INFLUENCE OF MICROPATTERNS ON HUMAN MESENCHYMAL STEM CELL FATE

A THESIS SUBMITTED TO
THE GRADUATE SCHOOL OF NATURAL AND APPLIED SCIENCES
OF
MIDDLE EAST TECHNICAL UNIVERSITY

BY

ONUR HASTÜRK

IN PARTIAL FULFILLMENT OF THE REQUIREMENTS
FOR
THE DEGREE OF MASTER OF SCIENCE
IN
BIOTECHNOLOGY

JUNE 2016

Approval of the thesis:

INFLUENCE OF MICROPATTERNS ON HUMAN MESENCHYMAL STEM CELL FATE

submitted by **ONUR HASTÜRK** in partial fulfillment of the requirements for the degree of **Master of Science in Biotechnology Department, Middle East Technical University** by,

Prof. Dr. Gülbin Dural Ünver _____
Dean, Graduate School of **Natural and Applied Sciences**

Doç. Dr. Çağdaş Devrim Son _____
Head of Department, **Biotechnology**

Prof. Dr. Vasıf Hasırcı _____
Supervisor, **Dept. of Biological Sciences, METU**

Prof. Dr. Nesrin Hasırcı _____
Co-supervisor, **Dept. of Chemistry, METU**

Examining Committee Members:

Prof. Dr. Menemşe Gümüşderelioğlu _____
Dept. of Chemical Engineering, Hacettepe University

Prof. Dr. Vasıf Hasırcı _____
Dept. of Biological Sciences, METU

Prof. Dr. Ayşe Eser Elçin _____
Stem Cell Institute, Ankara University

Doç. Dr. Tülin Yanık _____
Dept. of Biological Sciences, METU

Doç. Dr. Çağdaş Devrim Son _____
Dept. of Biological Sciences, METU

Date: 07.06.16

I hereby declare that all information in this document has been obtained and presented in accordance with academic rules and ethical conduct. I also declare that, as required by these rules and conduct, I have fully cited and referenced all material and results that are not original to this work.

Name, Last Name: Onur Hastürk

Signature:

ABSTRACT

INFLUENCE OF MICROPATTERNS ON HUMAN MESENCHYMAL STEM CELL FATE

Hastürk, Onur

M.S., Department of Biotechnology

Supervisor: Prof. Dr. Vasıf Hasırcı

Co-Supervisor: Prof. Dr. Nesrin Hasırcı

June 2016, 201 pages

Mesenchymal stem cells (MSCs) are promising cell sources for tissue engineering applications as they can differentiate into a variety of adult cells types including osteoblasts. *In vivo* microenvironment of stem cells is known to provide both biochemical signals and micro- and nanoscale physical cues that influence the behavior and fate of stem cells. The use of soluble chemical factors is the most common strategy to guide the commitment of MSCs to specific lineages, but it is a cause of concern such as unsatisfactory results or potential side effects. Therefore, engineering of the substrate surfaces with the aim of mimicking *in vivo* physical cues is a promising approach to understand cell-substrate interactions and modulate the fate of MSCs. For this purpose, poly(methyl methacrylate) films were designed to have surfaces decorated with 4x4 μm² (P4G4), 8x8 μm² (P8G8) and 16x16 μm² (P16G16) square prism pillars of 8 μm height separated by 4, 8 and 16 μm gaps, respectively. One set of the substrates were treated with oxygen plasma to improve surface hydrophilicity. Human MSCs isolated from dental pulp tissues were cultured on these substrates and the influence of the dimension and hydrophilicity of micropatterns on attachment, conformational changes, proliferation and differentiation of cells were studied. The results showed that micropatterns increased cell attachment but decreased proliferation rate on the hydrophobic substrates; however, oxygen plasma modification promoted both attachment and proliferation

rate on all substrates. Confocal micrographs and the following digital analysis of cell shapes revealed distinct deformations in varying degrees in the cytoskeleton induced by topographical features. These deformations were found to occur earlier and to a higher degree on plasma modified hydrophilic substrates. Cells cultured on substrates with smaller pillar and gap dimensions displayed significant deformations of their nuclei. The proliferation rates on these substrates were significantly lower compared to the control surfaces. The influence of micropatterns on the expression of stemness and osteogenesis related genes was determined by real time quantitative PCR method. Plasma modified substrates were found to downregulate the expression of stemness markers and did not lead to an increase in the expression of bone markers. Hydrophobic P4G4 and P8G8 surfaces having no oxygen plasma modification, however, caused a significant increase in the expression of the bone marker alkaline phosphatase (ALP) and demonstrated that unmodified hydrophobic micropillar structures induce osteogenesis without using any chemical osteogenic factors.

Keywords: Micropatterns, square prism pillar, poly(methyl methacrylate), mesenchymal stem cells, nucleus deformation, cytoskeleton, cell surface interactions, gene expression, osteogenic differentiation

ÖZ

MİKRODESENLERİN İNSAN MEZENKİMAL KÖK HÜCRELERİNİN YAZGISI ÜZERİNE ETKİLERİ

Hastürk, Onur
Yüksek Lisans, Biyoteknoloji Bölümü
Tez Yöneticisi: Prof. Dr. Vasıf Hasırcı
Ortak Tez Yöneticisi: Prof. Dr. Nesrin Hasırcı
Haziran 2016, 201 sayfa

Mezenkimal kök hücrelerin (MKH) kemik hücresi de dahil birçok hücre çeşidine farklılaşabilmesi, bu hücreleri doku mühendisliği uygulamaları açısından umut veren bir kaynak haline getirmektedir. Kök hücrelerin *in vivo* mikroortamlarının, biyokimyasal sinyallerin yanı sıra mikro- ve nanoölçekte fiziksel sinyaller de sağlayarak hücrelerin davranışlarını ve farklılaşmalarını yönlendirdiği bilinmektedir. Çözünür kimyasal faktörlerin kullanımı, MKH'in belirli hücre tiplerine farklılaşmasını kontrol etmekte en sık kullanılan yöntemdir. Ancak bu yöntem, yeterince etkin olmayan sonuçlar ve olası yan etkiler açısından kaygıları da beraberinde getirmektedir. Bu nedenle, malzeme yüzeylerinin hücrelerin *in vivo* ortamlarını taklit edecek şekilde tasarlanması, hücre-yüzey ilişkilerini anlama ve kök hücrelerin farklılaşma yönünü kontrol etme bakımından oldukça önemlidir. Buradan yola çıkarak, yüzeyleri sırasıyla 4, 8 ve 16 μm boşluklar ile ayrılmış 4x4 μm² (P4G4), 8x8 μm² (P8G8) ve 16x16 μm² (P16G16) boyutlara ve 8 μm yüksekliğe sahip kare prizma sütunlar ile bezenmiş poli(metil metakrilat) filmler tasarlanmıştır. Elde edilen filmlerin bir grubuna yüzey hidrofilikliğini arttırmak üzere oksijen plazması uygulanmıştır. Diş pulpasından izole edilen insan MKH'i, mikrodesenli yüzeyler üzerinde kültür edilmiş, mikrodesenlerin boyut ve hidrofilikliğinin hücre tutunması, yapısal değişiklik, hücre çoğalması ve farklılaşması üzerine etkileri

incelenmiştir. Elde edilen sonuçlar, mikrodesenlerin hidrofobik yüzeylerde hücre tutunmasını arttırırken çoğalma hızını düşürdüğünü, oksijen plazma işleminin ise, tüm örneklerde hem tutunmayı hem çoğalma hızını arttırdığını göstermiştir. Konfokal mikroskopi görüntüleri ve hücre biçimlerinin dijital analizleri, hücre iskeletlerinde yüzey desenlerinden kaynaklanan ciddi biçim bozulmalarının meydana geldiğini göstermiştir. Bu bozulmalar plazma işlemi görmüş yüzeylerde daha erken ve daha yüksek düzeyde gerçekleşmiştir. Daha küçük sütun ve sütunlararası boşluk boyutlarına sahip yüzeylerdeki hücre kültürlerinde, hücrelerin çekirdeklerinde ciddi şekil değişiklikleri oluşmuştur. Bu örneklerde hücre çoğalma hızı kontrol yüzeylere göre belirgin derecede azalmıştır. Mikrosütunların kök hücre ve kemik işaretçisi (marker) genlerin ifadesi üzerine etkileri gerçek zamanlı kantitatif PCR metodu ile incelenmiştir. Plazma işlemi görmüş desenli yüzeyler kök hücre işaretçilerinin ifadesinde bir azalmaya neden olurken, kemik hücresi işaretçilerinin ifadesinde bir artışa sebep olmamıştır. Oksijen plazma işlemi görmemiş hidrofobik P4G4 ve P8G8 yüzeyler ise kemik işaretçisi alkalen fosfatazın (ALP) ifadesinde artışa sebep olarak işlem görmemiş hidrofobik desenlerin kimyasal osteojenik faktörler olmadan da kemik hücresine farklılaşmayı tetiklediğini göstermiştir.

Anahtar kelimeler: Mikrodesenler, kare prizma sütun, poli(metil metakrilat), mezenkimal kök hücreler, hücre çekirdeği deformasyonu, hücre iskeleti, hücre-yüzey etkileşimleri, gen ifadesi, hücre farklılaşması

Dedicated to my lovely family

ACKNOWLEDGEMENTS

I would like to express my deepest gratitudes to my thesis supervisor, Prof. Dr. Vasıf Hasırcı for his continuous guidance, encouragement and insight throughout this study. I am very happy and proud of having the privilege of doing research under his supervision.

I am also grateful to my co-supervisor, Prof. Dr. Nesrin Hasırcı for her support, suggestions and guidance during this research.

I would like to offer my special thanks to Prof. Dr. Utkan Demirci and Dr. Pu Chen of Stanford University Bio-Acoustic-MEMS in Medicine (BAMM) Laboratory for the micropatterned silicon wafers.

I would like to extend my thanks to Doç. Dr. Ercüment Önder for the dental pulp tissues provided for stem cell isolation.

I am particularly grateful for the assistance given by Prof. Dr. Bülent Karasözen and Abdullah Sivas of METU Institute of Applied Mathematics in the coding of the shape descriptors into the MatLab software.

I would like to acknowledge to TÜBİTAK for their support through BIDEB 2210-E Scholarship.

I wish to acknowledge the help, guidance and support provided by MD. Menekşe Ermiş Şen throughout this study. I would also like to thank to Dr. Arda Büyüksungur for his guidance in microscopy and for his support and good advices.

I would like to thank to Deniz Sezlev Bilecen, Aylin Kömez, Menekşe Ermiş Şen, Gökhan Bahçecioğlu, Ezgi Antmen, Gözde Eke and Senem Heper for their invaluable friendship, encouragement and support.

I want to thank to the rest of the members of METU BIOMATEN Center of Excellence in Biomaterials and Tissue Engineering. Thanks to Tuğba Dursun, Büşra Günay, Esen Sayın, Cemile Bektaş, Ayşe Selcen Alagöz, Ayla Şahin, our postdoctoral fellow Türker Baran and our technician Zeynel Akın.

Finally, I would like to express my deepest gratitude to my lovely family İnci Hastürk, Bülent Hastürk and Simge Hastürk for their understanding, caring, trust, support and endless love throughout my life.

TABLE OF CONTENTS

LIST OF TABLES

TABLES

LIST OF FIGURES

FIGURES

LIST OF ABBREVIATIONS

B-GP	Beta-Glycerophosphate
μm	micrometer
μCP	Microcontact Printing
2D	Two Dimensional
3D	Three Dimensional
AFM	Atomic Force Microscopy
Al_2O_3	Alumina
ALP	Alkaline Phosphatase
AR	Aspect Ratio
BDI	1,4-diisocyanatobutyrate
BMSCs	Bone Marrow Mesenchymal Stem Cells
BMP	Bone Morphogenetic Protein
BSA	Bovine Serum Albumin
BSP	Bone Sialoprotein
CA	Contact Angle
CLSM	Confocal Laser Scanning Microscopy
CoCr	Cobalt-Chromium
CO_2	Carbon Dioxide
Col1a1	Collagen Type 1 Alpha-1
d	days
Da	Dalton
DAPI	4', 6-diamidino-2-phenylindole
DMEM	Dulbecco's Modified Eagle Medium
DMSO	Dimethyl Sulfoxide
DPSCs	Dental Pulp Stem Cells

E	Young’s Modulus
ECM	Extracellular Matrix
EDTA	Ethylenediaminetetraacetic Acid
EGF	Epidermal Growth Factor
ESB	European Society for Biomaterials
ESCs	Embryonic Stem Cells
FAK	Focal Adhesion Kinase
FBS	Fetal Bovine Serum
FDA	Food and Drug Administration
FITC	Fluorescein Isothiocyanate
g	gram
h	hour
hOP	Healthy Osteoprogenitor
HSCs	Hematopoetic Stem Cells
GPa	Gigapascal
hESC	Human Embryonic Stem Cells
HMDSO	Hexadimethylsiloxane
HUVEC	Human Umbilical Vein Endothelial Cells
IGF-1	Insulin-Like Growth Factor
iPSCs	Induced Pluripotent Cells
ISCT	International Society for Cellular Theraphy
kDa	Kilodalton
KOH	Potassium Hydroxide
kPa	Kilopascal
kV	Kilovolt
LBPs	Lamin Binding Proteins
LDI	Lysine diisocyanate
LINC	Linker of Nucleus and Cytoskeleton
M	Molarity
mg	milligram

min	minute
mL	milliliter
mm	millimeter
mM	millimolar
MPa	Megapascal
MW	Molecular Weight
Na_2CO_3	Sodium Carbonate
Na_2HPO_4	Sodium Phosphate Dibasic
NaCl	Sodium Chloride
NaH_2PO_4	Sodium Phosphate Monobasic
NaOH	Sodium Hydroxide
NIL	Nanoimprinting Lithography
nm	nanometer
OC	Osteocalcin
OsO_4	Osmium Tetroxide
PAAm	Polyacrylamide
PBS	Phosphate Buffer Saline
PCL	Poly(caprolactone)
PDMS	Poly(dimethylsiloxane)
PDLSCs	Periodental Ligament Stem Cells
PE	Polyethylene
PEG	Polyethylene Glycol
Pen/Strep	Penicillin/Streptomycin
PET	Poly(ethylene terephthalate)
PGA	Poly(glycolic acid)
PHAs	Polyhydroxyalkanoates
PHBV	Poly(3-hydroxybutyrate-co-3-hydroxyvalerate)
PHB	Poly(3-hydroxy butyrate)
PIPES	Piperazine-N, N'-Bis(Ethanesulfonic Acid)
PLA	Poly(lactic acid)

PLGA	Poly(lactic acid-co-glycolic acid)
PLLA	Poly(l-lactic acid)
PMMA	Poly(methyl methacrylate)
PS	Polystyrene
PVC	Poly(vinyl chloride)
RGD	Arginine, Glycine, Aspartic Acid Sequence
RMS	Root Mean Square
RP	Rapid Prototyping
Runx-2	Runt-related Transcription factor-2
SAMs	Self assembled monolayers
SCAP	Stem Cells from Apical Papilla
SEM	Scanning Electron Microscopy
SHED	Stem Cells from Exfoliated Deciduous Teeth
TCPs	Tissue Culture Polystyrene
TGF-β1	Transforming Growth Factor Beta-1
TPL	Two Photon Lithography
UC	Unpatterned Control
UTS	Ultimate Tensile Strength
UV	Ultraviolet
VSMCs	Vascular smooth muscle cells
v/v	volume/volume ratio
w	weight
w/v	weight/volume ratio
ZrO_2	Zirconia

CHAPTER 1

INTRODUCTION

1.1. Cell-Substrate Studies

Adherent cells of the vertebrates overlie on basement membranes that serve as a substrate and also provide biochemical and mechanical cues to the cells. These cues modulate cellular behaviors such as adhesion, distribution and orientation of cytoskeletal elements, survival, growth, migration and differentiation. In addition to biochemical and mechanical properties, three dimensional (3D) topography of the basement membranes that consists of micro- and nanoscale features has also been shown to affect cell behavior. Therefore, it is important to gain fundamental knowledge of cell-substrate interactions for the development of medical implants, tissue engineering applications and production of pharmaceuticals (Flemming et al., 1999). The influence of solid substrates on cell orientation, cytoskeletal organization and migration was first emphasized by Harrison in 1911. He grew embryonic cells on spider web and observed that cells oriented themselves in the direction of silk fibers in a phenomenon called physical guidance or stereotropism. In 1934, Paul Weiss showed that nerve cells aligned and elongated in the direction of topographical features by a mechanism called contact guidance. In 1962 and 1963, Rosenberg claimed that nanometer sized features influenced cell orientation and behavior. Later in 1964, Curtis and Varde investigated the behavior and morphology of fibroblasts on silica substrates with varying topology and proposed that cells respond to the substrate topography. In 1980s, microfabricated devices have been started to be used

in biology and medicine. In 1983, Brunette et al. used photolithography to create patterned surfaces and studied cell behavior on them. Since then, advances in micro- and nanostructure fabrication methods in the silicon microelectronics industry have enabled researchers to design variety of surface structures to study the responses of cells to the surface topography (Voldman et al., 1999; Chen and Pépin, 2001). Numerous studies have shown that micro- and nanoscale topographical cues of artificial substrates also influence cell behavior such as adhesion, alignment, morphology, proliferation, gene expression and differentiation (Hasirci and Kenar, 2006). It is now an accepted fact that the role of substrates is not only acting as a structural support but also providing chemical and topographical signals that guide cell fate (Martinez et al., 2009). In this study, an example of the influence of cell-substrate interface on stem cell fate will be studied.

1.2. Primary Cells and Stem Cells

The use of tissue specific cell types is desired on the designed scaffolds for regenerative medicine applications. One way to harvest cells is to obtain autologous organ specific cells by biopsy. However, this method is not feasible for several tissues such as heart valves, spinal cord or peripheral nerves. The most common approach to solve the difficulty of finding a cell source is the isolation of stem cells (Stock and Vacanti, 2001). Stem cells are undifferentiated cells, which have the ability of self renewal and differentiation into multiple lineages. Stem cells are able to generate a differentiated progeny under specific molecular signals such as growth factors, cytokines, microRNAs and transcription factors provided within the niche (Martino et al., 2012). The use of stem cells in cell replacement therapies and tissue engineering applications by controlling the self-renewal and lineage/tissue specific differentiation is of great interest (Hwang et al., 2008). The fate of stem cells was shown to be regulated by both biochemical and physical cues provided by their vivo microenvironment. Therefore, stem cell-substrate studies are crucial to establish

artificial environments that mimic the key features of original stem cell microenvironments (Nikkhah et al., 2012).

1.2.1. Properties of Cells

1.2.1.1. Cell and Nucleus Structure and Organization

Cells are the smallest, membrane enclosed units of living organisms. They are composed of a cytosol that contains organelles with distinct functions and a plasma membrane that separates the cytosol from the external environment (Fig.1.1). The plasma membrane is composed of a phospholipid bilayer and transmembrane proteins. In addition to exchange of nutrients and waste products, plasma membrane also links the cytoskeleton to the extracellular matrix and allows cells to receive information from their environment by the activities of the transmembrane receptor proteins. Unlike prokaryotes, eukaryotic cells have membrane enclosed organelles and a nucleus, which contains genetic information in the form of DNA surrounded by a nuclear envelope (Alberts et al., 2013).

The cell cytoskeleton is a large network of protein filaments. It connects cells physically and biochemically to their microenvironment and enables them to organize cellular contents, move and change shape. Constant flux of the cytoskeletal components provides a dynamic and adaptive structure rather than a fixed skeleton. There are three main cytoskeletal protein fibers: actin filaments, microtubules and intermediate filaments. The polymerization and depolymerization of actin filaments and microtubules generates a directed force and modulates changes in cell shape in response to external stimuli. Unlike actin filaments and microtubules, intermediate filaments are not polarized; therefore they cannot support directional movement. Instead, they are crosslinked to each other or to actin filaments and microtubules by proteins called plectins, and maintain the shape and structural integrity of cells under mechanical stress. One specialized class of intermediate filaments is the nuclear

lamins, which contributes to the mechanical integrity of the nucleus (Fletcher and Mullins, 2010).

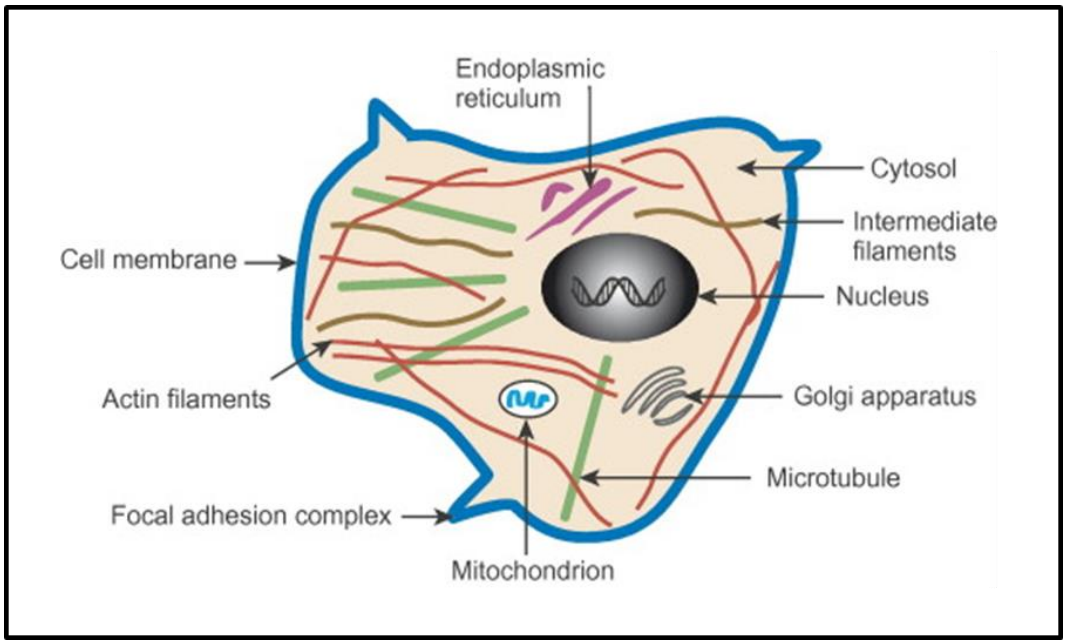

Figure 1.1. Schematic representation of the major features of a eukaryotic cell (Suresh, 2007).

The cell nucleus is the largest and the stiffest organelle in eukaryotic cells. It is composed of a nuclear envelope that encloses the nucleoplasm. The nuclear envelope consists of two phospholipid bilayer membranes and a dense protein network called the nuclear lamina. Nuclear lamina regulates and supports proteins involved in nuclear positioning, DNA replication and repair, and gene expression. There are two types of nuclear lamins, namely A-type and B-type. B-type lamins are expressed in all types of cells and essential for survival, while A-type lamins are fully expressed only in differentiated cells but absent in embriyonic stem cells. The main component of the nucleoplasm is the chromatin, which consists of DNA and histone proteins. Chromatin is structurally heterogeneous and composed of densely packed,

transcriptionally inactive regions called heterochromatin and more open, gene rich regions called euchromatin. Euchromatin is located at the interior of the nucleoplasm, whereas the heterochromatin is often located at the periphery of the nucleus and connected to the lamins through lamin binding proteins (LBPs) (Stuurman et al., 1998; Rowat et al. 2008; Dahl et al., 2008). The degree of packing and condensation of the chromatin have also been shown to contribute to the nuclear stiffness. For example, the chromatin of embryonic stem cells is loosely packed and exhibit high accessibility, which explains low nuclear stiffness together with the lack of A-type lamin expression. Chromatin of differentiated cells, however, is highly condensed and leads to a much stiffer nucleus (Pajerowski et al., 2007). The shape of the cell nucleus is typically spheroidal or ellipsoid. However, nuclear shape may undergo dramatic changes during differentiation or maturation as a result of altered expression of structural proteins. The nuclei of human embryonic stem cells are round and contain no lamin A/C. As the cells differentiate, chromatin movement increases and the expression of the A-type lamins is upregulated, which changes nucleus stiffness and shape (Constantinescu et al., 2006; Pajerowski et al., 2007).

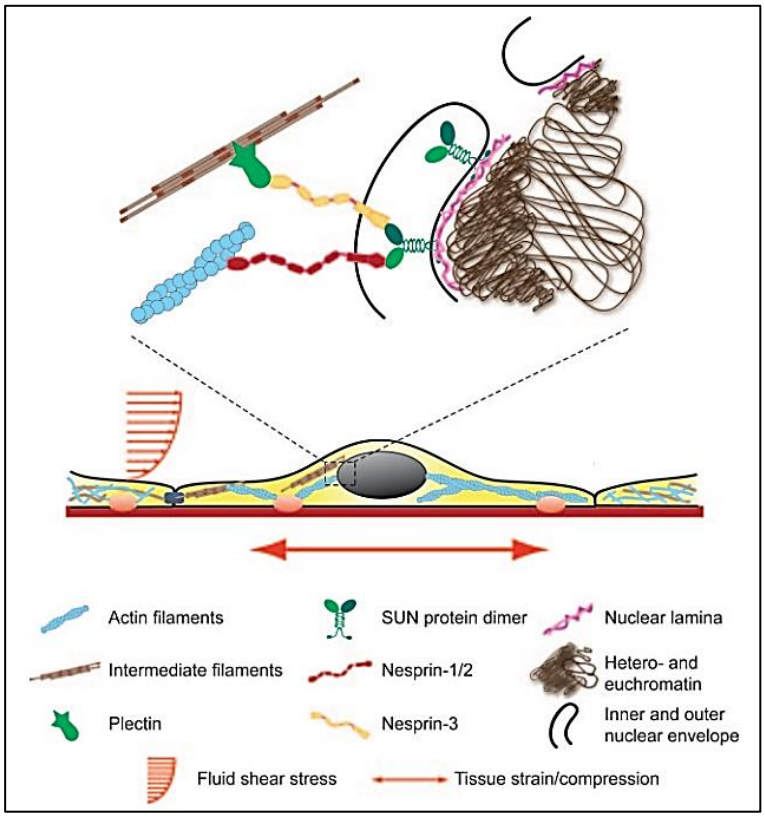

Figure 1.2. Schematic representation of the pathways of the force transmission from the extracellular matrix to the nucleus through cytoskeletal and nuclear elements (Dahl et al., 2008).

There are physical connections between the cytoskeleton and the nuclear envelope (Fig. 1.2). Nuclear lamins are connected to the inner nuclear membrane proteins SUN1 and SUN2, which are extended into the perinuclear space. SUN proteins interact with the adaptor protein nesprins, which can bind to actin and intermediate filaments. Association of A-type lamins, SUN proteins and nesprins forms a protein complex called linker of nucleus and cytoskeleton (LINC). There are also some direct connections between the microtubules and the nuclear envelope (Dahl et al., 2008; 2010). The mechanical stimuli collected from the microenvironment are transmitted to the cell nucleus as mechanical signals across the cytoskeleton through

a mechanism called mechanotransduction, which are then converted into biochemical responses (Orr et al., 2006).

1.2.1.2. Adhesion and Migration of Cells

Adhesion of mammalian cells to the ECM is a crucial step for fundamental processes such as survival, growth and differentiation. Cells express a variety of surface adhesion receptors including integrins, syndecans and cadherins. Among them, integrin family of transmembrane heterodimeric receptors forms the most critical connection between a cell and the ECM. The extracellular domains of integrins bind to specific sequence motifs of ECM proteins such as fibronectin, vitronectin and collagen and this binding brings a conformational change in the cytoplasmic tail of integrins. This change promotes the formation of a linkage to the actin cytoskeleton through several cytoskeletal and signaling proteins such as focal adhesion kinase (FAK), paxillin, vinculin and talin. The resulting multiprotein complex is called focal adhesion complex (Fig. 1.3). Cell adhesion through formation and maturation of the focal adhesions is crucial for cells to sense mechanical and physical cues of their microenvironment (Parsons et al., 2010).

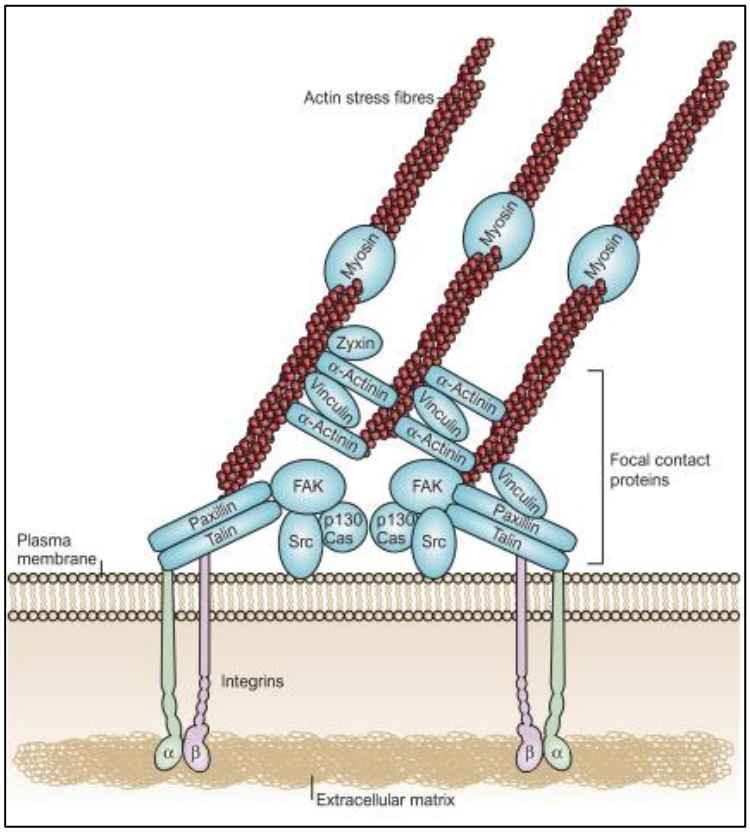

Figure 1.3. Schematic representation of the focal adhesion complex at the integrin-extracellular matrix binding sites (Mitra et al., 2005).

Directional migration of motile cells can be initiated by extracellular cues including gradients of growth factors or chemokines, mechanical forces such as stretching and fluid flow, electrochemical gradients, and the topography and mechanics of the ECM. Cells exhibit an asymmetric morphology while migrating. The migration cycle is initiated by the polarization and extension of cell protrusions at the leading edge. These protrusions include a broad, flat lamellipodia and spike-like filopodia (Fig.1.4.A). Lamellipodia are composed of a branched meshwork of actin filaments and moves forward upon the polymerization of actin filaments. Filopodia are formed at the periphery of lamellipodia and their tips are rich in cell adhesion receptors such as integrins and cadherins, therefore cells use these tentacles to probe their

microenvironment during protrusion. Cell protrusions are formed by a continuous process of actin polymerization and stabilized by the focal adhesions that link actin cytoskeleton to the underlying ECM. A traction force is generated by the contraction of actomyosin, and cells move forwards upon the disassembly of the focal adhesions at the cell rear. Actomyosin is composed of actin stress fibers and myosin II motor proteins that move antiparallel actin filaments. The contraction of actomyosin translocates the cell body and nucleus forward and the retraction fibers pull the cell rear (Fig.1.4.B) (Mattila and Lappalainen, 2008).

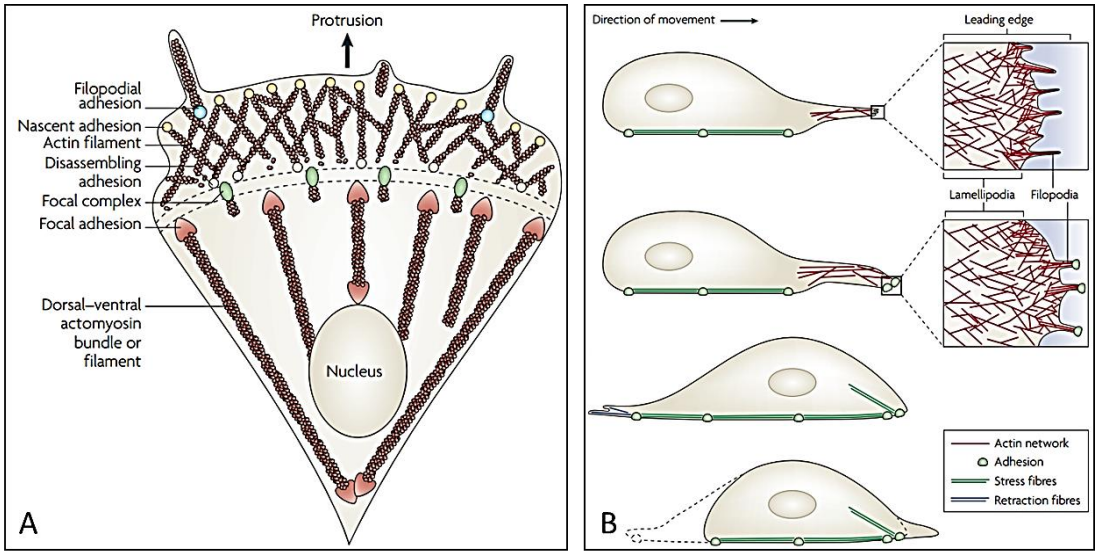

Figure 1.4. Schematic representation of the conformation and structural elements of migrating cells. (A) Components of the leading edge of a migrating polarized cell and their connections to cell cytoskeleton and nucleus (Parsons et al., 2010), (B) protrusion, extension and retraction of translocating cells during directional migration (Mattila and Lappalainen, 2008).

1.2.1.3. Mechanical Properties of Cells

External mechanical signals such as tension, compression, fluid shear stress and hydrostatic pressure or the mechanical properties of substrates such as the stiffness were shown to influence the growth, development and maintenance of cells greatly. These mechanical stimuli are sensed by cells using mechanosensitive receptors and cause intracellular tensile forces, which results in cytoskeletal reorganization and conversion of these mechanical stimuli into biochemical information via mechanotransduction (Castillo and Jacobs, 2010).

Upon the formation of a focal contact, focal adhesion kinase (FAK) is recruited by integrin binding proteins paxillin and talin. Activated FAK phosphorylates the cytoskeletal protein α-actinin and attaches actomyosin stress fibers to the focal contacts. FAK also influences the activity of Rho-family GTPases such as RhoA, Rac and Cdc42, which direct the assembly of local actin into stress fibers, lamellipodia and filopodia, respectively (Mitra et al., 2005). This mechanoresposive meshwork of stress fibers bidirectionally transfers the traction forces generated by actin polymerization and myosin II dependent contraction to the focal adhesions and nucleus. The synthesis and organization of the focal contacts and stress fibers are regulated so that they balance these bidirectional mechanical relations between the forces generated by cells and the external forces or mechanical properties of the ECM (MacQueen et al., 2013). These intracellular forces can be transmitted to the nucleus by the LINC complex across the cytoskeleton and may result in changes in nuclear shape. During these changes, conformation of DNA or higher order chromatin structures could be altered, which might lead to changes in accessibility of genes to transcription factors and alteration of the total gene expression profile (Marko and Poirier, 2003). In addition to generating cytoskeletal stress, FAK also activates a number of biochemical pathways (Fig. 1.5). Phosphorylated FAK recruits the Grb2/SOS complex and activates Ras and (ERK2)/MAP kinase signaling cascades. Activation of Ras and ERK/MAPK cascades regulates the activities and

expression levels of several transcriptional factors, which leads to altered transcription of genes that are important for biological processes such as cell cycle and differentiation (Schaller, 2001).

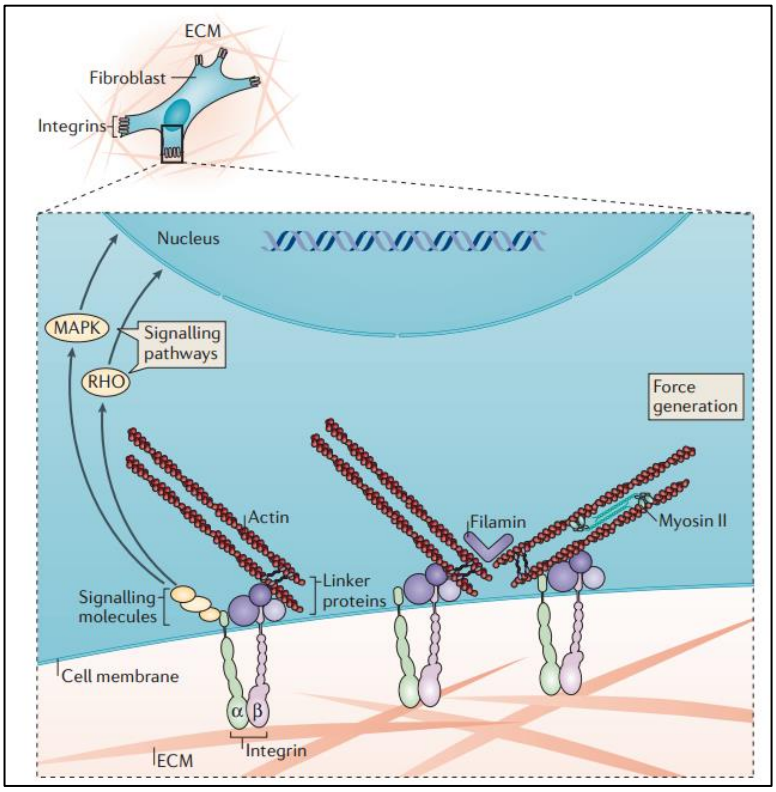

Figure 1.5. Mechanotransduction. Schematic representation of integrin binding to the ECM and mechanical and biochemical signalling to nucleus (Humprey et al., 2014).

The mechanical forces in the niche of embriyonic stem cells are known to play a critical role on differentiating fetal tissues and guide the development of functional organisms. Adult stem cells are also influenced by their mechanical environment. Mesenchymal stem cells, for instance, are susceptible to mechanical signals during

the development of skeleton. Mechanical tests carried out with single cells suggested that embriyonic and adult stem cells are more deformable than their differentiated forms, therefore they are influenced by the mechanical signals to a greater extent. Since the nucleus is the stiffest organel, it determines the stiffness of cells. The micropipette aspiration testing of ESCs showed that their nuclei stiffen 6-fold upon differentiation and this phenomenon was associated with the lamin A/C as it is not expressed in ESCs but expressed in differentiated cells. Similarly, micropipette aspiration of MSCs showed that undifferentiated cells had an equilibrium Young's modulus of 100 Pa, which increased significantly upon osteogenic differentiation and reached a value around twice that of undifferentiated cell (Lee et al., 2011).

1.2.2. Stem Cell Biology

Human embryonic stem cells, induced pluripotent stem cells and mesenchymal stem cells (MSCs) are the main types of stem cells used in regenerative medicine (Martino et al., 2012) (Fig. 1.6). Embryonic stem cells (ESCs) are isolated from the inner mass of blastocysts. They display high telomerase activity and express high levels of Oct3/4, Nanog and Sox2 genes that play a key role in the self-renewal (Mitsui et al., 2003). ESCs able to differentiate into all three germ layers: endoderm, mesoderm (including muscle, bone and blood) and ectoderm (epidermal tissues and nervous system). Several cell types such as hematopoietic precursors, neural cells, adipocytes, muscle cells, chondrocytes and bone cells have been successfully generated from mouse ESCs *in vitro* by controlling the culture conditions (Buttery et al., 2001). The use of ESCs, however, raises some concerns including ethical issues about the use of fetal tissues, potential immunological risks and ejection of the ESCs derived cellular grafts and formation of ESCs derived tumors (Odorico et al., 2001).

Moral and legal controversies concerning the use of ESCs for clinical and therapeutic applications have encouraged the examination of the progenitor cell sources that are

found within the adult organisms (Tuan et al., 2003). There are several types of adult stem cells that contribute to the maintenance and regeneration of post-natal tissues. Some of them are epithelial stem cells in epidermis and intestinal crypts, neural stem cells in the central nervous system and hematopoietic and stromal stem cells that reside in the bone marrow (Meirelles et al., 2006). These cells display a similar self-renewal capacity but a more restricted differentiation potential compared to ESCs (Galli et al., 2008). Among the adult stem cell sources, post-natal mammalian bone marrow is the most widely examined tissue, which hosts hematopoietic stem cells (HSCs) and stromal cells including vascular endothelial and mesenchymal stem cells (MSCs) (Strobel et al., 1986).

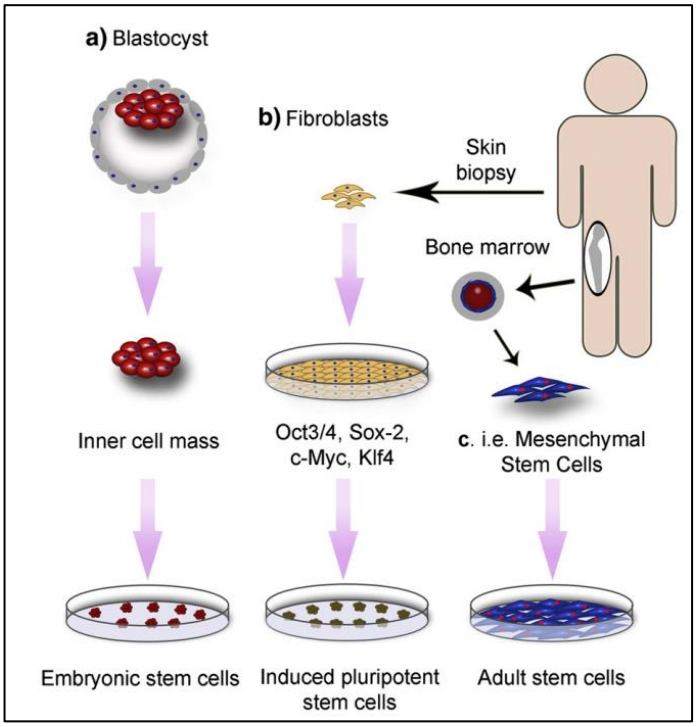

Figure 1.6. Schematic representation of stem cell biogenesis. (a) Embryonic stem cells derived from inner mass of the blastocyst, (b) induced pluripotent stem cells generated *in vitro* and (c) mesenchymal stem cells isolated from adult tissues (Martino et al., 2012).

1.2.2.1. Mesenchymal Stem Cells (MSCs)

Friedenstein, Owen and their colleagues first identified MSCs as the rodent bone marrow derived fibroblastoid cells that can adhere to the tissue culture plastic (Friedenstein et al., 1970; Owen et al., 1988). The Mesenchymal and Tissue Stem Cell Committee of the International Society for Cellular Therapy (ISCT) proposes three criteria to define a cell as mesenchymal stem cell: adherence to plastic, specific expression of surface antigens such as CD90, CD105 and CD73, and multipotent differentiation potential towards osteogenic, chondrogenic and adipogenic lineages (Dominici et al., 2006). Bone marrow MSCs (BMSCs) are multipotent cells and they were shown to be capable of differentiating into multiple mesenchymal cell lineages such as bone, adipose, cartilage cells. They were also reported to transdifferentiate into unrelated germline lineages such as muscle, endothelial and neuron-like cells (Uccelli et al., 2008) (Fig. 1.7). This versatility for multipotent differentiation makes these MSCs an attractive cell source for tissue engineering applications.

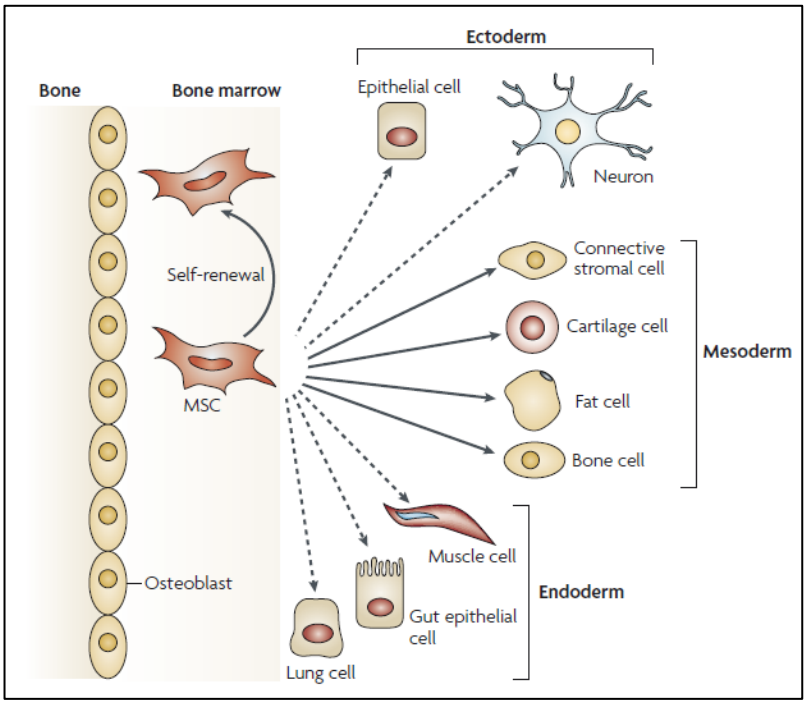

Figure 1.7. Schematic diagram of the lineages that bone marrow MSCs can differentiate. Straight solid arrows: differentiation into mesodermal lineage. Dashed arrows: transdifferentiation into ectodermal and endodermal lineages (Uccelli et al., 2008).

1.2.2.1.1. Bone Cells and Osteogenic Differentiation of MSCs

Bones of the skeleton forms the skeletal system together with cartilages, ligaments and several other connective tissues. In addition to providing structural support, bones also protect vital organs, store minerals and lipids, and produce blood cells. The walls of the shaft of long bones consist of compact bone, which forms a solid protective layer around the marrow cavity. The basic functional unit of compact bone is osteon (Haversian systems). In the center of osteons, a Haversian canal takes place, which contains one or more blood vessels that feed the bone. In addition to the central canals that run parallel to the bone surface, there are Volkmann canals extending perpendicular to the surface. The central canal is surrounded by cylindrical

layers called lamellae, which consist of collagen fibers and hydroxyapatite crystals. Between these lamellae, pockets called lacunae are sandwiched and they host osteocyte cells. Lacunae are interconnected by narrow passageways called canaliculi (Martini, 1998) (Fig. 1.8). The size of lacunae is in the order of 10 µm while the size of tubular canaliculi is in the order of 0.5 µm (Zhou et al., 2009).

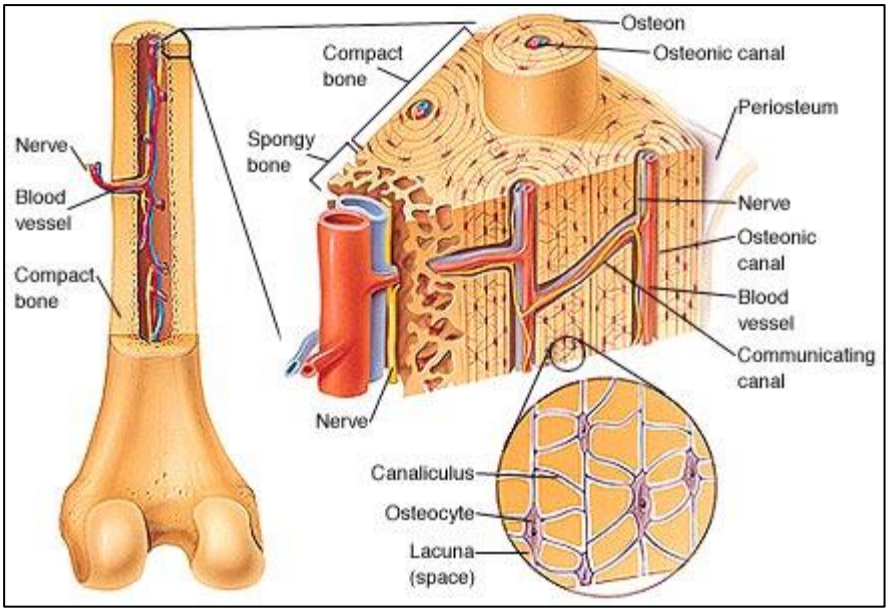

Figure 1.8. Schematic representation of the organization of osteons and lamellae of compact bone (Raven et al., 2010).

The remodeling of bone is carried out by specialized mature bone cells, which are osteoclasts, osteoblasts and osteocytes. Osteoclasts are large, multinucleated cells that dissolve the mineral components of the bone matrix by creating an acidic environment. Fully differentiated osteoblasts are responsible for new bone formation by producing and secreting bone matrix proteins, mainly collagen type I. Osteoblasts become mechanosensitive osteocytes when they are buried within the lacunae of the mineralized matrix. Osteocytes have a highly branched, stellate morphology and they

are the most abundant cell type in the bone tissue. They communicate with each other and other cells via the branching extensions of their plasma membrane that run along the canaliculi (Manolagas, 2000). Osteoblasts are derived from multipotent mesenchymal stem cells that reach bone by migrating from neighboring connective tissues (Triffitt, 1996). Differentiation into osteoblasts brings distinct changes in both morphology and physiology of MSCs. Their fibroblastic shape transforms into a cuboidal shape, and cells start to produce ECM that is mainly composed of collagen type I. In later stages, calcium phosphate aggregates and nodules are formed on the ECM as a result of increased expression of the enzyme alkaline phosphatase (ALP) and calcium accumulation (Vater et al., 2011).

The differentiation and development of osteoblasts from MSCs is controlled by soluble factors as well as the cell-cell and cell-ECM interactions and the mechanical signals provided in the cell microenvironment (Rosen and Wozney, 1996). At the molecular level, commitment of MSCs into the osteogenic lineage is controlled by the interactions between several transcription factors and hormones. The main regulator of osteogenic differentiation and bone formation is the transcriptional activity of the Runt-related transcription factor-2 (Runx2 (a.k.a. Cbfa1)). Expression of bone specific genes such as osterix (Sp7), osteocalcin, bone sialoprotein (BSP) and collagen type 1 alpha-1 (Col1a1) are induced upon binding of the Runx2 to the promoters of corresponding genes (Salasznyk et al., 2007). The zinc finger containing transcription factor osterix was shown to lie downstream of Runx2 and it is essential for the osteogenic differentiation (Nakashima et al., 2002). Osteoblastogenesis related growth factors, particularly the bone morphogenetic proteins (BMPs), stimulate the expression of Runx2. Aggregation of $\alpha_2\beta_1$ and $\alpha_v\beta_3$ integrins and activation of FAK at focal adhesion complexes have been also shown to stimulate Runx2 activity by starting intracellular signaling cascades including ERK/MAPK pathways, indicating the importance of focal adhesions and mechanical stimuli in osteogenesis (Salasznyk et al., 2007).

1.2.2.1.2. Dental Pulp Stem Cells (DPSCs)

There are some limitations associated with the bone marrow MSCs. These include painful procedure for the procurement of the tissue, high morbidity of the tissue site (Miller et al., 2008) and low ratio of the stem cells to the total isolated cells (Puissant et al., 2005). Thus, several other tissues have also been characterized as alternative MSC sources. Of these, progenitor cells isolated from adipose tissue, umbilical cord, amniotic fluid (Klemmt et al., 2011) and dental tissues have been shown to fulfill the requirements to be defined as MSCs. Among these, dental tissues become prominent as an easily accessible MSCs source. Up to the present, four types of dental tissue derived MSCs populations have been isolated and characterized: stem cells from exfoliated deciduous teeth (SHED), periodontal ligament stem cells (PDLSCs), stem cells from apical papilla (SCAP) and dental pulp stem cells (DPSCs) (Huang et al., 2009). DPSCs are progenitor cells that are extracted from the pulp tissue of impacted third molars (wisdom teeth) and have been shown to share a similar *in vitro* immunophenotype with the BMSCs. These progenitor cells proliferate and differentiate into odontoblasts to regenerate tooth specific structures such as cementum, periodontal ligaments and periapical follicles (Gronthos et al., 2000). DPSCs have been also reported to be multipotent MSCs with the ability to undergo adipogenic, chondrogenic and osteogenic differentiation. Thus, extracted human third molars could be an easily accessible source of MSCs for clinical applications (Perry et al., 2008).

There are two isolation methods for DPSCs: the outgrowth and enzyme digestion. In outgrowth method, pulp tissues are cut into pieces and placed directly in cell culture flask, so the cells crawl out from the tissue. In the enzyme digestion method, pulp tissue is degraded in a solution containing proteases such as collagenase and dispase, which digest the pulp tissue and release the cells. Even though both methods have been shown to give rise to cells with stem cell properties, some morphological differences were observed between two cell populations. Enzyme digestion method

gives a higher number of compact cells with a higher mineralization rate compared to the outgrowth method (Yildirim, 2013). DPSCs isolated with enzyme digestion method were shown to exhibit a broad, flattened shape, and they can successfully undergo adipogenic, chondrogenic and osteogenic differentiation (Khanna-Jain et al., 2012). DPSCs isolated by enzyme digestion method have been reported to express embryonic stem cell markers including Oct3/4 and Nanog, and maintain their normal karyotype and proliferation rate during at least 25 passages (Kerkis et al., 2007). In addition to high self-renewal capacity, these cells have been found to be able to differentiate into mechanoresponsive cells and form bone-like tissue *in vivo*, which suggests that DPSCs could be very useful for bone tissue engineering applications (Kolind et al., 2014).

1.2.2.2. *In Vitro* Differentiation of Stem Cells

The *in vivo* fate of stem cells has been shown to be controlled by the combination of chemical, physical and biological cues present in the microenvironment, which is called the "stem cell niche". Therefore, the studies on directing the differentiation of stem cells *in vitro* have been focused on the optimization of the combination of culture conditions, growth factors and extracellular matrix (Hwang et al., 2008).

1.2.2.2.1. Use of Growth Factors and Small Molecules

Growth factors are soluble secreted signaling molecules that bind to specific transmembrane receptors and instruct cells during the developmental stages by regulating their survival, migration, proliferation and differentiation (Cross et al., 1991). They have short half-lives and act locally, because they exhibit a slow, short-range diffusion through the extracellular matrix. Enabling control over the delivery of growth factors has been attracting much attention in order to achieve tissue

regeneration in adult organisms. Transforming growth factor-beta 1 (TGF-β1) and bone morphogenetic proteins (BMPs) are the most widely used growth factors for the osteogenic differentiation of MSCs. They induce cell growth, promote osteogenic differentiation in early stages and control the bone formation by modulating the remodeling of the components of bone matrix such as collagen type I (Hildebrandt et al., 2009). The response induced by a growth factor depends on the cell type, the receptor type on the same cell and some external factors such as the ability of the factor to bind to the extracellular matrix, concentration of the factor and the location of the target cell (Lamalice et al., 2007). In addition to the localized delivery of one specific factor, simultaneous or sequential delivery of multiple factors has been shown to determine the effect and the efficiency of the delivery (Huri et al., 2013).

In addition to the growth factors, some cell permeable small molecules such as dexamethasone, vitamin C, sodium pyruvate, thyroid hormones, prostoglabdin E2, dibutyrl cAMP and retinoic acid have been shown to regulate the fate of stem cells (Hwang et al., 2008). These small molecules were identified to be agonists and antagonists of classical developmental biology pathways such as Hedge-hog, Wnt and Notch, which are known to regulate the differentiation of stem cells (McNeish, 2007). Dexamethasone, beta-glyserophosphate (β-GP) and ascorbic acid are the most widely used small molecules as osteogenic supplements. Dexamethasone is a synthetic glucocorticoid that was shown to promote the osteogenic differentiation by activating Runx-2 dependent transcriptional regulation. β-GP acts as a crucial source of inorganic phosphate, which is important for matrix mineralization together with calcium ions, upon enzymatic cleavage by alkaline phosphatase. Ascorbic acid is utilized by the cells as a cofactor for the hydroxylation of proline and lysine residues of the collagens found in the ECM. Ascorbic acid was shown to enhance integrin signaling by increasing in the synthesis of collagen type 1, which is coupled with Runx-2 directed osteogenic differentiation (Langenbach and Handschel, 2013).

1.2.2.2.2. Engineering of the Extracellular Microenvironment

The main problem with the soluble factors is the difficulty of delivering them in a combined, controlled manner at the right place and time for the accurate duration in order to obtain satisfactory effects (Lee et al., 2011). Moreover, such soluble factors have been usually used in doses that are much higher than the physiological doses to obtain obvious results. However, this situation brings safety concerns such as tumorigenicity and little is known about the side effects of these chemicals (Anderson et al., 2011). Besides soluble factors, some material cues including substrate stiffness, surface chemistry and topographical cues such as micro/nanostructures have been found to influence the differentiation of stem cells. The ECM of stem cells contains topographical features inherent to its architecture. Depending on the functional requirements, each tissue exhibits varying amounts of matrix macromolecules and specific organization in the ECM, creating features ranging in size of nano- to microscale (Martinez et al., 2009). Together with the biochemical cues, these surface features of the microenvironment play an important role in regulation of stem cell renewal and differentiation (Edalat et al., 2011). Thus, surface modification of substrates with the aim of mimicking the key surface features of stem cell microenvironment is very important to study and modulate the fate of stem cells. It could be also a safer and more durable approach for directing stem cell fate than the delivery of soluble factors (Zhao et al., 2012). The influence of surface features on the fate of stem cells will be discussed in detail in Section 1.5.3.4.

1.3. Substrate Materials

Severe damage or degeneration of tissues caused by disease, injury or trauma requires treatments to replace damaged tissue or facilitate the repair when the self-regeneration of the body is slow or insufficient. In such cases, grafting techniques are employed, which currently focus on the transplantation of tissues from one site to

another in the same patient (an autograft) or from another individual (an allograft) or an animal (a xenograft) to the patient. However, harvesting autografts is expensive, donor tissue is scarce and there are the risks of donor site hematoma, infection and morbidity in addition to the pain. Similarly, allografts and xenografts introduce the risks of rejection by the immune system of the patient and transmission of disease from the donor. At this point, the fields of biomaterials and tissue engineering come to the forefront, with the aims of developing substitutes for the replacement or regeneration of the damaged tissue.

The term biomaterial is defined by the European Society for Biomaterials (ESB) as "a material intended to interface with biological systems to evaluate, treat, augment or replace any tissue, organ or function of the body" (O'Brien, 2011). Biomaterials can be designed to replace the lost or diseased tissues and restore the function or the form as in the examples of stents in blood vessels, artificial valves in the heart, replacement implants in hips, knees, shoulders, elbows, ears and orodental structures (Geetha et al., 2008). Alternatively, biomaterials can be used as cell scaffolds for tissue engineering applications with the aims of restoring, maintaining or improving the tissue function until it fully regenerates, instead of replacing them (Langer, 2000). Biomaterials that are designed for either replacement purposes that aim the ingrowth and differentiation of cells from surrounding tissues in situ or cell-based therapies for the induction of morphogenesis in bioengineered tissues should provide a three dimensional support to cells and guide their functions (Atala, 2004). Considering the importance of the basal membranes for cell behavior and fate, implants and scaffolds should be designed to mimic the characteristics of the ECM of the target tissue (Gauvin et al, 2012).

1.3.1. Types of Substrate Materials

The main types of the substrate materials used as biomaterials can be classified as metals, ceramics, polymers and composites. Metals exhibit excellent mechanical properties in addition to electrical and thermal conductivity. Metallic substrates are typically used as substitutes for hard tissue replacement such as total hip and knee joints, bone plates and screws, spinal fixation devices and dental implants. Metal alloys are employed for more active roles such as vascular stents, catheter guide wires and cochlea implants. Most common examples of metallic alloys used in biomedical field are the stainless steel that is used for the fabrication of fracture plates, screws and hip nails, cobalt-chromium (CoCr) alloys used in stems of prosthesis, nickel alloys of titanium that exhibits shape memory and is used in dental archwires, vascular stents and orthopedic staples, or aluminum and vanadium alloys of titanium used in orthopedic joint replacements and bone plates. Corrosion is the biggest disadvantage of metallic substrates, because it causes weakening and release of harmful particles (Park and Kim, 2003).

Ceramics are hard, polycrystalline compounds that have very high stiffness and compressive strength but exhibit inherent brittleness and low tensile and impact strengths. The relative inertness to body fluids and aesthetically pleasing appearance led the use of ceramics especially as dental crowns. Some carbons are utilized in blood interfacing applications such as heart valves. Ceramics are also used as filling materials in polymer matrices to enhance their mechanical, thermal and biological properties. Biomedical ceramics are classified as inert and biodegradable. Examples of inert ceramics are wear resistant alumina (Al_2O_3) and zirconia (ZrO_2), which are used for the fabrication of femoral ball head of total hip joint prostheses. Carbons such as graphite and pyrolytic carbon are used for the coating of implants to provide hemacompatibility (Lemons, 1996). Among the ceramic materials, titania has been widely employed for the fabrication of micro- and nanoscale surface structures to study cell-surface interactions (Sjöström et al., 2009; Zhao et al., 2012).

Biodegradable ceramics such as hydroxyapatite and tricalcium phosphate are typically used in dental and orthopedic surgery to fill bone defects and to coat surface of metallic implants to improve osteointegration. They resemble the mineral phase of native bone both chemically and structurally, therefore exhibit excellent biocompatibility (O'Brien, 2011).

Composites are solids that are composed of two or more distinct constituents or phases. Many natural structures such as bone, wood, dentin, cartilage and skin are composite materials. Composites offer a variety of advantages such as higher mechanical, thermal and biological properties compared to homogenous materials. Some biomedical applications of composites are dental filling, bone cements and orthopedic implants with porous surfaces. In addition to these, biodegradable polymer-calcium phosphate based ceramic composites have been widely investigated as scaffold materials for bone tissue engineering applications (Lakes, 2000).

1.3.1.1. Polymers

Polymers are the most versatile and widely investigated class of biomaterials and they are extensively used in biomedical applications such as implantable medical devices, prostheses, dental materials, contact lenses, drug delivery systems and scaffolds for tissue engineering applications. The unique property of biodegradable polymers to become weaker and completely resorbed over time makes them excellent candidates as scaffolds for tissue engineering approaches. Polymeric substrates that are used as biomaterials can be classified as naturally derived and synthetic polymers (Kariduraganavar et al., 2014).

1.3.1.1.1. Natural Polymers

Living organisms synthesize a variety of polymers, which can be classified as proteins, polysaccharides and polyesters based on their chemical structures. The biodegradability of these biological materials enables cells replace the degrading scaffold fabricated from them with their own extracellular matrix over time. Natural polymers can be extracted from plants, animals or algae, or can be obtained by the fermentation of microorganisms. ECM derived proteins including collagen, fibronectin, fibrin are of particular interest since they exhibit intrinsic recognition signals and promote excellent cellular adhesion and growth. The most widely investigated ECM protein is collagen that is found in skin, blood vessels, tendons, cartilage and bone. The cell adhesion sequence arginine-glycine-aspartic acid (RGD) found on ECM proteins was shown to allow many types of cells including fibroblasts and chondrocytes to retain their phenotype and activity. Once coupled with osteogenic factors such as bone morphogenetic proteins or hydroxyapatite, collagen grafts were shown to enhance bone tissue incorporation. Fibronectin is a glycoprotein that induces cell attachment and spreading, and it is generally incorporated onto the surface of biomaterials rather than being used for the fabrication of the biomaterial itself. Fibrin, which is the polymerized form of the blood plasma protein fibrinogen in the presence of thrombin, has been used as cell delivery matrix as the composites of other natural substrates such as alginate or hyaluronic acid in cartilage and skin tissue engineering applications (Mano et al., 2007). Silks are another class of protein based natural polymers used in biomedical applications. Natural or recombinant silk fibroins of silkworms and spiders have been processed into films, fibers, nets, meshes, membranes and sponges. These structures were shown to exhibit high tensile strength and elasticity and also support stem cells adhesion, proliferation and differentiation, making them promising scaffolds for skeletal and connective tissue engineering applications (Wang et al., 2006). Alginate, hyaluronic acid and chitosan are the most widely investigated polysaccharide based substrates, which exhibit a wide range of properties and

physiological functions, and offer a variety of biomedical applications. These polysaccharides undergo gelation upon crosslinking and have been investigated for the design of soft tissue scaffolds (Mano et al., 2007).

1.3.1.1.2. Synthetic Polymers

The use of synthetic polymers in biomedical applications dates back to the emergence of the field of polymer science in 1940s. Experimental surgical studies of almost every new synthetic polymer have been investigated soon after its invention. Use of Nylon sutures has been reported in early 1940s, and studies of the use of polymers such as poly(methyl methacrylate) (PMMA), Dacron polyester and polyvinyl chloride (PVC) in surgery started to appear in medical journals in the mid-1940s (Griffith, 2000). While the original use of synthetic polymers was primarily on replacement implants for connective tissues such as synthetic bone grafts and dental implants, the emergence of novel biomedical technologies including controlled drug delivery, bionanotechnology and tissue engineering have driven development of new biomaterials fabricated from synthetic polymers. Synthetic polymers can be classified as biodegradable polymers that erode in aqueous media and biostable (long lasting) polymers that are nondegradable or very resistant to degradation.

Synthetic biodegradable polymers contain functional groups susceptible to hydrolysis such as esters, orthoesters, anhydrides carbonates, amides and urethanes (Kohane and Langer, 2008). Most widely investigated synthetic biodegradable polymers are poly(α-esters), some polyurathanes, polyanhydrides and polycarbonates. Poly(α-esters) are thermoplastics which have short aliphatic chains between ester bonds that can degrade hydrolytically over time. Most common members of poly(α-esters) are poly(α-hydroxy acid)s, poly(ε-caprolactone) (PCL), poly(trimethylene carbonate) and bacterial polyesters including poly(3-hydroxybutyrate) (PHB) and its copolymer with 3-hydroxyvalerate (PHBV). Poly(α-

hydroxy acid)s include poly(glycolic acid) (PGA), stereoisomers of poly(lactic acid) (PLA) and their copolymer poly(lactide-co-glycolide) (PLGA). Highly crystalline PGA and semi-crystalline PLLA exhibit excellent fiber forming ability; therefore they have been employed for developing resorbable sutures. In addition to sutures, PLGA has been used as controlled delivery systems and skin replacement materials (Nair and Laurencin, 2007). PGA, PLA and PLGA are also the most popular Food and Drug Administration (FDA) approved synthetic polymeric materials used in bone tissue engineering applications because of their good mechanical properties and nontoxic degradation products (Liu and Ma, 2004). Semicrystalline PCL can be processed into various forms easily due to its low melting and glass transition temperatures, and its potential uses as drug delivery vehicles and scaffolds for bone tissue engineering (especially its composites with calcium phosphate based ceramics) and for meniscus substitutes as the composite of hyaluronic acid (Nair and Laurencin, 2007). Several aliphatic diisocyanates such as lysine diisocyanate (LDI) and 1,4-diisocyanatobutyrate (BDI) have been investigated for the development of biodegradable polyurathanes and studied as injectable systems for orthopedic applications (Bonzani et al.2007).

Biostable polymers are inert materials that give minimum or no reaction when interact with living tissue, and they retain their properties for years. Such polymers cause minimal response in the surrounding tissue and are generally used as endoprosthesis and sutures (Rokkanen, 2002). Most common examples of the biostable polymers and their biomedical applications are listed in Table 1.1.

Table 1.1. Some biostable polymers and some of their biomedical applications (Vert, 2007).

Polymers	**Biomedical Applications**
Nylon-type polyamides	Sutures
Poly(vinyl chloride)	Blood pushes and catheters
Poly(ethylene terephthalate)	Vascular prostheses and cardiac valves
Polytetrafluoroethylene	Orthopedic implants, vascular clips
Polyurethanes	Catheters, cardiac pumps and pacemakers
Silicones	Plastic surgery, tubes and oxygenators
Poly(2-hydroxyethyl methacrylate)	Flexible contact lenses, plastic surgery and hemocompatibility of surfaces
Methyl methacrylate based compounds	Acrylic cements for orthopedics and odontology, joint surgeries, bone filling and facial prostheses
Poly(methyl methacrylate)	Rigid contact lenses and intraocular lenses

1.3.1.1.2.1. Poly(methyl methacrylate) (PMMA)

Poly(methyl methacrylate) (PMMA), also known as the acrylic glass, is an amorphous thermoplastic, which can be produced by emulsion polymerization, solution polymerization or bulk polymerization of methyl methacrylate (Fig. 1.9). It exhibits very high transparency and often used as an alternative to glass due to its

lower density and higher impact strength. The environmental stability of PMMA is much better than other plastics such as polystyrene and polyethylene, and it exhibits very low water absorption. PMMA has also good mechanical properties and it has been shown to exhibit a Young's modulus of up to 3 GPa depending on the molecular weight of the polymer and the processing technique. PMMA is biocompatible with human tissues. Rigid intraocular lenses, which are used in the replacement of the original lens that is removed in the treatment of cataracts, have been manufactured from PMMA. It is also used in fabrication of hard contact lenses, while soft ones are made of related hydrophilic methacrylates containing hydroxyl groups such as pHEMA. PMMA is also used as bone cement to fix implants or to remodel lost bone. It fills the space between the bone and the implant to prevent the motion of the implant, but does not bond either to the implant or to the bone. PMMA is also utilized in dental applications. Dentures are generally fabricated from PMMA and colored to match the patients gum tissue. It also forms the main organic component of many white dental filling composites. PMMA microspheres suspended in biological fluids have been injected under the skin in cosmetic surgery to reduce wrinkles or scars. In addition to prostheses and filling materials, PMMA is also employed in biotechnology and biomedical research. It has been used to create microfluidic lab-on-a-chip devices with micron scale features (Kariduraganavar et al., 2014).

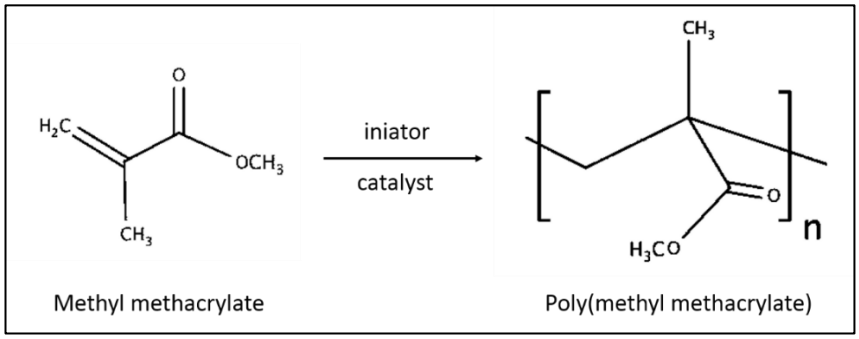

Figure 1.9. Synthesis of poly(methyl methacrylate).

1.3.2. Properties of Substrate Materials

In natural tissues, most of the mammalian cells are embedded in an extracellular matrix (ECM). Macromolecular composition and physicochemical properties of ECM differs between specific tissues depending on the local requirements (Hasirci and Kenar, 2006). Thus, long term *in vivo* success of a biomaterial is strongly determined by the matching of the chemical, mechanical and physical properties of the site of implantation on the nano and micron scale (Roach et al., 2007). In this section, physical, chemical and mechanical properties of the bulk and chemical and topographical properties of the surface of substrate materials that influence biomaterial performance and cell behavior are given.

1.3.2.1. Bulk Properties

Bulk of the solid materials possesses a variety of properties including chemical, physical, thermal, optical, electrical and magnetic properties. For most biomedical applications, physical, chemical and mechanical properties are of greatest importance (Ratner, 2004).

1.3.2.1.1. Physical and Chemical Properties

Physical and chemical properties of the bulk of a biomaterial remain during the lifetime of the implant and influence the function, biocompatibility and duration of it. The long term success of material in contact with the physiological environment depends on how well these properties match the site of implantation (Roach et al., 2007). One important physical property is the porosity, especially for bone implants. Interconnected pores allow cells to infiltrate into the material and provide vascularization and mechanical interlocking between the implant and surrounding tissue. However, pores lower the mechanical properties of implants and increase the

degradation rate of resorbable materials since it increases the total surface area (Karageorgiou and Kaplan, 2005). Chemistry of the matrix that forms the bulk of the material is also an important feature in terms of the reactions taking place in the physiological environment. Biostability or biodegradability of materials directly depends on the chemical properties including chemical groups, hydrophilicity, water adsorption and crystallinity. For example, amide (peptide) bonds of the protein based polymers make them prone to enzymatic degradation while synthetic polymers with short aliphatic ester bonds degrade hydrolytically. Presence of polar or charged hydrophilic groups increases the water uptake and swelling as in the hydrogel structure as well as the rate of hydrolytic degradation. Branching and tacticity of polymer chains determine the crystallinity and influence the rate of water diffusion to the matrix and hydrolytic degradation of the bulk. Chemical character of the bulk material also determines the nature and effects of the degradation products. During the degradation of poly(α-hydroxyacids) such as PLLA, for instance, acidic byproducts are released, which decreases the pH of the microenvironment (Nair and Laurencin, 2007).

1.3.2.1.2. Mechanical Properties

The mechanical properties of the tissues in human body range from soft (brain, around 0.5 kPa) to moderately stiff (muscles and skin, around 10 kPa) and stiff (bone, >30 kPa). These well-defined mechanical microenvironments support the development of distinct cellular architecture and have profound impact on cell behavior and morphogenesis of the tissues such as bone, cartilage and cornea. The mechanical stimuli provided by the cell microenvironment are transduced into biochemical signals and regulate a number of cellular processes such as adhesion, cytoskeleton remodeling and spreading (Mitragotri and Lahann, 2008). Therefore, mechanical properties of the native ECM provide a rough guide for the selection and

design of biomaterials with physiologically relevant mechanical properties in order to get optimum cell response (Wong et al., 2004).

Mechanical properties of polymers are typically determined by a tensile test, which gives information about the yield and ultimate tensile strengths, elongation in break and the elastic modulus. Elastic modulus is typically determined by the strength of the interatomic bonds and is used as a measure of stiffness (Ratner, 2004). Polymers are generally described as viscoelastic materials as they exhibit an intermediate behavior between viscous liquids and elastic solids. Elastic modulus of a polymeric substrate depends on the processing technique, temperature, crosslinking density and the molecular weight. Tensile strength and elastic modulus of polymeric substrates increases up to a limiting value with increasing molecular weight. For example, solvent cast PMMA thin films fabricated from higher molecular weight polymer was shown to exhibit higher elastic modulus than the ones fabricated from lower molecular weight polymer (Bae et al., 2009).

1.3.2.2. Surface Properties

The interactions of cells with their environment are based on the specific binding of the cell surface receptors to their ligands through a process called biorecognition. In natural tissues, most of the mammalian cells are embedded in an extracellular matrix (ECM) and their attachment to this matrix is mediated by binding of specialized surface receptors called integrins to adhesion proteins such as fibronectin, vitronectin, laminin and collagen present in the matrix. Similar interaction mechanisms are also valid for biomaterial surfaces. When a biomaterial comes in contact with body fluid or culture medium, the first reaction is the adsorption of proteins onto the material surface prior to cell attachment. Then various cells reach the surface, interact with these proteins and attach (Ma et al., 2007). In the body, adhered cells give specific responses that determine the biocompatibility and

functionality of the biomaterial depending on the physicochemical properties of the material surface including hydrophilicity/hydrophobicity, functional groups, type and density of the surface charges and topography (Wang et al., 2004). For example, methyl (-CH_3) but not hydroxyl (–OH) or carboxyl (–COOH) groups on the substrate surface were shown to change the conformation of adsorbed proteins so that they expose inflammatory epitopes to inflammatory cells and induce an immune reaction (Thevenot et al., 2008). On the surface of biologically inactive materials, fibroblasts produce a nonadherent fibrous capsule, which walls off and isolates the material from the host (Hench and Wilson, 1993), and the thickness of this fibrous tissue was shown to depend on the functional groups available on the surface (Barbosa et al., 2005). Besides chemical properties, surface roughness and porosity were shown to promote integration of bone tissue to the orthopedic and oral/maxillofacial implants (Wennerberg, 1998). Modulation of cell response by physicochemical surface features has also been investigated *in vitro* and it was shown that cells respond to chemical and topographical properties of surfaces. There are many studies showing that surface features influence adhesion, morphology, migration, survival, proliferation and even differentiation of cells (Wong et al., 2004).

1.3.2.2.1. Surface Chemistry

Chemical reactions and interactions occur at the substrate surface immediately after a biomaterial interacts with physiological fluids *in vivo* or culture media *in vitro*. The very first reaction is the formation of a water shell around the material in a few nanoseconds. The second stage is the adsorption of proteins found in physiological environments such as immunoglobulins, vitronectin, fibrinogen and fibronectin onto the material surface. In the third stage, cells reach the material surface and interact with this layer of adsorbed proteins rather than the bare material surface (Roach et al., 2007; Wilson et al., 2005). The type, quantity, conformation and activity of adsorbed proteins regulate focal adhesion composition and signaling through integrin

binding, which influences adhesion, morphology and differentiation of cells (Keselowsky et al., 2005). Since the profile of adsorbed proteins is mainly determined by the surface chemistry, there has been a great interest in modulating the surface chemistry to control cell response (Roach et al., 2007).

One important parameter of material surfaces is the type and density of functional groups. Methyl ($-CH_3$), hydroxyl (-OH), amino ($-NH_2$) and carboxyl (-COOH) groups are found on the biological surfaces and they determine the surface hydrophobicity and charge, which influence the protein adsorption. Hydrophobic substrates generally adsorb a larger quantity of proteins but cause severe changes in the native conformation of them. In a study, cell adhesive protein fibronectin was shown to maintain its active conformation on hydrophilic surfaces compared to hydrophobic counterparts. A stronger adsorption of cell repellent proteins such as albumin was also reported on highly hydrophobic surfaces (Baujard-Lamotte et al., 2008).

1.3.2.2.2. Topography

In natural tissues, cells are surrounded by micro- and nanoscale structures of the extracellular matrix (ECM) with different geometries, which influence cellular behaviors including morphology, adhesion, motility and differentiation. For example, the structure and alignment of collagen fibrils in bone, muscle and cartilage form different microstructures, which influence morphology and function of cells residing on them (Alberts et al., 2002). Besides the microscale features provided by the collagen matrix, nanoscale hydroxyapatite crystals in the bone tissue also influence cells by enhancing the number and extension of filopodia over the matrix to sense their microenvironment (Benoit and Anseth, 2005). Considering the influence of surface textures on the cell behavior, there is an increasing effort to develop materials that mimic naturally available complex structures (Martinez et al., 2009).

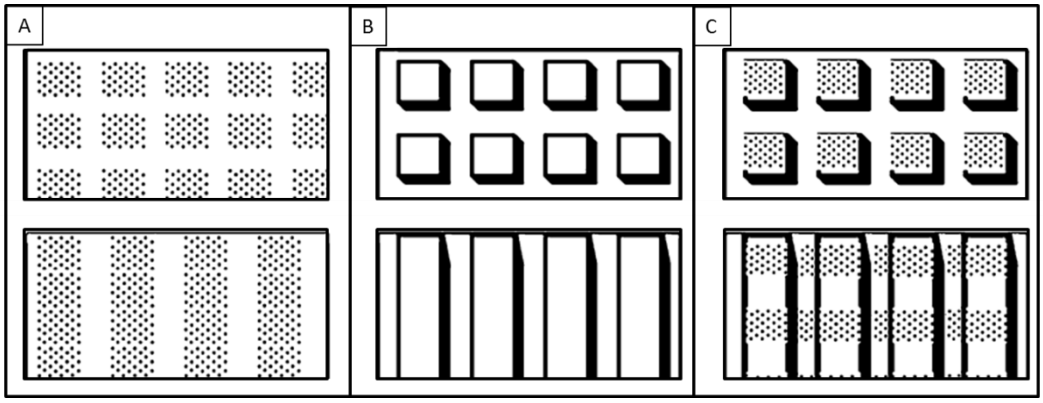

Figure 1.10. Schematic representation of surface chemical and topographic patterning examples. (A) 2D island and strip patterns, (B) 3D pillar and channel topographic patterns, and (C) mixed chemical and topographic patterns. Dots represent chemical patterning (Adapted from Roach et al., 2007).

Lithographic micro- and nanopatterning methods have been used to create topographic patterns in the size range of cells (Fig. 1.10.B). Different types of topographical features including micro- and nanoscale ridges and grooves, randomly or evenly distributed pits, pillars, wells, posts, pyramids and isotropically etched cavities with curved surfaces have been created (Nikkhah et al., 2012). There are also examples of physical features and chemical patterns together on the same surface (Fig. 1.10.C). In a study, microgroove structures and chemical patterns were produced on a substrate alone and together. It was observed that osteoblast cells were significantly aligned on physical or chemical patterns. When the surface was modified with a combination of both patterns at perpendicular directions, however, cells were observed to align to the physical topography, indicating that the physical patterns influence orientation and morphology of the cells stronger than chemical cues do (Charest et al., 2006).

3D surface features have been shown to modulate cell adhesion, morphology and orientation, migration, proliferation and gene expression. For example, a wide range

of cells including fibroblasts, osteoblasts, nerve cells and mesenchymal stem cells have been found to align themselves and elongate in the major axis of groove structures (Martinez et al., 2009). The extent of alteration depends on pattern geometry and dimensions. For instance, morphology of fibroblasts on micropillar structures was shown to be similar to that of cells grown on flat surface when the pillar height or interpillar spacing is small. On widely spaced pillars, however, cells exhibited bi- to tripolar morphology (Ghibaudo et al., 2009). Response to a certain surface feature also differs between different cell types. In a study, adhesion of fibroblasts was reported to be lower (Gallagher et al., 2002) while adhesion of muscle cells (Thapa et al, 2003) and astrocytes (Baac et al., 2004) were found to be higher on nanostructured surfaces compared to unpatterned control. In another study, bone marrow MSCs and Saos-2 osteosarcoma cells were shown to exhibit different adhesion behaviors on organized nanopillar structures. Saos-2 cells were observed to adhere preferentially on the nanopillar arrays with narrow spacing while BMSCs avoided those fields and adhered on nanopillars with larger spacing (Ozcelik et al., 2014). Owen et al. (2005) have reported differences in the proliferation of two cell types on micro- and nanopatterned PLGA surfaces. Epithelial cells were shown to exhibit reduced proliferation and migration while osteoblasts displayed higher proliferation and directional migration. Micro- and nanoscale topographical features have also been shown to influence gene expression and differentiation. For instance, mesenchymal stem cells were shown to exhibit a higher expression of neural and osteogenic markers on nanogratings (Yim et al., 2007) and on random circular nanostructures (Dalby et al., 2007), respectively.

1.3.2.2.3. Wettability

Protein adsorption, cell adhesion and spreading have been shown to be influenced by the wettability of substrate surfaces (Dowling et al., 2010). The chemical composition of the material surfaces greatly influences the wettability since it

determines the surface free energy. $–CF_3$ groups, for example, provide the lowest reported free energy and highest hydrophobicity. The maximum water contact angle (CA) measured on the flat surfaces terminated with these groups, however, was about 120^o, which is far from being superhydrophobic ($CA > 150^o$). In the nature, structures such as lotus leaves (Sun et al., 2005) and the scales on the skin of fast moving sharks show a water contact angle up to 160^o and have been reported to display nonwetting and antifouling properties. It was shown that it is the micron sized riblets of the dermal denticles of the sharks (Fig.1.11.A) and the micrometer scale papillae structures of the lotus leaves (Fig.1.11.B) that lead to very high water contact angle values (Bixler and Bhushan, 2013). Indeed, surface roughness or micro- and nanoscale three dimensional (3D) structures have been shown to enhance the intrinsic hydrophobic nature of surfaces and increase the contact angle of water droplets resting on them. Such 3D patterned surfaces have been used as highly nonwetting antifouling surfaces that exhibit extreme water repellency (Roach et al., 2008).

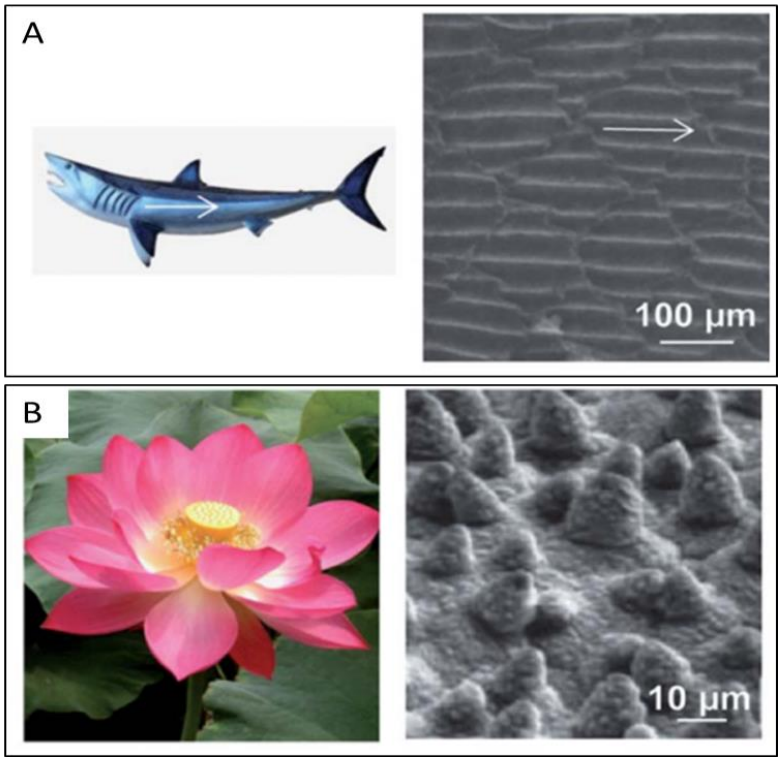

Figure 1.11. Nonwetting surface examples found in nature. (A) Shark skin and (B) lotus leaf (Bixler and Bhushan, 2013).

The concept of topographically induced superhydrophobicity was first explained by Wenzel, who proposed that a liquid completely fills the gaps on a rough surface where it contacts and the surface roughness emphasizes the intrinsic wetting tendency towards reduced or enhanced contact angle (Wenzel, 1936). In 1944, Cassie and Baxter suggested that water forms incomplete contact with the rough surface as air is trapped between the liquid and the solid, and the bridging of gaps always results in an increase in contact angle. On surfaces that display simple roughness, wetted (Wenzel) and bridging (Cassie-Baxter) states are easy to define, but complex roughness may exhibit a mixture of two states (Fig. 1.12). On many surfaces, a transition from Cassie-Baxter to Wenzel state is possible, and the

resistance of transition depends on the intrinsic chemical hydrophobicity and the distance between and the shape of topographic features (Shirtcliffe et al., 2005).

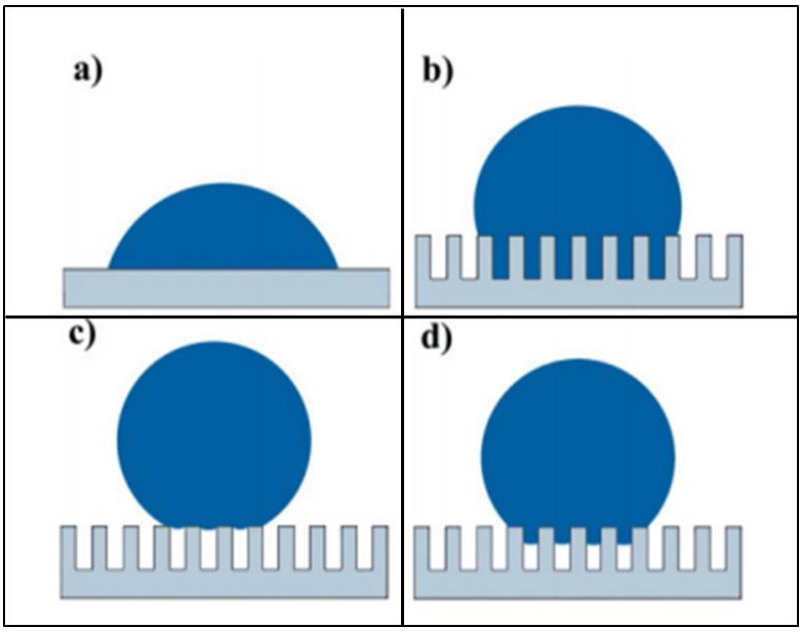

Figure 1.12. Schematic representation of the wetting behavior of solid substrates. (a) A liquid drop on a flat surface, (b) Wetted (Wenzel) state of the liquid on a rough surface, (c) Non-wetted bridging (Cassie-Baxter) state on a rough surface and (d) Intermediate state between Cassie-Baxter and Wenzel states (Feng and Jiang, 2006).

1.4. Design of Polymeric Surfaces for Cell-Substrate Interactions

A polymeric material that is selected because of its favorable bulk properties may not satisfy the surface characteristics for the intended application. In such cases, several chemical and physical modification strategies have been implemented to improve surface properties such as wettability, bioactivity and topography in order to control cell behavior (Penn and Wang, 1994). A well-engineered surface modification provides the enhancement of biocompatibility and biofunctionality while the bulk

properties stay unchanged (Ratner, 1995). Two main strategies are often employed for the engineering of the polymeric surfaces: (i) modification of the surface chemistry such as composition, hydrophilicity and surface charge and (ii) modification of the surface topography by introducing 2D or 3D micro-/nanoscale patterns to manipulate cellular behavior (Ma et al., 2007).

1.4.1. Chemical Modification

When the surface chemistry of a polymeric substrate is not suitable to fulfil certain biological goals such as reduced thrombogenicity or the promotion of the protein adsorption and cell adhesion, the strategy of surface chemical modification is implemented. The most widely employed procedures can be categorized as the attachment of polymer chains and biomolecules, formation of the self-assembled monolayers of silanes and chemical oxidation by reactive solutions, UV exposure or ionized gas treatment (Penn and Wang, 1994; Goddard and Hotchkiss, 2007).

Various polymer chains with a range of chemical properties and biomolecules including cell adhesive proteins and growth factors can be conjugated onto the substrate surface either chemically or physically. Graft polymerization of the monomers directly on the reactive sites of the substrate surface and grafting of polymer chains such as poly(ethylene glycol) (PEG) by physical adsorption are the most common methods (Penn and Wang, 1994). Proteins and growth factors can be immobilized on the substrate surface either covalently after creating reactive groups such as hydroxyl, carboxyl and amino groups on inert polymeric materials or by physical adsorption after appropriate modification of the material surface. ECM derived cell adhesive proteins (such as fibronectin, laminin, vitronectin and collagen or their cell adhesion promoting sequence RGD tripeptide) and growth factors (such as epidermal growth factor (EGF), insulin and bone morphogenetic proteins (BMPs))

are the most commonly immobilized biomolecules on polymeric surfaces in order to modulate cellular behaviors (Ma et al., 2007).

Silanization of substrate surfaces is another common chemical modification method used. Organofunctional alkoxysilane molecules form self assembled monolayers (SAMs) either by forming covalent –Si-O-Si- bonds with the hydroxyl groups available on the surface or by forming thiol linkages with gold, copper or silver coating of the substrates (Goddard and Hotchkiss, 2007). This method was originally adapted by Whiteside's group for the fabrication of micropatterns on the substrate surfaces to study cell behavior. By altering the functional groups of the long chain molecules exposed at the surface, chemical properties of the monolayer can be modulated. For instance, use of alkanethiols terminated in highly hydrophilic oligo(ethylene glycol) results in formation of an protein and cell repellent layer. Inversely, relatively more hydrophobic SAMs adsorb proteins rapidly and promote adhesion of cells. Surfaces can also be patterned by microcontact printing method into SAM regions that alternately promote or prevent protein adsorption and cell adhesion (Chen et al., 1998; Mrksich, 2000).

Oxidation of the polymeric substrates is a strategy to generate new functional groups on the substrate surface rather than coating them with a new layer. It can be achieved by the treatment with oxidative liquid reagents such as chromic acid, nitric acid, sulfuric acid or potassium permanganate to produce hydroxyl, carbonyl, or carboxylic acid groups (Piiroja et al., 1980). This method is, however, classified as non-specific since it result in a range of oxygen-rich functional groups and it may also produce hazardous byproducts and lead to irregular surface etching, which might influence the topography of the material (Desai and Singh, 2004). Another oxidation method is the exposure of polymers to UV radiation. This method generates reactive sites, which can be converted to new functional groups upon exposure to a gas or can be used as the start points for graft polymerization (Chan et al., 1996). The most commonly used surface oxidation method is the ionized gas

treatment, in which an electrically induced stream of gas bombards the polymeric surface and creates new functional groups upon the reaction of gas molecules with the created reactive sites. The flowing gas can be ionized either in the absence of vacuum as in the corona discharge method or under vacuum in plasma treatment technique. Corona discharge creates a broad range of oxygenated groups on the substrate surface, but there is the risk of contamination due to the absence of vacuum and lack of control on operation parameters due to the variations in local temperature and humidity (Goddard and Hotchkiss, 2007). Plasma treatment creates various functional groups depending on the selection of plasma gas (Ar, N_2, O_2, H_2O, CO_2, NH_3 etc.) and the operation parameters such as plasma pressure, power, duration and the flow rate of the plasma gas (Lane et al., 1993).

1.4.1.1. Oxygen Plasma Treatment

Plasma is a complex, high energy gaseous state of matter, which can be created by applying continuous electrical discharge on an inert or reactive gas. It contains neutral and partially ionized gas molecules as well as reactive particles such as free radicals, electrons and photons (Dinklage et al., 2005). A typical plasma chamber is composed of a reactor vessel, a vacuum pump and a power source. In the treatment process, the reactor vessel is first evacuated by the vacuum pump and then filled with a low-pressure gas. An energy source such as electric discharge, heat, radio-frequency, microwaves or alternating/direct current is used to excite the plasma gas, leading to the ionization of the gas atoms or molecules into high energy species. The bombardment of the substrate with these energetic species causes an energy transfer to the material surface and leads to a series of chemical and physical changes. Plasma treatment can modify the surface up to a depth of several hundred angstroms to 10 microns without altering the bulk properties. High energy species in the plasma can react with the activated atoms at the surface, creating new functional groups (Katti et al., 2008). Oxygen plasmas are the most commonly used plasma treatments for the

modification of polymer surfaces, because it can react with a wide range of polymers including PMMA, PCL, and PE and produces oxygen-rich functional groups including hydroxyl, carbonyl and carboxyl (Chan et al., 1996). Plasma treatment may cause etching of the substrate surface as well as creating new groups. Removal of the volatile products generated during the chemical reactions etches the surface physically, which is typically used as a cleaning procedure. Surface etching and cleaning especially occurs upon oxygen plasma treatment of polymeric substrates with a carbon backbone. The biggest advantage of plasma treatment is the chemical modification of polymeric surfaces without the use of highly corrosive liquids and generation of chemical waste. It causes less degradation and surface roughening compared to wet chemical treatments (Goddard and Hotchkiss, 2007). The main drawback of the plasma treatment, however; is the ageing. It is defined as the returning of treated surfaces to their untreated state upon the reorientation of the newly formed functional groups into the bulk polymer or moving of the small polymer segments into the matrix in time. Plasma treated polymers incubated in an aqueous environment, on the other hand, were shown to maintain their hydrophilicity since the medium forces polar groups to stay on the surface (Vesel and Mozetic, 2012).

1.4.2. Micro- and Nanopattern Fabrication

Considering that the cell microenvironment is composed of structures on the scale of nano- to micrometer, a need for controlling cell behavior at these length scales have arisen. In the last 20 years, an increased effort has been paid to establish new fabrication technologies to produce structures with greater geometrical complexity at reduced cost and time (del Campo and Arzt, 2008; Nikkhah et al., 2012). Random surface features are generally produced by using classical processing techniques such as acid etching, plasma spraying, machining, grinding, abrasion, sandblasting and grit-blasting. Ordered structures such as grooves, wells, pits and pillars, on the other

hand, are produced by using lithographic micro- and nanofabrication methods that were originally developed by semiconductor and microelectronics industries (Nikkhah et al., 2012).

1.4.2.1. Photolithography

Lithography is a routinely employed technique in the microelectronics industry to fabricate micro- and nanoscale patterns on silicon wafers. These 3D surface structures on the silicon wafer can be easily replicated on the surface of a biomedical polymer (Thompson et al., 1994). Brunette et al. (1983) was among the first who employed photolithography to study cell behavior on patterned surfaces. Since then, the technique has been used to produce surface features in the majority of the studies on cell-surface interactions. In the photolithographic process, a substrate is coated with a thin layer of photoresist. This resist is exposed to UV light through a photomask, which selectively irradiates certain regions of the resist. Depending on the type of the resist, irradiated regions become more or less soluble in the developer solution. Therefore; a positive- or negative- tone of the mask is obtained on the substrate upon immersion into the developer solution. Due to the diffraction limitations, the lateral resolution of the method is equal to the size scale of the wavelength of the light source used. Thus, the photolithographic methods using UV light are able to create surface features with lateral dimensions of 220-250 nm (Flemming et al., 1999). The most widely used photolithograpic technique is the UV photolithography, in which a photocurable resist such as SU-8 that is crosslinked upon UV radiation is used to fabricate the positive-tone of the transparent regions of the photomask on the substrate (del Campo and Arzt, 2008). Obtained patterns can be used directly or transferred to the underlying substrate by etching the regions that are not covered with the resist. Reactive ion etching and potassium hydroxide (KOH) wet etching of silicon substrates were shown to yield anisotropic square and V-shaped gaps, respectively. After the etching is completed, the remaining resist is

removed and a three-dimensional negative or positive of the transparent regions of photomask is obtained. Most commonly encountered problems with the etching process are the yielding shapes with different dimensions than the intended design, curved sides and roughened surfaces (Thompson et al., 1994 and Madou et al., 2002).

The patterns obtained on the original wafer by photolithography are transferred to polymer surfaces by the molding process. The basic idea behind molding is the transfer of the surface features of a master tool called mold or stamp into a soft material. The same mold can be used repeatedly to fabricate large number of structures, which allows scaled up patterning of large areas at low cost. Most widely employed molding techniques are temperature based processing, photo- or thermally induced polymerization and solvent casting. Temperature based molding techniques are thermal injection molding and hot embossing/nanoimprint lithography (NIL) of thermoplastics. These methods are based on the shaping of thermoplastic polymers that is in contact with the mold under heat and pressure. Upon heating the mold or the substrate itself, the viscosity of polymer decreases significantly and it flows into the cavities of the mold under the applied pressure. When cooled back, the polymer hardens and then the mold is separated from the replica. In injection molding technique, melted thermoplastic is injected into a closed cavity containing the mold through a nozzle under high pressure. In hot embossing technique, the mold is pressed into a sheet of thermoplastic material at elevated temperatures. In photopolymerization method, a photosensitive polymer is coated onto a planar substrate and then pressed against a UV-transparent mold. Upon exposure to UV radiation, the polymer is cured and it hardens. PDMS molds are widely used for photopolymerization since PDMS is UV-transparent within the 340-600 nm region. Thermally induced polymerization is based on the production of a thermoset (such as epoxy substrates) or elastomer (such as PDMS) negative replica of the hard master by casting and thermal curing of the prepolymer on the master. In solvent-assisted molding techniques, the polymer substrate is softened or completely dissolved in an

appropriate solvent and then brought in contact with an elastomer mold. The polymer solution is drawn into the cavities of the mold by gravity or capillary forces depending on the relative positions of the polymer solution and the mold. Upon complete removal of the solvent by evaporation or diffusion into the mold, a hardened accurate polymer replica is obtained (del Campo and Arzt, 2008).

1.4.2.2. Soft Lithography and Microcontact Printing

Soft lithography is the name given to a family of techniques which utilize an elastomeric, "soft" material to create chemical structures on material surfaces. The most widely known technique of this family is the microcontact printing (μCP). μCP was originally developed for microelectronics applications and soon adapted by Whiteside's group to produce micropatterns on substrate surfaces for the selective attachment of cells. Since then, the method has become very popular for biological applications due to its simplicity, low cost and flexibility. The process of μCP includes use of an elastomeric stamp, which is typically fabricated from polydimethyl siloxane (PDMS) by casting its uncured liquid phase over a micropatterned master. Elastomeric stamp is inked with the specific solution to be printed, and then pressed onto the substrate surface. After the ink is transferred to the substrate, non-stamped areas are generally backfilled with a second molecule (Singhvi et al., 1994; Coutinho et al., 2011). Patterning molecules can be transferred to the substrate surface directly or indirectly. In direct patterning, a solution of target molecules such as cell adhesive ECM proteins is used as the ink and directly transferred to the activated substrate surface. Indirect patterning is typically performed by producing geometrically controlled patches of SAMs and then selective adsorption of target molecules (Singhvi et al., 1994).

1.4.2.3. Electron Beam and Ion Beam Lithography

Charged particles (electrons or ions) can be used to pattern surfaces without using a mask. Great flexibility they offer in the feature design makes them frequently used methods in micro- and nanopatterning of substrate surfaces in academic research. In electron beam lithography, an electron sensitive resist is exposed to an electron beam of 10-100 eV. When electrons reach the surface, they create a cascade of secondary electrons and these low energy electrons form free radicals and radical cations. Chemical change in the resist occurs upon reaction with these intermediate species and the resist material is either broken down or crosslinked. In theory, patterns with the size of the wavelength of electrons on the order of 1 A can be formed. However, electron scattering limits the achievable resolution to ~10 nm. Since the low energy electrons can penetrate into only a small depth, this method is restricted to patterns with a height below 100 nm (del Campo and Arzt, 2008; McMurray et al., 2011). Mechanism of ion beam lithography is quite similar to e- beam lithography. In this method, instead of electrons high energy ions such as Ga^+, H^+ and He^+ are trajected to the resist material and they deeply penetrate the resist depending on the ion energy. High energy ions run through a well-defined path in the resist, which allows fabrication of densely packed structures with high aspect ratio and smooth and vertical walls. Deep penetration of ions enables formation of structures with micrometer scale height, which is the main advantage of this method over the e-beam lithography (del Campo and Arzt, 2008).

1.4.2.4. Laser Prototyping

Laser prototyping methods include stereolithography and two photon lithography (TPL). They are maskless fabrication techniques in which a resist surface is scanned with a laser beam. Like photolithography, these techniques are also based on the photoactivation and development of a resist layer. In stereolithography, photosentive

monomeric or polymeric resins are polymerized by exposure of a scanning UV laser and 2D patterns are obtained. The process is repeated sequentially through layer by layer addition of new resist on the cured one and subsequent UV laser exposure allows creation of 3D patterns with micrometer precision. TPL method is based on the absorption of two photons coming from two separate beams at defined locations of the resist. Polymerization of the resist is activated locally upon absorption of two photons at the same time (del Campo and Arzt, 2008; Nikkhah et al., 2012).

1.4.2.5. Rapid Prototyping

Rapid prototyping (RP) is the name given to a family of techniques that are used to produce a physical model directly from computer designed data. RP methods are additive processes and rely on the layer by layer construction of structures. In RP, each layer is generated by extrusion of a strand of melt material through a needle while it moves across a plane. Upon cooling, the material solidifies and it is fixed on the previous layer. Successive formation of each layer on top of previous one can be used to form complex 3D solid objects. The resolution of RP is relatively low, at 250 μm, compared to other micropatterning methods. Natural polymers cannot be processed since the material must be melted into a semiliquid phase before extrusion at very high temperatures that biomolecules cannot withstand (Yeong et al., 2004).

1.5. Responses of Cells to Substrate

1.5.1. Responses to Mechanical Cues

The influence of the mechanical properties of substrates on cell behavior has been typically studied by growing cells on hydrogels with tunable stiffness. Such hydrogel substrates are generally fabricated from agarose and polyacrylamide (PAAm) and their stiffness is controlled by changing the crosslinking density (Rehfeldt et al.,

2007). Stiffness of substrates has been shown to influence morphology, proliferation and differentiation of cells. For example, chondrocytes grown on alginate hydrogels spread less on soft substrates compared to stiff ones (Genes et al., 2004). Similarly, fibroblasts and vascular smooth muscle cells (VSMCs) were shown to migrate towards stiffer regions and spread more when grown on polyacrylamide (PAAm) with spatial gradient in elastic modulus (Wang et al., 2000). In a study, gels with moderate stiffness were shown to promote proliferation of muscle cells while very soft and stiff gels reduced proliferation (Griffin et al., 2004). In another study, fibroblasts, epithelial cells and endothelial cells were reported to exhibit increased proliferation on stiffer substrates while neurons displayed greater proliferation on softer substrates (Engler et al., 2004). Morphologies and gene expression profiles of MSCs on gels with variable elastic moduli were also studied. For instance, MSCs cultured on gels that mimic the elasticities of brain, muscle and bone tissues were reported to exhibit neuron-like highly branched morphology on soft gels, whereas they exhibited myoblast-like spindle shapes on moderately stiff gels and osteoblast-like polygonal morphologies on very stiff gels. Expressions of neurogenic, myogenic and osteogenic markers were also shown to be higher on substrates with relevant stiffness (Engler et al., 2006).

The mechanical cues in their microenvironment regulate the functions and determine the fate of stem cells (Pajerowski et al., 2007). For instance, exposure to fluid shear stress has been reported to increase the expression of cardiovascular lineage specific genes in ESCs (Yamamoto et al., 2005). In a study with human MSCs, uniaxial cyclic compression of scaffolds was reported to upregulate the chondrogenesis associated genes, while cyclic tension enhanced the expression of osteogenic genes (Haudenschild et al., 2009). Similarly, tensile strain was shown to enhance commitment of MSCs grown in monolayer into osteogenic lineage and inhibit adipogenesis (Sen et al., 2008).

The levels of traction forces exerted by differentiated cells such as muscle cells, fibroblasts, epithelial cells and neurons on the same substrate have been shown to differ, and this leads to differences in the cellular morphologies of the cells as a result of different force-balance between the cell and the substrate. In a study, human BMSCs were cultured on collagen coated polyacrylamide hydrogels with tunable stiffness and expression of osteogenic markers such as Runx2, osteocalcin and collagen type I were shown to increase on stiffer matrices. These findings were reinforced with the demonstration of increased kinase activities of ROCK, FAK and ERK1/2 on stiffer matrices, which are known to be involved in mechanotransduction of matrix stiffness during osteogenesis (Shih et al., 2011). Therefore, it can be proposed that the mechanical properties of the substrate surface could affect the stem cell fate (Hwang et al., 2008). Indeed, differentiation of MSCs has been demonstrated to be modulated by varying mechanical properties of substrates.

1.5.2. Responses to Surface Chemistry

1.5.2.1. Adhesion and Proliferation

Surface chemistry determines the net charge and hydrophilicity and modulates the type and amount of proteins adsorbed onto the material surface. The profile of adsorbed proteins directly affects the adhesion and migration of cells cultured on the substrates. Early studies reported that moderate hydrophilicity at a water contact angle range of 40^{o}-70^{o} is optimum for mammalian cells to adhere effectively on polymeric surfaces (Tamada and Ikada, 1993; Lee et al., 1998). Surface charge also seems to be an important parameter in conformation and bioactivity of adsorbed proteins. In a study, binding of fibronectin to $\alpha_5\beta_1$ integrin was shown to be higher when adsorbed on negatively charged (–COOH) than neutral (–OH) surface (Lee et al., 2006). Influence of surface chemistry on cell adhesion also depends on the cell type. In a study, surfaces modified with SAMs were used to examine adhesion of

HUVECs and HeLa cells. It was shown that HUVECs adhere best on $–CH_3$/-OH mixed SAMs with a contact angle of 40^o while the number of adhered HeLa cells was maximum on both $–CH_3$/-OH and $–CH_3$/-COOH mixed SAMs with a contact angle of 50^o (Arima and Iwata, 2007).

Proliferation of the adhesion dependent cells is induced by the attachment and subsequent signal transduction responses that are mediated through integrin-ECM interactions. Therefore, substrate surface chemistry controlling the adsorption of ECM proteins modulates the proliferation of cells as well as the adhesion. The most commonly employed approach to modulate surface chemistry to study its influence on cell proliferation is the production of self assembled monolayer films. In one such study, SAMs of alkythiols bearing terminal methyl ($-CH_3$) and carboxylate (-COOH) groups were produced on gold coated poly(ethylene terephthalate) surface and the adhesion and proliferation of Swiss 3T3 fibroblasts on these surfaces were investigated. It was shown that fibroblasts on on −COOH terminated SAMs displayed adhesion and proliferation rate comparable to that of TCPs, while the cells on −CH3 terminated SAMs displayed much lower attachment and reduced rate of proliferation (McClary et al., 1999). In a similar study, MG-63 osteoblasts were cultured on SAMs terminated by $–NH_2$, $-CH_3$ and $–CF_3$ and the cell attachment and proliferation were observed to be similar on $–CH_3$ and $–NH_2$ terminated SAMs but much lower on $–CF_3$ terminated SAMs (Schweikl et al., 2007). There are studies showing that increased hydrophilicity of polymeric substrates upon oxygen plasma treatment leads to higher cell attachment and proliferation. For instance, human BMSCs were cultured on oxygen plasma treated PLLA films displaying a water contact angle of 58^o and an increased attachment, distribution and proliferation compared to pristine films (CA: 76^o) was reported (Hanson et al., 2007). In another study, 3T3 fibroblasts were cultured on untreated and oxygen plasma treated low density polyethylene (LDPE) films and the cell proliferation was found to be higher on plasma treated hydrophilic surface compared to pristine films. Expressions of proto-oncogene c-myc and cell cycle regulator gene p53, which are known to

promote proliferation and influenced by the interactions of cells with cell adhesive proteins, were also found to increase on plasma treated hydrophilic LDPE (Kim et al., 2007).

1.5.2.2. Differentiation

It is known that integrin binding to ECM proteins influences the differentiation of mesenchymal stem cells by regulating focal adhesion composition and signaling. Integrin binding has been shown to be influenced by the species, concentration and conformation of adsorbed proteins, which are mainly determined by the surface chemistry. Thus, surface chemistry of substrates plays a crucial role in the differentiation of stem cells by regulating the integrin binding (Keselowsky et al., 2005). Chemical modification of substrate surfaces has been widely employed to investigate the influence of surface chemistry on stem cell fate. In a recent study, –OH or $–NH_2$ groups were created on PCL films by hydrolysis or aminolysis, respectively. When human amniotic MSCs were grown on these films, it was observed that hydroxyl groups supported osteogenic differentiation while amino groups induced chondrogenic differentiation (Zhao et al, 2016). A similar observation about the negative effect of amino groups on osteogenic differentiation was made on ammonia plasma treated polypropylene substrates. MSCs cultured on these substrates in differentiation medium were shown to express osteogenic markers in much lower quantity compared to untreated controls (Mwale et al., 2006). Oxygen plasma treatment has been shown to enhance osteogenic differentiation of human MSCs on PDMS substrates. It was shown that oxygen plasma treatment converted silane ($Si-CH_3$) groups on the surface of PDMS substrates to silanol (Si-OH) groups and increased the formation of focal adhesions and mineral deposition by MSCs (Yang et al., 2012). Similarly, a blend of starch and PCL polymeric fiber mesh was shown to induce osteogenic differentiation in the absence of osteogenic supplements when functionalized with silanol groups (Rodrigues et al., 2014). In another study,

MSCs were grown on substrates which were surface grafted with gradients of acrylic acid and diethylene glycol dimethyl ether in the opposite directions. Competitive differentiation analysis of rat BMSCs in mixed (50% osteogenic and 50% adipogenic) medium have shown that adipogenic differentiation of cells was not influenced significantly by the surface chemistry. Osteogenic differentiation and calcium deposition, however, increased gradually towards increasing acrylic acid coating, which has –COOH groups (Wang et al., 2015).

1.5.3. Responses to Surface Topography

1.5.3.1. Adhesion and Migration

It has been shown that topography influences the site of focal contacts and promotes the maturation of focal adhesions complex (Seo et al., 2011) (Fig.1.13). However, it is hard to generalize the adhesion behavior of cells on micro- and nanostructures reported in the literature. For example, adhesion of osteoblasts was shown to be similar on microgroove structures and flat controls (Charest et al., 2004). Similarly, number of adhered fibroblast cells on micropost structures and flat surfaces were close to each other even though the number of focal adhesion sites was higher on micropatterned surfaces (Estévez et al., 2015). Decrease in cell adhesion in response to topographical cues has also been reported by several studies. Dalby et al., for instance, showed that fibroblasts adhered less on PCL and PMMA surfaces decorated with nanopits compared to flat counterparts (2004). In another study, adhesion rat astrocyte cells on microscale grooves was observed to be lower compared to unpatterned control surface (Recknor et al., 2004).

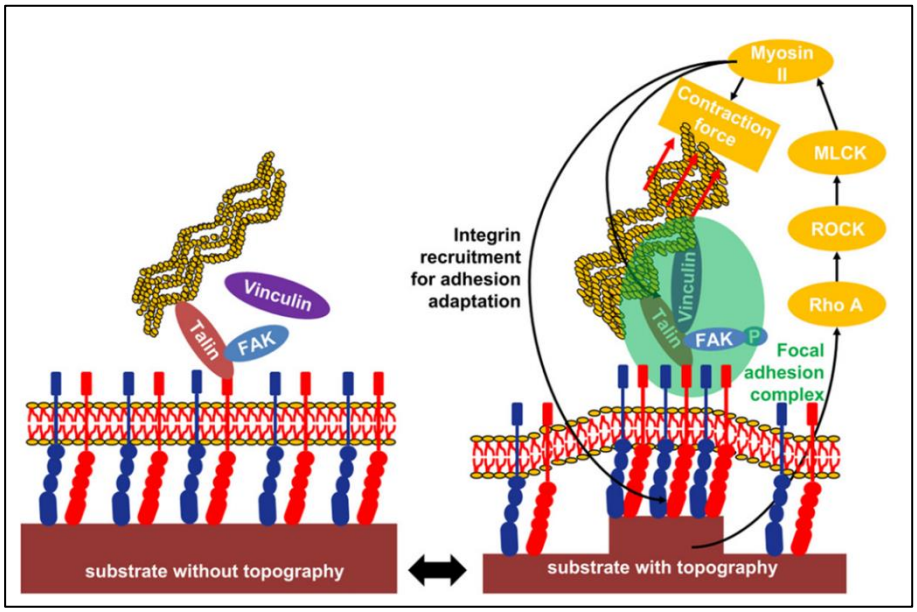

Figure 1.13. Schematic representation of the mechanism of topography induced maturation of focal adhesions and actin organization (Seo et al., 2011).

Several other studies, on the other hand, have reported increased cell adhesion on the surfaces carrying micro- and nanostructures. In a study, human astrocyte cells were shown to exhibit higher adhesion on surfaces decorated with nanoscale grooves (Baac et al., 2004). Smooth muscle cells were also observed to adhere better on random nanoscale structures compared to cells grown on flat surface (Thapa et al., 2003). In a more recent study, adhesion of dental pulp stem cells was shown to be higher on surfaces with micropillar structures and the number of adhered cells decreased as the pillar size was decreased and the interpillar spacing was increased (Kolind et al., 2014). Finally, the shape of topographical structures has been shown to influence the cell adhesion. It was found that adhesion of cells was enhanced on nanograting structures while decreased on nanopost and nanopit patterns (Bettinger et al., 2009).

Physical structure and geometry of the surface features of the ECM were shown to influence migration of cells by restricting adhesion sites and direct cells through contact guidance. Similarly, topographical features of artificial substrates were reported to affect and guide cell migration. Micro- and nanoscale groove structures, for example, have been shown to guide the migration of many cell types including fibroblasts, neurons, epithelial, endothelial and smooth muscle cells unidirectionally on the major axis and increase their migration speed (Nikkhah et al., 2012). In addition to groove structures, migration of cells has also been investigated on lattice and pillar structures. In a study, rectangular lattice grids, especially the ones with higher aspect ratio, were shown to direct cells to elongate and migrate along the direction of the long side (Mai et al., 2007; Jeon et al., 2010). In another study, spatial organization and dimensions of micropillar structures were shown to influence migration of fibroblasts. Cells were observed to follow zigzag pattern of the pillars and move faster compared to the cells cultured on flat surfaces (Frey et al., 2006).

1.5.3.2. Proliferation

There are only a few studies on the influence of micro- and nanostructures on cell proliferation and the observations vary depending on the types of cells and the surface structures. Several studies have reported that surface micro- and nanotopography did not influence cell proliferation. For instance, proliferation of fibroblast cells has been shown to be unaffected by the presence or the dimensions of microscale grooves on silicon substrates (Braber et al., 1996). Similarly, rat bone marrow osteoblast-like cells were shown to exhibit similar proliferation on the microgrooves of PLLA and PS surfaces and on the unpatterned counterparts (Matsuzaka et al., 2000). Another study has reported no distinct differences in the proliferation of OCT-1 osteoblast-like cells cultured on PLLA surfaces with nano- or microscale bumps compared to flat control surfaces (Wan et al., 2005). There are

also studies that have reported reduced or increased proliferation on patterned surfaces. Human embryonic stem cells, for instance, were observed to exhibit significantly reduced proliferation on PDMS surfaces carrying nanoscale ridges. Interestingly, when the cells were exposed to actin disrupting agents, influence of nanotopography on the cell proliferation was found to disappear, indicating that cytoskeletal stress directs proliferative effects of the topographical features (Gerecht et al., 2007). Another study, however, reported a 40% increase in the proliferation of mouse bone marrow mesenchymal stem cells on nanoporous alumina surfaces compared to flat control surfaces (Popat et al., 2006). A similar observation was made by Moroni and Lee (2008), who reported higher proliferation of fibroblasts on PLGA films decorated with micropits or channels compared to smooth counterparts. The effect of surface topography has been also found to depend on the structures involved and the cell type. For example, proliferation of osteoblasts was shown to be higher on epoxy surfaces carrying discontinuous microgrooves but lower on micropillar structures compared to flat control surface (Hamilton et al., 2006). Liliensiek et al. (2006) reported that proliferation of corneal epithelial cells reduced as the spacing of nanogroove structures decreased while corneal fibroblasts did not exhibit significant difference on patterned and flat surfaces in term of cell growth. In a more recent study, proliferation of HeLa cells has been shown to be unaffected by the surface microtopography, while proliferation of vascular smooth muscle cells (VSMCs) was inhibited as a response to mechanical trapping of their nuclei. Both cell types exhibited remarkable deformation of their nuclei on PDMS surfaces decorated with micropillars, which was speculated to induce chromatin condensation and inhibit the proliferation of VSMCs but not HeLa cells (Nagayama et al., 2015).

1.5.3.3. Conformational Change

1.5.3.3.1. Changes in Cytoskeletal Morphology

Spreading of cells on the underlying substrate is known to alter the cytoskeletal organization and intracellular forces, which ultimately changes cell morphology (Ingber, 1997). Groove structures, which are typically composed of repeating ridges and grooves with equal width, are one of the most widely investigated surface patterns that have been shown to influence the cell morphology. In nearly all instances, the majority of cell types have been observed to align along the major axis of the grooves and display a highly elongated shape. For example, osteoblasts cultured on microgrooved polyimide surfaces were observed to exhibit an elongated shape (Charest et al., 2004). However, morphology of cells has been shown to depend strongly on the dimensions of ridges and grooves. Cells cultured on surfaces with very narrow and deep grooves were found to bridge the ridges instead of aligning in the grooves. Rat bone cells cultured on PS micrograting arrays, for instance, were observed to align through the long axis of the grooves when the groove width was above 5 μm. Cells on narrower grooves, however, were shown to bridge the structures and exhibited a well spread morphology (Matsuzaka et al., 2003). Cell morphology has also been investigated on nano- and microscale pillar structures. For example, T24 human bladder carcinoma cells were shown to display a less rounded, satellite morphology when grown on silicon nanopillar structures (Anderson et al., 2003). Fibroblasts cultured on PMMA surfaces decorated with nanopillar structures, on the other hand, have been observed to exhibit poorly spread, rounded morphology with less organized actin cytoskeleton compared to the flat surfaces (Dalby et al., 2004). Turner et al. (2000) have investigated the morphology of astroglial cells on 1 μm high silicon micropillars with a width of 0.5-2 μm and spacing of 1-5 μm. Cells were found to exhibit preferential adhesion to the top of the pillars and highly polarized cytoskeleton compared to flat controls. In another study, fibroblasts have been shown to exhibit a branched morphology when they were

cultured on PS micropillars (Ghibaudo et al., 2009). Height and spacing of pillars were shown to influence cell morphology and spreading.

1.5.3.3.2. Changes in Nuclear Morphology

Nucleus exhibits viscoelastic properties and it is known to be much stiffer than the cytoplasm. Micropipette aspiration experiments have been extensively used to investigate the mechanical properties of cells and nuclei (Rowat et al., 2006). In addition to the alteration cytoskeletal morphology, 3D microstructures have also been reported to cause deformations in the cell nuclei. For example, slight elongation of the cell nuclei was observed in the cells grown on microgroove structures (Dalby et al., 2003; Gerecht et al., 2007). In a study by Steinberg et al. in 2007, keratinocytes cultured on PDMS substrates decorated with micropillars had deformed nuclei, but these deformations were not discussed. Severe deformation of cell nucleus on micropillar structures has been emphasized by Davidson et al. for the first time in 2009. Saos-2 osteosarcoma cells grown on PLLA substrates carrying square micropillars were shown to exhibit significantly deformed nuclei after 7 days of incubation, while healthy osteoprogenitor (hOP) cells showed very little deformation (Davidson et al., 2009). In the following study of the same group, degree of nucleus deformation was found to depend on the cell type. Nuclei of osteosarcoma-derived cancer cell lines were observed to deform extensively while the nuclei of immortalized cells deformed less and the nuclei of healthy cells deformed slightly only at short incubation types (Davidson et al., 2010). In another study, degree of nucleus deformation of the same cell type has been shown to depend on the pillar dimensions and spacing rather than the substrate type. Nuclei of Saos-2 cells exhibited limited deformation between pillars spaced by 2-4 μm as the cells were not entirely inserted between pillars, while they were remarkably deformed between pillars spaced by 5-10 μm and not deformed at all between pillars spaced by 11-20 μm (Badique et al., 2013). Nuclei of mesenchymal stem cells have also been shown

to deform in response to micropillar structures. Self deformation of the nuclei of rat bone marrow MSCs was shown on PLGA substrates carrying micropillars with sufficient height but not on surfaces with micropits. In the same study, it was also shown that the shape of nuclei can be controlled by modulating the orientation and density of micropillars (Pan et al., 2012). In a more recent study, porcine vascular smooth muscle cells and cervical cancer HeLa cells have been shown to spread in the space between circular micropillars of PDMS substrate and the nuclei of both cells have been demonstrated to deform as a result of mechanical trapping. The degree of nuclear deformation, however, was significantly higher for HeLa cells, which are known to exhibit lower nucleus stiffness compared to healthy cells (Nagayama et al., 2015).

1.5.3.4. Differentiation

Increased local tension causes clustering of integrins and phosphorylation of FAK, which activates small GTPases of Rho-family. RhoA and its effector kinase ROCK were shown to be involved in regulation of transcription factors and gene expression via mechanotransduction (Vogel et al., 2006; Jaalouk et al., 2009). For example, the activity of Runx2, a transcriptional factor responsible for regulation of the osteogenic differentiation, has been shown to be modulated by the intracellular signaling cascades ERK/MAPK as a result of integrin signaling (Salasznyk et al., 2007). Since the formation and maturation of focal adhesion complexes and modeling of cytoskeletal elements were reported to be influenced by the surface micro- and nanoscale structures, these topographical cues have also been shown to modulate the gene expression profile of the cells and influence their survival, proliferation and differentiation (Seo et al., 2011).

It has been suggested that cell shape and size can direct the fate of MSCs by generating higher degrees of cytoskeletal tension (McBeath et al., 2004; Bhadriraju

et al., 2007). In one study, pentagonal, round, flower, star or rectangular shaped cell adhesive microislands of same area were created on gold surfaces by SAMs method. Human BMSCs that attached and spread on these micropatterns were cultured in a 1:1 mixture of osteogenic and adipogenic differentiation media and the expression of bone and fat cell specific marker genes were investigated. The results showed that the cells on micropatterns with sharp corners and curvature such as stars differentiated towards osteoblasts whereas the cells on smoother patterns like round islands or flowers undergo adipogenic differentiation. Moreover, the degree of osteogenic differentiation has been shown to increase as the aspect ratio of the rectangular microislands increased, demonstrating that and elongated shape commits cells into osteogenesis (Kilian et al., 2010).

Besides 2D micropatterns, 3D micro- and nanostructures have also been created on polymer surfaces to control cell behavior and direct stem cell fate. For example, in a study by Dalby et al. (2006), osteogenic differentiation of human BMSCs was found to be enhanced on PMMA surfaces carrying random nanopit structures. In another study, human BMSCs cultured on collagen coated PDMS surfaces with nanoscale grooves were reported to express neural and muscular gene markers significantly higher compared to flat controls and surfaces decorated with microscale grooves (Yim et al., 2007). Several studies have reported that not only the shape but also the dimensions of patterns influence fate of cells. In a study, umbilical cord derived MSCs were grown on PDMS substrates with micrograting surface structures and were shown to exhibit enhanced neuronal cell differentiation on narrower grooves compared to wider ones (Kim et al., 2008). In another study, adipose derived MSCs were grown on microgroove structures with different ridge witdth in 1:1 mixture of adipogenic and osteogenic media. It was shown that surfaces with narrow ridges enhanced osteogenic differentiation while the ones with wider ridges promoted adipogenic differentiation (Abagnale et al., 2015). Yang et al (2011) used PDMS surfaces carrying micropillar structures with constant diameter and center to center space and variable heights to regulate the differentiation of human MSCs. They

reported enhanced expression of osteogenic markers on shorter pillars, while adipogenic differentiation was observed on tall pillars as a result of rounded morphology. Spacing between patterns has also been shown to influence lineage commitment of cells. In one study, murine MSCs were cultured on PDMS surfaces carrying lattice micropatterns with constant width and height but varying interval length. The results showed that the expression of osteogenic markers increased as the interval length increased from flat to 3 μm but decreased after 3 μm (Seo et al., 2011). There are also a few studies that have investigated the influence of surface features on stem cell fate in the absence of soluble factors. In 2007, Dalby et al. has reported that nanopatterns can induce commitment of MSCs into osteogenic lineage in the absence of differentiation medium. They cultured human BMSCs on PMMA surfaces with nanoscale circular pillar structures that were aligned in an ordered or random manner, and observed that slightly irregular nanopillars induced osteogenesis and significantly enhanced expression of bone cell specific marker genes. In 2012, Watari et al., have found that nanoscale grooves promote expression of osteogenic marker genes and calcium deposition of human MSCs in a scale dependent manner without the use of osteoinductive agents. In another study published in 2014, Kolind et al. have reported that microscale pillar structures induced DPSCs to express osteogenic markers and deposit calcium in the absence of soluble factors. They showed that it is the pillar size and interpillar gap that influences stem cell fate, not the pillar shape or arrangement.

1.6. Aim and Novelty of the Study

Many studies have shown that the interactions between cells and the substrate surface influence the behavior and the fate of cells. This topic has been investigated by many researchers, and topographical modulation of cell behavior has been investigated extensively in the last 20 years. Micro- and nanoscale surface patterns have been shown to cause distinct morphological changes and affect the cellular

behavior such as adhesion, migration, proliferation and differentiation (Hasirci and Kenar, 2006; Dalby et al., 2004; Curtis et al., 2006; Martinez et al., 2009; Nikkhah et al., 2012). In addition to the changes in cytoskeletal morphology, topographically induced self deformation of the cell nuclei has also been investigated on micropillar structures by several research groups recently (Davidson et al., 2009; 2010; Pan et al., 2012, Ermis et al., 2013; Badique et al., 2013; Nagayama et al.; 2015). The effect of the changes in cytoskeletal morphology on stem cell fate has been studied particularly on 2D surface micropatterns (McBeath et al., 2004; Bhadriraju et al., 2007; Kilian et al., 2010), but the topographically induced deformation of the cell nucleus has not been correlated to lineage commitment of stem cells. In only a few studies, researchers have reported topographically induced differentiation of stem cells on surface 3D nano- and microstructures in the absence of soluble differentiation supplements (Dalby et al., 2007; Watari et al., 2012; Kolind et al., 2014), but none of the surface structures used have been reported to cause deformations in the cell nuclei.

The aim of this study was to study the influence of the dimensions, spacing and hydrophilicity (and therefore surface chemistry and stiffness) of the micropillar structures on the morphologies of the cell body and the nuclei as well as the attachment, proliferation and osteogenic differentiation of mesenchymal stem cells without using any differentiation media. The pattern dimensions were selected to mimic the dimensions of the lacunae structures of the cortical bone tissue, and to cause changes in cytoskeletal or in both nuclear and cytoskeletal morphologies. By increasing the hydrophilicity of patterned surfaces via oxygen plasma treatment, it was aimed to modulate the degree of these deformations in order to investigate their influence of this chemistry change on cell fate.

CHAPTER 2

MATERIALS AND METHODS

2.1. Materials

Dulbecco's Modified Eagle Medium (DMEM) High Glucose, DMEM:F12 1:1 mixture, DMEM High Colorless, Pen-Strep (10.000 $U.mL^{-1}$ Penicillin and 10.000 $U.mL^{-1}$ Streptomycin), and L-glutamine (200 mM in 0.85% NaCl solution) were obtained from Lonza (Switzerland). Sylgard 184 Silicone PDMS polymer and Sylgard 184 Curing agent were bought from Dow Corning Company (UK). Poly(methyl methacrylate) (PMMA; with molecular weights $\overline{M}_w$ = 120,000, 350,000 and 996,000 Da), Trypsin-EDTA (0.25%), amphotericin-B (0.25 $\mu g.mL^{-1}$), potassium chloride (KCl), β-glycerophosphate disodium salt hydrate, dexamethasone, L-ascorbic acid, bovine serum albumin (BSA), piperazine-N,N'-bis(ethanesulfonic acid (PIPES), dispase II and collagenase type I proteases were purchased from Sigma-Aldrich (USA). Fetal bovine serum (FBS) was from Biowest (France). Chloroform and ethanol were obtained from Avantor J.T. Baker (USA). Alamar Blue® Cell Viability Assay, Alexa Fluor® 488 conjugated phalloidin, ethidium bromide (10 $mg.mL^{-1}$), dimethyl sulfoxide (DMSO), RevertAid First Strand cDNA Synthesis Kit, Ambion DNA-free™ DNA Removal Kit were purchased from Thermo Fisher Scientific (USA). NucleoCasette was from ChemoMetec (Denmark). Alexa Fluor® 488 anti-human CD31, CD45 and Mouse IgG1κ; and Alexa Fluor® 647 CD90 and CD105 antibodies were bought from BioLegend (USA). 4',6-

diamine-2-phenylindole dihydrochloride (DAPI) and DRAQ5 were bought from Cell Signalling Technology (USA). Sodium chloride (NaCl), potassium dihydrogen phosphate (KH_2PO_4) and disodium hydrogen phosphate (Na_2HPO_4) were obtained from Merck Millipore (Germany). Osmium tetroxide (OsO_4) (4%) was bought from Polysciences (USA) and Triton-X 100 was purchased from PanReac Applichem (Germany). GoTaq® qPCR Mastermix was obtained from Promega (USA). Marker specific primers were synthesized by Sentegen (Turkey).

2.2. Methods

2.2.1. Mechanical Testing of PMMA Films of Different Molecular Weights

PMMA films for mechanical testing were prepared by solvent casting of PMMA (M_w = 120,000, 350,000 and 996,000 Da) solutions (10%, w/v) in chloroform in a glass petri dish. Films were air dried at room temperature overnight and gently peeled off from the petri dish. Five tensile specimens (10 mm wide x 50 mm long x 0.10-0.15 mm thick) were cut from the cast PMMA sheets. Tensile tests of PMMA samples were conducted with Shimadzu AGS-X universal test machine (Japan). PMMA strips with a gauge length of 20 mm were attached and a uniaxial tensile load was applied to the specimen at a pulling rate of 1 $mm.min^{-1}$. Force and elongation values were recorded and the stress and strain graphs were plotted using the values calculated with the following equations:

$$Stress\ (\sigma) = \frac{F}{A} \quad (1)$$

$$Strain\ (\varepsilon) = \frac{\Delta l}{l} \quad (2)$$

where F is the force (N), A is the crosssectional area (width x thickness, mm^2), Δl the change in length (mm) and l the initial length (mm). Ultimate tensile strength (UTS) of the samples was defined as the highest stress value on the stress-strain curve. The tensile moduli (Young's Modulus, E) were calculated as the slope of these curves using the following equation:

$$E = \frac{\sigma}{\varepsilon} \qquad (3)$$

where σ is the stress (MPa) and ε the strain in the elastic region (Fig. 2.1).

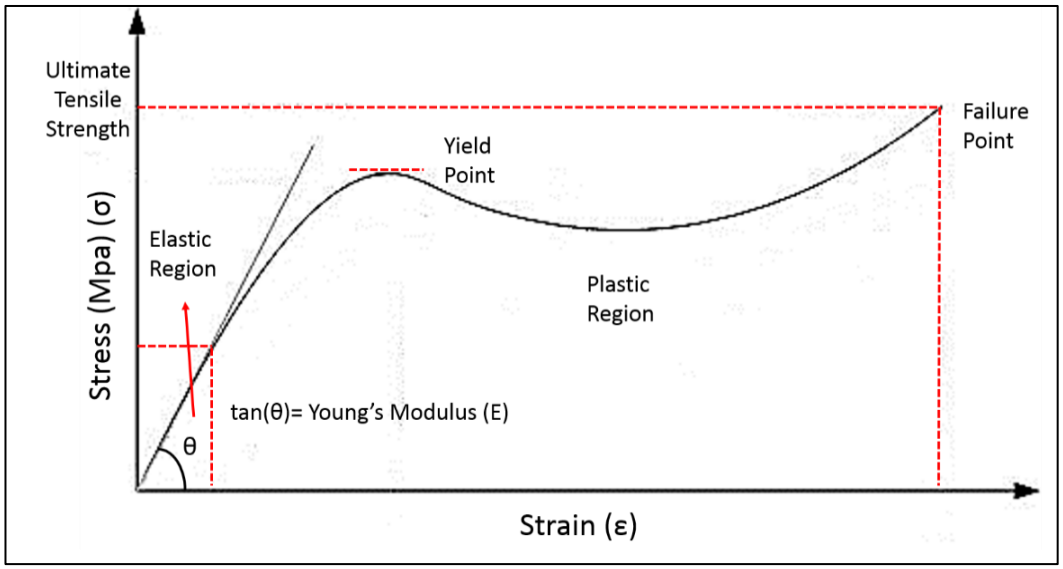

Figure 2.1. The representative stress-strain curve of thermoplastic polymers.

2.2.2. Preparation of PMMA Films Decorated with Micropillars

2.2.2.1. Preparation of Silicon Wafers Decorated with Micropillars

SU-8 micropillar arrays chips were fabricated at Prof. U. Demirci's Bio-Acoustic-MEMS in Medicine (BAMM) Laboratory, Stanford University (USA) using standard photolithography procedures (Fig. 2.2). Micropillar geometries and dimensions were designed as presented in Table 2.1. The pillars were 8 µm tall square prisms with areas of 4x4, 8x8 and 16x16 μm^2. The pillars were separated from each other by 4, 8 and 16 µm gaps. Pattern designs were printed on a custom-designed photomask (Fineline Imaging, CO).

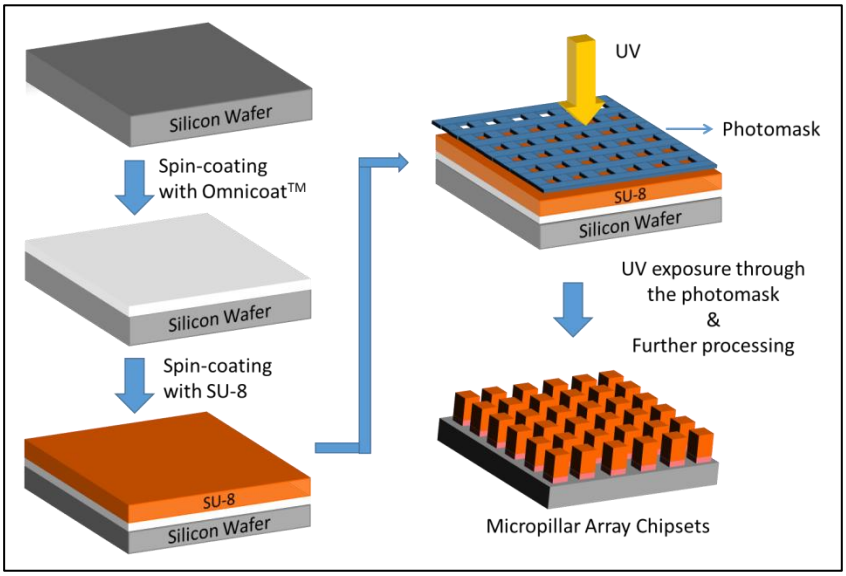

Figure 2.2. Schematic presentation of the fabrication of micropillar covered arrays.

2.2.2.2.Preparation of Polydimethylsiloxane (PDMS) Templates

Copies of the silicon wafers were fabricated using PDMS templates (Fig.2.3.A). Sylgard 184 silicone prepolymer solution and the curing agent were mixed at a ratio of 10:1 (w/w). The mixture was kept under vacuum at -600 mm Hg for 1 h at room

temperature to remove bubbles. The mixture was then poured onto the silicon wafers, kept under vacuum for 30 min and then incubated at 70 ^{o}C for 4 h in an oven for curing the polymer. The PDMS templates produced were gently peeled off from the silicon wafers and stored in glass petri dishes.

Table 2.1. Pillar dimension and organization on the surfaces of the micropatterned PMMA films.

Surface Features	**Abbreviation**	**Top View**	**Side View**
4x4 μm^2 pillar 4 μm gap	P4G4	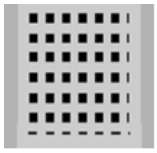	
8x8 μm^2 pillar 8 μm gap	P8G8	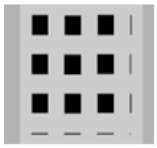	
16x16 μm^2 pillar 16 μm gap	P16G16	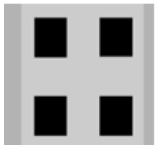	

2.2.2.3. Preparation of PMMA Replicas of the Silicon Wafers

Solvent casting method was used to produce PMMA replicas of the original silicon wafers by using the PDMS negatives (Fig. 2.3.B). PMMA solution (10% w/v in chloroform) was poured onto the PDMS mold and air dried overnight at room temperature for the evaporation of chloroform. Dry films were then peeled off from the PDMS molds and stored in 12 well TCPs plates at room temperature until use.

One set of the films were kept in vacuum oven at 50 ^{o}C in order to remove any remaining solvent, and then tested for tensile properties and cell viability. Since no difference was observed between untreated and treated films, incubation in vacuum oven was not applied for the rest of the study.

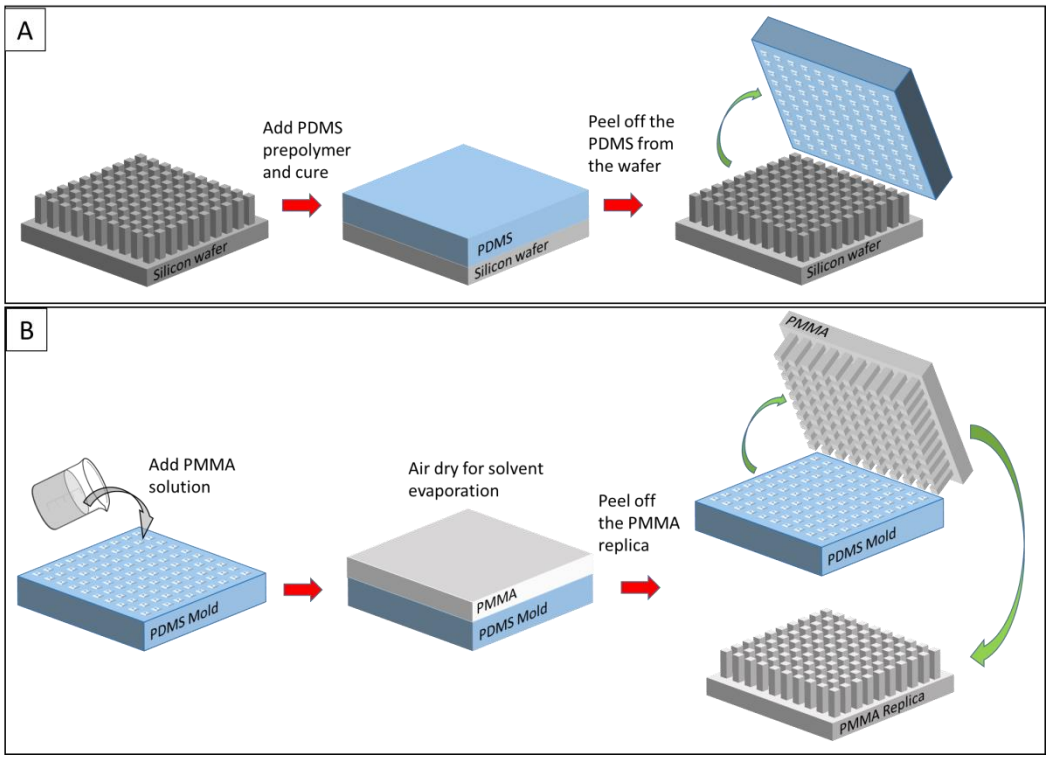

Figure 2.3. Schematic presentation of the fabrication of PMMA films decorated with micropillars. (A) Production of PDMS molds of the original silicon wafers, and (B) production of PMMA replicas of the original silicon wafers using the PDMS molds and solvent casting method.

2.2.3. Oxygen Plasma Treatment of the Films

Oxygen plasma modification was employed to increase surface hydrophilicity of the PMMA films. In order to choose optimum plasma parameters, surfaces of the unpatterned smooth films were modified by oxygen plasma treatment at different power and exposure durations and then water contact angles were measured. Films were placed in the plasma reaction chamber (Femto 40 kHz, Diener Electronic, Germany) and the plasma pressure was maintained at 20 mbar by the introduction of the oxygen gas at a controlled rate. The power was set to 20, 30, 50, 75 and 100 W and the films were exposed to oxygen plasma for 2.5 or 10 min. After the plasma treatment was ceased, the gas flow was continued for 10 min for the termination of the created reactive groups. Exposure to plasma at 100W for 10 min was selected and smooth and micropatterned samples were plasma modified. One set of the films were then immediately used in contact angle measurements and the other set was used in *in vitro* studies.

2.2.4. Characterization of the Films

2.2.4.1. Scanning Electron Microscopy (SEM) Analysis

Surface features of the untreated and oxygen plasma treated PMMA films were examined with SEM (400D Field Emission SEM, USA). Films were coated with Au-Pd under vacuum and micrographs of top and side view were taken. Pillar and gap dimensions of the films were measured using the SEM micrographs and the image analysis software ImageJ (NIH, 1.48v).

2.2.4.2. Atomic Force Microscopy (AFM) Analysis

In order to study the effect of plasma modifications, AFM analysis had to be carried out along with the contact angle measurements. The surface morphologies of the untreated and oxygen plasma treated smooth PMMA surfaces were examined with an atomic force microscope (Universal SPM, Ambios Technology, Korea) in intermittent tapping mode. The mean surface roughness and the average height of three sample surfaces from each group were measured, and 2D and 3D wavemode micrographs were recorded.

2.2.4.3. Contact Angle Analysis

Contact angles of the all untreated and oxygen plasma treated PMMA films were measured by the static sessile drop method using a goniometer (Attension, Biolin Scientific, Sweden) (n=3). The measurements were made with distilled water with a drop volume of 7 μL.

2.2.5. *In Vitro* Studies

2.2.5.1. Isolation of Human Dental Pulp Mesenchymal Stem Cells (DPSCs)

Impacted human third molars were obtained with informed written consent at METU Medical Center, Ankara, Turkey with the approval of the Human Subjects Ethics Committee of Middle East Technical University, Ankara, Turkey (28620816/505-69). Human dental pulp extracts were obtained from 3 patients (2 female, 1 male), aged 18-22 years (20 ± 1.6 years) by Dr. Ercument Onder of METU Medical Center, Department of Dentistry. The pulp tissue extracts were brought to the laboratory in DMEM High Glucose medium containing 3% Pen-Strep and 0.25 $\mu g.mL^{-1}$ amphotericin B. Dental pulp fragments were washed with sterile phosphate buffered

saline (PBS; 137 mM NaCl, 2.7 mM KCl, 10 mM Na_2HPO_4 and 1.8 mM KH_2PO_4, pH 7.4) twice and minced into small pieces by using sterilized scalpels. Pulp pieces were then digested in DMEM High Glucose medium containing 3 $mg.mL^{-1}$ collagenase type I and 4 $mg.mL^{-1}$ dispase II for 1 h at 37 ^oC with gentle agitation. The homogenate was centrifuged at 5000 rpm for 5 min, the pellet was resuspended in 600 µL DMEM High Glucose medium and the suspension was filtered through a 100 µm cell strainer. Cell suspension was transferred to T25 tissue culture flasks.

2.2.5.2. Human DPSCs Culture

Isolated DPSCs were cultured in DMEM:F12 1:1 medium supplemented with 5 mM L-glutamine, 10% FBS, 1% Pen-Strep and 0.25 $\mu g.mL^{-1}$ amphotericin B. DPSCs used in osteogenic differentiation analysis were cultured in regular DMEM:F12 1:1 growth medium supplemented with 100 nM dexamethasone, 10 mM β-glycerophosphate and 50 µM L-ascorbic acid. Cells were incubated at 37 ^oC in a 5% CO_2 incubator and the growth medium of the cells was replaced with fresh medium every 2 days. Cells at 70 - 80% confluency were removed from the tissue culture flasks with Trypsin-EDTA. Cells were stored frozen at -80˚C in FBS with 10% (v/v) DMSO, and were thawed and allowed to proliferate in tissue culture flasks prior to use. Cells at passages 2 – 5 were used in the tests.

2.2.5.3. Flow Cytometry Analysis of the Isolated Cells

Isolated cells cultured in growth medium were analyzed for cell surface antigens of mesenchymal stem cells by flow cytometry (BD Accuri C6, USA). After the cells were trypsinized and centrifuged, the pellet was washed with FACS buffer (1:1000 sodium azide and 1:100 BSA in PBS) and fixed in 4% paraformaldehyde solution for 15 min. Fixed cells were stained with mouse IgG1 anti-human monoclonal antibodies (Biolegend, USA) against CD31 (#303110), CD45 (#304017), CD90

(#328116) and CD105 (#323212) surface markers. Mouse IgG1κ monoclonal antibody was used as the negative control for the detection of nonspecific binding. The cell population was gated on the forward and side scatter chart and flow cytometry was performed on 10^5 cells per sample. Positive expression was defined as the level of fluorescence greater than 50% of the corresponding unstained cell sample.

2.2.5.4. Sterilization of the Films

The PMMA films were sterilized under UV light in a laminar flow hood at room temperature. Both sides of the films were exposed to UV (254 nm) for 15 min prior to cell seeding.

2.2.5.5. Cell Seeding onto the Films

Cells were detached from the tissue culture flasks by Trypsin-EDTA (37 ^oC for 5 min). Then trypsin was blocked by the addition of DMEM:F12 1:1 growth medium and the cell suspension was centrifuged (3000 g, 5 min). Obtained cell pellet was resuspended in the culture medium and the cell number was determined by using the Nucleocounter (Chemometec, Denmark). Cells were seeded onto the films at a density of 2000 cells/film for fluorescence and confocal microscopy analyses, 7500 cells/film for proliferation analysis and $2x10^4$ cells/film for attachment analysis and RNA isolation. After allowing the cells to adhere for 2 h, 2 mL of growth medium was added into each well of the 12 well plate. Plates were incubated at 37 ^oC and 5% CO_2 incubator for 1, 7, 14, 21 and 28 days and the growth medium was replaced every 2 days.

2.2.5.6. Cell Attachment and Proliferation on the Films

Cell numbers were determined at 16 h for attachment and also on Days 3, 7, 14 and 21 for proliferation with the Alamar Blue cell viability assay. The films were washed with PBS twice and incubated in 500 µL Alamar Blue solution (10% in DMEM High Glucose colorless supplemented with 100 $U.mL^{-1}$ Pen-Strep) for 2 h at 37 ^{o}C and 5% CO_2. After incubation, 200 µL of the Alamar Blue solution was transferred into a 96 well plate and the absorbances of the transferred solutions were determined at 570 nm (λ_1) and 595 (λ_2) with a plate reader (Multiscan Spectrum, Thermo Scientific, USA). The absorbance values were converted to percent reduction by using the following equation:

$$\text{Reduction (\%)} = \frac{((\varepsilon_{ox})_{\lambda_2} \text{ x } A_{\lambda_1}) - ((\varepsilon_{ox})_{\lambda_1} \text{ x } A_{\lambda_2})}{((\varepsilon_{red})_{\lambda_1} \text{ x } A'_{\lambda_2}) - ((\varepsilon_{red})_{\lambda_2} \text{ x } A'_{\lambda_1})} \; x \; 100 \qquad (4)$$

where,

λ_1 = 570 nm

λ_2 = 595 nm

$A_{\lambda 1}$ and $A_{\lambda 2}$= Absorbance of cell seeded films,

$A'_{\lambda 1}$ and $A'_{\lambda 2}$= Absorbance of the negative control (unseeded unpatterned film)

Molar Extinction Coefficients were:

$(\varepsilon_{ox})_{\lambda 1}$= 80.586 $(\varepsilon_{red})_{\lambda 1}$= 155.677

$(\varepsilon_{ox})_{\lambda 2}$= 117.216 $(\varepsilon_{red})_{\lambda 2}$= 14.652

In order to convert the percent reduction values to cell numbers, a calibration curve was constructed (Fig.A.1) by applying the same experimental procedure presented above with a series of known number of cells cultured in the wells of a 24 well plate.

Three samples were used for each group and the absorption of each sample was measured twice.

2.2.6. Microscopic Studies

2.2.6.1. Scanning Electron Microscopy (SEM) Analysis

The PMMA films with seeded DPSCs were washed twice with PBS and incubated in 4% paraformaldehyde for 5 min at room temperature. After fixation, the specimens were washed twice with PIPES (piperazine-N,N'-bis(ethanesulfonic acid)) buffer and then incubated in 1% osmium tetroxide (OsO_4) in PIPES buffer at room temperature for 1 h. Then, the samples were washed twice with PIPES buffer and dehydrated by incubating in a series of ethanol concentrations (50, 70 and 100% in distilled water) at room temperature for 5 min each. Samples were Au-Pd coated under vacuum and examined with a SEM (400F Field Emission SEM, USA).

2.2.6.2. Fluorescence Microscopy Analysis

The PMMA films with seeded DPSCs were washed with PBS (10 mM, pH 7.4) and incubated for 15 min at room temperature in paraformaldehyde (4% w/v) for fixation. Cells were permeabilized with Triton X-100 solution (0.1%, v/v, in PBS) for 5 min at room temperature. After washing with PBS twice, films were incubated in BSA blocking solution (1%, w/v, in PBS) at 37 ^{o}C for 30 min. Films were then incubated in Alexa Fluor 488® labelled Phalloidin solution (1:50 dilution in 0.1% BSA in PBS) for 1 h at 37 ^{o}C and in DAPI solution (1:1000 dilution in 0.1% BSA in PBS) for 15 min at room temperature. Films were washed twice with PBS and stored in 12 well plates in 1 mL PBS solution at 4 ^{o}C and the plates were wrapped in aluminum foil for light protection until analysis. Samples were analyzed with the fluorescence microscope (Zeiss Axio Imager M2, Germany).

2.2.6.3. Confocal Laser Scanning Microscopy (CLSM) Analysis

The PMMA films with seeded DPSCs were fixed and blocked as described in Section 2.2.6.2., and then incubated in Alexa Fluor 488® labelled phalloidin solution (1:50 dilution in 0.1% BSA in PBS) for 1 h at 37 ^{o}C and in DRAQ5 solution (1:1000 dilution in 0.1% BSA in PBS) for 45 min at room temperature. After staining, films were washed twice with PBS and stored in 12 well plates in 1 mL PBS solution at 4 ^{o}C until analysis with a confocal laser scanning microscope (Leica SPE CLSM, Germany).

2.2.7. Digital Analysis of Morphological Changes in the Nucleus and Cytoskeleton of DPSCs

2.2.7.1. Analysis of Nuclear Deformation

CLSM micrographs of the nuclei of DPSCs on Days 1, 3, 7, 14 and 28 were analyzed by using the image analysis software Image J (1.48v, NIH, USA) to determine the circularity of the nuclei of cells. ImageJ uses the following equation to calculate circularity:

$$f_{\text{circularity}} = \frac{4\pi A}{P^2} \quad (5)$$

where A and P denote the area and perimeter, respectively. Circularity of a shape takes values between 0 and 1, and the circularity of a perfect sphere is repesented as 1. Since the circularity value decreases with an increase in the deviation from the sphere (Fig. 2.4), the following equation was used to quantify nuclear deformation:

$$f_{\text{Nuclear Deformation}} = 1 - f_{\text{Circularity}} \quad (6)$$

Nuclear deformation values were calculated from 100 nuclei per surface and the distribution of the data was presented as box-whisker plots.

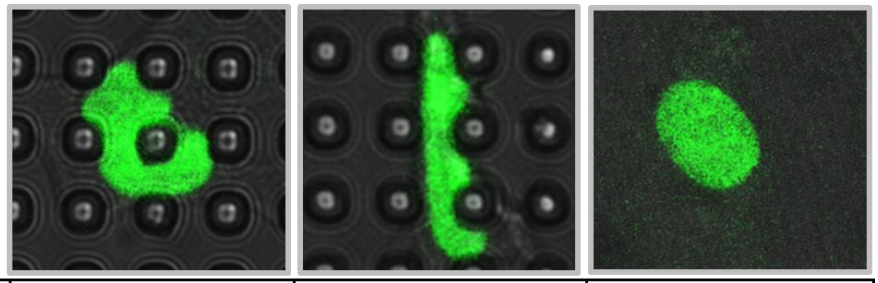

Circularity	0.43	0.45	0.85
Nucleus Deformation (1-circularity)	0.57	0.55	0.15

Figure 2.4. A representation of the quantification of nuclear deformation using the CLSM images of the nuclei of DPSCs.

2.2.7.2. Analysis of Elongation and Branching of the Cytoskeleton of DPSCs

Fluorescence micrographs of DPSCs on PMMA films on Days 1, 3 and 7 were analyzed by using the Image Processing Toolbox of the MatLab (R2013a) software to determine the elongation and branching of cell cytoskeleton from the cell boundaries (Fig. 2.5). Elongation and solidity formulas were embedded into a MatLab code by Abdullah Sivas of METU Institute of Applied Mathematics, Ankara, Turkey.

As it can be seen in Fig. 2.5, elongation of a quite circular cell (Fig.2.5.A) is much smaller than that of a linearly stretched cell (Fig.2.5.B), while for a branched cell

(Fig.2.5.C) this value is similar to the circular cell. However, the branching values of the circular and branched cells are distinctly different. Thus, classification and analysis become possible by using several of these parameters simultaneously.

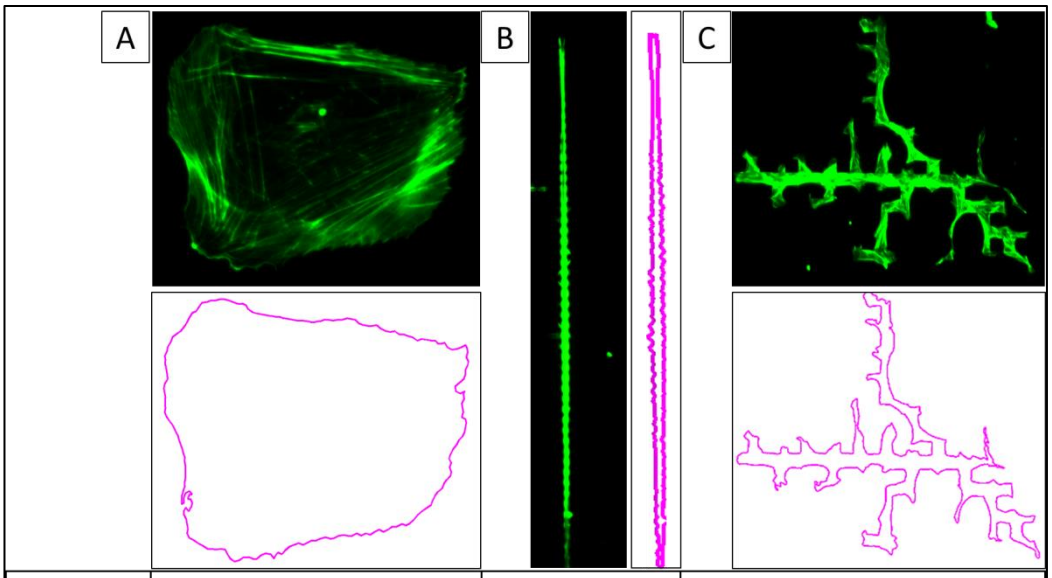

	A	B	C
Elongation	1.271	13.952	1.257
Solidity	0.945	0.629	0.234
Branching (1/Solidity)	1.058	1.590	4.274

Figure 2.5. Quantification of the elongation and branching of cell cytoskeleton from the cell boundaries obtained from fluorescent micrographs of DPSCs. Digital analysis of a relatively (A) circular, (B) elongated and (C) branched cell from the cell boundaries.

2.2.7.2.1. Analysis of the Elongation of Cell Cytoskeleton

The following equation derived by Stojmenovic & Zunic (2008), which calculates the elongation of polygonal shapes using their shape boundary, was used to measure the elongation of the cytoskeletons:

$$\mathcal{E}(P) = \frac{\sum_{1\le i\le n} |e_i| + \sqrt{(\sum_{1\le i\le n} |e_i|\cos(2\alpha_i))^2 + (\sum_{1\le i\le n} |e_i| \cdot \sin(2\alpha_i))^2}}{\sum_{1\le i\le n} |e_i| - \sqrt{(\sum_{1\le i\le n} |e_i| \cdot \cos(2\alpha_i))^2 + (\sum_{1\le i\le n} |e_i| \cdot \sin(2\alpha_i))^2}} \quad (7)$$

where P is a shape with polygonal boundary, $\varepsilon(P)$ is the elongation function of the shape P, e_i ($1\le i \le n$) are the edges of the boundary of P and α_i ($1\le i \le n$) are the angles between the edges e_i and the x axis. This equation defines the elongation of polygonal shapes as the ratio of the maximum and minimum values of their shape orientation function, which is composed of the boundary edges and the angles that those edges make with the x-axis. Elongation values were calculated using 100 cells per surface and the distribution of the data was presented as box-whisker plots.

2.2.7.2.2. Analysis of the Branching of Cell Cytoskeleton

The branching of the cells was quantified using the shape descriptor solidity, which is defined with the following equation:

$$f_{\text{Solidity}} = \frac{\text{Shape Area}}{\text{Convex Area}} \quad (8)$$

where the convex area is the smallest convex hull that contains the original region (Fig. 2.6).

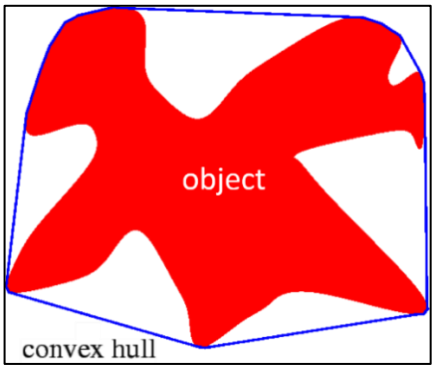

Figure 2.6. Schematic representation of the convex hull of a polygonal shape.

The solidity value of a shape decreases as its branching increases. Thus, the following equation was derived to calculate branching of the cell cytoskeleton:

$$f_{\text{Cell Branching}} = 1 / f_{\text{Solidity}} \quad (9)$$

Cell branching values were calculated using 100 cells per surface and the distribution of the data was presented as box-whisker plots.

2.2.8. Gene Expression Studies

2.2.8.1. RNA Isolation

Total RNA content of DPSCs cultured on PMMA films were extracted by using Masterpure RNA Purification Kit according to the manufacturer's instructions. RNA isolation was done on two biological replicas of each group of surface and six films were pooled for each biological replicate. DNA-free™ DNA removal Kit was used to remove any DNAs contaminating the RNA samples. RNA concentrations were measured by Nanodrop 2000C (Thermo Scientific, USA). Isolated RNA samples (1.5

μL) were mixed with 1 μL of loading dye and run on 1% agarose gel with EtBr at 100 V for 45 min. Agarose gels were visualized under UV exposure using ChemiDoc – It^2 Imager (UVP, USA).

2.2.8.2. Reverse Transcription PCR (RT-PCR)

First-strand cDNA synthesis via RT-PCR was performed with 1 μg RNA from each sample with RevertAid First Strand cDNA Synthesis Kit and a thermal cycler (iCycler, BIO-RAD, USA) with the oligo$(dT)_{18}$ primers supplied with the kit. The reverse transcription step ran for 60 min at 42 ^{o}C, followed by reaction termination for 5 min at 70 ^{o}C.

2.2.8.3. Quantitative Real Time PCR (qRT-PCR)

Quantitative RT-PCR was conducted using forward and reverse primers specific for GAPDH (glyceraldehyde 3-phosphate dehydrogenase) as the house keeping gene, primers specific for stemness markers were Oct3/4 (octamer-binding transcription factor ¾) and Nanog, and primers specific for bone markers were OSX (Osterix/Sp7), ALP (alkaline phosphatase) and OC (osteocalcin) (Table 2.2). To exclude signals from contaminating DNA, primers were designed on different exons (except OSX, which is composed of one large exon). GoTaq® qPCR Mastermix (Promega, USA) was used for quantitative PCR reactions according to the manufacturer's instructions. Briefly, 12.5 μL of mastermix solution was mixed with 9.5 μL of RNase free dH_2O, 0.5 μL of forward primer (10 mM) and 0.5 μL of reverse primer (10 mM). The volume was completed to 25 μL by adding 2 μL of cDNA template (50 ng/reaction). The reactions were performed with Rotor-Gene Q real-time PCR cycler (Qiagen, Germany). Following the denaturation step at 95 ^{o}C for 2 min, 35-45 cycles were run, consisting of 15 s denaturation at 95 ^{o}C and 60 s of annealing/extension at 60 ^{o}C. RT-qPCR was run for each marker with no reverse

transcriptase (No-RT) control RNA from each group in order to detect any nonspecific amplification caused by contaminating genomic DNA. Samples were assayed in duplicate, and the C_t values for Oct3/4, Nanog, Osx, ALP and OC were normalized to that of the housekeeping gene GAPDH. Gene expression levels of the cells cultured on TCPs in osteogenic media were normalized to the cells cultured in regular growth medium (reference group), while the expression levels of the cells cultured on micropatterned PMMA films were normalized to that on unpatterned control according to the following equations:

$$\Delta C_t \text{ (Treated)} = C_t \text{ (Treated }_{\text{target}}\text{)} - C_t \text{ (Treated }_{\text{reference}}\text{)} \quad (10)$$

$$\Delta C_t \text{ (Control)} = C_t \text{ (Control }_{\text{target}}\text{)} - C_t \text{ (Control }_{\text{reference}}\text{)} \quad (11)$$

$$\Delta\Delta C_t = \Delta C_t \text{ (Treated)} - \Delta C_t \text{ (Control)} \quad (12)$$

$$\text{Normalized target gene expression level} = 2^{(-\Delta\Delta Ct)} \quad (13)$$

where C_t is the threshold cycle. All qRT-PCR products were run on 2% agarose gel with EtBr at 100V for 45 min and the gels were visualized using the ChemiDoc – It^2 imaging system.

Table 2.2. Primer sequences for qRT-PCR analysis. F: forward primer, R: reverse primer.

Marker		Primer (5' – 3')	Amplicon Size (bp)	NCBI Accession #
GAPDH	**F**	CACCCACTCCTCCACCTTTG	110	NM_001289746.1
	R	CCACCACCCTGTTGCTGTAG		
Oct3/4	**F**	ACTGCAGCAGATCAGCCACATCG	124	NM_002701
	R	ATCCTCTCGTTGTGCATAGTCGC		
Nanog	**F**	AAAGAATCTTCACCTATGCC	110	NM_024865
	R	GAAGGAAGAGGAGAGACAGT		
Osx	**F**	CCCCACCTCTTGCAACCA	102	NM_001173467
	R	GGCTCCACCACTCCCTTCTAG		
ALP	**F**	GGAACTCCTGACCCTTGACC	86	NM_000478
	R	TCCTGTTCAGCTCGTACTGC		
OC	**F**	CTCACACTCCTCGCCCTATTGG	121	NM_199173.5
	R	CGCTGCCCTCCTGCTTGG		

2.2.9. Statistical analysis

All quantitative data in this study are expressed as mean ± standard deviations with n≥2 unless otherwise stated. Normality test on all collected data was performed by Anderson-Darling method. Statistical analysis was performed by one-way ANOVA (analysis of varience) test followed by Tukey's test for normally distributed data and Kruskal-Wallis test for non-normally distributed data. *p*-values less than 0.05 were considered statistically significant.

CHAPTER 3

RESULTS AND DISCUSSION

3.1. Tensile Testing of Solvent Cast PMMA Films

Mechanical properties of the substrates are known to influence the fate of stem cells. Matrices that mimic the mechanical properties of the natural tissues have been shown to promote differentiation towards the related lineage (Engler et al., 2006). In this section, the mechanical properties of the solvent cast films prepared by using three different molecular weights (120, 350 and 996 kDa) of PMMA were determined by a tensile test. The stress-strain curves and the Young's moduli and ultimate tensile strengths determined from these curves are represented in Fig. 3.1. and Fig. 3.2 (also in Table B.1), respectively. The elastic moduli of the films prepared with Mw 996 kDa and 350 kDa PMMA were found to be close to each other (1255 ± 15 MPa and 1285 ± 29 MPa, respectively) and significantly higher than that of the films prepared with 120 kDa PMMA (870 ± 6 MPa). A similar trend was also observed with the ultimate tensile strengths (41.5 ± 0.3 MPa, 41.6 ± 2 MPa and 25.2 ± 0.5 MPa for 996 kDa, 350 kDa and 120 kDa, respectively). The influence of MW on mechanical properties is generally explained by the entanglement of the polymer chains. For amorphous polymers such as polystyrene and PMMA, the number of entanglements were shown to increase with increasing molecular weight up to a certain limit, restrict the viscous flow of polymer chains, which in turn increases the UTS and E values (Landel and Nielsen, 1993). It was also shown that the tensile strength and

modulus of amorphous polymers are independent from MW above a certain limit. For instance, tensile strengths of the PMMA films were reported to be independent of the molecular weight at values higher than 150 kDa but diminish significantly with decreasing MW below this value (Kishi and Kamata, 1961). A similar observation was made by Bae et al. (2009) who produced thin films by spin coating PMMA solution in chloroform and showed that the Young's moduli of the films prepared by using 996 kDa and 350 kDa PMMA (~2.8 GPa) were similar at low strain rates (10 $\mu\varepsilon.s^{-1}$). It was noticed that the stress-strain curves of the samples (Fig.3.1) did not follow the general trend of increasing stress after necking up to the failure point observed for thermoplastic materials (Fig.2.1 in Section 2.2.1). Instead, stress decreased continuously until the failure point. A similar behavior was observed by Moy et al. (2011) for PMMA, and it was shown that the behavior of the material varies with the temperature and the strain rate.

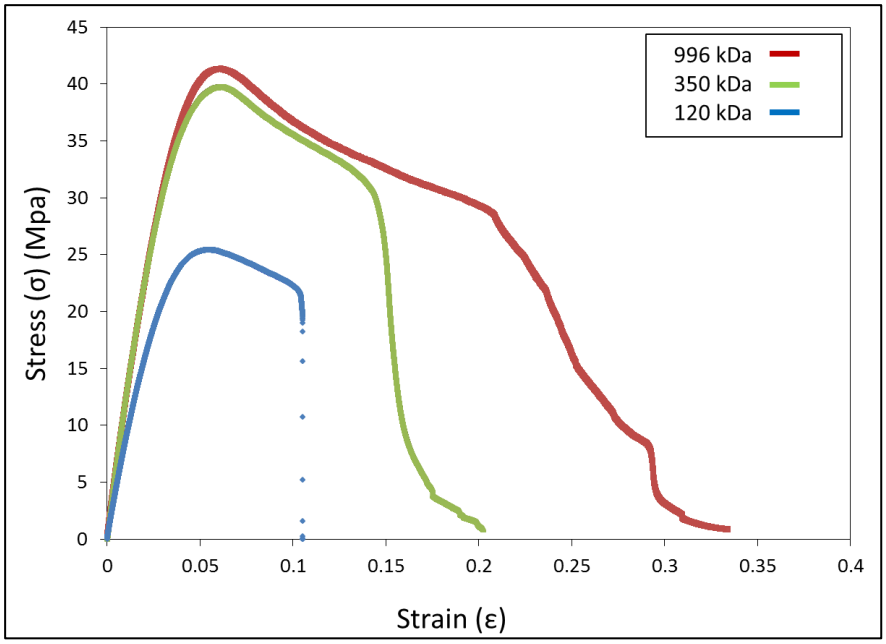

Figure 3.1. Representative stress vs. strain curves of the solvent cast films prepared by using 120, 350 and 996 kDa PMMA.

The Young's moduli of PMMA films determined in this study were in the range of 0.8 – 1.3 GPa. In the literature, however, this range is given as 1.8 – 3.1 GPa (Kariduraganavar et al., 2014), which is above the values obtained in this study. The reason of this difference is probably the processing method used. The PMMA films used in this study were produced by solvent casting, which was shown to decrease the mechanical properties. Rhim et al. (2006) prepared PLA films by thermocompression and solvent casting methods and showed that Young's modulus and ultimate tensile strength values were significantly higher for thermocompressed films. Lower tensile strength and elastic modulus of the solvent cast product was explained with loosely packing of the polymer chains and a part of the solvent that remain in the bulk and act as a plasticizer. In our study, however, no significant difference was observed in tensile properties or cell viability upon incubating the films under vacuum at 50 ^{o}C, indicating that no chloroform remained in the bulk in the standard procedure. Elastic moduli and tensile strengths of the cortical bone (E: 3-30 GPa, UTS: 80-150 MPa) and the cancellous bone (E: 0.1-0.4 GPa, UTS: 5-10 MPa) (Weiner and Wagner, 1998) are given in the literature. It can be seen that the mechanical properties of the solvent cast PMMA films lie between these of cortical and cancellous bone tissues. In order for the products to display stiffness that is closer to that of the cortical bone, PMMA with MW of 996 kDa was selected for the fabrication of the micropatterned substrates.

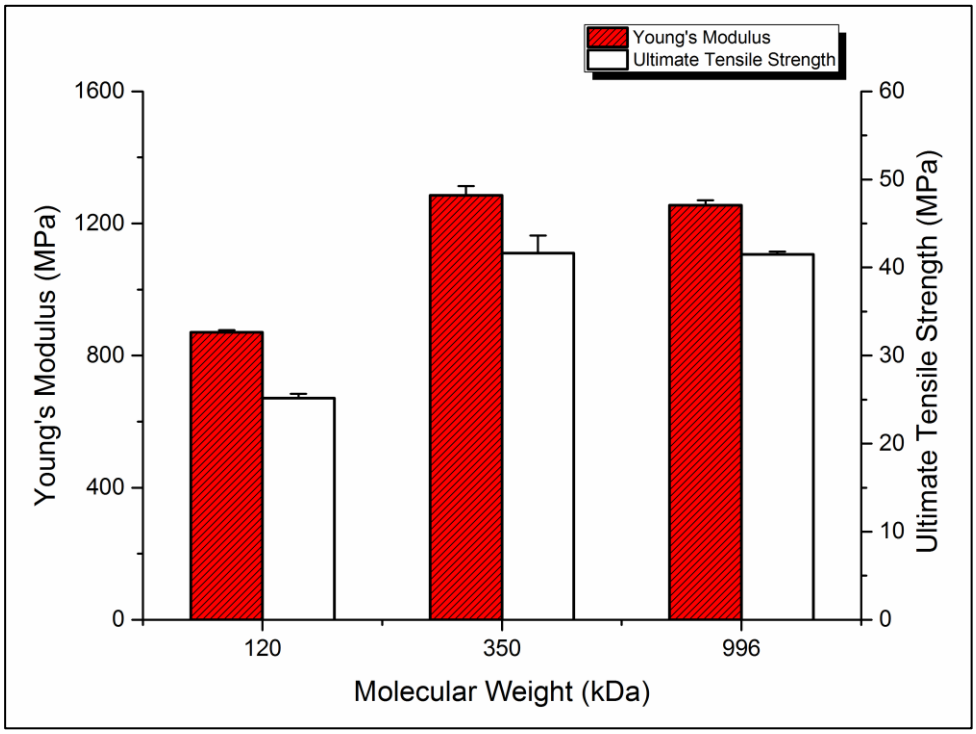

Figure 3.2. Young's modulus and ultimate tensile strength of the solvent cast PMMA films with molecular weights 120, 350, and 996 kDa.

3.2. Oxygen Plasma Modification of Unpatterned PMMA Films

Wettability is a function of surface free energy and topography. It is one of the surface characteristics that affect adsorption and desorption of proteins and influences adhesion, proliferation and migration of mammalian cells on polymeric materials (Lee et al., 1993; Arima et al., 2007). Substrates with water contact angles below 90^o are called wettable and above 90^o are called non-wettable. PMMA is considered by some as a hydrophilic polymer because it exhibits a water contact angle around 70^o, but others (Borges et al., 2013) have found it to be higher (83^o). The water contact angle of pristine PMMA films produced in this study was determined to be around 87^o (Fig. 3.3.). Unpatterned PMMA films were exposed to oxygen plasma treatment to increase their hydrophilicity. In order to obtain a series

of polymeric surfaces with varying surface wettability, power was increased while keeping the pressure and flow rate contant. Since the aim was to decide optimum plasma parameters, 1 sample was plasma modified and used for contact angle measurement for each condition. The effects of different plasma power and durations on water contact angle of smooth PMMA surfaces are shown in Figure 3.3 (Numerical values in Table B.2). A decrease in the contact angle with an increase in the power was observed. Meanwhile, an increase in the duration of the plasma treatment from 2.5 min to 10 min caused a significant drop in contact angle from 33^{o} to 14^{o}. This was expected as it was previously shown that increasing the duration of exposure or the power increases the surface wettability of PMMA films by increasing polar components and surface free energy (Ozcan et al., 2008). In order to study the influence of 3D surface cues on cell morphology and behavior, untreated surface (contact angle 87^{o}) and oxygen plasma treated (100W, 10 min, contact angle 14^{o}) were selected as two extreme surfaces for the *in vitro* studies. In the rest of the study, plasma treated surface stands for PMMA films exposed to oxygen plasma at 100W for 10 min.

During the oxygen plasma treatment, reactive species (ions, radicals etc.) interact with the surface not only chemically but also physically. In addition to the introduction of new functional groups, some low MW molecules are removed from the polymer surface. This results in etching of the surface and an increase in the surface roughness (Cvelbar et al., 2003). In order to study this on our samples PMMA surfaces were analyzed by AFM. It was observed that the relatively smooth surface of the unpatterned substrates was transformed into a rough surface as shown in the AFM micrographs and by the root mean square (RMS) values (Fig. 3.3, Table 3.1). Upon treatment, the average height increased from 33.08 to 54.59 nm and RMS deviation increased from 6.36 to 15.88 nm, indicating an increase in surface roughness as a result of the etching effect of oxygen plasma treatment. This was expected because oxygen plasma modification was reported to create nanotextures and increase surface roughness of organic polymers including PMMA (Vesel et al.,

2012), PLA, PLGA (Khorasani et al., 2009) and polystyrene (PS) (Dowling et al., 2010).

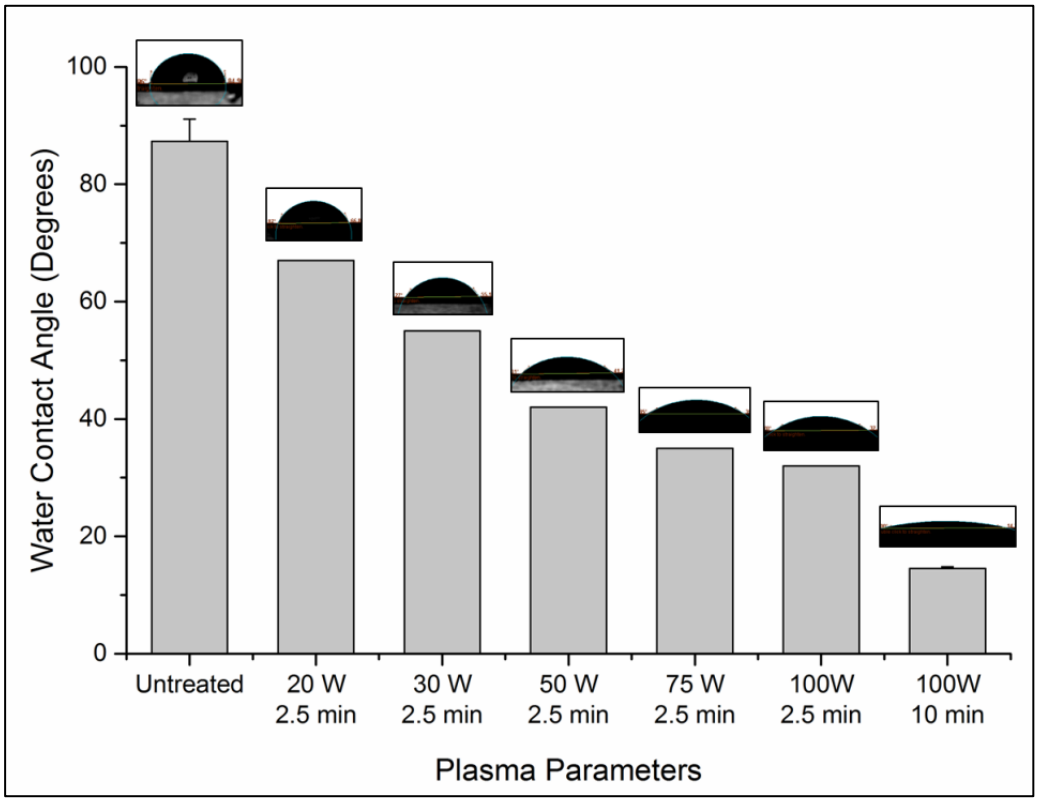

Figure 3.3. Water contact angles of unpatterned PMMA surfaces after oxygen plasma treatment at different power and durations.

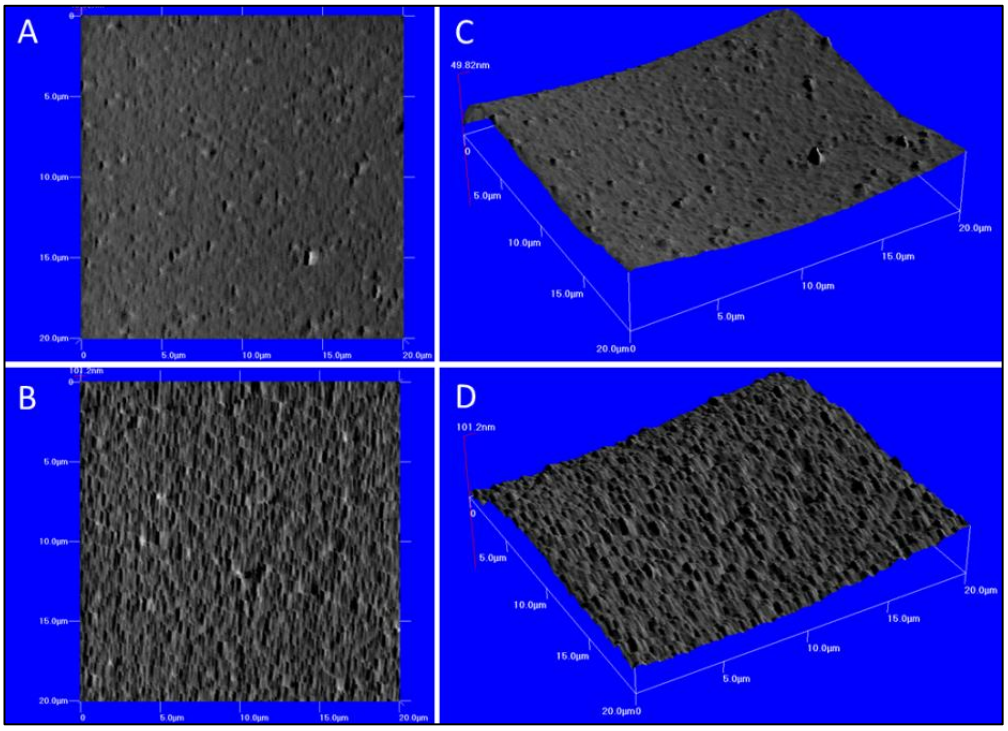

Figure 3.4. AFM micrographs of unpatterned PMMA films. 2D and 3D micrographs of (A, C) untreated, and (B, D) oxygen plasma treated surfaces.

Table 3.1. Quantitation of the surface roughness of unpatterned PMMA films before and after oxygen plasma treatment.

Sample	RMS Deviation (nm)	Average Height (nm)
Untreated PMMA Film	6.36	33.08
O_2 Plasma Treated PMMA Film	15.88	54.59

3.3. Surface Characterization of Substrates

Three types of silicon wafers decorated with micropillars were prepared as described in Section 2.2.2.1. These were P4G4, P8G8 and P16G16, where P is the square prism pillar dimension and G is the interpillar gap, both in μm (Fig. 3.5.). Unpatterned smooth wafers were used for the fabrication of negative control surfaces. PDMS molds were prepared using these wafers as explained in Section 2.2.2.2 and served as negative templates for the production of the PMMA replicas of the original wafers. Surfaces of the films were characterized by SEM and contact angle measurements.

3.3.1. SEM Analysis

SEM micrographs of the top and side views of surface micropillar structures are given in Fig. 3.5. It was observed that the micron scale pillars were quite successfully replicated on PMMA surfaces. It was, however, observed that the micropillars with small dimensions had smooth edges rather than 90^{o} angles. As the size of the pillars increased, the sharpness of the edges increased implying a problem of wafer preparation with low micron features. The dimensions of the pillars and interpillar distances measured by image analysis software ImageJ on the top view SEM micrographs are presented in Table 3.2. The measurements revealed some deviations in both pillar and gap dimensions. These observations suggest that the transfer of the features from photomask to the silicon wafer, then to PDMS and finally to PMMA film could not be perfect due to a number experimental steps used during this sequence. It is stated that since the resolution of photolithography is determined by the wavelength of the UV light used, which is generally around 350 nm, the deviations in this scale become more apparent as the dimensions of the structures get smaller (Maalouf et al., 2008). Pillar constructs can be produced more accurately by electron beam lithography that offers higher resolution and quality compared to UV photolithography (McMurray et al., 2011). However, the discrepancy introduced in

the transfer process was not larger than 10% and this was satisfactory for the study performed.

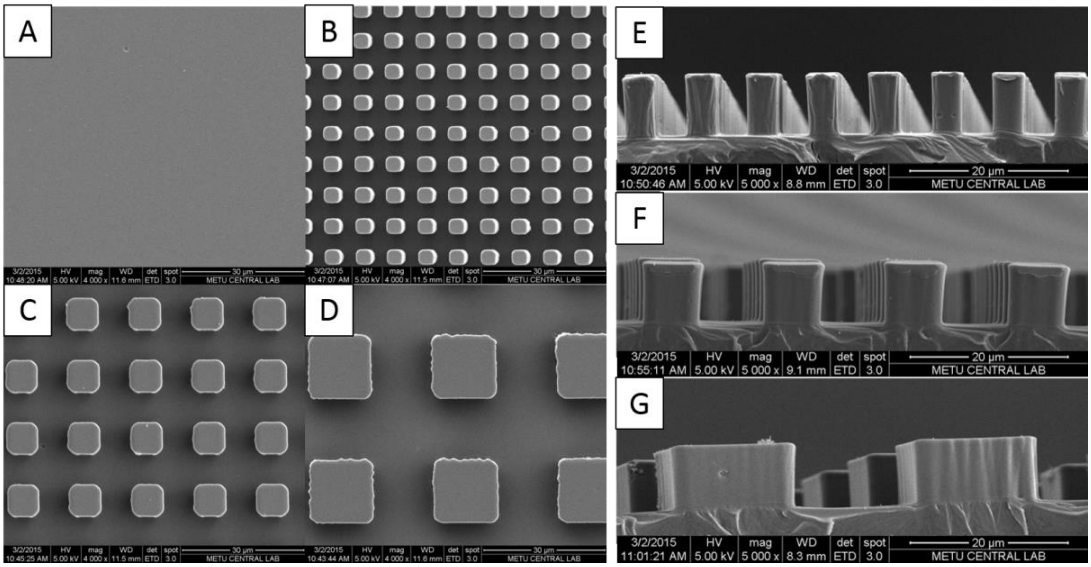

Figure 3.5. SEM micrographs of the pristine unpatterned and micropatterned PMMA films. (A) The top view of the unpatterned control, and (B, E) the top and side views of the P4G4, (C, F) P8G8, and (D, G) P16G16 surfaces. Scale bar on top view: 30 µm and on side view: 20 µm.

Table 3.2. Designed and obtained pillar dimensions of PMMA films

	Designed // Obtained		
Sample	**Pillar Area (μm^2)**	**Gap Length (µm)**	**Pillar Height (µm)**
P4G4	4x4//3.87 ± 0.08 x 3.83 ± 0.09	4//3.78 ± 0.08	8//7.57 ± 0.05
P8G8	8x8//7.74 ± 0.11 x 7.81 ± 0.14	8//7.49 ± 0.11	8//7.59 ± 0.03
P16G16	16x16//15.87 ± 0.22 x 15.63 ± 0.18	16//14.98 ± 0.14	8//8.17 ± 0.03

3.3.2. Water Contact Angle Measurements

It is known that the wettability of a surface depends on both the chemical composition such as the functional groups available and the topography including roughness and micro- and nanostructures (Blondiaux et al., 2009). In order to study the influence of roughness or patterns on the wettabilities of untreated and oxygen plasma treated PMMA films, contact angles (CA) of the substrates were measured (Fig. 3.6, Fig. 3.7, Table B.3). CA of untreated micropatterned substrates were much higher than that on the untreated smooth surface (Fig. 3.6.A-D), suggesting that the micropillar features decreased the wettabilities of the substrates. This was expected, because the surface texture, or roughness up to a certain value; is known to enhance the intrinsic hydrophobicity of substrates and used to produce superhydrophobic (CA > 150^{o}), highly water-repellent antifouling surfaces (Roach et al., 2008). This phenomenon is explained with the models of Wenzel and Cassie-Baxter, which emphasize the water droplet forming equilibrium shapes to minimize the changes in surface free energy at solid-air, solid-liquid and water-air interfaces resulting from surface texture (Shirtcliffe et al., 2005). The highest contact angle was observed on P4G4 ($131.7^{o} \pm 1.2^{o}$) while the lowest value was on P16G16 ($113^{o} \pm 1.2^{o}$), suggesting that the wettability decreases as the pillar and/or gap size decreases.

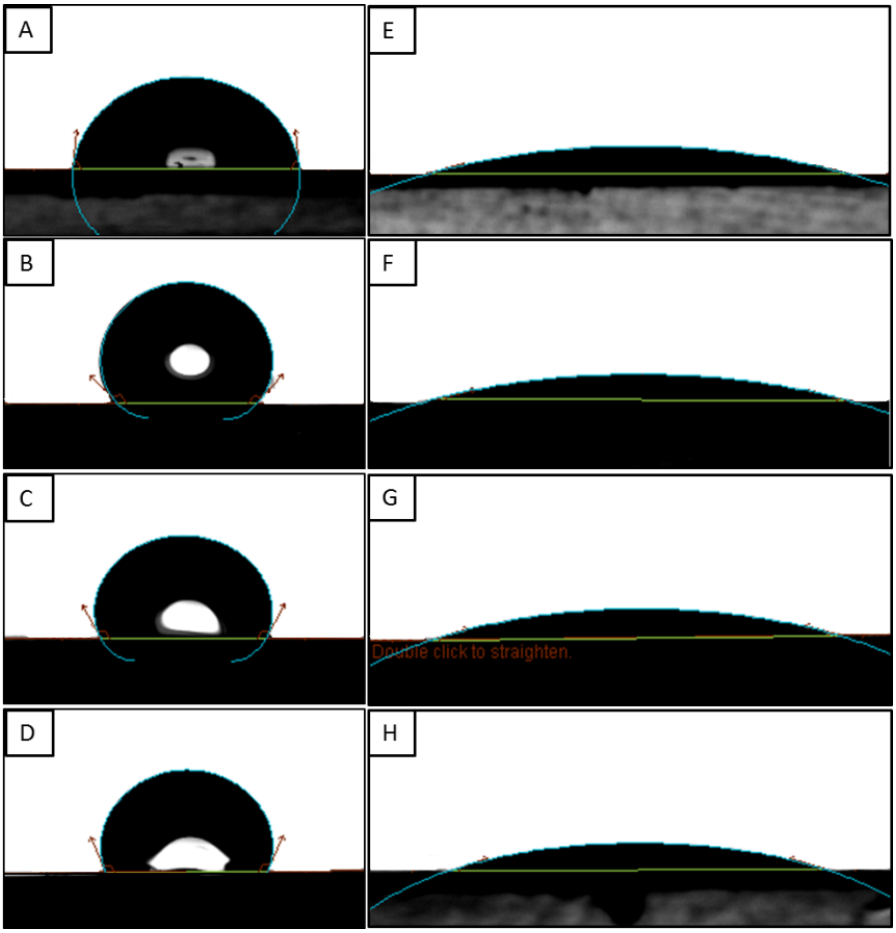

Figure 3.6. Water sessile drops on untreated and oxygen plasma treated samples. (A, E) unpatterned control, (B, F) P4G4, (C, G) P8G8 and (D, H) P16G16 surfaces.

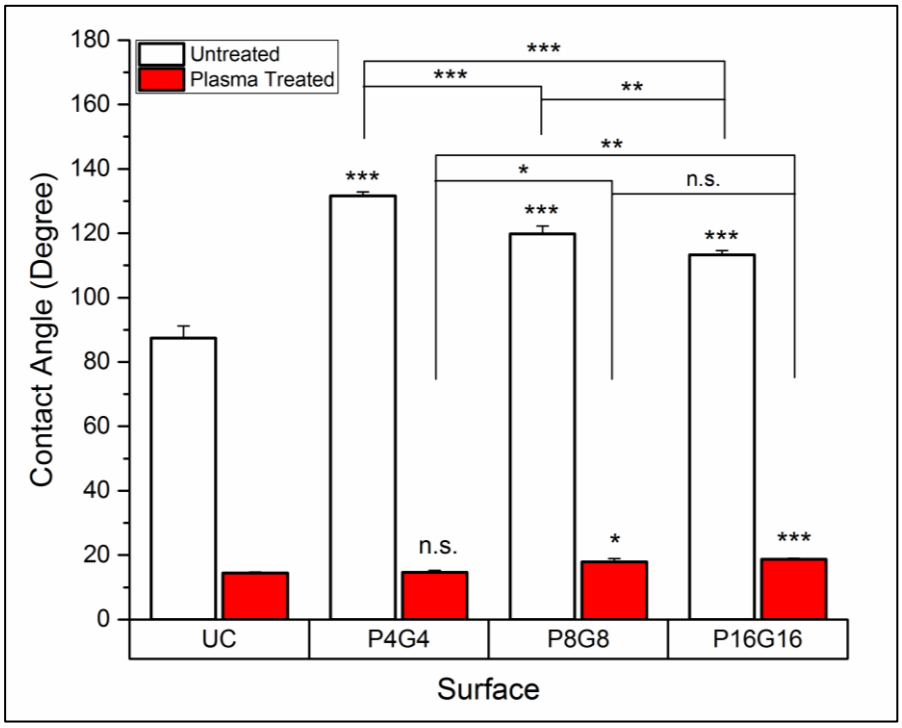

Figure 3.7. Water contact angles of untreated and oxygen plasma treated unpatterned control (UC) and micropatterned PMMA films. The data of water contact angle was shown as the mean ± SD for three determinations, *p < 0.05, **p < 0.01, and ***p < 0.001. Asterisks above the bars represent significance compared to the unpatterned counterpart. n.s: not significant.

On the plasma treated surfaces, water droplets spread immediately and wetted the surface completely (Fig. 3.6.E-H). This significant decrease upon plasma treatment can be attributed to the increase in the polar groups containing oxygen atoms (Chai et al, 2004). Upon plasma treatment, the increase in the contact angles with decrease in pillar/gap size observed on untreated surfaces disappeared and the contact angles did not change significantly among the substrates. This change of response could be explained with the difference in the states of untreated and plasma treated surfaces. On the untreated surfaces, the water droplet was probably in Cassie-Baxter state (Fig.1.12.c) where the droplet made incomplete contact with the patterned surface as

a result of air trapped between the liquid and the solid, and a contact angle larger than that on the unpatterned surface was obtained. He et al. (2014) proposed the following equations for Wenzel (Eqn. 14) and Cassie (Eqn. 15) states on micropillar decorated surfaces:

$$\cos Q_W = r \cos Q = \left(1 + \frac{4h/a}{\left(1+\frac{b}{a}\right)^2}\right) \cos Q \quad (14)$$

$$\cos Q_C = f\,(1 + \cos Q) - 1 = \frac{1}{\left(1+\frac{b}{a}\right)^2}(\cos Q + 1) - 1 \quad (15)$$

In the Wenzel equation, Q_W is the Wenzel contact angle on the patterned surface, r is the roughness factor (specific surface area) and h is the height of the pillars. In the Cassie equation, Q_C is the Cassie contact angle on patterned surface and f is the ratio of the solid to the liquid at the interface beneath the droplet. In both equations, a is the side length of the square pillars, b is the length of the interpillar gaps and Q is the contact angle on the smooth control surface. Wenzel equation (14) yielded a Q_W of 82^o while Cassie equation (15) yielded a Q_C of 137^o for the untreated P4G4 (h=8, a=4 and b=4) when Q was taken as 87^o (CA of the untreated smooth surface). The experimental contact angle for untreated P4G4 surface was $131.6^o \pm 1.25$, a value closer to the outcome of the Cassie equation (137^o), confirming that the water droplet was indeed in bridging (Cassie-Baxter) state. The Cassie equation proposed by He at el., however, does not explain the decrease observed in contact angles of the untreated samples with increasing pillar/gap dimensions. f values on P4G4, P8G8 and P16G16 surfaces are equal to each other as the b/a is constant for all surfaces, but the contact angle values were not. In order to formulate a more accurate relationship, Zheng et al. (2010) proposed the following equation, a modified version of the original Cassie-Baxter equation:

$$\cos Q^* = f\,(1-\frac{lcr}{S})(1+\cos Q)-1 \qquad (16)$$

where l_{cr} is a hypothetical constant and S is the shape dependent roughness scale. S was taken as a/4 for pillar structures that have square crosssections, where a is the side length of the square pillars. Based on this equation, it was shown that S value increases as the pillar and gap dimensions increase even when *f* remains constant; increasing S was shown to result in a lower contact angle on square prism micropillars as it can also be inferred from the equation 16.

On the plasma treated surfaces, water droplets were probably in Wenzel state (Fig.1.12.b), they completely filled the gaps between the pillars as a result of increased hydrophilicity of the surface. According to the Wenzel equation (14), r is calculated for P4G4, P8G8 and P16G16 surfaces as 3, 2 and 3/2, respectively. It can be inferred from the equation that when $Q < 90^o$, Q_W increases as r decreases. This explains the increase in contact angle from P4G4 (14.6 ± 0.6) to P16G16 (18.7 ± 0.2) for plasma treated surfaces. However, contact angles on all plasma treated surfaces were similar within ($\pm 3^o$) as the contact angle on the smooth control was very low (14.5 ± 0.2), indicating that surface features do not affect the water contact angle on hydrophilic surfaces as drammatically as on hydrophobic surfaces.

3.4. *In vitro* Studies

3.4.1. Characterization of Isolated Cells

The morphologies and expressions of surface markers of the cells isolated from dental pulps were studied in order to verify their mesenchymal stem cell nature. Confocal micrographs of the isolated cells are represented in Fig. 3.8. Isolated cells were expanded in DMEM:F12 growth medium on TCPs for 7 days and were observed to have a flattened, broad shape (Fig.3.8.B), consistent with the shapes of

the DPSCs isolated enzymatically and expanded in growth media with FBS reported by Khanna-Jain et al. (2012) and Yildirim et al. (2013). Even though the seeding density was quite low, cells covered almost the whole well of a 12 well plate over 7 days due to their very high proliferation rate.

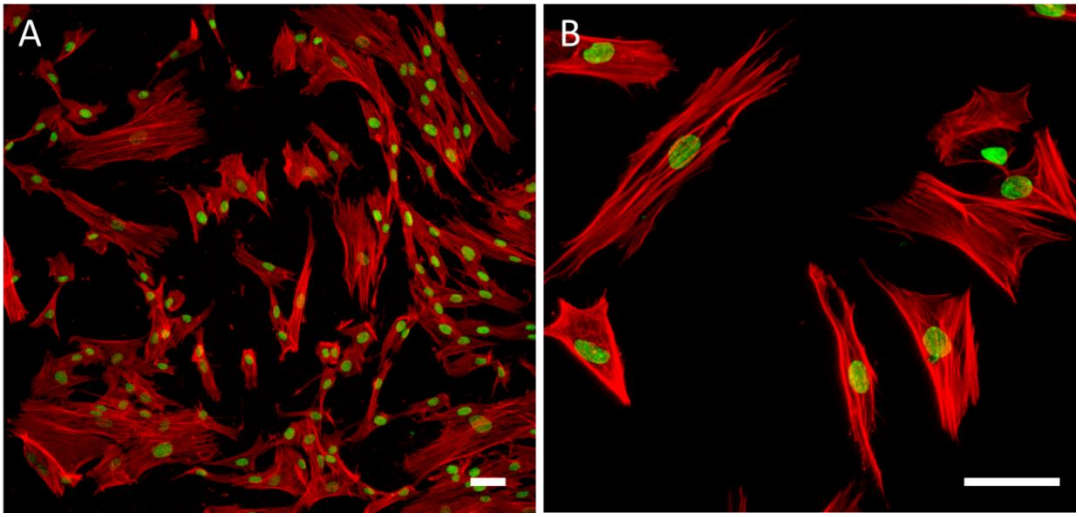

Figure 3.8. Confocal micrography of the isolated cells cultured on TCPs on Day 7. Magnification: (A) x100 and (B) x300. Red: Actin cytoskeleton (Alexa Fluor 488® conjugated phalloidin), green: Nucleus (DRAQ5). Cell seeding density: 2.5 x 10^3. Scale bar: 50 μm.

The Mesenchymal and Tissue Stem Cell Committee of the International Society for Cellular Theraphy (ISCT) proposes three criteria to define a cell as MSC: adherence to plastic, expression of specific surface antigens including CD105, CD90 and CD73, and multipotent differentiation potential (Dominici et al., 2006). Isolated cells were expanded in tissue culture flask in DMEM:F12 growth medium and analyzed using flow cytometry for the expression of surface markers CD105, CD90, CD45 and CD31. CD105 (SH2, endoglin) is a mesenchymal adhesion molecule and CD90

(Thy-1) is a surface protein speculated to be responsible for cell-cell and cell-ECM interactions (Deans et al., 2000; Lindroos et al., 2009). Hematopoetic CD45 (Leukocyte common antigen) and endothelial CD31 (PECAM) markers are absent on MSCs and are used as negative markers (Crisan et al., 2009). In order to detect any nonspecific interaction between the cell surface and the Fc (constant) region of the antibodies used, fixed cells were also incubated with the IgG1κ isotype control and the fluorescence intensity was compared with the unstained cells.

No nonspecific binding was detected as the fluorescence intensity of cells stained with isotype control highly overlapped (99.7%) with the instensity of unstained cells (Fig. 3.9.B). Isolated cells were found to be negative (<2%) for the markers CD45 (0.4%) and CD31 (0.3%) (Fig 3.9.C and D), while they displayed positive expression (>50%) for the mesenchymal markers CD105 (73.6%) and CD90 (100%) (Fig.3.9.E and F). The expression profiles were consistent with other studies reporting DPSCs positive for CD105 and CD90 but negative for CD31 and CD45 (Perry et al., 2008 & Khanna-Jain et al., 2012). A lower fraction of the total population was found to be positive for CD105 while all population was positive for CD90. The unusually low expression of CD105 was also observed in similar studies (Miura et al., 2003; Mokry et al., 2010 and Kanafi et al., 2013), and was explained with the presence of ectomesenchymal stem cells that share a common origin with neural crest cells and are negative for CD105 (Ibarretxe et al., 2012). The expression of CD105 by DPSCs was shown to increase with passage number (Kanafi et al., 2013).

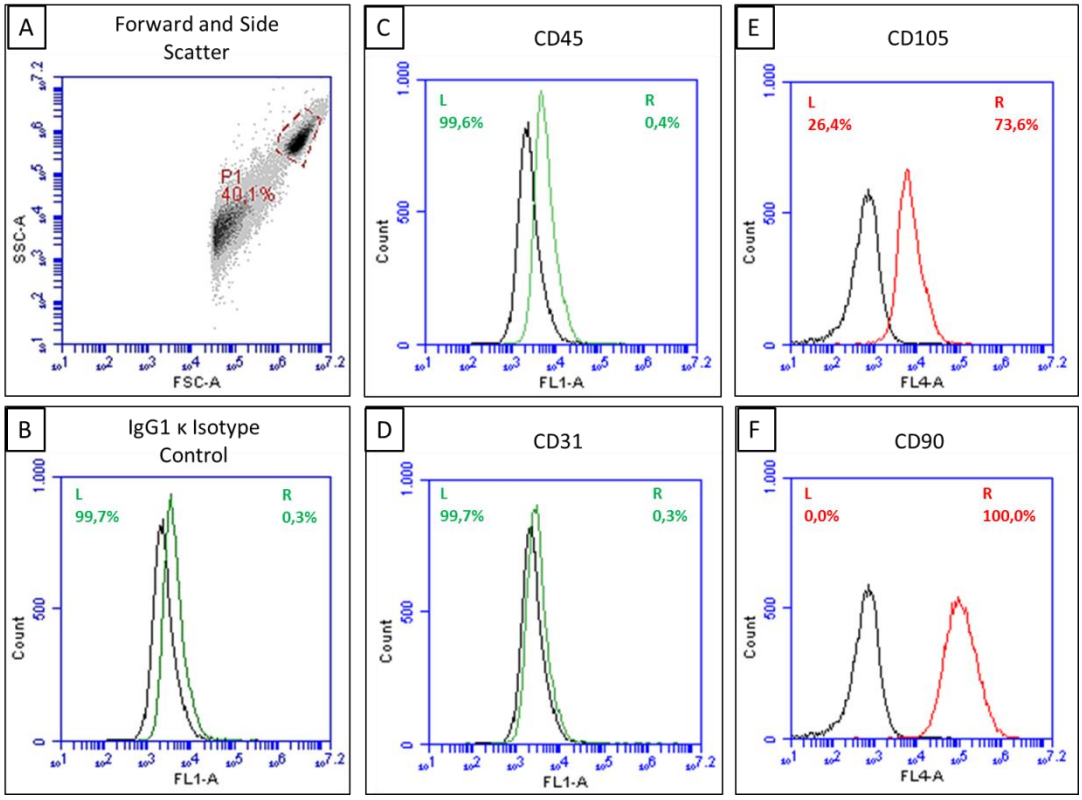

Figure 3.9. Flow cytometry analysis of the expression of surface markers by DPSCs. (A) Gating of the cell population on the forward and side scatter of particles. Histograms of the cells stained with (B) antimouse IgG1 isotype control, (C) CD45, (D) CD31, (E) CD105 and (F) CD90 antibodies. Black: Unstained control, Green: negative markers, Red: positive markers.

3.4.2. Attachment of DPSCs on Substrates

Attachment of DPSCs onto PMMA films was determined by Alamar Blue cell viability assay 16 h after cell seeding (Fig.3.10, Table B.4). Number of cells attached on PMMA substrates, particularly on pristine films, was significantly lower than on TCPs. Only a quarter of the number of cells seeded managed to attach on pristine smooth surface, and micropillar features increased cell attachment remarkably. Oxygen plasma treatment significantly increased the number of cells attached on all

substrates (except P4G4). The cell numbers on plasma treated smooth surface was 5 fold higher than on the untreated surface. For the untreated samples, the highest attachment was observed on P4G4, while there was no significant difference in the number of cells attached on P8G8 and P16G16. For the untreated patterned samples, increased cell attachment with decreasing pillar and gap size was observed. Meanwhile, there was no significant difference between plasma treated smooth, P4G4 and P8G8 surfaces; attachment on P16G16 was slightly higher. It can, therefore, be proposed that surface topography and chemistry have equal effect on cell attachment if the roughness is less (as in P4G4), and the surface chemistry has a stronger influence than topography if the pattern dimensions are larger.

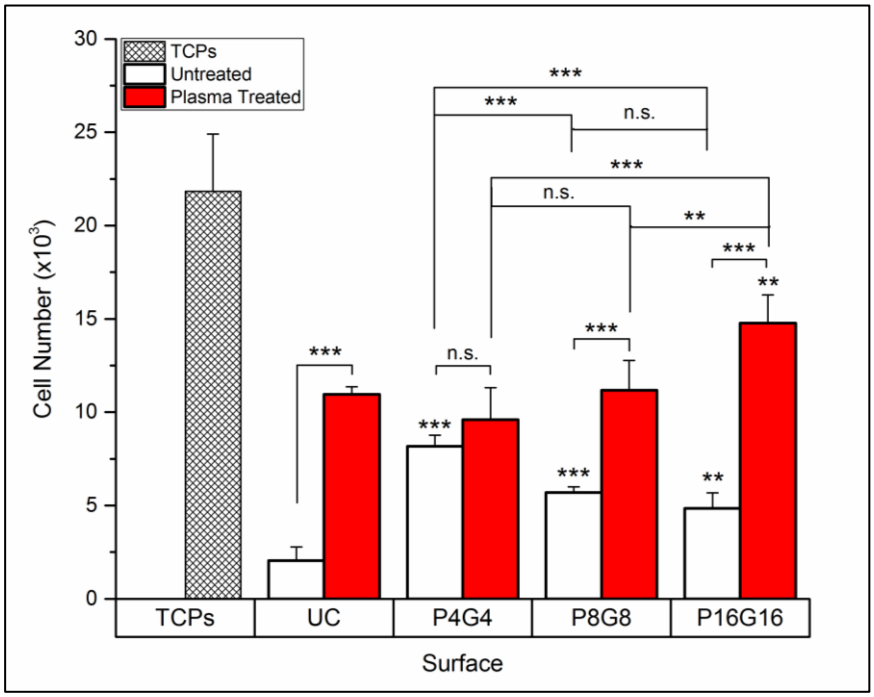

Figure 3.10. DPSC attachment on untreated and oxygen plasma treated PMMA films. Time: 16h. Cell seeding density: 2 x 10^4 per sample. Data represent the mean ± SD of three replicates, *p < 0.05, **p < 0.01 and ***p < 0.001. Asterisks above the bars represent significance compared to the unpatterned control. n.s.: not significant.

Cell adhesion mainly depends on the proteins adsorbed onto the substrate surface. Therefore, higher number of attached cells on the plasma treated surfaces suggests that the type and conformation of the proteins adsorbed onto the hydrophilic surface from the culture medium promoted cell adhesion. Antibodies specific to the Arg-Gly-Asp (RGD) tripeptide were shown to bind preferentially to the proteins adsorbed onto the hydrophilic surfaces. This observation indicates that the cell adhesive sequences tend to be exposed more on hydrophilic surfaces (Grinnell et al., 1982). The number of attached L929 murine fibroblast cells was shown to be significantly higher on oxygen plasma treated polystyrene (PS), PMMA and PMMA/PS blends with water contact angles of 37^{o}, 45^{o} and 59^{o} compared to the untreated controls (Borges et al., 2013). In another study, the highest attachment of 3T3 fibroblasts was reported to be on oxygen plasma treated PMMA surface with a water contact angle of 35^{o}, however, the attachment level decreased when the contact angle was further decreased to 27^{o} (Ozcan et al., 2008). In these studies, the water contact angles upon oxygen plasma treatment were in the range 40^{o}-70^{o}, which was reported to be the optimum wettability for mammalian cells to adhere on polymeric surfaces (Lee et al., 1998) but in the current study the contact angles of the oxygen plasma treated surfaces were in the range 14^{o}-19^{o}. There are however studies that reported significant increases (6-fold) in the attachment of B65 nerve cells on super-hydrophilic surfaces (10^{o}) (Khorasani et al., 2008). Another study carried out with oxygen plasma treated hexamethyldisiloxane (HMDSO) surfaces showed that the competitive adsorption of fibronectin and the initial attachment of MC3T3-E1 osteoblast cells were the highest on the most hydrophilic surface (CA: 0^{o}), and the cell attachment decreased as the contact angle increased (106^{o}) (Wei et al., 2009). These studies show that cell attachment depends on the cell type and surface chemistry as well as the hydrophilicity.

Another parameter that was observed to influence the cell attachment was the surface features. Several other research groups have also reported increase in cell attachment on 3D surface features. For example, primary astrocyte cells were shown to have a

higher tendency to attach on the silicon surfaces decorated with 0.5 μm wide columns with 1 μm spacing rather than the unpatterned surface (Craighead et al., 1998). Similarly, rat cardiac myocytes were found to exhibit enhanced attachment on micropegged and microgrooved silicone substrates (Deutsch et al., 2000). Su et al. (2009) reported increased attachment of mouse bone marrow stromal cells onto the silicon-based substrates decorated with 1 μm wide micropillars separated by 9 μm long gaps and suggested that the surface features increase the total contact area available for the interactions between the cell and the substrate through focal adhesions. Indeed, several studies reported that micro- and nanoscale topography enhanced the formation and maturation of focal adhesions. For instance, focal adhesion maturation and actin polymerization of murine mesenchymal stem cells were found to be promoted on fibronectin coated PDMS surfaces decorated with 2 μm wide lattice patterns with 3 μm intervals, and the pillar tops and edges were shown to be the regions where the highest number of focal adhesion contacts were made (Seo et al., 2011). These observations could explain the attachment of highest number of cells on the untreated P4G4 surface, on which the number of pillars a cell could interact was the highest compared to the other patterned samples.

3.4.3. Changes of Cell Conformation on Micropatterned Surfaces

In this section, DPSCs were cultured on pristine and oxygen plasma treated micropatterned substrates and the cells and their nuclei were visualized using SEM and confocal microscopy. The influence of dimensions and hydrophilicity of micropillars on the morphologies of mesenchymal stem cells was investigated and conformational changes in cell cytoskeleton and nuclei were quantified by the digital analysis of the fluorescent micrographs of the cells.

3.4.3.1. SEM Analysis

SEM micrographs of the DPSCs cultured on pristine and oxygen plasma treated micropillared PMMA substrates are presented (Fig.3.11-Fig.3.15). Fig. 3.11 shows DPSCs cultured on untreated and plasma treated flat substrates on days 1, 7, 14 and 21 and reveals the temporal effects of the surface hydrophilicity on the cells. On day 1, cells are seen attached on both untreated and treated unpatterned smooth surfaces that had water contact angles of 84^{o} and 14^{o}, respectively. On the untreated surface, cells spread less and exhibited a compact body (that can be seen as lighter region pointed out with red arrow) compared to oxygen plasma treated samples (Fig. 3.11.A). At the leading edge lamellipodia were extended (pointed out with blue arrow) with little or no filopodia. On the oxygen plasma treated surface, on the other hand, cells were observed to have a well spread morphology with numerous long filopodia (pointed out with yellow arrow) protruding from the lamellipodia (pointed out with blue arrow) (Fig.3.12.E). Filopodia are rich in activated cell adhesion molecules such as integrins and cadherins, and enable cells to probe their environment and migrate by acting as sites for signal transduction (Mattila and Lappalainen, 2008). Thus, a higher number of filopodia on the plasma treated surface suggests enhanced adhesion and migration of the cells compared to that on the untreated smooth surface. A similar influence of increased hydrophilicity on the spreading of fibroblasts and the number of filopodia was reported on thermally oxidized silicon surfaces. Cells grown on hydrophilic surfaces were reported to spread well and exhibit areas of dense filopodia extensions while the cells grown on hydrophobic counterparts were much smaller and had less filopodia (Ranella et al., 2010). Similarly, Vero fibroblasts grown on oxygen plasma functionalized PHBV surfaces were shown to have thicker and a higher number of filopodia compared to untreated control surface (Lucchesi et al., 2008). On day 7, cell spreading on untreated flat substrate was observed to increase (Fig.3.11.B), even though there still were a few unorganized cells. On plasma treated flat surface (Fig.3.11.F), the cell density was increased significantly and a relatively elongated and aligned

morphology was noticed. On day 14, both untreated and plasma treated surfaces were completely covered by cells so that distinguishing individual cells was not possible. Cells on the untreated surface were observed to extend a thin mesh of filopodia (Fig. 3.11.C) similar to the cell protrusions on plasma treated counterpart (Fig.3.11.G), suggesting that the cell-surface interactions on this surface were improved. The change in the cell density and spreading on untreated surface from day 7 to day 14 could be explained with the interactions of cell surface receptors with the proteins of the extracellular matrix that was laid down by the cells over the two weeks. On day 21, both surfaces were covered with cells. On the plasma treated surface (Fig.3.11.H), formation of a thick cell sheet that started to peel off from the surface was apparent because the surface probably became over confluent.

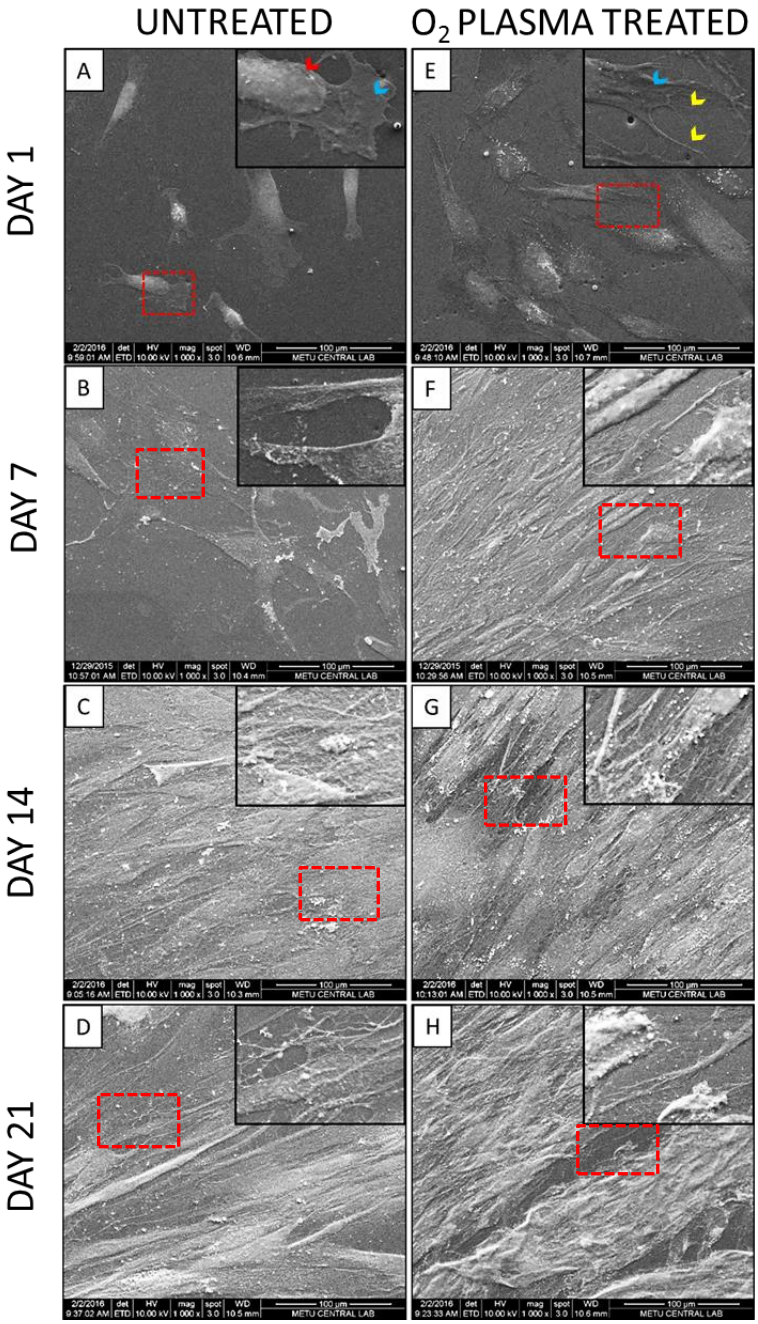

Figure 3.11. SEM micrographs of DPSCs on unpatterned PMMA films. Cells on untreated and oxygen plasma treated surfaces on (A, E) day 1, (B, F) day 7, (C, G) day 14, and (D, H) day 21. Magnification: X1000. Scale bar: 100 μm. The upper right inlets show the images of a higher magnification (X4000) of the regions enclosed in red boxes. Cell seeding density: 7.5 x 10^3 per sample.

On the micropatterned surfaces, cells were observed to exhibit distinct morphologies and spreading behavior that varied with surface hydrophilicity and the pillar/gap dimensions. The overall observation was that the pattern dimensions and hydrophilicity determined the positioning of cells; either on pillar tops or on the substrate floor between the pillars, and this resulted in morphological differences. On day 1, cells on untreated P4G4 surface (Fig. 3.12.A) were seen located on the pillar tops and had a bulkier appearance than the cells grown on smooth control. Cell bodies were observed to bridge over the interpillar spaces (pointed out with yellow arrow) and the cell protrusions at the leading edge were extended from above downward to the substrate floor (pointed out with red arrow). On plasma treated P4G4 (Fig.3.12.D), however, most of the cells penetrated into the interpillar gaps and elongated while a few cells adhered to the top of the pillars and extended a single long protrusion through the space between pillars. A large portion of the cell bodies were squeezed between the pillars (pointed out with yellow arrow), and their lamellipodia and filopodia were extended to the pillar tops (pointed out with red arrow). The same difference in the positioning of the cell bodies was also observed between untreated and plasma treated P8G8 surfaces. The cells on untreated P8G8 surface (Fig.3.12.B) placed their bodies on the pillar tops (pointed out with yellow arrow) and extended their lamellipodia (with no filopodia) to the floor of the gaps (pointed out with red arrow). They bridged a lower number of pillars compared to the untreated P4G4 surface since the interpillar distance was twice that of the P4G4. Cells on plasma treated P8G8 surface (Fig.3.12.E) inserted their bodies between the pillars (pointed out with yellow arrow) and stretched their lamellipodia with thin, long filopodia pointing towards the side surfaces of the pillars (pointed out with red arrow). Apparently, the interpillar distance on P16G16 surfaces was too high for the cells to suspend themselves on the pillar tops, therefore, they were positioned on the floor. On untreated P16G16 surface (Fig.3.12.C), cells were observed to probe pillar tops with cytoskeletal protrusions (pointed out with yellow arrow) while many cells on the plasma treated P16G16 surface (Fig.3.12.F) spread freely without even touching the pillars.

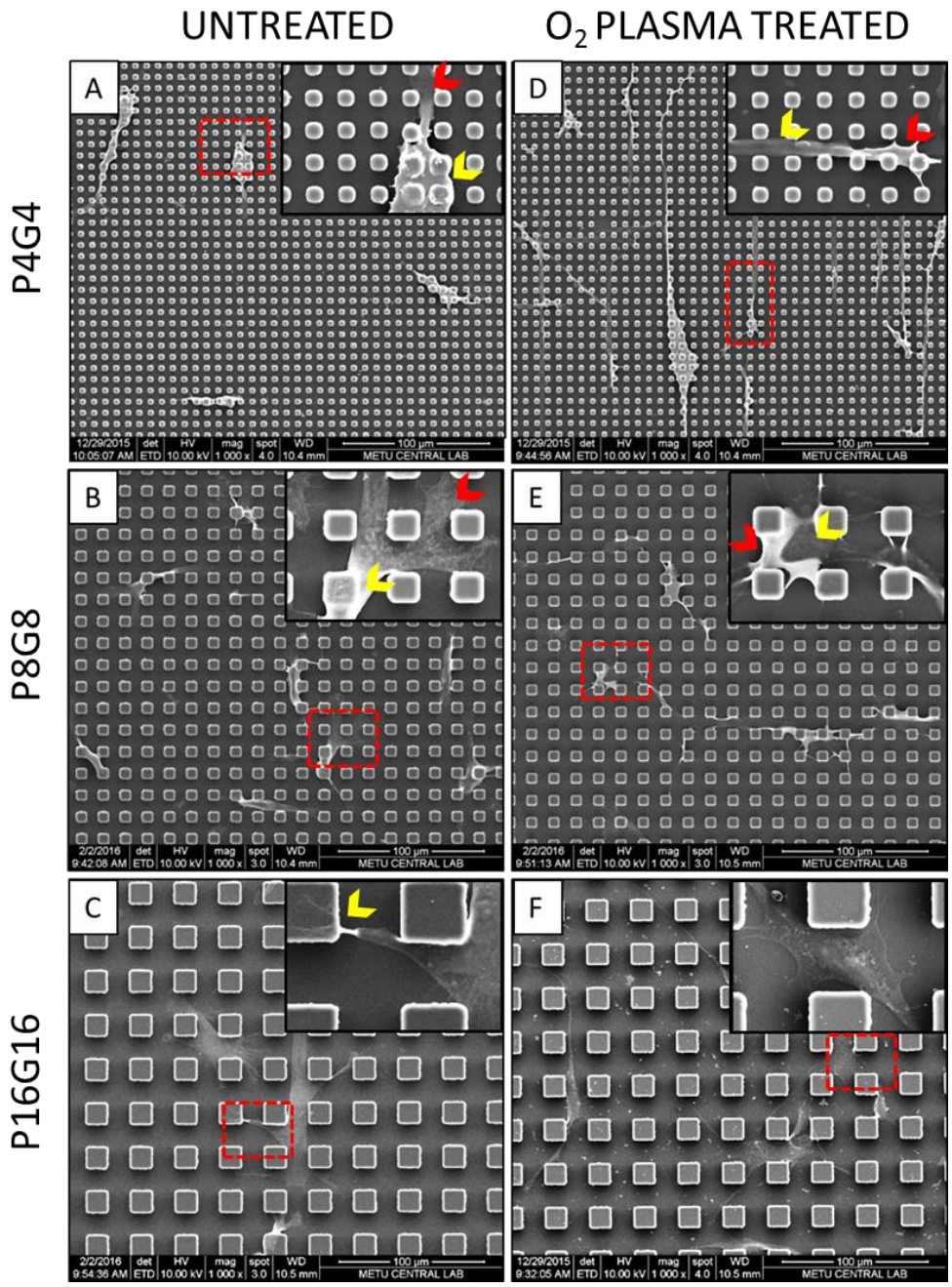

Figure 3.12. SEM micrographs of DPSCs on micropatterned PMMA films on Day 1. Cells on untreated and oxygen plasma treated (A, D) P4G4, (B, E) P8G8 and (C, F) P16G16 surfaces. Magnification: X1000. Scale bar: 100 µm. The upper right inlets show the images of a higher magnification (X4000) of the regions enclosed in red boxes. Cell seeding density: 7.5 x 10^3 per sample.

On day 7, cells on the untreated P4G4 surface (Fig.3.13.A) were still located at the pillar tops but lost their bulky appearance and exhibited a highly elongated morphology by extending their bodies perpendicularly or diagonally. On the plasma treated P4G4 surface (Fig.3.13.D), however, cells invaded the interpillar spaces with their protrusions attached to the side walls of the pillars. Cells on untreated P8G8 (Fig.3.13.B) surface were also seen to attach to the side surfaces of the pillars and suspend themselves by stretching out diagonally over the interpillar space. Since a diagonal line between two pillars is the largest interpillar distance on micropillared surfaces, cells might specifically elongate diagonally in order to minimize their contact with the substrate material. On plasma treated P8G8 (Fig.3.13.E), however, cells spread well on the substrate floor and stretched their lamellipodia towards the side walls of the pillars. Cells on untreated P16G16 surface (Fig.3.13.C) were observed to start climbing up the pillars with their bodies stretched between the pillars and substrate floor and their extensions suspended between the pillars. On plasma treated P16G16 (Fig.3.13.F), the interaction between the cells and pillars was still minimum and the cells proliferated on the substrate floor between the pillars. The difference in the positioning of the cell bodies between the untreated and plasma treated P4G4 and P8G8 surfaces can be explained with the hydrophilicity of surface that was shown to influence cell adhesion and spreading on the unpatterned substrates (Fig.3.12.A-H). Cell location on pillar tops with the untreated micropatterned surfaces suggests that cells try to minimize contact with the hydrophobic substrate material by suspending a part of their body in the air over the interpillar floor. A similar observation was made by Papenburg et al. (2010) with myoblast cells cultured on hydrophobic PDMS (C.A.: ~120^{o}) and relatively hydrophilic PLLA (C.A.:~70^{o}) substrates decorated with micropillar structures. Cells were shown to remain on the pillar tops of the PDMS and elongate by bridging over to anchor adjacent pillars separated by 5 μm gaps, in order to minimize contact with the hydrophobic substrate. On PLLA substrates, on the other hand, cells were observed to grow on the underlying substrate surface.

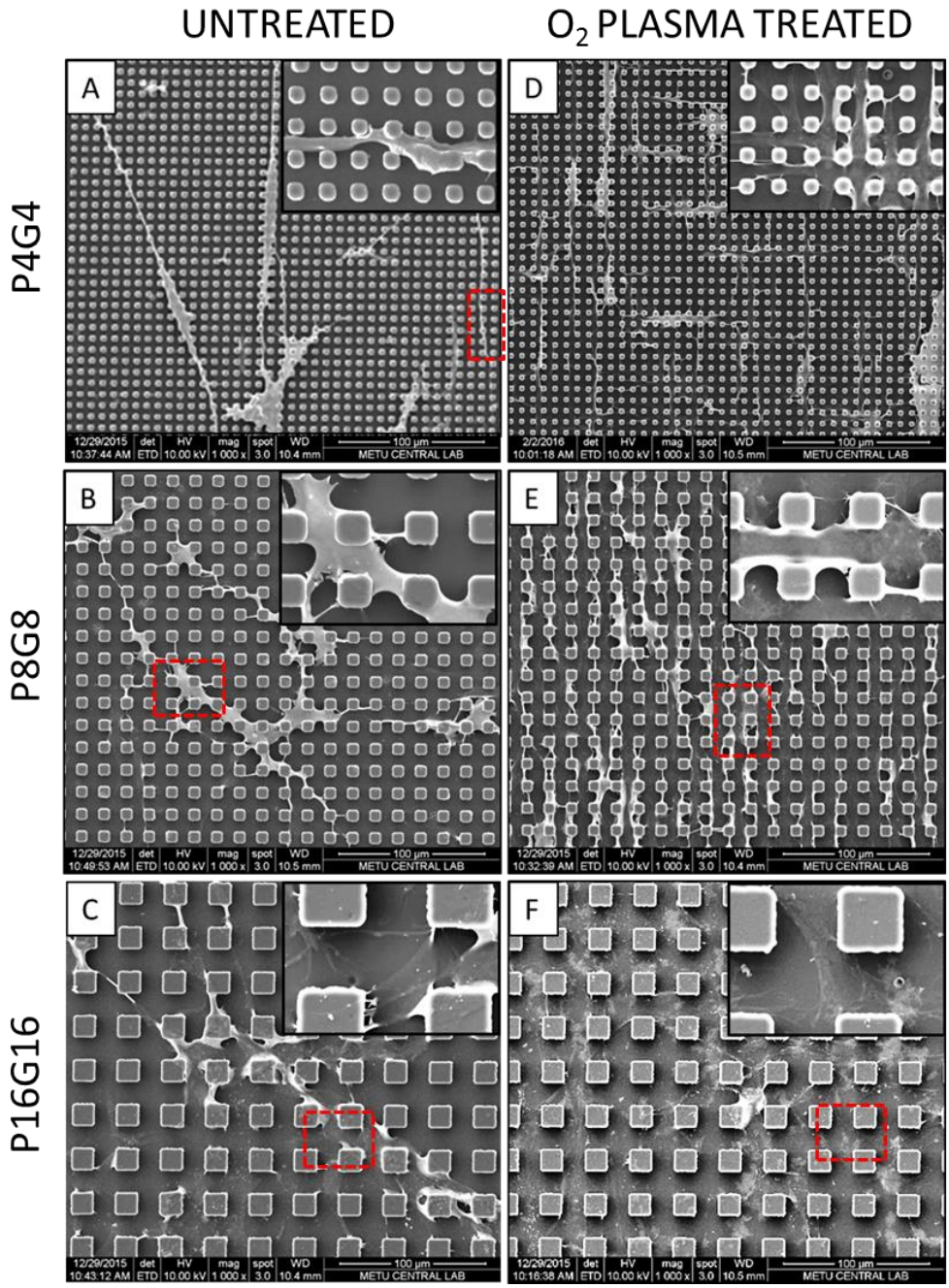

Figure 3.13. SEM micrographs of DPSCs on micropatterned PMMA films on Day 7. Cells on untreated and oxygen plasma treated (A, D) P4G4, (B, E) P8G8 and (C, F) P16G16 surfaces. Magnification: X1000. Scale bar: 100 µm. The upper right inlets show the images of a higher magnification (X4000) of the regions enclosed in red boxes. Cell seeding density: 7.5 x 10^3 per sample.

On day 14, cell patches had formed on the pillar tops of untreated P4G4 (Fig.3.14.A) and P8G8 (Fig.3.14.B) surfaces as a result of increased cell number. Interestingly, similar cell patches were also observed on plasma treated P4G4 (Fig.3.15.D) and P8G8 (Fig.3.14.E). When viewed more closely with the plasma treated samples, it can be seen that the substrate floor was also covered with cells, indicating that cells first reached confluency between the pillars and then started occupying the pillar tops in need for more space to proliferate. More surprisingly, cells on the untreated P16G16 surface (Fig.3.14.C) also formed patches on the top of the pillars as well as lying on the ground of interpillar spaces, which was not observed on days 1 and 7. Apparently, increased spreading of cells and secretion of ECM over time enabled them to stretch through the large interpillar distances of P16G16. On plasma treated P16G16 (Fig.3.14.F), however, cells were observed to cover the interpillar spaces and the pillar tops completely but did not bridge the gaps. Instead, pillars were encapsulated by the cell bodies. This observation suggested that bridging pillars separated by 16 μm gaps was still difficult feat for the cells and they instead spread over the solid surface as long as the surface chemistry promoted adhesion. On day 21, the general appearance of the cells on the substrates (Fig. 3.15) did not change significantly. The major difference was the size of cell patches on micropatterned surfaces, which grew larger as a result of increased cell number. Moreover, cells on P4G4 surfacea (Fig.3.15.A and D) were observed to form large cell patches that were highly aligned to each other. Cell alignment is typically observed on anisotropic nano- or microscale surface features such as grooves. For instance, osteoblast cells were shown to align to the microgrooves (width: 1-6 μm, depth: 1.6 μm) of the silicone surfaces (Hasirci and Kenar, 2006). The pillar structures in this study, however, were ordered isotropically and still observed to cause cell alignment on day 28 but not at earlier time points. The same observation was also made on the unpatterned surfaces (Fig.3.11.D and H), suggesting that the alignment at confluency is a trait of DPSCs. Since P4G4 surfaces resemble the unpatterned surface the most because of having the narrowest gaps among the micropatterned surfaces, it did not restricted cell alignment as other micropillared surfaces did.

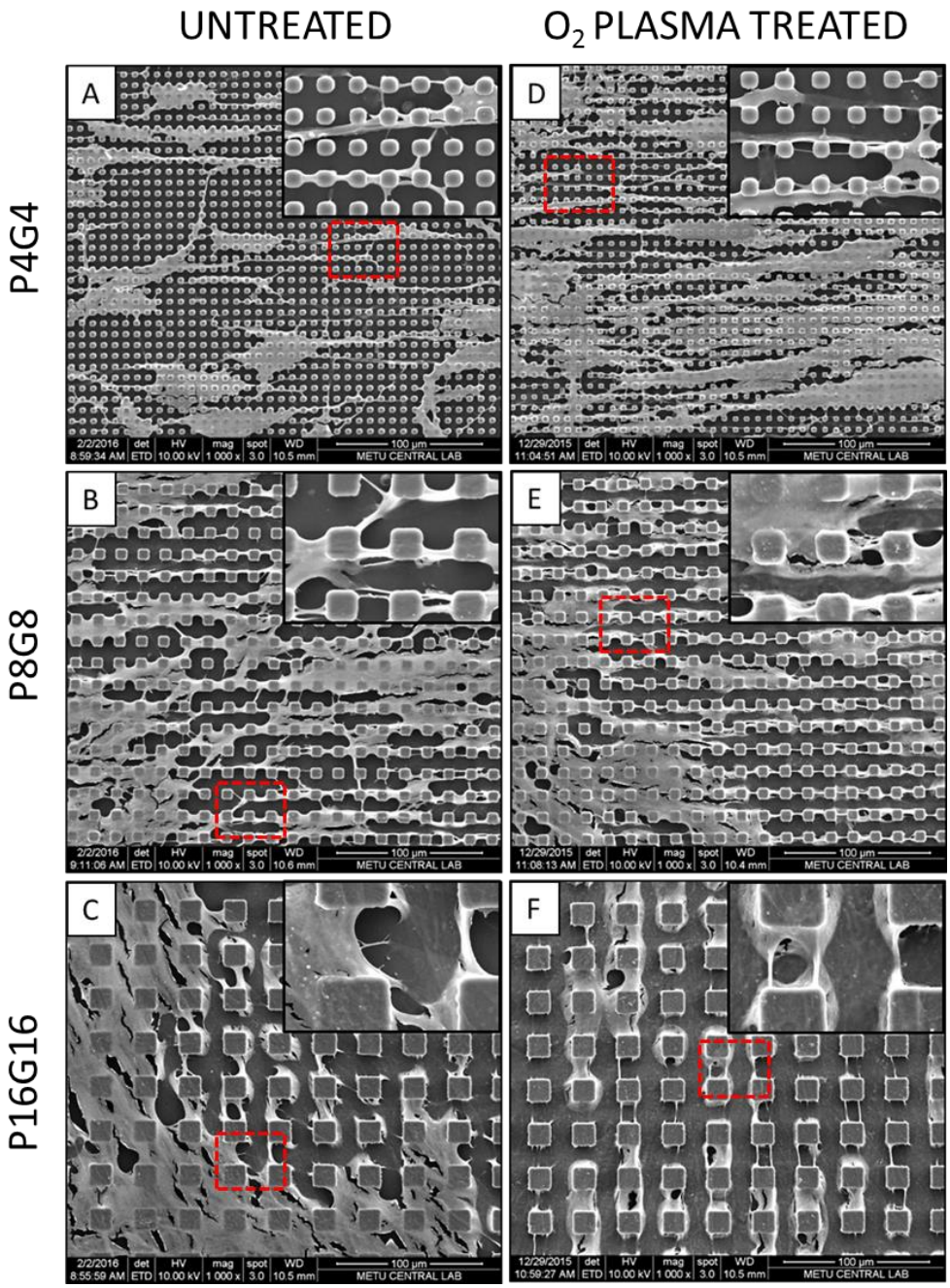

Figure 3.14. SEM micrographs of DPSCs on micropatterned PMMA films on Day 14. Cells on untreated and oxygen plasma treated (A, D) P4G4, (B, E) P8G8 and (C, F) P16G16 surfaces. Magnification: X1000. Scale bar: 100 µm. The upper right inlets show the images of a higher magnification (X4000) of the regions enclosed in red boxes. Cell seeding density: 7.5 x 10^3 per sample.

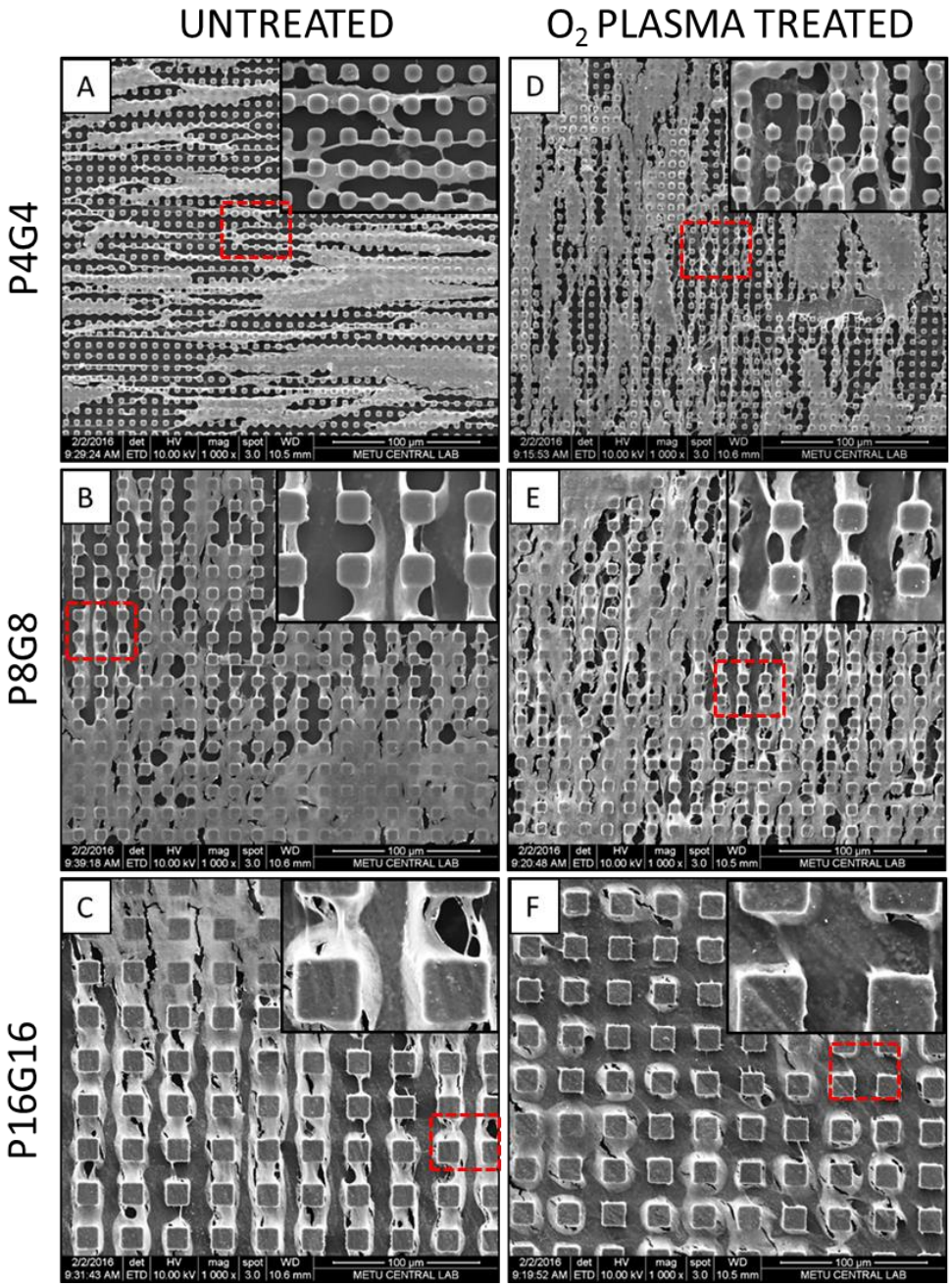

Figure 3.15. SEM micrographs of DPSCs on micropatterned PMMA films on Day 21. Cells on untreated and oxygen plasma treated (A, D) P4G4, (B, E) P8G8 and (C, F) P16G16 surfaces. Magnification: X1000. Scale bar: 100 µm. The upper right inlets show the images of a higher magnification (X4000) of the regions enclosed in red boxes. Cell seeding density: 7.5 x 10^3 per sample.

3.4.3.2. Confocal Microscopy

3.4.3.2.1. Imaging of Cells by Confocal Microscopy

Confocal micrographs of the DPSCs cultured on unpatterned smooth PMMA substrates for 4 weeks are presented in Fig. 3.16. On day 1, cells on the plasma treated substrate (Fig.3.16.F) were distributed individually and displayed a well spread, relatively more elongated morphology than on the untreated counterpart. Multinucleated cell clusters observed on the untreated surface (Fig.3.16.A) indicate the lack of separation and spreading of the cells. On day 3, there were no multinucleated cell clusters (Fig.3.16.B) and cells started to migrate and spread. There were more cells on the plasma treated surface on day 3, and these cells displayed a higher elongation than on untreated counterpart. As the time progressed the difference in cell numbers between the untreated and oxygen plasma treated samples decreased. On days 14 and 21, covering of all the surface and confluency was observed. Cells got oriented on both untreated and plasma treated surfaces and their nuclei were distinctly elliptical.

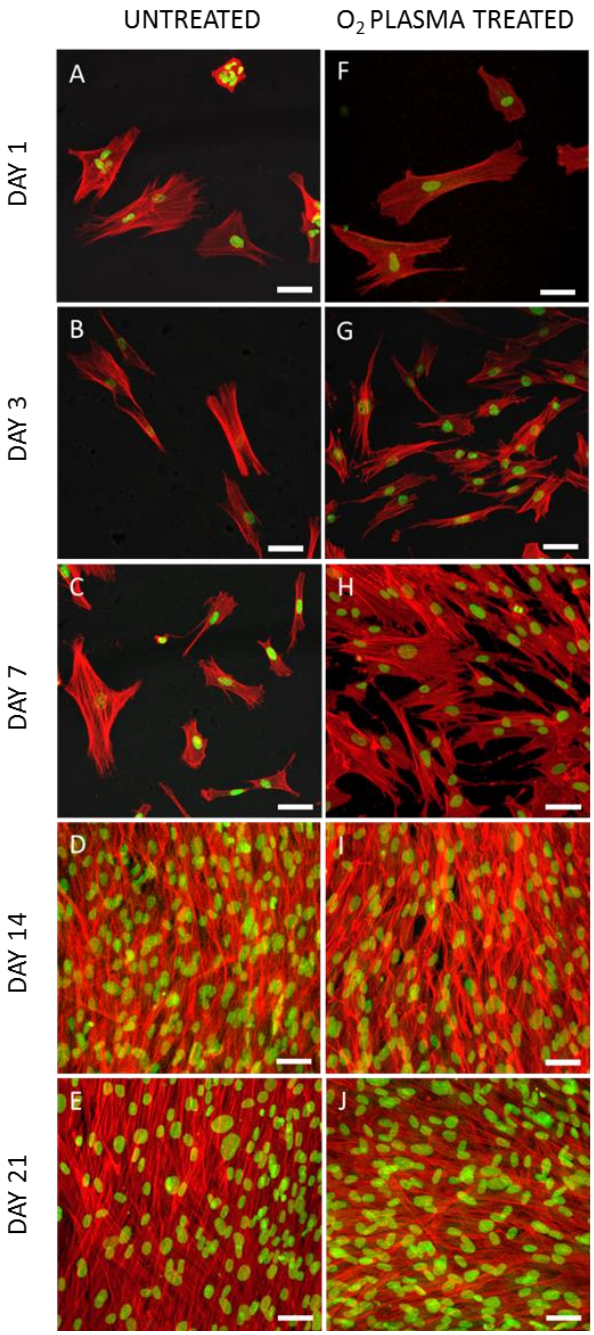

Figure 3.16. Confocal micrographs of the DPSCs on unpatterned PMMA films. Cells on untreated and oxygen plasma treated on (A, E) day 1, (B, F) day 3, (C, G) day 7, (D, H) day 14 and (E, J) day 28. Green: Nucleus (DRAQ5), red: Actin cytoskeleton (Alexa Fluor 488® conjugated phalloidin). Cell seeding density was 2.5 x 10^3 per sample. Scale bar: 50 μm.

On the micropatterned substrates, cells exhibited remarkable deformations ranging from extensively elongated to highly branched. These characteristic morphologies were found to depend on the pillar/gap dimensions. The general observation on day 1 (Fig.3.17) was that the cells on the untreated surfaces were larger and spread on the pillar tops while upon plasma treatment they placed themselves in between the pillars and get branched as the cell body thickness conformed to the gap dimensions. On day 3, cells on the untreated substrates started to spread and deform. Cells on the untreated P4G4 surface (Fig.3.18.A) were still located on the pillar tops but displayed relatively higher elongation compared to day 1, while the cells on the plasma treated counterpart were positioned between the pillars and displayed a highly elongated morphology. Contrary to day 1, most of the cells on untreated P8G8 (Fig.3.18.B) and P16G16 (Fig. 3.18.C) introduced their bodies between the pillars and displayed a branched morphology on day 3. The major difference between the untreated and plasma treated P8G8 surfaces was the degree of spreading. Cells on the untreated surface (Fig.3.18.B) were observed to have very thin protrusions while the branches of the cells on plasma treated surface (Fig.3.18.E) were fully conformed to the gaps. Micrographs of the cells on day 7 were the most explicit visual proof of the influence of pattern and gap dimensions on the cell morphology and showed that the conformational changes in the cell bodies were not transient. The majority of the cells on untreated P4G4 surface (Fig.3.19.A) were located between the pillars and displayed an elongated morphology that resembles cells on plasma treated P4G4 on day 3. A network of highly elongated cells that invaded the interpillar spaces of the plasma treated P4G4 surface (Fig.3.19.D) was observed. Spreading of the cells on the untreated P8G8 (Fig.3.19.B) and P16G16 (Fig.3.19.C) surfaces increased compared to day 3, and the majority of the cells had a branched morphology with three or more extensions probing the gaps and pillar walls. On plasma treated P8G8 (Fig.3.19.E) and P16G16 (Fig.3.19.F), cells exhibited a branched morphology similar to the cells on pristine counterparts but the extent of branching was still higher on hydrophilic surfaces, particularly on plasma treated P16G16.

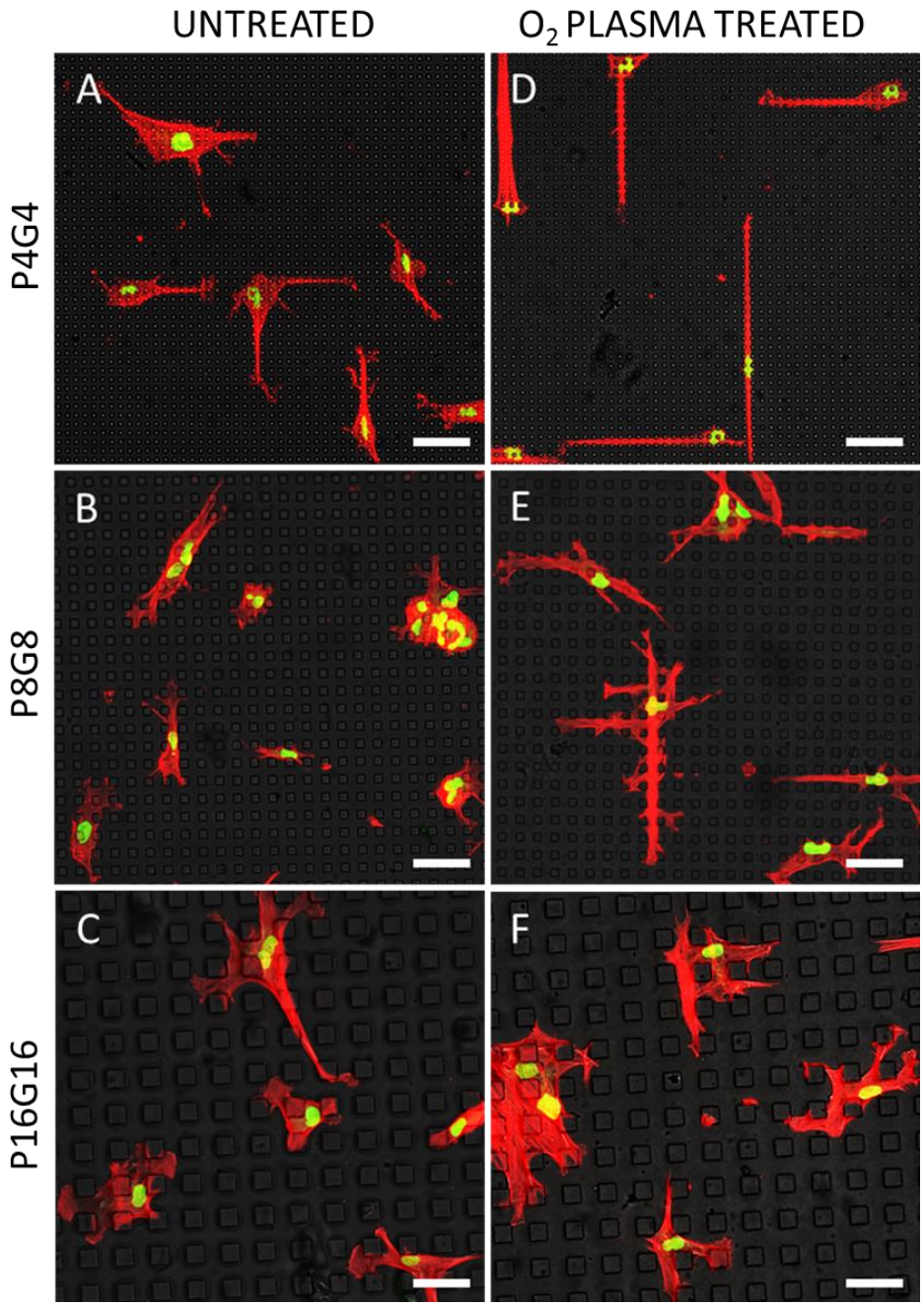

Figure 3.17. Confocal micrographs of the DPSCs on micropatterned PMMA films on Day 1. Cells on untreated and oxygen plasma treated (A, D) P4G4, (B, E) P8G8 and (C, F) P16G16. Green: Nucleus (DRAQ5), Red: Actin cytoskeleton (Alexa Fluor 488® conjugated phalloidin). Background: Transmission channel. Cell seeding density: 2.5 x 10^3 per sample. Scale bar: 50 μm.

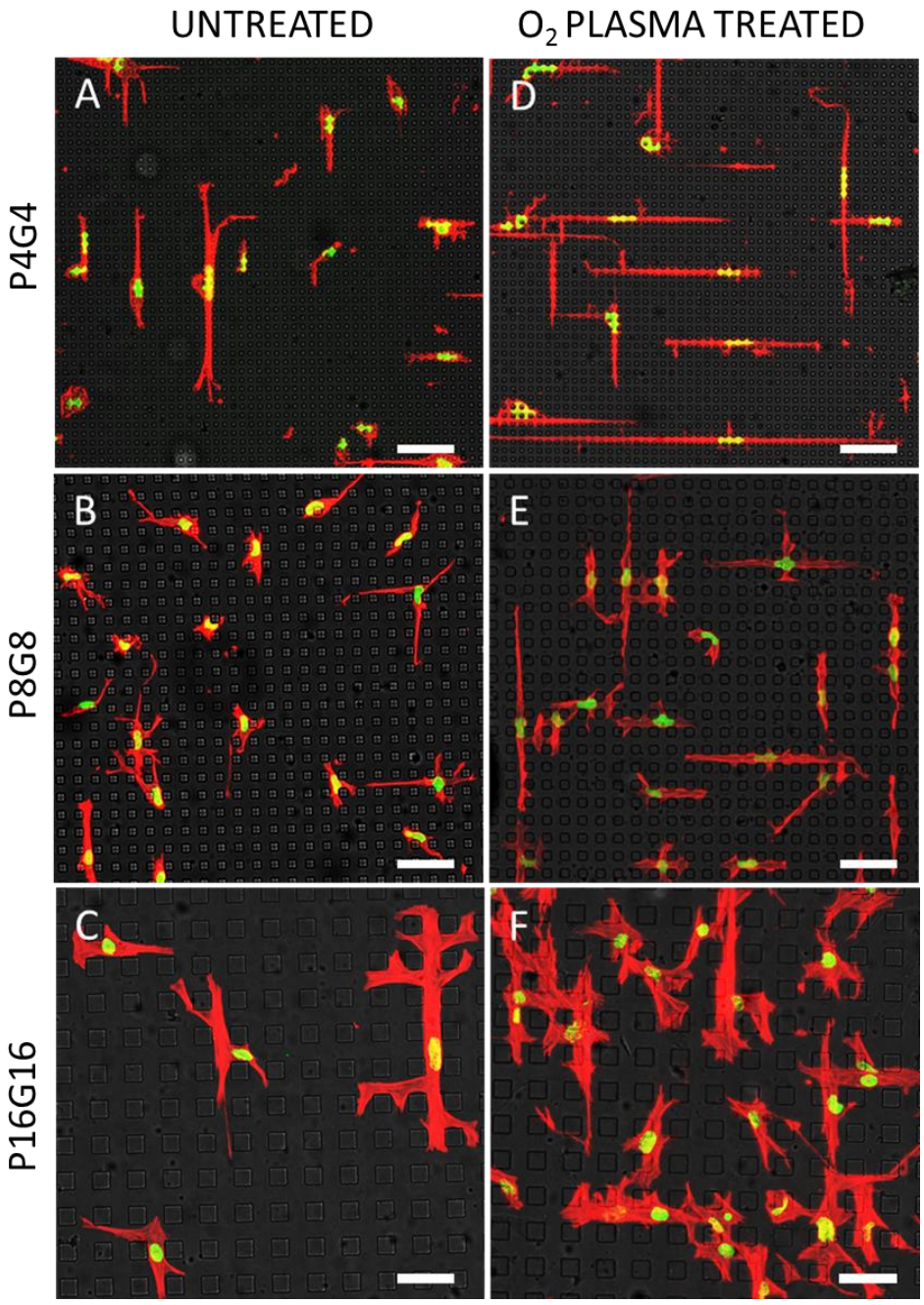

Figure 3.18. Confocal micrographs of the DPSCs on micropatterned PMMA films on Day 3. Cells on untreated and oxygen plasma treated (A, D) P4G4, (B, E) P8G8 and (C, F) P16G16. Green: Nucleus (DRAQ5), Red: Actin cytoskeleton (Alexa Fluor 488® conjugated phalloidin). Background: Transmission channel. Cell seeding density: 2.5 x 10^3 per sample. Scale bar: 50 μm.

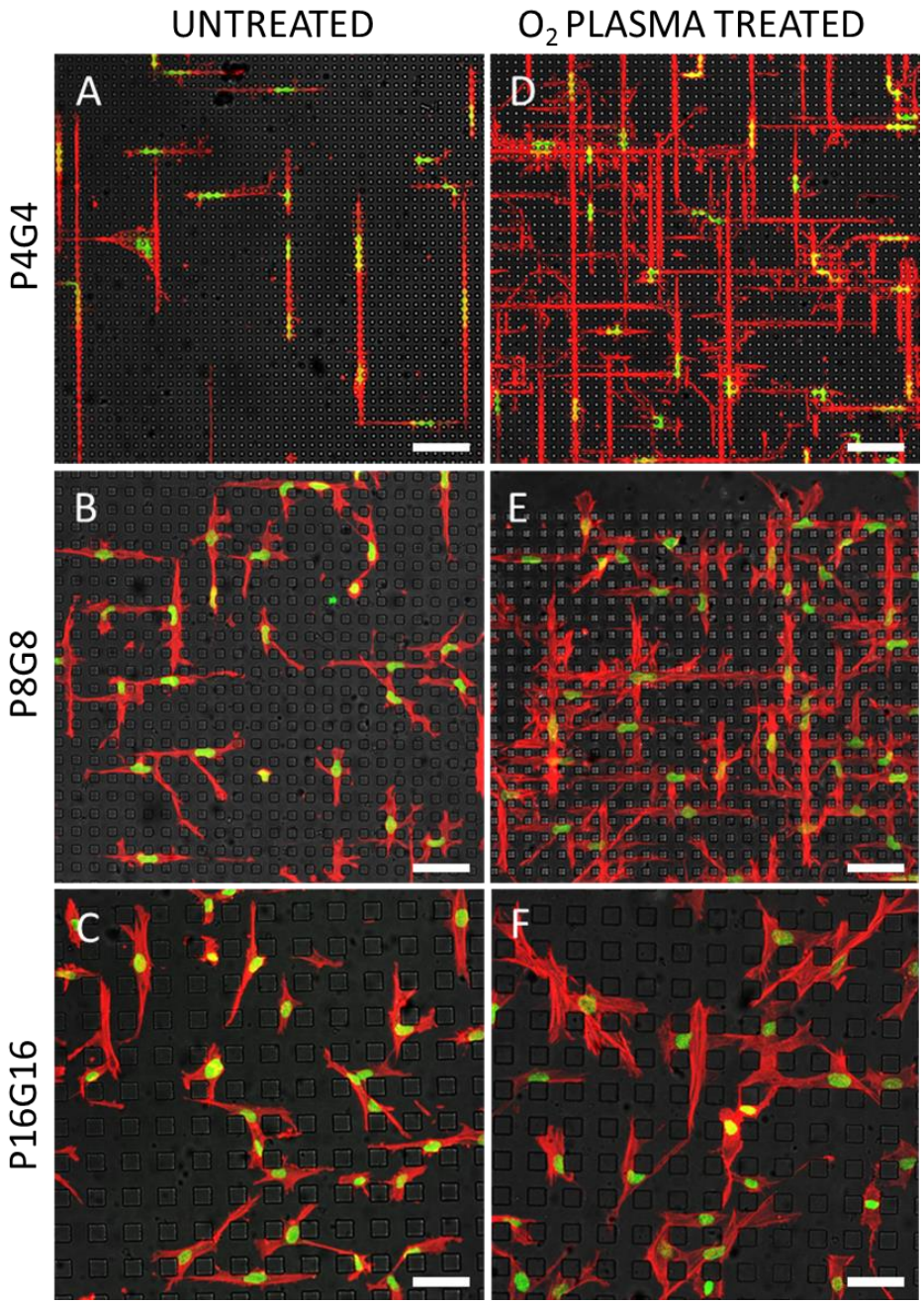

Figure 3.19. Confocal micrographs of the DPSCs on micropatterned PMMA films on Day 7. Cells on untreated and oxygen plasma treated (A, D) P4G4, (B, E) P8G8 and (C, F) P16G16. Green: Nucleus (DRAQ5), Red: Actin cytoskeleton (Alexa Fluor 488® conjugated phalloidin). Background: Transmission channel. Cell seeding density was 2.5 x 10^3 per sample. Scale bar: 50 µm.

In order to study the general scheme of the cells at the time points of RNA isolation for the gene expression analysis, the cells on the substrates were also recorded with confocal microscopy on days 14 and 28. At both time points, it was nearly impossible to distinguish individual cells due to very high cells density. The most remarkable difference observed on days 14 (Fig.3.20) and 28 (Fig.3.21) was the cells started growing on the pillar tops. Confocal and SEM micrographs have shown that the cells on the untreated substrates suspended themselves over the interpillar gaps without touching the floor by attaching to the side surfaces of the pillars at earlier time points and displayed deformed body and nucleus. On the plasma treated surfaces, on the other hand, cells located their bodies on the floor between the pillars. On day 14, however, cells with non-deformed cytoskeleton were observed on both untreated and plasma treated micropatterned substrates, which was also demonstrated on the SEM micrographs. These cells displayed a well spread, undeformed cytoskeleton and undeformed nuclei on the untreated substrates. On day 28, the number of cells on the pillar tops increased, particularly on the untreated substrates.

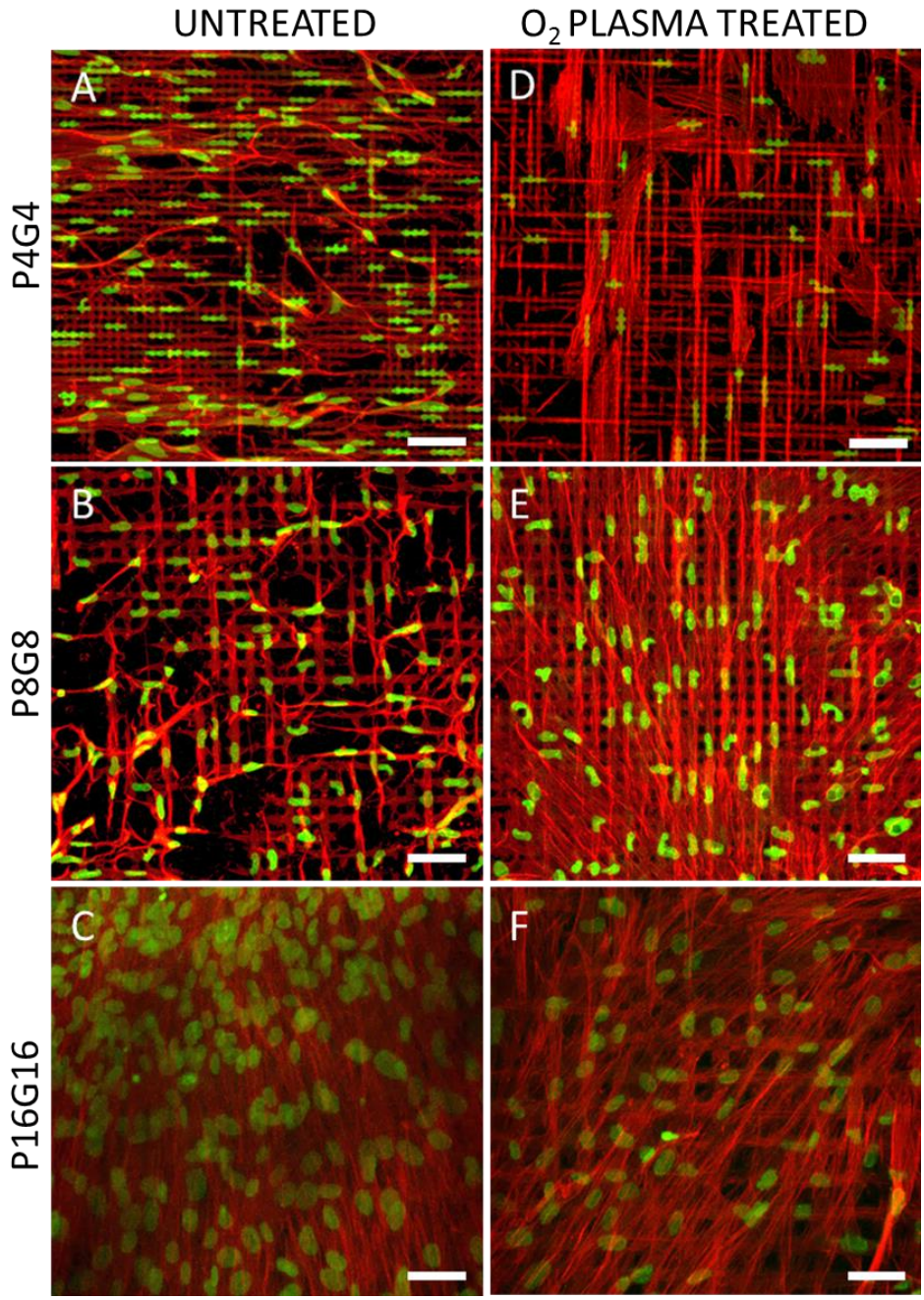

Figure 3.20. Confocal micrographs of the DPSCs on micropatterned PMMA films on Day 14. Cells on untreated and oxygen plasma treated (A, D) P4G4, (B, E) P8G8 and (C, F) P16G16. Green: Nucleus (DRAQ5), Red: Actin cytoskeleton (Alexa Fluor 488® conjugated phalloidin). Cell seeding density was 2.5 x 10^3 per sample. Scale bar: 50 μm.

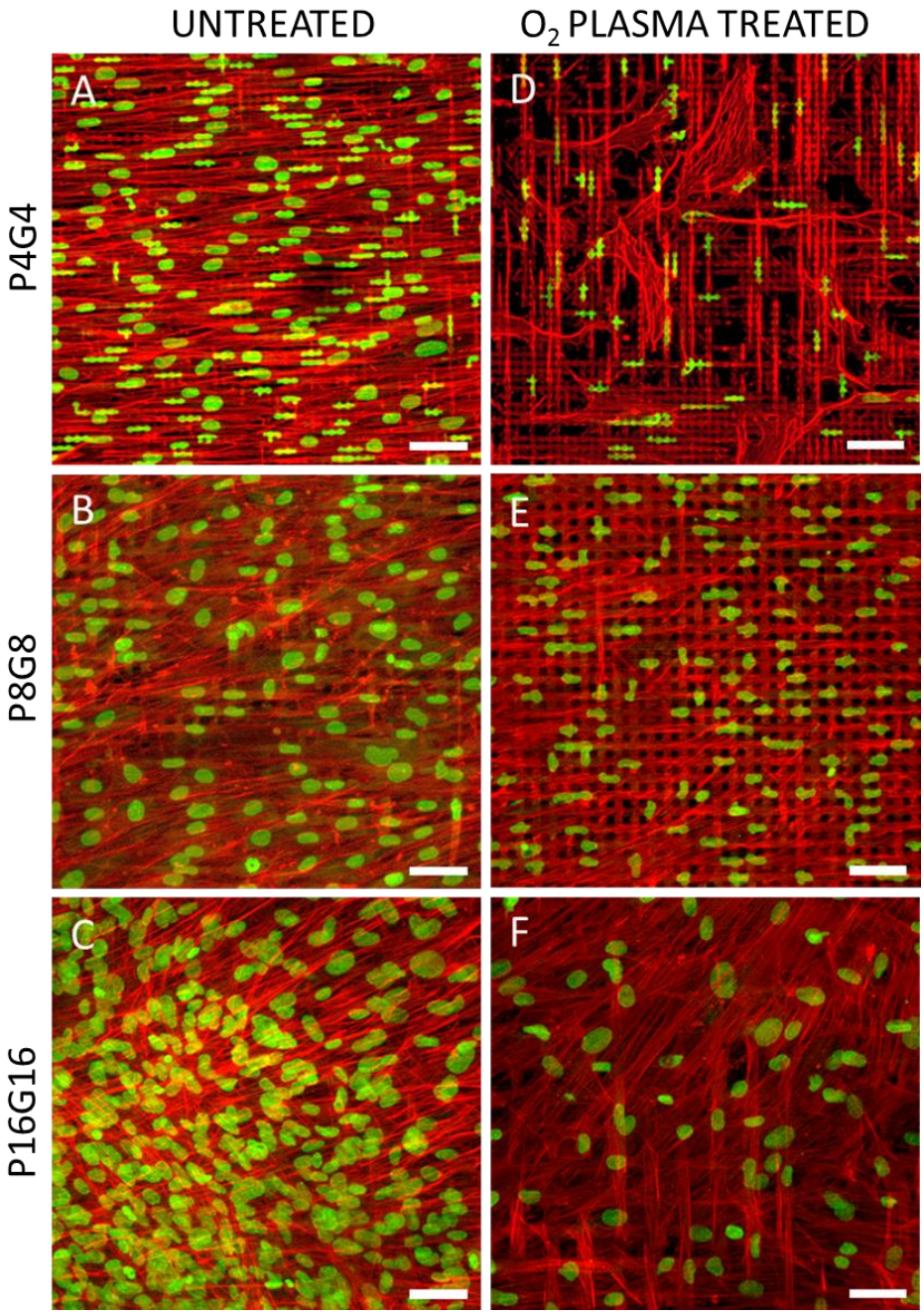

Figure 3.21. Confocal micrographs of the DPSCs on micropatterned PMMA films on Day 28. Cells on untreated and oxygen plasma treated (A, D) P4G4, (B, E) P8G8 and (C, F) P16G16. Green: Nucleus (DRAQ5), Red: Actin cytoskeleton (Alexa Fluor 488® conjugated phalloidin). Cell seeding density was 2.5 x 10^3 per sample. Scale bar: 50 μm.

3.4.3.2.2. Imaging of Cell Nuclei by Confocal Microscopy

The confocal micrographs of the nuclei of the cells incubated on unpatterned and micropatterned substrates for 4 weeks are given in Fig. 3.22. Nuclei on unpatterned surfaces were elliptical but became more and more elongated later time points as a result of cell elongation in a confluent population. Severe deformation of the nuclei was observed on micropatterned substrates, particularly on P4G4. P8G8 surfaces were found to cause milder deformations while there was almost no deformation on P16G16. This observation suggests that the nuclear deformations occur when the nuclei are inserted between the pillars that are separated by a distance smaller than the diameter of the nucleus. The gaps of P16G16 were large enough for the nuclei to fit in between the pillars without any deformations. Still, some nuclei were observed to bend slightly on P16G16 surfaces when the cells followed the contours of the pillar walls. An important difference between the nuclei on smooth and micropatterned surfaces was the areas of the nuclei. On smooth surfaces, nuclei appeared much larger as a result of spreading while on micropillar decorated surfaces nucleus area was lower; it decreased in parallel with the pillar and gap size decreases.

It is notable that the nuclear deformations were apparent on plasma treated P4G4 and P8G8 surfaces starting from day 1, while it took the nuclei longer to deform on untreated counterparts. On day 3, there were still undeformed nuclei on untreated P4G4 and P8G8, while all nuclei had lost their elliptical shape on their plasma treated counterparts. On day 7, the proportion of deformed nuclei had become similar on both type of surfaces. The trend in nuclear deformation was in parallel with the deformations in cell cytoskeleton (Section 3.3.4.2.1). Apparently, the force (gravity) that drags the nuclei in between the pillars was generated by the cytoskeletal stress along with that from the physical resistance of the rigid pillars since no nucleus deformation was observed when the cells were located on the pillar tops. On day 14 and day 28, very few undeformed elliptical nuclei were observed on untreated P4G4 and P8G8 surfaces. On plasma treated substrates, all nuclei were still deformed but the number of undeformed nuclei was somewhat increased. The reason for this

observation could be that the cells had reached confluency and started to grow on pillar tops. Deformations of the nuclei of osteosarcoma cells caused by surface micropillar structures were first reported by our group (Davidson et al. 2009), where it was proposed that the cytoskeleton drags the nucleus down upon adhesion to micropatterns. Similar deformations in the nuclei of mesenchymal stem cells cultured on PLLA substrate decorated with 5 μm high and 3 μm wide micropillars separated by 6 μm gaps were later reported by Pan et al. (2012). The expression of lamin A/C, which provides the stiffness of the nucleus, is absent in embriyonic stem cells and upregulated in adult stem cells. Both embriyonic and mesenchymal stem cells were studied using micropipette aspiration and the stiffness of the nuclei were found to be at least 2 fold lower compared to fully differentiated cells, suggesting that stem cells are more deformable (Lee et al., 2011).

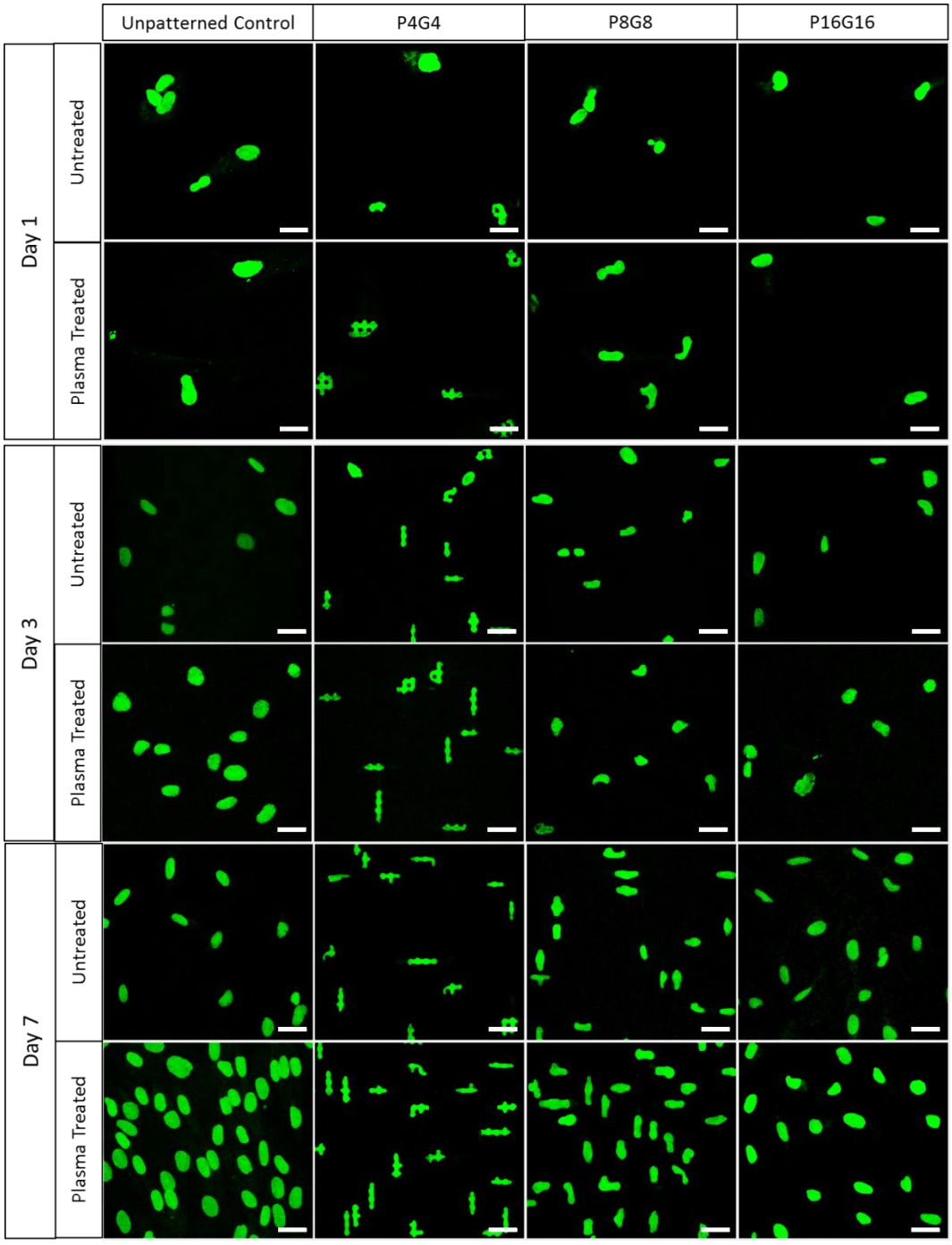

Figure 3.22. Confocal micrographs of the nuclei of DPSCs cultured on untreated and oxygen plasma treated unpatterned control and micropatterned PMMA films on 1, 3, 7, 14 and 28 days of culture. Green: Nucleus (DRAQ5). Cell seeding density was 2.5 x 10^3. Scale bar: 25 μm.

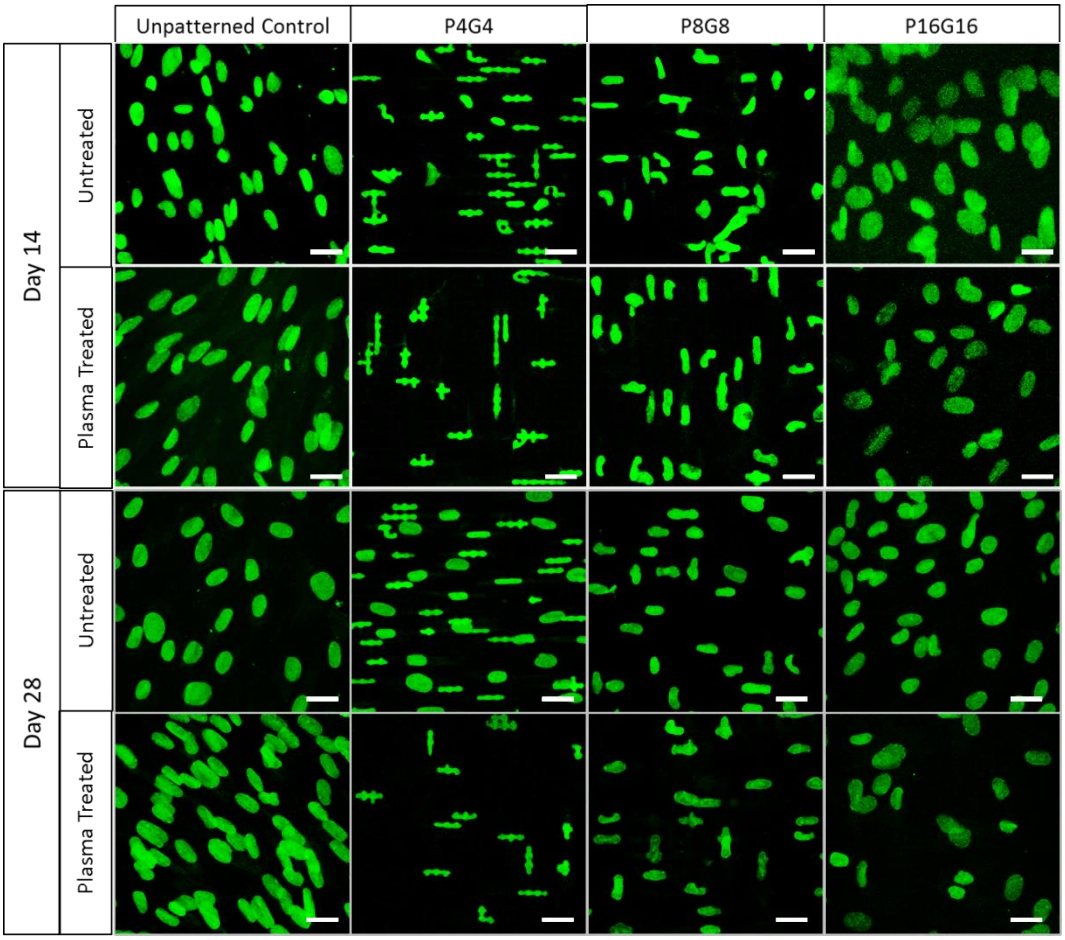

Figure 3.22 (continued)

The z-stack constructs of the side views of the cells cultured on P4G4 surfaces are given in Fig.3.23. These constructs give information about the relative positions of the deformed nuclei and cytoskeletons on untreated and plasma treated P4G4 substrates. It was observed that the highly elongated cells on untreated (Fig.3.23.A) and plasma treated (Fig.3.23.D) surfaces on day 7 were indeed located in the interpillar space and their nuclei were also inserted between the pillars together with the cytoskeleton. On days 14 and 28, some cells were found to spread on pillar tops on both untreated and plasma treated P4G4 surfaces. The z-stack micrographs showed that the nuclei of these cells were located on the pillar tops (pointed out with blue arrows in Fig. 3.23.C) while the nuclei of the cells that were trapped were deformed and between the pillars (pointed out with yellow arrows). On plasma treated P4G4 (Fig. 3.23.F), however, the nuclei were observed to be still deformed (pointed out with blue arrows) even though the cell body was positioned on the pillar tops. The number of undeformed nuclei were higher on Day 28 compared to Day 14.

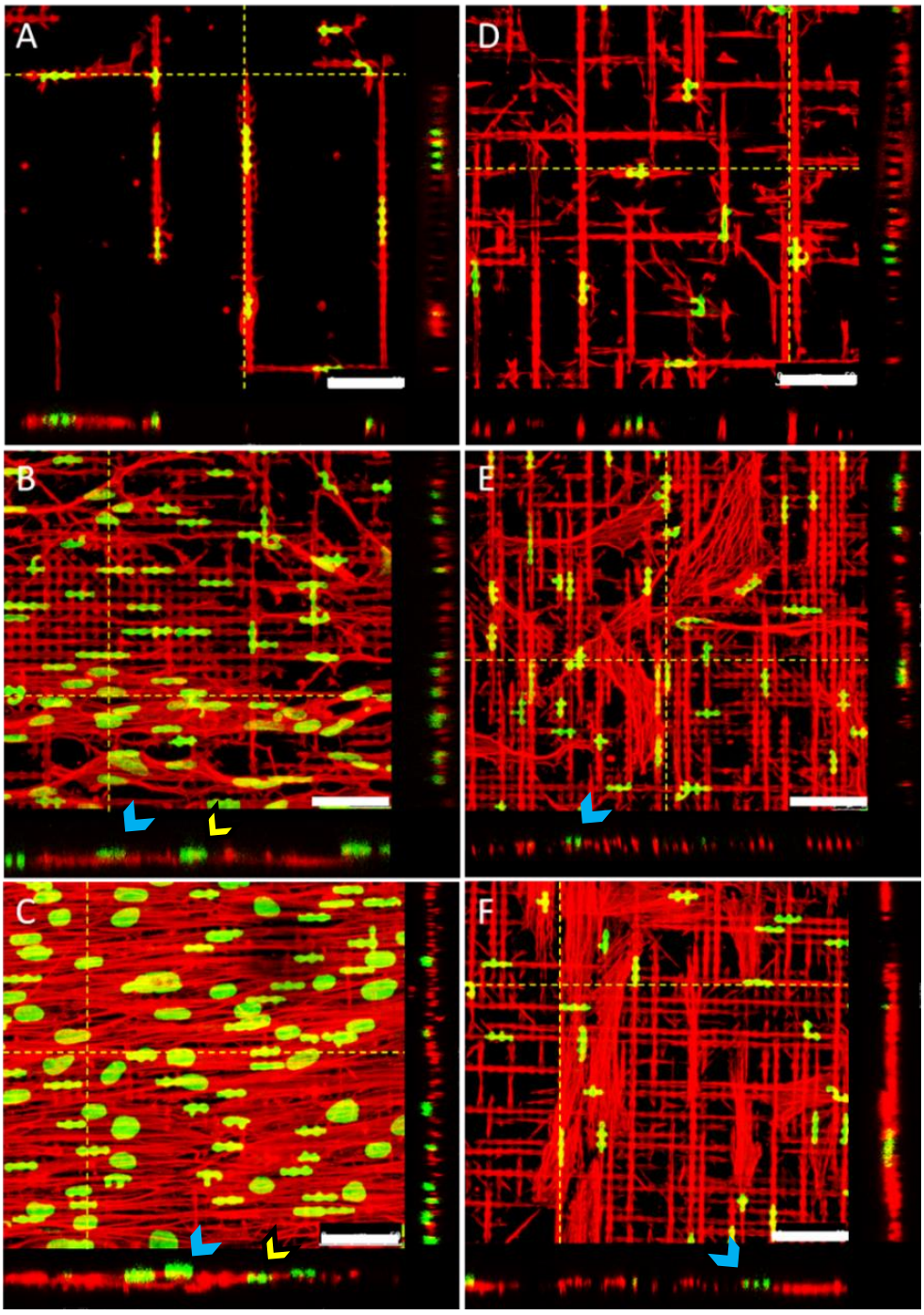

Figure 3.23. Z-stack constructs of the side views of the nuclei and cytoskeletons on P4G4 surfaces. Untreated and plasma treated P4G4 surfaces on (A, D) Day 7, (B, E) Day 14 and (C, F) Day 28. Red: Actin cytoskeleton (Alexa Fluor 488® conjugated phalloidin), green: nucleus (DRAQ5). Scale bar: 50 µm.

SEM and confocal micrographs provided an insight of the relative positioning of the cells with respect to the pillars. Based on the observations, 3 different positionings were proposed as presented in Fig.3.24.A and B. The first one is the complete penetration between the pillars and spreading on the floor (Fig.3.24.A.a and Fig.3.24.B.a). This behavior was observed on the plasma treated micropatterned substrates. Cells exhibiting this behavior were shown in the SEM micrographs to touch the floor and in the confocal micrographs they display a highly deformed morphology between the pillars (Fig.3.24.C.c). The second positioning style was stretching between the pillars by attaching appandages to the side surfaces of the pillars and occasionally to the pillar tops without contacting the floor (Fig.3.24.A.b and Fig.3.24.B.b). This behavior suggests that cells tried to minimize contact with the substrate by suspending themselves in the air. It was the SEM micrographs that clearly showed this position; in the confocal micrographs (Fig.3.24.C.a) it was not possible to distinguish between the untreated and plasma treated surfaces. Cells on both surfaces were practically localized between the pillars and displayed a highly deformed morphology. The final positioning type was spreading over the pillar tops (Fig.3.24.A.c and Fig.3.24.B.c). This behavior was observed on both untreated and plasma treated surfaces at late time points (days 14, 21 and 28). The cells with this position displayed no cytoskeletal or nuclear deformations on the untreated surfaces (Fig.3.24.C.c), and displayed nuclear but not cytoskeletal deformations on the plasma treated surfaces (Fig.3.24.C.d). Cells on the untreated substrates were shown to contact only with the pillar tops while the cells on the plasma treated counterparts were in contact with the top and the side surfaces of the pillars and fully covered the upper parts.

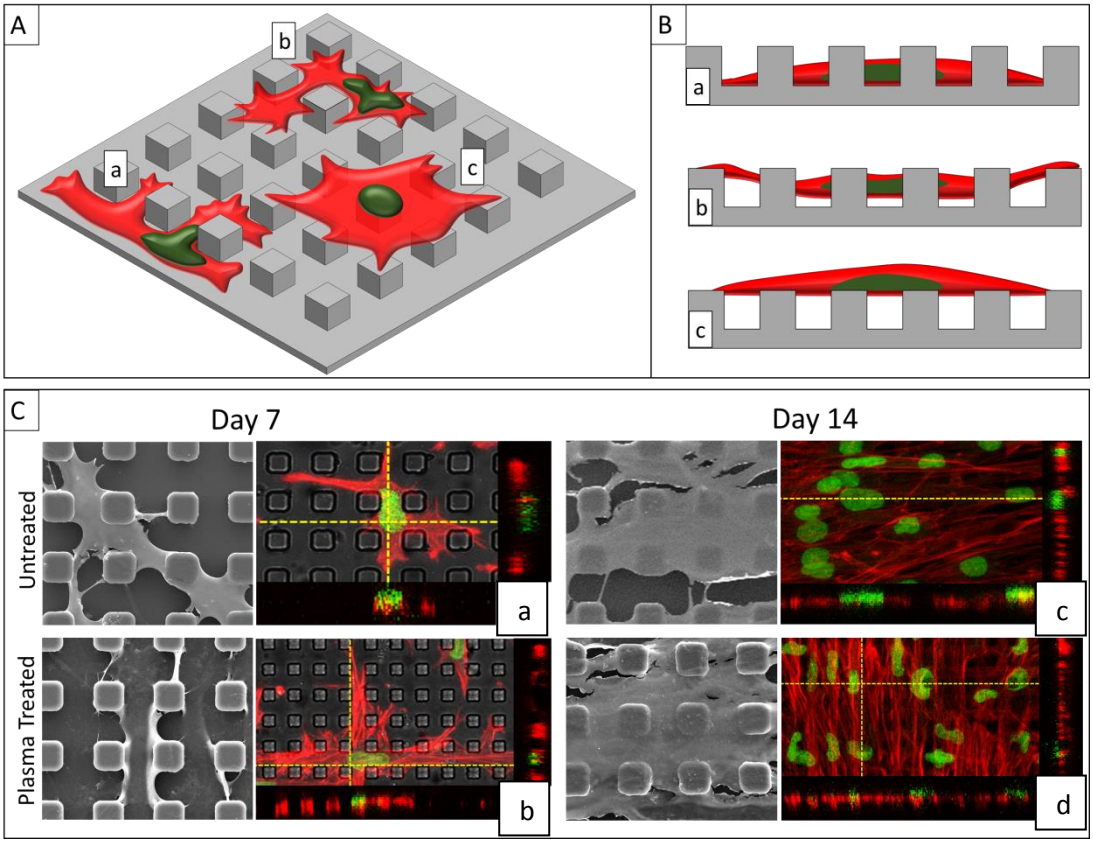

Figure 3.24. Relative positioning of the cells with respect to the micropillars. Schematic representations of the possible localizations of the cells from the (A) top, and (B) side views. (C) Examples of the positionings of the cells shown in SEM micrographs and z-stack constructs of the untreated and plasma treated P8G8 surfaces on days 7 and 14.

3.4.3.3. Digital Analysis of Cytoskeletal and Nuclear Morphology

3.4.3.3.1. Cytoskeletal Morphology

Distinct conformational changes were observed in the cytoskeleton of the cells cultured on micropatterned substrates. In general, cells on P4G4 surfaces were found to have a highly elongated morphology and severely deformed nuclei. On P8G8

surfaces, a mixed population of cells exhibiting nuclei deformed to varying degrees was observed at early time points and in time the frequency of branching (the most extensive cytoskeletal deformation) increased. On P16G16 surfaces, cells was highly branched but with no significant deformation of their nuclei. These conformational changes were also observed to take place earlier and to a higher degree on the O_2 plasma treated surfaces than on the untreated hydrophobic counterparts. However, these observations had to be quantified to arrive at a general conclusion. In order to quantify the morphologies of the cells, fluorescence micrographs of cytoskeletons on days 1, 3 and 7 were digitally analyzed based on two shape descriptors (parameters), namely elongation and branching. Cells cultured for more than 7 days could not be analyzed due to overcrowding.

The most widely used method in the quantification of cell elongation is the use of Feret diameter and the aspect ratio. Feret diameter is defined as the longest distance between any two points on the shape outline. Aspect ratio is calculated by dividing Feret diameter to the shortest distance between two points on perimeter (Poellmann et al., 2010). This method, however, gave misleading results in this study because two cells with similar aspect ratios were observed to have quite different morphologies. Therefore, the elongation equation introduced by Stojmenovic and Žunic (2008) was transformed into a MatLab code and used for the quantification of the degree of elongation. This equation computes elongation of polygonal shapes from their boundary and it is independent of the area, rotation or size. The distribution of the elongation values of 100 cells per surface are shown in Fig. 3.25. Since the values obtained were not normally distributed, the results were represented as box-whisker plots instead of bar graphs representing mean and standard deviation.

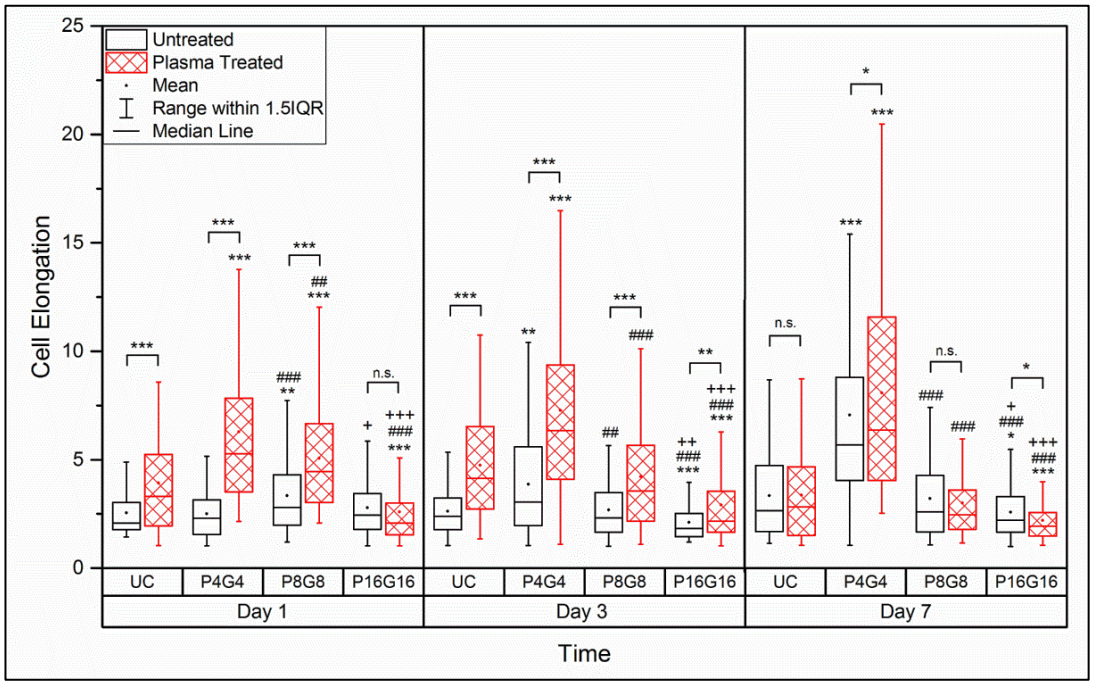

Figure 3.25. Distribution of the cell elongation on untreated and oxygen plasma treated smooth and micropatterned substrates on days 1, 3 and 7. P: Square pillar width (µm), G: Interpillar distance (µm), UC: Unpatterned control. *p < 0.05, **p < 0.01 and ***p < 0.001. *, # and + on the whiskers represent comparison with unpatterned smooth, P4G4 and P8G8 surfaces, respectively. n.s: not significant.

The elongation values on days 1, 3 and 7 reflected the observations on the confocal micrographs. On the untreated surfaces the cell elongation was insignificant on day 1. This was in agreement with the observations made on the SEM and confocal micrographs of the cells on untreated P4G4 (Fig. 3.12A and Fig.3.17.A) and P8G8 (Fig.3.12.B and Fig.3.17.B). It was observed that the highest cell elongation was on P4G4 surface among the treated substrates, and elongation decreased as the pillar and the gap size increased. On day 3, this trend did not change on hydrophilic surfaces, but it can be noted that the elongation increased on P4G4 while decreased P8G8 compared to day 1. This was expected, because the mixed population of elongated and branched cells on P8G8 on day 1 was observed to shift to branched cells on day

3. On day 3 elongation was also increased as the pillar/gap sized decreased for both the untreated and plasma treated surfaces. On day 7, the elongation profile on plasma treated surfaces took its final form as the cell elongation on P8G8 and P16G16 surfaces decreased while it increased for the P4G4 compared to day 3. The same trend was also valid for the untreated surfaces and elongation on P4G4 surface further increased compared to day 3. Elongation on plasma treated P4G4, however, was still significantly higher than on untreated P4G4.

Another parameter, solidity, is defined as the ratio of the shape area to the area of convex that surrounds target shape (Fig.2.6 in section 2.2.7.2.2.), and it decreases as the branching of a shape increases. Branching is the reciprocal of solidity. As in the case of elongation, branching values of 100 cells per surface were determined and found to be not normally distributed. Therefore they are represented as a box-whisker plot in Fig. 3.26. On day 1, cell branching was found to be higher on all plasma treated micropatterned surfaces than their untreated counterparts. This was expected as the cells on pristine surfaces did not spread well on the first day of cell seeding while the cells on plasma treated surfaces did. The branching between hydrophilic P8G8 and P16G16 surfaces was not significantly different, but they were both higher than that of P4G4 surface. On day 3, branching increased on both untreated and plasma treated micropatterned surfaces, but the trend was the same. Branching increased as the pillar (and gap) size increased on plasma treated surfaces. On untreated substrates, however, there was no significant difference in cell branching between the untreated P4G4 and P8G8. The frequency of branched cells on Day 7 was lower on P4G4 surfaces while it increased on P8G8 and P16G16 surfaces. This was the opposite of the elongation trend discussed above, suggesting that the cell elongation and branching occurred antagonistically as expected.

In brief, it can be proposed that cell elongation increases and branching decreases as the pillar and gap size decreases, and these deformations occur earlier and to a higher extent on oxygen plasma treated surfaces. These can be explained with the differences in surface hydrophobicity. Apparently, cells on hydrophilic surfaces

spread readily after seeding while the cells on hydrophobic substrates minimize their contact with surface structures and their spreading is delayed until the cells lay down their own ECM and modify the surface. As a result of enhanced spreading on the substrate floor between the pillars of the plasma treated surfaces compared to the untreated counterparts, higher elongation on treated P4G4 and branching on treated P16G16 were observed.

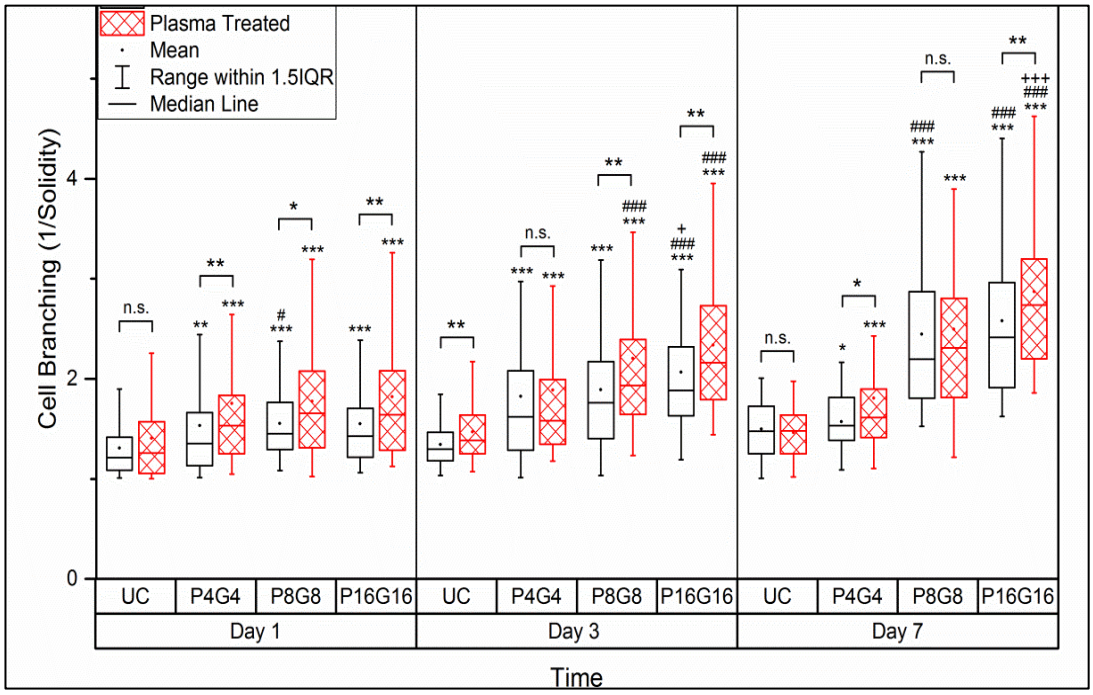

Figure 3.26. Distribution of the cell branching on untreated and oxygen plasma treated flat and micropatterned substrates on Days 1, 3 and 7. UC: Unpatterned control. *p < 0.05, **p < 0.01 and ***p < 0.001. *, # and + on the dashed lines represent comparison with smooth, P4G4 and P8G8, respectively. n.s: not significant.

In the literature, highly elongated morphologies were generally attributed to the cells cultured on micro- or nanoscale channel structures. For instance, human mesenchymal stem cells cultured on polyurethane substrates carrying 300 nm deep and 1400 or 4000 nm wide channels were reported to display highly elongated morphology (Watari et al., 2012). This phenomenon was explained with the term contact guidance by Curtis and Wilkinson (1997), who proposed that cells align themselves along the surface structures. They also emphasized that cells sense these structures as continuous or discontinuous, and can react discontinuities as long as the discontinuity is larger than the distance between the sensing elements such as the focal adhesion complexes. The surface features used in this study were discontinuous, but the cells on P4G4 surfaces reacted to them as they were continuous ridges and elongated linearly rather than taking sharp turns as observed on P8G8 and P16G16 surfaces. The same observation was made by Alapan et al. (2015), who reported that human MSCs and cardiomyocytes exhibited highly elongated morphology on PDMS substrates carrying 5x5 μm^2 square pillars separated by 5 μm. Apparently, the distance between the sensing elements was larger than the interpillar distance, so the cells could not sense the discontinuities of 4 μm length. Interestingly, Alapan et al. showed that cells cultured on 7x7 μm^2 square pillars separated by 7 μm also exhibited an elongated morphology, even though the extent was lower compared to substrates with shorter gap lengths. In our study, a mixed population of elongated and branched cells was observed on P8G8 surfaces at earlier time points, but the fraction of the DPSCs that were able to follow the contours of the pillars and had a branched morphology increased as the time progressed. The hydrophilicity of the substrates might also influence the discrimination of continuous and discontinuous structures by the cells. PDMS is more hydrophobic (CA: ~120^o) than PMMA (CA: ~84^o), and reduced cell spreading on PDMS might have caused elongation rather than branching in the work of Alapan et al. Increased cell branching with an increase in interpillar distance was also reported in other studies. 3T3 fibroblast cells cultured on fibronectin coated PDMS substrates carrying circular pillars were shown to exhibit higher branching as the gap

size increases. Cells on P5G5 (5 μm wide pillars separated by 5 μm gap) were reported to have long protrusions following the grooves while the ones cultured on P10G10 substrates extended pseudopodia like protrusions on the flat parts between the pillars (Ghibaudo et al., 2009). In another study, epithelial cells were shown to exhibit highly elongated morphology on titanium substrates decorated with 15 μm wide channels, while the cells on 15 μm wide square ridges separated by 15 μm gaps were reported to exhibit a branched morphology rather than elongated (Andersson et al., 2003).

3.4.3.3.2. Nuclear Morphology

The nuclear deformations on PMMA substrates were quantified using 100 cells per surface and calculating the circularity (Fig. 3.27) for 28 days. The highest deformation was on P4G4 surfaces among both untreated and plasma treated surfaces at all time points examined, and it decreased as the pillar and gap size increased. The homogeneity in deformations at early time points was observed to change upon plasma treatment. On untreated P4G4, there were both highly deformed and almost undeformed nuclei on Days 1 and 3, because some cells did not interact fully with hydrophobic pillars. Thus, the range of its box-whisker plot was quite wide. On day 7, the distribution became narrower and got close to the distribution of plasma treated P4G4 as a result of increased spreading and interactions with the substrate. On plasma treated P4G4, the distribution of nuclear deformation was quite narrow at a high level on days 1, 3 and 7, indicating that all nuclei were highly deformed. Cells on hydrophilic surfaces readily started inserting both their cytoplasm and nucleus between the pillars as can be seen in the confocal micrographs of day 1 (Fig.3.17.D), thus the distribution was in agreement with the microscopical observations. On day 14, however, these narrow distributions of nuclear deformation on P4G4 surfaces were not observed, particularly for the untreated substrate. This observation became more apparent on day 28. This phenomenon can be explained with the cells that were

shown to climb up the pillars and locate their nuclei on the pillar tops on days 14 and 28. Overall, it can be concluded that the nuclear deformations increased as the pillar and gap size decreased, and the extent of these deformations was higher on the plasma treated surfaces. On both untreated and plasma treated substrates, nucleus deformation increased and the distribution of nuclear deformations became narrower from Day 1 to Day 7. From Day 7 to Day 28, however, the distribution of nucleus deformation widened because some cells started reside on the pillar tops rather than on the interpillar gaps due to reaching confluency and displayed no deformation in their nuclei.

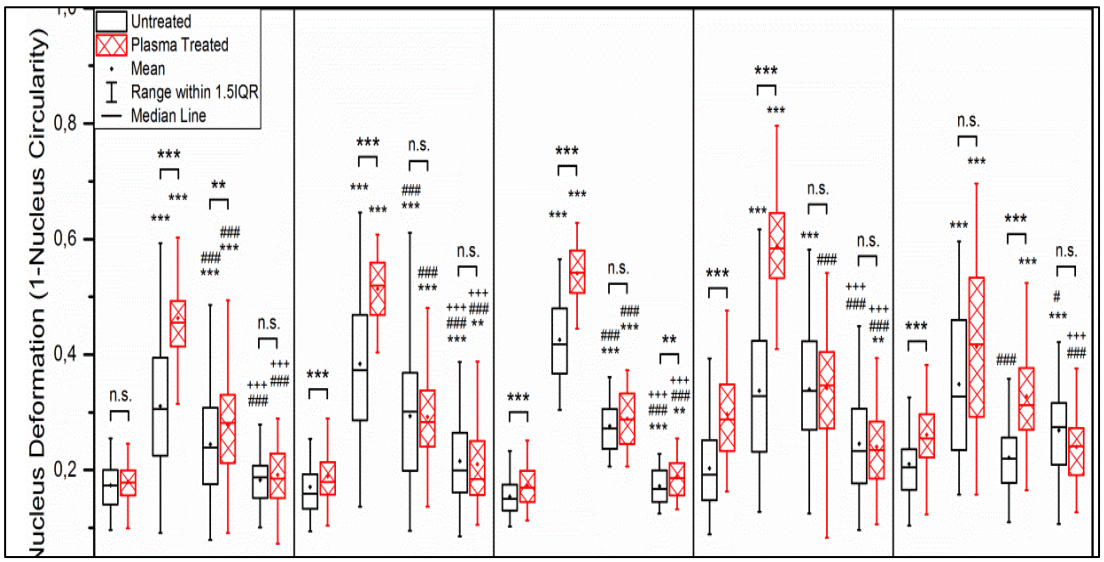

Figure 3.27. Distribution of the nucleus deformation values of the DPSCs on 1, 3, 7, 14 and 21 days of culture on untreated and oxygen plasma treated smooth and micropatterned PMMA films. P: Square pillar width (μm), G: Interpillar distance (μm). *p < 0.05, **p < 0.01 and ***p < 0.001. *, # and + on the whiskers represent comparison with smooth, P4G4 and P8G8, respectively. n.s: not significant.

3.4.4. Cell Proliferation

The numbers of DPSCs and the rate of proliferation of the cells on PMMA films and TCPs for 4 weeks in the culture were determined by using the calibration curve prepared with known cell numbers (Fig.3.28 and Fig.3.29, numerical values in Table B.5 and B.6). It was observed that the number of cells on plasma treated smooth and micropatterned surfaces was higher compared to the untreated counterparts at each time point. The cell numbers on untreated flat control film was significantly lower than on TCPs control. The number of cells on the plasma treated unpatterned film was relatively closer to that on TCPs. The proliferation rate on the plasma treated unpatterned substrate was also higher compared to its untreated counterpart between days 3 and 7. These observations suggested that increased hydrophilicity upon oxygen plasma treatment promoted cell proliferation. Between Days 7 and 21, however, proliferation rate significantly increased on the pristine unpatterned substrate but decreased on the treated counterpart. Increasing surface hydrophilicity by applying oxygen plasma has been reported to increase proliferation on polymers. In one study, 3T3 fibroblasts were cultured on oxygen plasma treated low density polyethylene (LDPE) films and the cell proliferation was found to be higher on plasma treated surfaces than on the untreated counterparts (Kim et al., 2007). The decrease in the proliferation rate on the plasma treated surface after day 7 can be explained with the contact inhibition, which is defined as the arrest of cell cycle upon increased cell-cell contact (Polyak et al., 1994). As it can be seen on the SEM micrograph given in Fig. 3.12.F, the surface of the plasma treated smooth surface became very crowded already on day 7 due to very high initial proliferation rate and the resulting increase in the cell-cell contact probably slowed down the proliferation on the subsequent days.

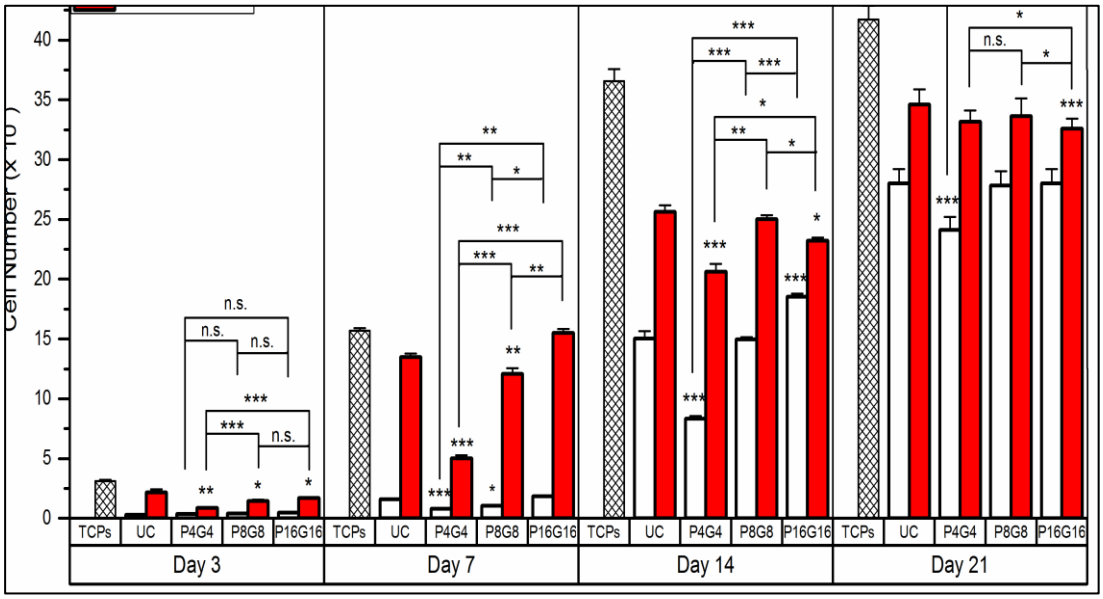

Figure 3.28. Cell numbers of DPSCs on untreated and oxygen plasma treated smooth and micropatterned PMMA films compared to TCPs on 3, 7, 14 and 21 days of culture. (7.5 x 10^3 cells were seeded per film). Data represent the mean ± SD for three samples, *p < 0.05, **p < 0.01, and ***p < 0.001. Asterisks above the bars represent significance compared to unpatterned smooth counterpart. n.s: not significant.

Besides the surface wettability, presence of 3D surface features and their dimensions were also found to influence the cell numbers and proliferation rate significantly. It was observed that the number of cells increased with an increase in the pillar and gap size on plasma treated substrates on days 3 and 7, and increased on untreated substrates at each time point examined. The same trend was also observed for the cell proliferation, proving the negative effect of smaller pillar/gap dimensions on proliferation. Between days 14 and 21, on the other hand, the proliferation rate on the untreated and plasma treated P4G4 surfaces increased significantly and even exceeded the rate on the other surfaces. In brief, the proliferation rate was initially

higher on the plasma treated surfaces than on untreated counterparts and it increased as the pillar and gap sizes increased on both untreated and treated surfaces. This trend was reversed in time and the highest proliferation rate was observed on P4G4 surfaces between days 14 and 21.

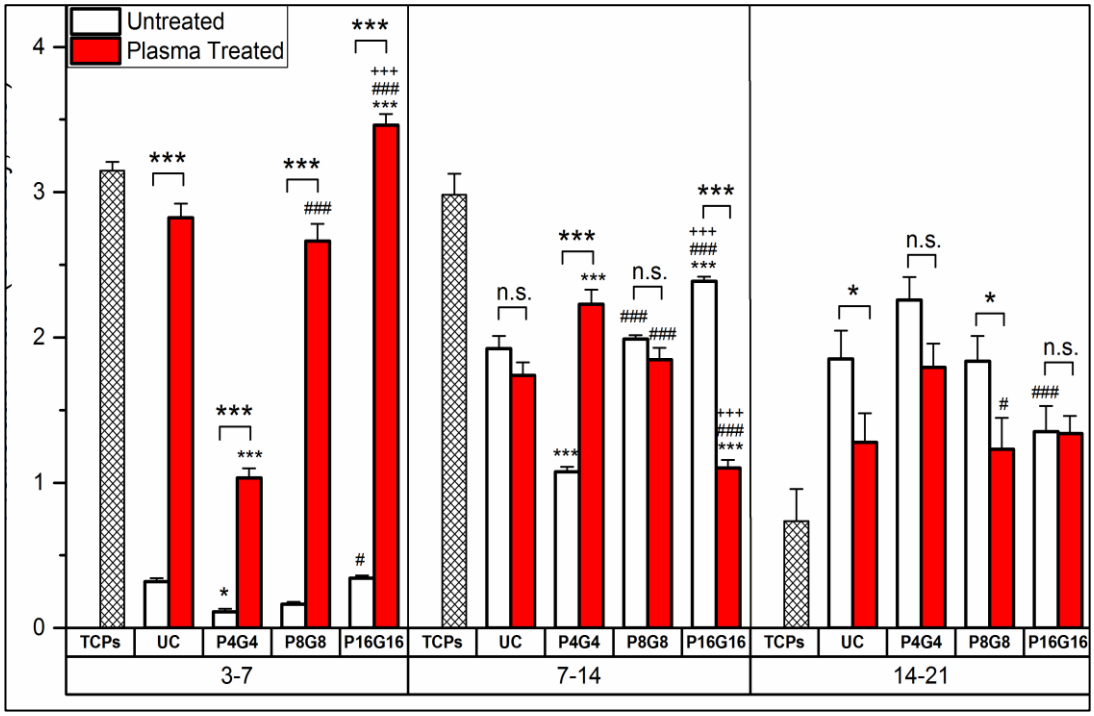

Figure 3.29. Proliferation of DPSCs on untreated and oxygen plasma treated smooth and micropatterned PMMA films compared to TCPs Data represent the mean ± SD for three samples, *p < 0.05, **p < 0.01 and ***p < 0.001. *, # and + above the bars represent significance compared to smooth, P4G4 and P8G8 surfaces, respectively. n.s: not significant.

The reason of the significantly reduced proliferation on P4G4 substrates between days 3 and 14 was probably the severe deformations in the nuclei. Mitosis is a highly organized process that undergoes with precise rearrangements in the nucleus, therefore, the severe deformations in the nuclei as a result of mechanical trapping between the micropillars might have inhibited proliferation. Reduced cell proliferation as a result of nuclear deformations was also reported by Nagayama et al. (2015), who demonstrated inhibition of the proliferation of vascular smooth muscle cells cultured on micropillar structures and explained this observation with the condensation of intranuclear chromatin in the relatively smaller nucleus of the muscle cells as a result of dramatic nuclear deformation. After day 14, cells on both untreated and plasma treated P4G4 surfaces were observed to spread on top of the pillars and exhibited reduced or no nuclear deformation (Fig.3.20.A and D). Apparently, these cells with undeformed nuclei displayed a high proliferation rate as on the unpatterned surfaces while the proliferation rates on the other substrates decreased due to reaching confluency. Thus, the highest proliferation rate was observed on P4G4 substrates between days 14 and 21.

3.4.5. Gene Expression Analysis

The changes caused by the micropillar structures on the expression of the stemness markers Oct3/4 and Nanog, and the osteogenic markers osterix (Osx), alkaline phosphatase (ALP) and osteocalcin (OC) by DPSCs were investigated using real time quantitative PCR (RT-qPCR). DPSCs were cultured on TCPs in the osteogenic medium (OM) for 14 and 28 days and the expression analysis was done in order to test the capability of isolated DPSCs to differentiate towards osteoblasts and determine the expression profile of the target genes during osteogenic differentiation at the selected time points. The expression levels of all markers were normalized to the expression of the housekeeping gene glyceraldehyde 3-phosphate dehydrogenase (GAPDH) and represented as the fold changes compared to the cells cultured in

regular growth media (Fig. 3.30, Table B.7). Interestingly, a small (0.5 fold) increase rather than a decrease was observed in the expression of Oct3/4 on days 14 and 28. The expression of the second stemness marker Nanog, on the other hand, was 2 fold lower than the control at both time points. The most significant change, however, was observed in the expression of the osteogenic transcription factor Osx (10 fold), suggesting that the cells were committed towards osteogenic lineage in the presence of osteogenic supplements. By day 28, the expression decreased to the level of the control. On day 14 about 3 fold increases were observed in ALP and OC. On day 28, their expression was substantially higher (around 10 fold).

Oct3/4 and Nanog together with Sox2 form a trio of transcription factors that are associated with the self-renewal and pluripotency of embryonic stem cells (Liu et al., 2011). Differentiation of embryonic stem cells was shown to repress expression of Oct4 and Nanog and downregulate ES cell specific genes that are bound to these transcription factors (Loh et al., 2006). Oct3/4 and Nanog expression in human mesenchymal stem cells derived from bone marrow, adipose tissue, heart, dermis (Riekstina et al., 2009), and dental pulp (Khanna-Jain et al., 2012) was also reported, but no clear evidence of the expression profile of these genes during differentiation was presented in the literature. Here we observed a small decrease in Nanog and a slight increase in the expression of Oct3/4. Even though Oct3/4 is associated with pluripotency of embryonic cells and expected to be downregulated during differentiation, this might not be the case with the mesenchymal stem cells. The increase and than returning back to initial levels observed in the expression of osteogenic transcription factor Osx was consistent with work of Igarashi et al. (2004), who demonstrated an increase in the expression of Osx by differentiating rat calvarial cells starting from day 11 until day 15, and then a gradual decrease to the initial levels. Dexamethasone is known to upregulate the expression of Osx, increases the ALP and OC mRNA and protein levels and stimulates osteoblastogenesis (Ahdjoudj et al., 2001) as observed in this study.

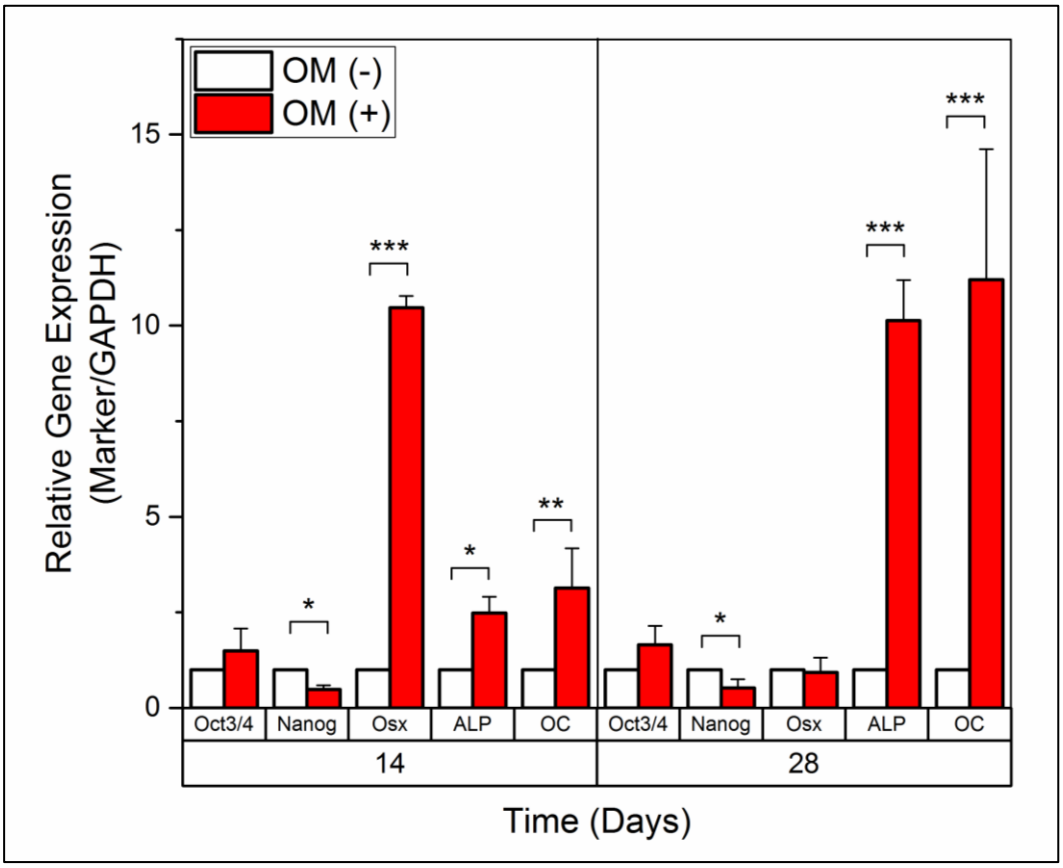

Figure 3.30. The relative expressions of the stemness markers Oct3/4 and Nanog and the osteogenic markers osterix (Osx), alkaline phosphatase (ALP) and osteocalcin (OC) by DPSCs after 14 and 28 days of culture on TCPs. Expressions in the presence of osteogenic supplemenents (OM(+)) were normalized to the corresponding expression level in the regular growth media without osteogenic supplements (OM(-)). *$p < 0.05$, **$p < 0.01$ and ***$p < 0.001$.

The expressions of the stemness and osteogenic markers were studied with the cells cultured on micropatterned substrates for upto 28 days in order to investigate the influence of micropillar cues and surface hydrophilicity on the fate of DPSCs (Fig. 3.31, Table B.8). It was observed that the expression of Oct3/4 was lower on patterned surfaces than on unpatterned surface on Day 14 regardless of the treatment with plasma (Fig.3.31.A). By day 28 the expression of Oct3/4 on untreated surfaces were significantly higher than the unpatterned control, while oxygen plasma treated were still as on Day 14, lower than the control (Fig.3.31.B). The expression of Nanog was found to be slightly lower only on untreated P4G4, while it was higher on P8G8 and unchanged on P16G16 compared to the flat surface. On day 28, this trend did not change but the expression was observed to decrease further on P4G4 and increase on P8G8 surface compared to day 14.

The expression levels of Osx on untreated micropatterned substrates were close to each other and around 2 fold lower than the control. Upon plasma treatment, the expression levels were increased but there was no distinct difference due to pattern presence (Fig.3.31.E). On day 28, expression levels of Osx on plasma treated and untreated samples were increased, with the increase being higher in the plasma treated samples (Fig.3.31.F).

Expression of ALP was found to be significantly higher on the patterned untreated surfaces except P16G16 than the unpatterned control. There was no change in the plasma treated samples (Fig.3.31.G). This trend was the same on Day 28 with the untreated samples that had increased difference with respect to the control (Fig.3.31.H). The expression of OC on the untreated samples on both days 14 and 28 was lower than the plasma treated samples and the treated samples were around the control (Fig. 3.31.I and J). This can be summarized as patterns have a detrimental effect on the expression of OC.

Based on the results obtained, it can be proposed that the surface micropatterns cause distinct changes in the gene expression of DPSCs and the extent of these changes are

affected by the surface hydrophilicity and pillar/gap dimensions. The expressions of the Oct3/4 and Nanog on plasma treated substrates suggest that DPSCs displayed a decrease in their capacity of self renewal and multipotency when cultured on plasma treated P4G4 and P8G8 surfaces. Apparently, severe deformations of cell nuclei on P4G4 (Fig.3.22) must have influenced the gene expression negatively, since the downregulation decreased with dimension increased. Deformation of cell nucleus leads to an increase in their surface to volume ratio, which might result in a higher fraction of chromatin material contacting the nuclear membrane. Since the genes close to the nuclear membrane are known to be turned off (Dahl et al., 2008), deformations in cell nuclei could cause the downregulated gene expression through increased contact.

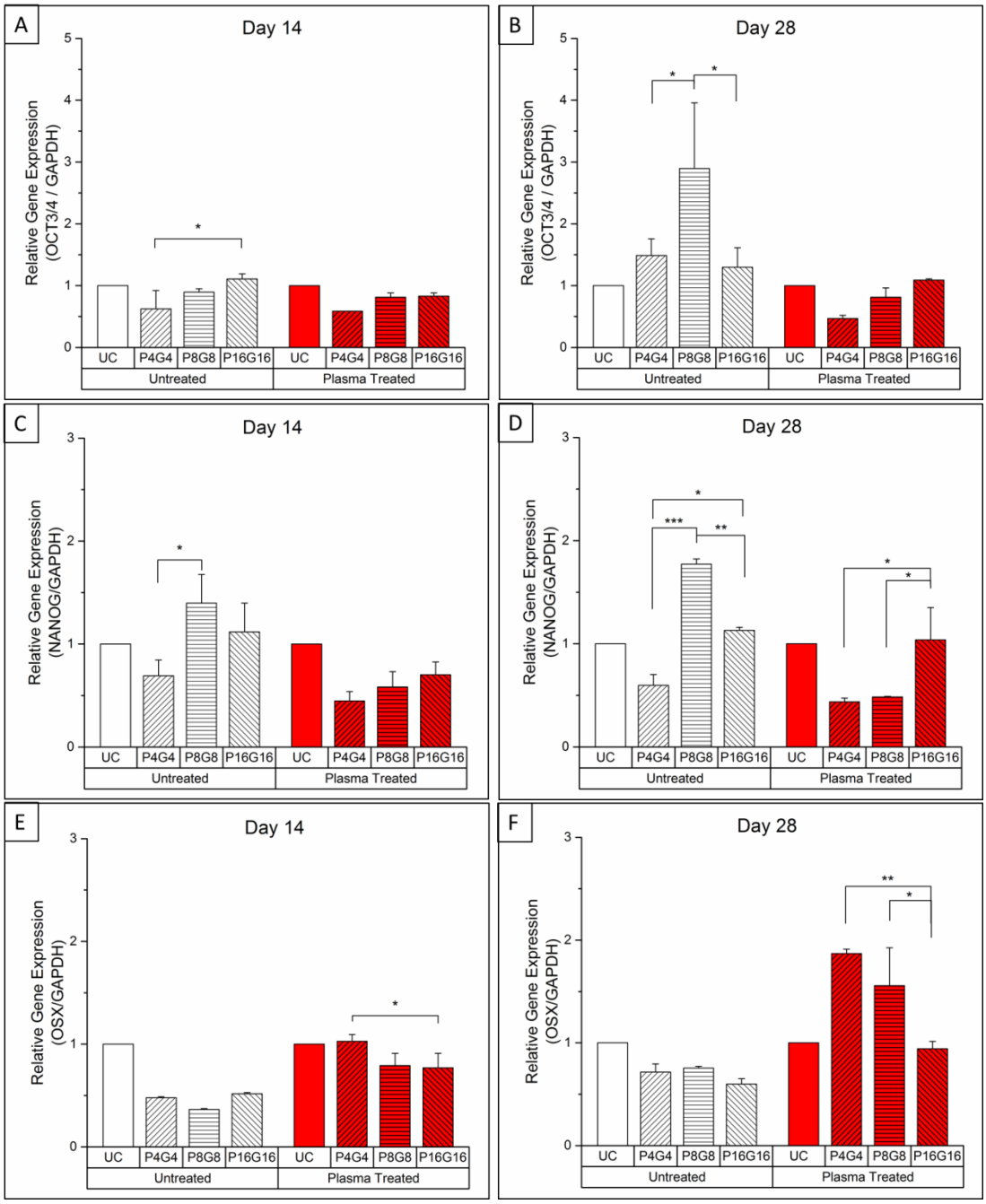

Figure 3.31. Relative expressions of stemness and osteogenic markers on untreated and plasma treated micropatterned substrates compared to unpatterned control. Expressions of (A,B) Oct3/4, (C,D) Nanog, (E,F) Osx, (G,H) ALP and (I,J) OC on Days 14 and 28.

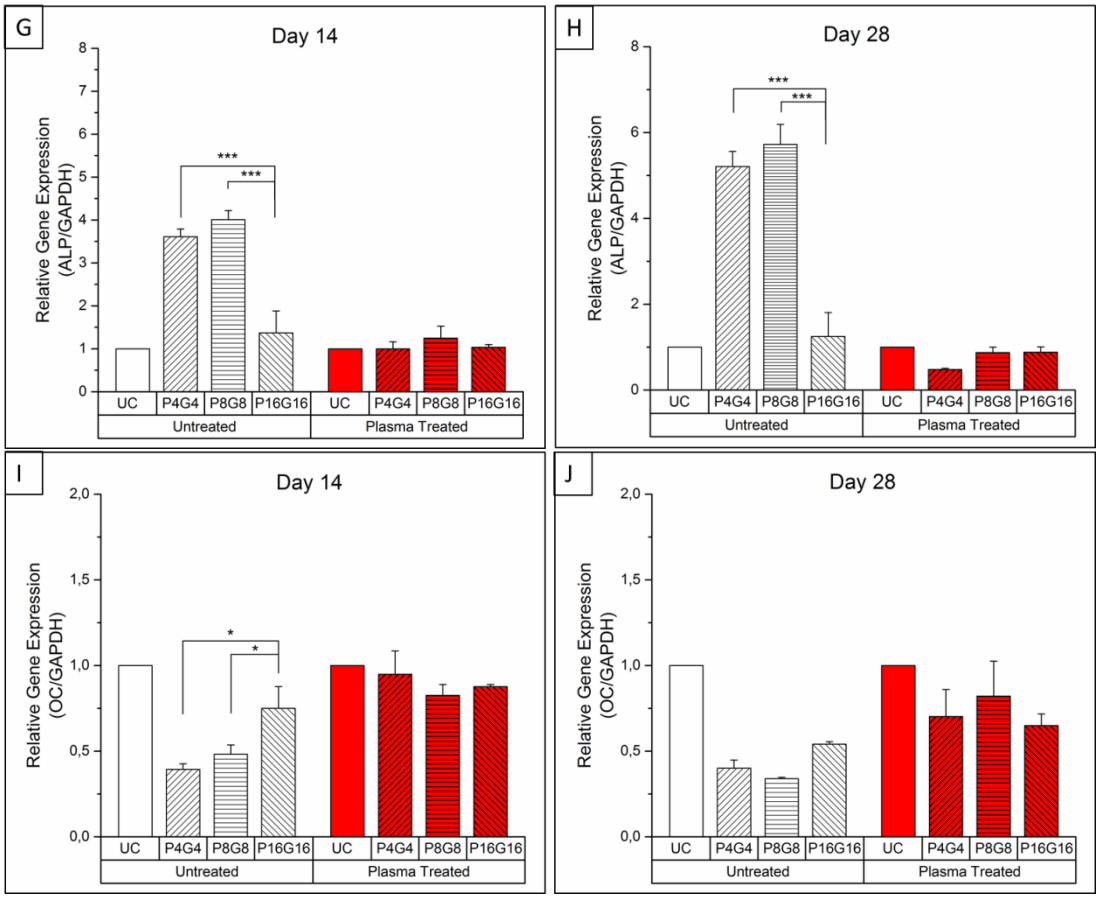

Figure 3.31 (continued).

The significant increase in the expression of ALP on untreated P4G4 and P8G8 (and a lesser increase on P16G16) suggests increased osteogenic differentiation of cells, something that was not observed on plasma treated counterparts. The increase in ALP was not accompanied by an increase in neither Osx nor OC. Osx is an early osteogenic marker and was shown to decrease upon commitment to osteogenic lineage. Therefore, it might have peaked at an earlier time point that was not examined in this study. Similarly, the absence of an increase in the late bone marker OC might be because the cells did not become fully differentiated in 28 day culture. It is possible that the increase was observed in ALP because ALP is one of the first expressed major osteogenic markers and might be induced at the gene level before

OC (Stein et al., 1993). A similar observation was reported by Song et al. (2015), who tested human MSCs on PDMS decorated with 10 μm sided cubic pillars separated by 10 μm for 6 weeks and observed a significant increase in ALP expression but not in OC. The increase in ALP on hydrophobic but not hydrophilic substrates could be related with their positions with respect to the pillars.

On untreated substrates, a large portion of the cells were shown to localize on the pillar tops and form aggregates, while on plasma treated substrates the cells completely occupied the interpillar spaces and then moved to the pillar tops as illustrated in Fig.3.24. It is known that cultures of human MSCs undergoing osteogenic differentiation form multilayered nodular structures *in vitro* (Jaiswal et al., 1997). Tang et al. (2010) reported a linear correlation between the cell-cell contact and osteogenic differentiation of the MSCs cultured on cell adhesive chemical patterns (islands), and the highest differentiation was observed in the largest cell "microislands". In another study, hydrophobic substrates were shown to force the aggregation of stem cells and lead to an increase in their differentiation. (Valamehr et al., 2008). Such cell aggregates were reported to form on hydrophobic nanopillars rather than microstructures. For instance, Brammer et al. (2011) reported formation of aggregates of mesenchymal stem cells with intense bone protein deposits on gold coated silicon substrates decorated with 2.5 μm high and 20 nm wide dense nanopillars but not on 2 μm wide and 2.5 μm high micropillars separated by 4 μm. Cells on the micropillars were shown to spread on both the pillars and the substrate floor as the pillars were relatively short and the cells were reported to fail to form aggregates. Dalby et al. (2007) also demonstrated the presence of intense cell aggregations and formations of osteocalcin and osteopontin positive early bone nodules when human MSCs were cultured on PMMA substrates carrying disordered 100 nm deep and 120 nm wide nanopillars. In this study, on the other hand, cells formed aggregates on the untreated hydrophobic pillar tops rather than stretching from pillar tops to the interpillar space, and these could explain the difference between the untreated and plasma treated substrates. Restricted contact of the cells

that invaded the interpillar spaces on the plasma treated substrates might have inhibited the osteogenic differentiation at early time points. The relative increase in the expression of Osx observed on plasma treated P4G4 and P8G8 on day 28 might be an indicator of osteogenic commitment at a much later time point. The major difference observed on day 28 on these surfaces was the large number of cells spread over the pillar tops as a result of reaching confluency at the substrate floor between the pillars, while at earlier time points the cells were between the pillars and had a smaller spread area which lead to deformed cytoskeleton, and might have inhibited osteogenesis. Human MSCs were shown to undergo osteogenesis as long as they are allowed to flatten and spread due to higher RhoA mediated cytoskeletal contractility, focal adhesion assembly and downstream integrin signaling. McBeath et al. (2004) reported that osteogenic differentiation of hMSCs occurs when they are cultured on microcontact printed fibronectin islands with an area of 10000 μm^2 but not on 1024 μm^2, and explained this with increased ROCK activity and shape mediated actomyosin contraction. In addition to the spread area, the interactions between the cells and pillars and the localization of the focal contacts could be also another factor in osteogenesis. Seo et al. (2011) showed that distribution of focal adhesions cultured on pillars 2 μm wide and separated by 3 μm gaps was primarily on pillar tops rather than the bottom. They also reported maturation of the focal adhesions on the pillars and subsequent organization of the actin organization through the RhoA/ROCK pathway. In another study, Salasznyk et al. (2007) showed that focal adhesion kinase signaling induces osteogenic differentiation of hMSCs through ERK dependent pathway by upregulating the expressions of osteogenic transcription factors Runx2 and osterix. Based on these, it can be proposed that the cells on the hydrophobic pillar tops could be committed to osteogenic lineage much earlier than the cells on plasma treated hydrophilic surfaces which climb up the pillars later, after confluency at the bottom.

The conformational changes in the cell cytoskeleton and nuclei also showed differences between plasma treated substrates and their controls which could also

influence the fate of DPSCs. On plasma treated P4G4, cells were elongated more than the population on untreated control. Yao et al. (2013) demonstrated that the extent of osteogenesis increases with increasing aspect ratio of cells up to an optimum point and then decreases. They cultured rat BMSCs on rectangular RGD microislands with same areas but different lateral aspect ratios and showed that the fraction of cells undergoing osteogenesis increased from aspect ratio 1 to 2, but decreased beyond 2. The aspect ratios of the cells cultured on plasma treated P4G4 surfaces in this study, however, were much higher than 2 when they resided between the pillars, which might have inhibited osteogenesis. Another difference between the untreated and plasma treated P4G4 and P8G8 were the fraction of deformed nuclei at late time points. On untreated surfaces the cells residing on the pillar tops were observed to have undeformed nucleus starting from day 14, while a large proportion of the cells on hydrophilic counterparts maintained their deformed nuclei until day 28. The presence of undeformed nuclei on untreated P4G4 and P8G8 substrates could be an indicator of the differentiating cells as the nucleus of stem cells become stiffer after differentiation as a result of increased lamin A/C expression.

CHAPTER 4

CONCLUSION

The interactions of cells with substrate surfaces regulate cellular behavior such as adhesion, migration, proliferation and differentiation. Cell-substrate studies are, therefore, important especially in the engineering of optimum biomaterial surfaces. In this study, PMMA films decorated with micropillars were fabricated and they were treated with oxygen plasma in order to study the influence of dimensions and the hydrophilicity of micropillars on the adhesion, proliferation, conformation and osteogenic differentiation of human dental pulp mesenchymal stem cells (DPSCs).

The present study showed that standard photolithography method makes production of micropatterned surfaces with tolerable deviation from the intended geometry and dimensions. Solvent casting of PMMA on the PDMS molds of the master template yielded accurate polymeric replicates which were satisfactory for use in the study of cell-surface interactions. Hydrophilicity (and therefore, wettability) of the resultant substrates was a function of both the surface chemistry and the pattern dimensions, and could be modulated remarkably upon oxygen plasma treatment.

Behavior of mesenchymal stem cells was affected by the micron scale topographical features on the substrate surface to varying extents depending on the dimensions and chemistry of the patterns. 3D structures on the substrate surface acted as anchorage sites and therefore, micropillars increased cell attachment even when the surface hydrophobicity was too high to promote cell adhesion. The number of attached cells

is directly proportional to the density of the pillars on the surface and the highest value was obtained for P4G4 in this study. Higher hydrophilicity induced by oxygen plasma had a stronger positive effect on cell attachment than physical topography.

Micropillars introduced distinct morphological changes in the cytoskeleton and nuclei of mesenchymal stem cells. Pattern dimensions influenced the type of deformations of the cytoskeleton, while the position of the cells, and the timing and extent of the deformations on these micropatterned surfaces were determined by the surface hydrophilicity. Substrates with pillar/gap dimensions that are too small relative to the average size of the cells caused extensive cell elongationand severe deformations of the nucleus. Cells displayed a more branched morphology on substrtaes with larger pillar/gap dimensions, and the deformations of the nuclei disappeared when the gap size was large enough for the nuclei to fit into the interpillar gaps. Digital analysis of the micrographs by using image analysis software made it possible to quantify the deformations observed. Selected shape descriptors, namely elongation and branching for cytoskeletal shape and circularity for the nuclear shape, were shown to be successful and quite useful to quantify the deformations and classify the substrates based on the type, timing and extent of the morphological changes they caused. The analysis results revealed that cell elongation and branching occurred antagonistically and depended on the pillar/gap dimensions. Surface hydrophilicty was also an important parameter in terms of the interactions of the cells with the patterned surfaces. Morphological changes occurred earlier and to a higher extent on oxygen plasma treated hydrophilic substrates than on their untreated counterparts.

Micropillar cues also influenced the proliferation of the mesenchymal stem cells. Surfaces with high density of pillars (small pillar/gap size) had a detrimental effect on cell proliferation at early time points, probably due to severe deformations in the cell nuclei. This negative effect vanished at later time points as a result of the growth of the cells on the pillar tops and no deformations was displayed in nuclei. Increased hydrophilicity significantly increased the proliferation rate of the cells, but it was not

enough to neutralize the negative effect of the nuclear deformations caused by the micropillars.

As expected topographical features of the substrates had a net effect on gene expression of the mesenchymal stem cells. Substrates with small pillar/gap dimensions led to a downregulation of stemness markers while larger dimensions had no distinct effect, suggesting the existence of a correlation between gene expression and nuclear deformation. Micropillar structures of untreated substrates also induced an upregulation in the expression of early bone marker genes. Morphological changes caused by the pillar cues might have induced osteogenic differentiation of the cells withouth any need for soluble factors such as dexamethasone or ascorbic acid, but further experiments such as immunostaining of the bone matric proteins or western blotting of the marker proteins are required to confirm cell differentiation.

This study showed that micropillar structures influence the fate of human dental pulp mesenchymal stem cells by altering the attachment, morphology, proliferation and expression of stemness and bone marker genes by the cells. To generalize these effects, mesenchymal stem cells of different origins (bone marrow, adipose etc.) could be cultured on the designed substrates to study their fate. In addition to osteogenesis, the analysis of the effect of micropillars on the expression of other genes and differentiation towards other lineages such as muscle or neural cells is possible by using large gene arrays.

REFERENCES

Abagnale, G., Steger, M., Nguyen, V. H., Hersch, N., Sechi, A., Joussen, S., & Schnakenberg, U. (2015). Surface topography enhances differentiation of mesenchymal stem cells towards osteogenic and adipogenic lineages. *Biomaterials*, 61, 316-326.

Ahdjoudj, S., Lasmoles, F., Oyajobi, B. O., Lomri, A., Delannoy, P., & Marie, P. J. (2001). Reciprocal control of osteoblast/chondroblast and osteoblast/adipocyte differentiation of multipotential clonal human marrow stromal F/STRO-1+ cells. *Journal of cellular biochemistry*, 81(1), 23-38.

Aita, H., Att, W., Ueno, T., Yamada, M., Hori, N., Iwasa, F., & Ogawa, T. (2009). Ultraviolet light-mediated photofunctionalization of titanium to promote human mesenchymal stem cell migration, attachment, proliferation and differentiation. *Acta Biomaterialia*, 5(8), 3247-3257.

Alapan, Y., Younesi, M., Akkus, O., & Gurkan, U. A (2015). Anisotropically Stiff Micropillars as a Unidirectional Cell Entrapment and Alignment Niche for Cardiomyocytes. Society for Biomaterials Annual Meeting & Exposition, April 15-18, Charlotte, NC, USA (Poster Presentation)

Alberts, B., Bray, D., Hopkin, K., Johnson, A., Lewis, J., Raff, M. & Walter, P. (2013). *Essential cell biology*. Garland Science.

Alberts, B., Johnson, A., Lewis, J., Raff, M., Roberts, K., & Walter, P. (2002). Cell junctions, cell adhesion, and the extracellular matrix. *Molecular Biology of the Cell*. Alberts B (Ed.). Garland, New York, USA 1065–1125

Anderson, J. M., Vines, J. B., Patterson, J. L., Chen, H., Javed, A., & Jun, H. W. (2011). Osteogenic differentiation of human mesenchymal stem cells synergistically enhanced by biomimetic peptide amphiphiles combined with conditioned medium. *Acta biomaterialia*, 7(2), 675-682.

Andersson, A. S., Olsson, P., Lidberg, U., & Sutherland, D. (2003). The effects of continuous and discontinuous groove edges on cell shape and alignment. *Experimental cell research*, 288(1), 177-188.

Arima, Y., & Iwata, H. (2007). Effect of wettability and surface functional groups on protein adsorption and cell adhesion using well-defined mixed self-assembled monolayers. *Biomaterials*, 28(20), 3074-3082.

Atala, A. (2004). Tissue engineering and regenerative medicine: concepts for clinical application. *Rejuvenation research*, 7(1), 15-31.

Baac, H., Lee, J. H., Seo, J. M., Park, T. H., Chung, H., Lee, S. D., & Kim, S. J. (2004). Submicron-scale topographical control of cell growth using holographic surface relief grating. *Materials Science and Engineering: C*, 24(1), 209-212.

Badique, F., Stamov, D. R., Davidson, P. M., Veuillet, M., Reiter, G., Freund, J. N., & Anselme, K. (2013). Directing nuclear deformation on micropillared surfaces by substrate geometry and cytoskeleton organization. *Biomaterials*, 34(12), 2991-3001.

Bae, J. S., Oh, C. S., Nam, J. E., Lee, J. K., & Lee, H. J. (2009). A tensile test technique for the freestanding PMMA thin films. *Current Applied Physics*, 9(1), S107-S109.

Barbosa, J. N., Madureira, P., Barbosa, M. A., & Águas, A. P. (2005). The attraction of Mac-1+ phagocytes during acute inflammation by methyl-coated self-assembled monolayers. *Biomaterials*, 26(16), 3021-3027.

Baujard-Lamotte, L., Noinville, S., Goubard, F., Marque, P., & Pauthe, E. (2008). Kinetics of conformational changes of fibronectin adsorbed onto model surfaces. *Colloids and Surfaces B: Biointerfaces*, 63(1), 129-137.

Benoit, D. S., & Anseth, K. S. (2005). The effect on osteoblast function of colocalized RGD and PHSRN epitopes on PEG surfaces. *Biomaterials*, 26(25), 5209-5220.

Bettinger, C. J., Langer, R., & Borenstein, J. T. (2009). Engineering substrate topography at the micro-and nanoscale to control cell function. *Angewandte Chemie International Edition*, 48(30), 5406-5415.

Bhadriraju, K., Yang, M., Ruiz, S. A., Pirone, D., Tan, J., & Chen, C. S. (2007). Activation of ROCK by RhoA is regulated by cell adhesion, shape, and cytoskeletal tension. *Experimental cell research*, 313(16), 3616-3623.

Bixler, G. D., & Bhushan, B. (2013). Fluid drag reduction and efficient self-cleaning with rice leaf and butterfly wing bioinspired surfaces. *Nanoscale*, 5(17), 7685-7710.

Blondiaux, N., Scolan, E., Popa, A. M., Gavillet, J., & Pugin, R. (2009). Fabrication of superhydrophobic surfaces with controlled topography and chemistry. *Applied Surface Science*, 256(3), S46-S53.

Bonzani, I. C., Adhikari, R., Houshyar, S., Mayadunne, R., Gunatillake, P., & Stevens, M. M. (2007). Synthesis of two-component injectable polyurethanes for bone tissue engineering. *Biomaterials*, 28(3), 423-433.

Borges, A. M. G., Benetoli, L. O., Licínio, M. A., Zoldan, V. C., Santos-Silva, M. C., Assreuy, J., & Soldi, V. (2013). Polymer films with surfaces unmodified and modified by non-thermal plasma as new substrates for cell adhesion. *Materials Science and Engineering: C*, 33(3), 1315-1324.

Brammer, K. S., Choi, C., Frandsen, C. J., Oh, S., & Jin, S. (2011). Hydrophobic nanopillars initiate mesenchymal stem cell aggregation and osteo-differentiation. *Acta biomaterialia*, 7(2), 683-690.

Brunette, D. M., Kenner, G. S., & Gould, T. R. L. (1983). Grooved titanium surfaces orient growth and migration of cells from human gingival explants. *Journal of Dental Research*, 62(10), 1045-1048.

Buttery, L. D. K., Bourne, S., Xynos, J. D., Wood, H., Hughes, F. J., Hughes, S. P. F., & Polak, J. M. (2001). Differentiation of osteoblasts and in vitro bone formation from murine embryonic stem cells. *Tissue engineering*, 7(1), 89-99.

Cassie, A. B. D., & Baxter, S. (1944). Wettability of porous surfaces. *Transactions of the Faraday Society*, 40, 546-551.

Castillo, A. B., & Jacobs, C. R. (2010). Mesenchymal stem cell mechanobiology. *Current osteoporosis reports*, 8(2), 98-104.

Chai, J., Lu, F., Li, B., & Kwok, D. Y. (2004). Wettability interpretation of oxygen plasma modified poly (methyl methacrylate). *Langmuir*, 20(25), 10919-10927.

Chan, C. M., Ko, T. M., & Hiraoka, H. (1996). Polymer surface modification by plasmas and photons. *Surface science reports*, 24(1), 1-54.

Charest, J. L., Bryant, L. E., Garcia, A. J., & King, W. P. (2004). Hot embossing for micropatterned cell substrates. *Biomaterials*, 25(19), 4767-4775.

Charest, J. L., Eliason, M. T., García, A. J., & King, W. P. (2006). Combined microscale mechanical topography and chemical patterns on polymer cell culture substrates. *Biomaterials*, 27(11), 2487-2494.

Chen, C. S., Mrksich, M., Huang, S., Whitesides, G. M., & Ingber, D. E. (1998). Micropatterned surfaces for control of cell shape, position, and function. *Biotechnology progress*, 14(3), 356-363.

Chen, Y., & Pepin, A. (2001). Nanofabrication: Conventional and nonconventional methods. *Electrophoresis*, 22(2), 187-207.

Constantinescu, D., Gray, H. L., Sammak, P. J., Schatten, G. P., & Csoka, A. B. (2006). Lamin A/C expression is a marker of mouse and human embryonic stem cell differentiation. *Stem cells*, 24(1), 177-185.

Coutinho, D., Costa, P., Neves, N., Gomes, M. E., & Reis, R. L. (2011). Micro-and nanotechnology in tissue engineering. *In Tissue Engineering* (pp. 3-29). Springer Berlin Heidelberg.

Craighead, H. G., Turner, S. W., Davis, R. C., James, C., Perez, A. M., John, P. S., & Banker, G. (1998). Chemical and topographical surface modification for control of central nervous system cell adhesion. *Biomedical Microdevices*, 1(1), 49-64.

Crisan, M., Yap, S., Casteilla, L., Chen, C. W., Corselli, M., Park, T. S., & Norotte, C. (2008). A perivascular origin for mesenchymal stem cells in multiple human organs. *Cell stem cell*, 3(3), 301-313.

Cross, M., & Dexter, T. M. (1991). Growth factors in development, transformation, and tumorigenesis. *Cell*, 64(2), 271-280.

Curtis, A. S. G., & Varde, M. (1964). Control of cell behavior: topological factors. *Journal of the National Cancer Institute*, 33(1), 15-26.

Curtis, A. S., Dalby, M., & Gadegaard, N. (2006). Cell signaling arising from nanotopography: implications for nanomedical devices. *Future Medicine* (1), 67-72

Cvelbar, U., Pejovnik, S., Mozetie, M., & Zalar, A. (2003). Increased surface roughness by oxygen plasma treatment of graphite/polymer composite. *Applied surface science*, 210(3), 255-261.

da Silva Meirelles, L., Chagastelles, P. C., & Nardi, N. B. (2006). Mesenchymal stem cells reside in virtually all post-natal organs and tissues. *Journal of Cell Science*, 119(11), 2204-2213.

Dahl, K. N., Booth-Gauthier, E. A., & Ladoux, B. (2010). In the middle of it all: mutual mechanical regulation between the nucleus and the cytoskeleton. *Journal of biomechanics*, 43(1), 2-8.

Dahl, K. N., Ribeiro, A. J., & Lammerding, J. (2008). Nuclear shape, mechanics, and mechanotransduction. *Circulation research*, 102(11), 1307-1318.

Dalby, M. J., Gadegaard, N., Riehle, M. O., Wilkinson, C. D., & Curtis, A. S. (2004). Investigating filopodia sensing using arrays of defined nano-pits down to 35 nm diameter in size. *The international journal of biochemistry & cell biology*, 36(10), 2005-2015.

Dalby, M. J., Gadegaard, N., Tare, R., Andar, A., Riehle, M. O., Herzyk, P. & Oreffo, R. O. (2007). The control of human mesenchymal cell differentiation using nanoscale symmetry and disorder. *Nature materials*, 6(12), 997-1003.

Dalby, M. J., McCloy, D., Robertson, M., Agheli, H., Sutherland, D., Affrossman, S., & Oreffo, R. O. (2006). Osteoprogenitor response to semi-ordered and random nanotopographies. *Biomaterials*, 27(15), 2980-2987.

Davidson, P. M., Fromigué, O., Marie, P. J., Hasirci, V., Reiter, G., & Anselme, K. (2010). Topographically induced self-deformation of the nuclei of cells: dependence on cell type and proposed mechanisms. *Journal of Materials Science: Materials in Medicine*, 21(3), 939-946.

Davidson, P. M., Özçelik, H., Hasirci, V., Reiter, G., & Anselme, K. (2009). Microstructured Surfaces Cause Severe but Non-Detrimental Deformation of the Cell Nucleus. *Advanced Materials*, 21(35), 3586-3590.

Deans, R. J., & Moseley, A. B. (2000). Mesenchymal stem cells: biology and potential clinical uses. *Experimental hematology*, 28(8), 875-884.

del Campo, A., & Arzt, E. (2008). Fabrication approaches for generating complex micro-and nanopatterns on polymeric surfaces. *Chemical reviews*, 108(3), 911-945.

Den Braber, E. T., De Ruijter, J. E., Smits, H. T. J., Ginsel, L. A., Von Recum, A. F., & Jansen, J. A. (1996). Quantitative analysis of cell proliferation and orientation on substrata with uniform parallel surface micro-grooves. *Biomaterials*, 17(11), 1093-1099.

Desai, S. M., & Singh, R. P. (2004). Surface modification of polyethylene. *In Long Term Properties of Polyolefins* (pp. 231-294). Springer Berlin Heidelberg.

Deutsch, J., Motlagh, D., Russell, B., & Desai, T. A. (2000). Fabrication of microtextured membranes for cardiac myocyte attachment and orientation. *Journal of biomedical materials research*, 53

Dinklage, A., Klinger, T., Marx, G., & Schweikhard, L. (Eds.). (2005). Plasma physics: confinement, transport and collective effects (Vol. 670). Springer Science & Business Media.

Dominici, M. L. B. K., Le Blanc, K., Mueller, I., Slaper-Cortenbach, I., Marini, F. C., Krause, D. S., & Horwitz, E. M. (2006). Minimal criteria for defining multipotent mesenchymal stromal cells. *The International Society for Cellular Therapy position statement. Cytotherapy*, 8(4), 315-317.

Dowling, D. P., Miller, I. S., Ardhaoui, M., & Gallagher, W. M. (2010). Effect of surface wettability and topography on the adhesion of osteosarcoma cells on plasma-modified polystyrene. *Journal of biomaterials applications*.

Edalat, F., Bae, H., Manoucheri, S., Cha, J. M., & Khademhosseini, A. (2012). Engineering approaches toward deconstructing and controlling the stem cell environment. *Annals of biomedical engineering*, 40(6), 1301-1315.

Engler, A. J., Griffin, M. A., Sen, S., Bönnemann, C. G., Sweeney, H. L., & Discher, D. E. (2004). Myotubes differentiate optimally on substrates with tissue-like stiffness pathological implications for soft or stiff microenvironments. *The Journal of cell biology*, 166(6), 877-887.

Engler, A. J., Sen, S., Sweeney, H. L., & Discher, D. E. (2006). Matrix elasticity directs stem cell lineage specification. *Cell*, 126(4), 677-689.

Ermis M., Antmen E., Gurkan U. A., Demirci U., Hasirci V (2013). Effect of Micropatterned PLGA and Collagen Surfaces on Cell Adhesion and Nuclear Deformation. MRS Fall Meeting, December 1-6, Boston, MA, USA. (Poster presentation).

Estévez, M., Martínez, E., Yarwood, S. J., Dalby, M. J., & Samitier, J. (2015). Adhesion and migration of cells responding to microtopography. *Journal of Biomedical Materials Research Part A*, 103(5), 1659-1668.

Fan, Y. X., Gu, C. H., Zhang, Y. L., Zhong, B. S., Wang, L. Z., Zhou, Z. R., & Wang, F. (2013). Oct4 and Sox2 overexpression improves the proliferation and differentiation of bone mesenchymal stem cells in Xiaomeishan porcine. *Genet Mol Res*, 12(4), 6067-79.

Fang, T. H., & Chang, W. J. (2003). Effects of AFM-based nanomachining process on aluminum surface. *Journal of Physics and chemistry of Solids*, 64(6), 913-918.

Feng, X. J., & Jiang, L. (2006). Design and creation of superwetting/antiwetting surfaces. *Advanced Materials*, 18(23), 3063-3078.

Flemming, R. G., Murphy, C. J., Abrams, G. A., Goodman, S. L., & Nealey, P. F. (1999). Effects of synthetic micro-and nano-structured surfaces on cell behavior. *Biomaterials*, 20(6), 573-588.

Fletcher, D. A., & Mullins, R. D. (2010). Cell mechanics and the cytoskeleton. *Nature*, 463(7280), 485-492.

Frey, M. T., Tsai, I. Y., Russell, T. P., Hanks, S. K., & Wang, Y. L. (2006). Cellular responses to substrate topography: role of myosin II and focal adhesion kinase. *Biophysical journal*, 90(10), 3774-3782.

Friedenstein, A. J., Chailakhjan, R. K., & Lalykina, K. S. (1970). The development of fibroblast colonies in monolayer cultures of guinea-pig bone marrow and spleen cells. *Cell Proliferation*, 3(4), 393-403.

Fu, H., Doll, B., McNelis, T., & Hollinger, J. O. (2007). Osteoblast differentiation in vitro and in vivo promoted by Osterix. *Journal of biomedical materials research Part A*, 83(3), 770-778.

Gallagher, J. O., McGhee, K. F., Wilkinson, C. D. W., & Riehle, M. O. (2002). Interaction of animal cells with ordered nanotopography. *NanoBioscience*, IEEE Transactions on, 1(1), 24-28.

Galli, R., Gritti, A., & Vescovi, A. L. (2008). Adult neural stem cells. *Neural Stem Cells: Methods and Protocols*, 67-84.

Gauvin, R., Chen, Y. C., Lee, J. W., Soman, P., Zorlutuna, P., Nichol, J. W., & Khademhosseini, A. (2012). Microfabrication of complex porous tissue engineering scaffolds using 3D projection stereolithography. *Biomaterials*, 33(15), 3824-3834.

Geetha, M., Singh, A. K., Asokamani, R., & Gogia, A. K. (2009). Ti based biomaterials, the ultimate choice for orthopaedic implants–a review. *Progress in Materials Science*, 54(3), 397-425.

Genes, N. G., Rowley, J. A., Mooney, D. J., & Bonassar, L. J. (2004). Effect of substrate mechanics on chondrocyte adhesion to modified alginate surfaces. *Archives of biochemistry and biophysics*, 422(2), 161-167.

Gerecht, S., Bettinger, C. J., Zhang, Z., Borenstein, J. T., Vunjak-Novakovic, G., & Langer, R. (2007). The effect of actin disrupting agents on contact guidance of human embryonic stem cells. *Biomaterials*, 28(28), 4068-4077.

Ghibaudo, M., Trichet, L., Le Digabel, J., Richert, A., Hersen, P., & Ladoux, B. (2009). Substrate topography induces a crossover from 2D to 3D behavior in fibroblast migration. *Biophysical journal*, 97(1), 357-368.

Goddard, J. M., & Hotchkiss, J. H. (2007). Polymer surface modification for the attachment of bioactive compounds. *Progress in polymer science*, 32(7), 698-725.

Griffin, M. A., Sen, S., Sweeney, H. L., & Discher, D. E. (2004). Adhesion-contractile balance in myocyte differentiation. *Journal of cell science*, 117(24), 5855-5863.

Griffith, L. G. (2000). Polymeric biomaterials. *Acta materialia*, 48(1), 263-277.

Grinnell, F., & Feld, M. K. (1982). Fibronectin adsorption on hydrophilic and hydrophobic surfaces detected by antibody binding and analyzed during cell adhesion in serum-containing medium. *J biol chem*, 257(9), 4888-4893.

Gronthos, S., Mankani, M., Brahim, J., Robey, P. G., & Shi, S. (2000). Postnatal human dental pulp stem cells (DPSCs) in vitro and in vivo. *Proceedings of the National Academy of Sciences*, 97(25), 13625-13630.

Hamilton, D. W., Wong, K. S., & Brunette, D. M. (2006). Microfabricated discontinuous-edge surface topographies influence osteoblast adhesion, migration, cytoskeletal organization, and proliferation and enhance matrix and mineral deposition in vitro. *Calcified tissue international*, 78(5), 314-325.

Han, S. M., Han, S. H., Coh, Y. R., Jang, G., Ra, J. C., Kang, S. K., & Youn, H. Y. (2014). Enhanced proliferation and differentiation of Oct4-and Sox2-overexpressing human adipose tissue mesenchymal stem cells. *Exp Mol Med*, 46, e101.

Hanson, A. D., Wall, M. E., Pourdeyhimi, B., & Loboa, E. G. (2007). Effects of oxygen plasma treatment on adipose-derived human mesenchymal stem cell adherence to poly (L-lactic acid) scaffolds. *Journal of Biomaterials Science*, Polymer Edition, 18(11), 1387-1400.

Harrison, R. G. (1911). On the stereotropism of embryonic cells. *Science*, 279-281.

Hasirci, V., & Kenar, H. (2006). Novel surface patterning approaches for tissue engineering and their effect on cell behavior. *Future Medicine*, 73-90.

Haudenschild, A. K., Hsieh, A. H., Kapila, S., & Lotz, J. C. (2009). Pressure and distortion regulate human mesenchymal stem cell gene expression. *Annals of biomedical engineering*, 37(3), 492-502.

He, Y., Jiang, C., Wang, S., Ma, Z., Tian, W., & Yuan, W. (2014). Tailoring Anisotropic Wettability Using Micro-pillar Geometry. Colloids and Interface Science Communications, 2, 19-23.

Hench, L. L., & Wilson, J. (Eds.). (1993). An introduction to bioceramics (Vol. 1). World Scientific.

Huang, G. J., Gronthos, S., & Shi, S. (2009). Mesenchymal stem cells derived from dental tissues vs. those from other sources: their biology and role in regenerative medicine. *Journal of dental research*, 88(9), 792-806.

Humphrey, J. D., Dufresne, E. R., & Schwartz, M. A. (2014). Mechanotransduction and extracellular matrix homeostasis. *Nature Reviews Molecular Cell Biology*, 15(12), 802-812.

Huri, P. Y., Huri, G., Yasar, U., Ucar, Y., Dikmen, N., Hasirci, N., & Hasirci, V. (2013). A biomimetic growth factor delivery strategy for enhanced regeneration of iliac crest defects. *Biomedical Materials*, 8(4), 045009.

Hwang, N. S., Varghese, S., & Elisseeff, J. (2008). Controlled differentiation of stem cells. *Advanced drug delivery reviews*, 60(2), 199-214.

Ibarretxe, G., O. Crende, M. Aurrekoetxea, V. García-Murga, J. Etxaniz, F. Unda (2012) Neural crest stem cells from dental tissues: a new hope for dental and neural regeneration. *Stem Cells Int* 2012: 103503

Igarashi, M., Kamiya, N., Hasegawa, M., Kasuya, T., Takahashi, T., & Takagi, M. (2004). Inductive effects of dexamethasone on the gene expression of Cbfa1, Osterix and bone matrix proteins during differentiation of cultured primary rat osteoblasts. *Journal of molecular histology*, 35(1), 3-10.

Ingber, D. E. (1997). Tensegrity: the architectural basis of cellular mechanotransduction. *Annual review of physiology*, 59(1), 575-599.

Jaalouk, D. E., & Lammerding, J. (2009). Mechanotransduction gone awry. *Nature reviews Molecular cell biology*, 10(1), 63-73.

Jaiswal, N., Haynesworth, S. E., Caplan, A. I., & Bruder, S. P. (1997). Osteogenic differentiation of purified, culture-expanded human mesenchymal stem cells in vitro. *Journal of cellular biochemistry*, *64*(2), 295-312.

Jeon, H., Hidai, H., Hwang, D. J., Healy, K. E., & Grigoropoulos, C. P. (2010). The effect of micronscale anisotropic cross patterns on fibroblast migration. *Biomaterials*, 31(15), 4286-4295.

Kanafi, M. M., Ramesh, A., Gupta, P. K., & Bhonde, R. R. (2013). Influence of hypoxia, high glucose, and low serum on the growth kinetics of mesenchymal stem cells from deciduous and permanent teeth. *Cells Tissues Organs*, 198(3), 198-208.

Karageorgiou, V., & Kaplan, D. (2005). Porosity of 3D biomaterial scaffolds and osteogenesis. *Biomaterials*, 26(27), 5474-5491.

Kariduraganavar, M. Y., Kittur, A. A., & Kamble, R. R. (2014). Chapter 1-Polymer synthesis and processing. *Nat. Synth. Biomed. Polym*. 1st ed., Elsevier Inc, 1-31.

Katti, D. S., Vasita, R., & Shanmugam, K. (2008). Improved biomaterials for tissue engineering applications: surface modification of polymers. *Current topics in medicinal chemistry*, 8(4), 341-353.

Kerkis, I., Kerkis, A., Dozortsev, D., Stukart-Parsons, G. C., Gomes Massironi, S. M., Pereira, L. V., & Cerruti, H. F. (2007). Isolation and characterization of a population of immature dental pulp stem cells expressing OCT-4 and other embryonic stem cell markers. *Cells Tissues Organs*, 184(3-4), 105-116.

Keselowsky, B. G., Collard, D. M., & García, A. J. (2005). Integrin binding specificity regulates biomaterial surface chemistry effects on cell differentiation. *Proceedings of the National Academy of Sciences*, 102(17), 5953-5957.

Khanna-Jain, R., Vanhatupa, S., Vuorinen, A., Sandor, G. K., Suuronen, R., Mannerstrom, B., & Miettinen, S. (2013). Growth and differentiation of human dental pulp stem cells maintained in fetal bovine serum, human serum and

serum-free/xeno-free culture media. *Journal of Stem Cell Research & Therapy*, 2012.

Khorasani, M. T., Mirzadeh, H., & Irani, S. (2008). Plasma surface modification of poly (L-lactic acid) and poly (lactic-co-glycolic acid) films for improvement of nerve cells adhesion. *Radiation Physics and Chemistry*, 77(3), 280-287.

Kilian, K. A., Bugarija, B., Lahn, B. T., & Mrksich, M. (2010). Geometric cues for directing the differentiation of mesenchymal stem cells. *Proceedings of the National Academy of Sciences*, 107(11), 4872-4877.

Kim, S. H., Ha, H. J., Ko, Y. K., Yoon, S. J., Rhee, J. M., Kim, M. S., & Khang, G. (2007). Correlation of proliferation, morphology and biological responses of fibroblasts on LDPE with different surface wettability. *Journal of Biomaterials Science*, Polymer Edition, 18(5), 609-622.

Kim, S. J., Lee, J. K., Kim, J. W., Jung, J. W., Seo, K., Park, S. B., Lee, Y. S. (2008). Surface modification of polydimethylsiloxane (PDMS) induced proliferation and neural-like cells differentiation of umbilical cord blood-derived mesenchymal stem cells. *Journal of Materials Science: Materials in Medicine*, 19(8), 2953-2962.

Kishi, N., & Kamata, K. (1961). The effects of gamma irradiation on poly(methyl methacrylate). J. *Appl. Phys*.(Japan), 30.

Klemmt, P. A., Vafaizadeh, V., & Groner, B. (2011). The potential of amniotic fluid stem cells for cellular therapy and tissue engineering. *Expert Opinion on Biological Therapy*, 11(10), 1297-1314.

Kohane, D. S., & Langer, R. (2008). Polymeric biomaterials in tissue engineering. *Pediatric research*, 63(5), 487-491.

Kolind, K., Kraft, D., Bøggild, T., Duch, M., Lovmand, J., Pedersen, F. S., & Besenbacher, F. (2014). Control of proliferation and osteogenic differentiation of human dental-pulp-derived stem cells by distinct surface structures. *Acta biomaterialia*, 10(2), 641-650.

Lakes, R. (2000). Composite biomaterials. The biomedical engineering handbook, 41, 1-13.

Lamalice, L., Le Boeuf, F., & Huot, J. (2007). Endothelial cell migration during angiogenesis. *Circulation research*, 100(6), 782-794.

Landel, R. F., & Nielsen, L. E. (1993). Mechanical properties of polymers and composites. CRC Press.

Lane, J. M., & Hourston, D. J. (1993). Surface treatments of polyolefins. *Progress in organic coatings*, 21(4), 269-284.

Langenbach, F., & Handschel, J. (2013). Effects of dexamethasone, ascorbic acid and β-glycerophosphate on the osteogenic differentiation of stem cells in vitro. *Stem Cell Res Ther*, 4(5), 117.

Langer, R. (2000). Biomaterials in drug delivery and tissue engineering: one laboratory's experience. *Accounts of Chemical Research*, 33(2), 94-101.

Lee, J. H., Khang, G., Lee, J. W., & Lee, H. B. (1998). Interaction of different types of cells on polymer surfaces with wettability gradient. *Journal of colloid and interface science*, 205(2), 323-330.

Lee, K., Silva, E. A., & Mooney, D. J. (2011). Growth factor delivery-based tissue engineering: general approaches and a review of recent developments. *Journal of the Royal Society Interface*, 8(55), 153-170.

Lee, M. H., Ducheyne, P., Lynch, L., Boettiger, D., & Composto, R. J. (2006). Effect of biomaterial surface properties on fibronectin–α 5 β 1 integrin interaction and cellular attachment. *Biomaterials*, 27(9), 1907-1916.

Lemons, J. E. (1996). Ceramics: past, present, and future. *Bone*, 19(1), S121-S128.

Liliensiek, S. J., Campbell, S., Nealey, P. F., & Murphy, C. J. (2006). The scale of substratum topographic features modulates proliferation of corneal epithelial cells and corneal fibroblasts. *Journal of biomedical materials research Part A*, 79(1), 185-192.

Lindroos, B., Boucher, S., Chase, L., Kuokkanen, H., Huhtala, H., Haataja, R., & Miettinen, S. (2009). Serum-free, xeno-free culture media maintain the proliferation rate and multipotentiality of adipose stem cells in vitro. *Cytotherapy*, 11(7), 958-972.

Liu, L., Wei, X., Ling, J., Wu, L., & Xiao, Y. (2011). Expression pattern of Oct-4, Sox2, and c-Myc in the primary culture of human dental pulp derived cells. *Journal of endodontics*, 37(4), 466-472.

Liu, X., & Ma, P. X. (2004). Polymeric scaffolds for bone tissue engineering. *Annals of biomedical engineering*, 32(3), 477-486.

Loh, Y. H., Wu, Q., Chew, J. L., Vega, V. B., Zhang, W., Chen, X., & Wong, K. Y. (2006). The Oct4 and Nanog transcription network regulates pluripotency in mouse embryonic stem cells. *Nature genetics*, 38(4), 431-440.

Lucchesi, C., Ferreira, B. M., Duek, E. A., Santos Jr, A. R., & Joazeiro, P. P. (2008). Increased response of Vero cells to PHBV matrices treated by plasma. Journal of Materials Science: Materials in Medicine, 19(2), 635-643.

Ma, Z., Gao, C., & Shen, J. (2003). Surface modification of poly-L-lactic acid (PLLA) membrane by grafting acrylamide: an effective way to improve

cytocompatibility for chondrocytes. *Journal of Biomaterials Science*, Polymer Edition, 14(1), 13-25.

Maalouf, A., Gadonna, M., & Bosc, D. (2008). An improvement in standard photolithography resolution based on Kirchhoff diffraction studies. *Journal of Physics D: Applied Physics*, 42(1), 015106.

MacQueen, L., Sun, Y., & Simmons, C. A. (2013). Mesenchymal stem cell mechanobiology and emerging experimental platforms. *Journal of The Royal Society Interface*, 10(84), 20130179.

Madou, M. J. (2002). Fundamentals of microfabrication: the science of miniaturization. CRC press.

Mai, J., Sun, C., Li, S., & Zhang, X. (2007). A microfabricated platform probing cytoskeleton dynamics using multidirectional topographical cues. *Biomedical microdevices*, 9(4), 523-531.

Mano, J. F., Silva, G. A., Azevedo, H. S., Malafaya, P. B., Sousa, R. A., Silva, S. S. & Neves, N. M. (2007). Natural origin biodegradable systems in tissue engineering and regenerative medicine: present status and some moving trends. *Journal of the Royal Society Interface*, 4(17), 999-1030.

Manolagas, S. C. (2000). Birth and death of bone cells: basic regulatory mechanisms and implications for the pathogenesis and treatment of osteoporosis 1. *Endocrine reviews*, 21(2), 115-137.

Marko, J. F., & Poirier, M. G. (2003). Micromechanics of chromatin and chromosomes. *Biochemistry and cell biology*, 81(3), 209-220.

Martinez, E., Engel, E., Planell, J. A., & Samitier, J. (2009). Effects of artificial micro-and nano-structured surfaces on cell behaviour. *Annals of Anatomy-Anatomischer Anzeiger*, 191(1), 126-135.

Martini, F. (1998). Anatomy and Physiology, 2007 Ed. Rex Bookstore, Inc.

Martino, S., D'Angelo, F., Armentano, I., Kenny, J. M., & Orlacchio, A. (2012). Stem cell-biomaterial interactions for regenerative medicine. *Biotechnology advances*, 30(1), 338-351.

Matsuzaka, K., Walboomers, F., Ruijter, A., & Jansen, J. A. (2000). Effect of microgrooved poly-l-lactic (PLA) surfaces on proliferation, cytoskeletal organization, and mineralized matrix formation of rat bone marrow cells. *Clinical oral implants research*, 11(4), 325-333.

Matsuzaka, K., Walboomers, X. F., Yoshinari, M., Inoue, T., & Jansen, J. A. (2003). The attachment and growth behavior of osteoblast-like cells on microtextured surfaces. *Biomaterials*, 24(16), 2711-2719.

Mattila, P. K., & Lappalainen, P. (2008). Filopodia: molecular architecture and cellular functions. *Nature reviews Molecular cell biology*, 9(6), 446-454.

McBeath, R., Pirone, D. M., Nelson, C. M., Bhadriraju, K., & Chen, C. S. (2004). Cell shape, cytoskeletal tension, and RhoA regulate stem cell lineage commitment. *Developmental cell*, 6(4), 483-495.

McClary, K. B., Ugarova, T., & Grainger, D. W. (2000). Modulating fibroblast adhesion, spreading, and proliferation using self-assembled monolayer films of alkylthiolates on gold. *Journal of biomedical materials research*, 50(3), 428-439.

McMurray, R., Dalby, M. J., & Gadegaard, N. (2011). Nanopatterned surfaces for biomedical applications. In: Laskovski A, (Ed.) Biomedical Engineering Trends in Materials Science

McNeish, J. D. (2007). Stem cells as screening tools in drug discovery. *Current opinion in pharmacology*, 7(5), 515-520.

Miller, J. P., Perry, E. H., Price, T. H., Bolan, C. D., Karanes, C., Boyd, T. M., & King, R. J. (2008). Recovery and safety profiles of marrow and PBSC donors: experience of the National Marrow Donor Program. *Biology of Blood and Marrow Transplantation*, 14(9), 29-36.

Mitra, S. K., Hanson, D. A., & Schlaepfer, D. D. (2005). Focal adhesion kinase: in command and control of cell motility. *Nature reviews Molecular cell biology*, 6(1), 56-68.

Mitragotri, S., & Lahann, J. (2009). Physical approaches to biomaterial design. *Nature materials*, 8(1), 15-23.

Mitsui, K., Tokuzawa, Y., Itoh, H., Segawa, K., Murakami, M., Takahashi, K., Yamanaka, S. (2003). The homeoprotein Nanog is required for maintenance of pluripotency in mouse epiblast and ES cells. *Cell*, 113(5), 631-642.

Miura, M., S. Gronthos, M. Zhao, B. Lu, L.W. Fisher, P.G. Robey, S. Shi (2003) SHED: stem cells from human exfoliated deciduous teeth. *Proc Natl Acad Sci USA 100*: 5807–5812.

Mokry, J., T. Soukup, S. Micuda, J. Karbanova, B. Visek, E. Brcakova, J. Suchanek, J. Bouchal, D. Vokurkova, R. Ivancakova (2010) Telomere attrition occurs during ex vivo expansion of human dental pulp stem cells. *J Biomed Biotechnol 2010*: 673513.

Moroni, L., & Lee, L. P. (2009). Micropatterned hot-embossed polymeric surfaces influence cell proliferation and alignment. *Journal of Biomedical Materials Research Part A*, 88(3), 644-653.

Moy, P., Gunnarsson, C. A., Weerasooriya, T., & Chen, W. (2011). Stress-strain response of pmma as a function of strain-rate and temperature. *In Dynamic Behavior of Materials*, 1, 125-13. Springer New York.

Mrksich, M. (2000). A surface chemistry approach to studying cell adhesion. *Chemical Society Reviews*, 29(4), 267-273.

Mwale, F., Wang, H. T., Nelea, V., Luo, L., Antoniou, J., & Wertheimer, M. R. (2006). The effect of glow discharge plasma surface modification of polymers on the osteogenic differentiation of committed human mesenchymal stem cells. *Biomaterials*, 27(10), 2258-2264.

Nagayama, K., Hamaji, Y., Sato, Y., & Matsumoto, T. (2015). Mechanical trapping of the nucleus on micropillared surfaces inhibits the proliferation of vascular smooth muscle cells but not cervical cancer HeLa cells. *Journal of biomechanics*, 48(10), 1796-1803.

Nair, L. S., & Laurencin, C. T. (2007). Biodegradable polymers as biomaterials. *Progress in polymer science*, 32(8), 762-798.

Nakashima, K., Zhou, X., Kunkel, G., Zhang, Z., Deng, J. M., Behringer, R. R., & de Crombrugghe, B. (2002). The novel zinc finger-containing transcription factor osterix is required for osteoblast differentiation and bone formation. *Cell*, 108(1), 17-29.

Nikkhah, M., Edalat, F., Manoucheri, S., & Khademhosseini, A. (2012). Engineering microscale topographies to control the cell–substrate interface. *Biomaterials*, 33(21), 5230-5246.

O'brien, F. J. (2011). Biomaterials & scaffolds for tissue engineering. *Materials Today*, 14(3), 88-95.

Odorico, J. S., Kaufman, D. S., & Thomson, J. A. (2001). Multilineage differentiation from human embryonic stem cell lines. *Stem cells*, 19(3), 193-204.

Orr, A. W., Helmke, B. P., Blackman, B. R., & Schwartz, M. A. (2006). Mechanisms of mechanotransduction. *Developmental cell*, 10(1), 11-20.

Owen, G. R., Jackson, J., Chehroudi, B., Burt, H., & Brunette, D. M. (2005). A PLGA membrane controlling cell behaviour for promoting tissue regeneration. *Biomaterials*, 26(35), 7447-7456.

Owen, M. (1988). Marrow stromal stem cells. *Journal of Cell Science*, 1988(Supplement 10), 63-76.

Ozcan, C., Zorlutuna, P., Hasirci, V., & Hasirci, N. (2008, August). Influence of oxygen plasma modification on surface free energy of PMMA films and cell attachment. *In Macromolecular symposia*, 269(1), 128-137

Ozcelik, H., Padeste, C., & Hasirci, V. (2014). Systematically organized nanopillar arrays reveal differences in adhesion and alignment properties of BMSC and Saos-2 cells. *Colloids and Surfaces B: Biointerfaces*, 119, 71-81.

Pajerowski, J. D., Dahl, K. N., Zhong, F. L., Sammak, P. J., & Discher, D. E. (2007). Physical plasticity of the nucleus in stem cell differentiation. *Proceedings of the National Academy of Sciences*, 104(40), 15619-15624.

Pan, Z., Yan, C., Peng, R., Zhao, Y., He, Y., & Ding, J. (2012). Control of cell nucleus shapes via micropillar patterns. *Biomaterials*, 33(6), 1730-1735.

Papenburg, B. J., Rodrigues, E. D., Wessling, M., & Stamatialis, D. (2010). Insights into the role of material surface topography and wettability on cell-material interactions. *Soft Matter*, 6(18), 4377-4388. (3), 267-275.

Park, B. J., & Kim, Y. K. (2003). Metallic biomaterials. *Balance*, 1, 50.

Parsons, J. T., Horwitz, A. R., & Schwartz, M. A. (2010). Cell adhesion: integrating cytoskeletal dynamics and cellular tension. *Nature reviews Molecular cell biology*, 11(9), 633-643.

Pearn, W. L., Kang, H. Y., Lee, A. I., & Liao, M. Y. (2009). Photolithography control in wafer fabrication based on process capability indices with multiple characteristics. *Semiconductor Manufacturing, IEEE Transactions on*, 22(3), 351-356.

Penn, L. S., & Wang, H. (1994). Chemical modification of polymer surfaces: a review. *Polymers for Advanced Technologies*, 5(12), 809-817.

Perry, B. C., Zhou, D., Wu, X., Yang, F. C., Byers, M. A., Chu, T. M. G., & Goebel, W. S. (2008). Collection, cryopreservation, and characterization of human dental pulp-derived mesenchymal stem cells for banking and clinical use. *Tissue Engineering Part C: Methods*, 14(2), 149-156.

Piiroja, E. K., Lippmaa, H. V., Metlitskaya, O. F., & Dankovics, A. (1980). Low-temperature oxidation of polyethylene. *European Polymer Journal*, 16(7), 641-645.

Poellmann, M. J., Harrell, P. A., King, W. P., & Johnson, A. J. W. (2010). Geometric microenvironment directs cell morphology on topographically patterned hydrogel substrates. *Acta biomaterialia*, 6(9), 3514-3523.

Polyak, K., Kato, J. Y., Solomon, M. J., Sherr, C. J., Massague, J., Roberts, J. M., & Koff, A. (1994). p27Kip1, a cyclin-Cdk inhibitor, links transforming growth factor-beta and contact inhibition to cell cycle arrest. *Genes & development*, 8(1), 9-22.

Popat, K. C., Chatvanichkul, K. I., Barnes, G. L., Latempa, T. J., Grimes, C. A., & Desai, T. A. (2007). Osteogenic differentiation of marrow stromal cells cultured on nanoporous alumina surfaces. *Journal of Biomedical Materials Research Part A*, 80(4), 955-964.

Puissant, B., Barreau, C., Bourin, P., Clavel, C., Corre, J., Bousquet, C., & Penicaud, L. (2005). Immunomodulatory effect of human adipose tissue-derived adult

stem cells: comparison with bone marrow mesenchymal stem cells. *British journal of haematology*, 129(1), 118-129.

Ratner, B. D., Hoffman, A. S., Schoen, F. J., & Lemons, J. E. (2004). Biomaterials science: an introduction to materials in medicine. Academic press.

Raven, P. H., Johnson, G. B., Mason, K. A., Losos, J., & Singer, S. (2010). Biology, McGraw-Hill. New York, NY.

Recknor, J. B., Recknor, J. C., Sakaguchi, D. S., & Mallapragada, S. K. (2004). Oriented astroglial cell growth on micropatterned polystyrene substrates. *Biomaterials*, 25(14), 2753-2767.

Rehfeldt, F., Engler, A. J., Eckhardt, A., Ahmed, F., & Discher, D. E. (2007). Cell responses to the mechanochemical microenvironment—implications for regenerative medicine and drug delivery. *Advanced drug delivery reviews*, 59(13), 1329-1339.

Reubinoff, B. E., Pera, M. F., Fong, C. Y., Trounson, A., & Bongso, A. (2000). Embryonic stem cell lines from human blastocysts: somatic differentiation in vitro. *Nature biotechnology*, 18(4), 399-404.

Rhim, J. W., Mohanty, A. K., Singh, S. P., & Ng, P. K. (2006). Effect of the processing methods on the performance of polylactide films: thermocompression versus solvent casting. *Journal of Applied Polymer Science*, 101(6), 3736-3742.

Riekstina, U., Cakstina, I., Parfejevs, V., Hoogduijn, M., Jankovskis, G., Muiznieks, I., & Ancans, J. (2009). Embryonic stem cell marker expression pattern in human mesenchymal stem cells derived from bone marrow, adipose tissue, heart and dermis. *Stem Cell Reviews and Reports*, 5(4), 378-386.

Roach, P., Eglin, D., Rohde, K., & Perry, C. C. (2007). Modern biomaterials: a review—bulk properties and implications of surface modifications. *Journal of Materials Science: Materials in Medicine*, 18(7), 1263-1277.

Roach, P., Shirtcliffe, N. J., & Newton, M. I. (2008). Progess in superhydrophobic surface development. *Soft matter*, 4(2), 224-240.

Rodrigues, M. T., Leonor, I. B., Gröen, N., Viegas, C. A., Dias, I. R., Caridade, S. G., & Reis, R. L. (2014). Bone marrow stromal cells on a three-dimensional bioactive fiber mesh undergo osteogenic differentiation in the absence of osteogenic media supplements: The effect of silanol groups. *Acta biomaterialia*, 10(10), 4175-4185.

Rokkanen, P. U. (2002). Bioabsorbable polymers for medical applications with an emphasis on orthopedic surgery. Polymeric biomaterials. 2nd ed. New York (NY): Marcel Dekker, 545-61.

Rosen, V., & Wozney, J. M. (1996). Bone morphogenetic proteins. *Principles of bone biology*, 2, 919-928.

Rosenberg, M. D. (1962). Long-range interactions between cell and substratum. *Proceedings of the National Academy of Sciences*, 48(8), 1342-1349.

Rosenberg, M. D. (1963). Cell guidance by alterations in monomolecular films. *Science*, 139(3553), 411-411.

Rowat, A. C., Lammerding, J., Herrmann, H., & Aebi, U. (2008). Towards an integrated understanding of the structure and mechanics of the cell nucleus. *Bioessays*, 30(3), 226-236.

Salasznyk, R. M., Klees, R. F., Williams, W. A., Boskey, A., & Plopper, G. E. (2007). Focal adhesion kinase signaling pathways regulate the osteogenic

differentiation of human mesenchymal stem cells. *Experimental cell research*, 313(1), 22-37.

Schaller, M. D. (2001). Biochemical signals and biological responses elicited by the focal adhesion kinase. *Biochimica et Biophysica Acta (BBA)-Molecular Cell Research*, 1540(1), 1-21.

Schweikl, H., Müller, R., Englert, C., Hiller, K. A., Kujat, R., Nerlich, M., & Schmalz, G. (2007). Proliferation of osteoblasts and fibroblasts on model surfaces of varying roughness and surface chemistry. *Journal of Materials Science: Materials in Medicine*, 18(10), 1895-1905.

Sen, B., Xie, Z., Case, N., Ma, M., Rubin, C., & Rubin, J. (2008). Mechanical strain inhibits adipogenesis in mesenchymal stem cells by stimulating a durable β-catenin signal. *Endocrinology*, 149(12), 6065-6075.

Seo, C. H., Furukawa, K., Montagne, K., Jeong, H., & Ushida, T. (2011). The effect of substrate microtopography on focal adhesion maturation and actin organization via the RhoA/ROCK pathway. *Biomaterials*, 32(36), 9568-9575.

Shih, Y. R. V., Tseng, K. F., Lai, H. Y., Lin, C. H., & Lee, O. K. (2011). Matrix stiffness regulation of integrin-mediated mechanotransduction during osteogenic differentiation of human mesenchymal stem cells. *Journal of Bone and Mineral Research*, 26(4), 730-738.

Shirtcliffe, N. J., McHale, G., Newton, M. I., & Perry, C. C. (2005). Wetting and wetting transitions on copper-based super-hydrophobic surfaces. *Langmuir*, 21(3), 937-943.

Singhvi, R., Kumar, A., Lopez, G. P., Stephanopoulos, G. N., Wang, D. I., Whitesides, G. M., & Ingber, D. E. (1994). Engineering cell shape and function. *Science*, 264(5159), 696-698.

Sjöström, T., Dalby, M. J., Hart, A., Tare, R., Oreffo, R. O., & Su, B. (2009). Fabrication of pillar-like titania nanostructures on titanium and their interactions with human skeletal stem cells. *Acta Biomaterialia*, 5(5), 1433-1441.

Song, S., Kim, E. J., Bahney, C. S., Miclau, T., Marcucio, R., & Roy, S. (2015). The synergistic effect of micro-topography and biochemical culture environment to promote angiogenesis and osteogenic differentiation of human mesenchymal stem cells. *Acta biomaterialia*, 18, 100-111.

Stein, G. S., & Lian, J. B. (1993). Molecular mechanisms mediating proliferation/differentiation interrelationships during progressive development of the osteoblast phenotype. *Endocrine reviews*, 14(4), 424-442.

Steinberg, T., Schulz, S., Spatz, J. P., Grabe, N., Mussig, E., Kohl, A., & Tomakidi, P. (2007). Early keratinocyte differentiation on micropillar interfaces. N*ano letters*, 7(2), 287-294.

Stock, U. A., & Vacanti, J. P. (2001). Tissue engineering: current state and prospects. *Annual review of medicine*, 52(1), 443-451.

Stojmenović, M., & Žunić, J. (2008). Measuring elongation from shape boundary. *Journal of Mathematical Imaging and Vision*, 30(1), 73-85.

Strobel, E. S., Gay, R. E., & Greenberg, P. L. (1986). Characterization of the in vitro stromal microenvironment of human bone marrow. *The International Journal of Cell Cloning*, 4(5), 341-356.

Stuurman, N., Heins, S., & Aebi, U. (1998). Nuclear lamins: their structure, assembly, and interactions. *Journal of structural biology*, 122(1), 42-66.

Sun, T., Feng, L., Gao, X., & Jiang, L. (2005). Bioinspired surfaces with special wettability. *Accounts of Chemical Research*, 38(8), 644-652.

Suresh S. Biomechanics and biophysics of cancer cells. *Acta Materialia*. 2007; 55:3989–4014.

Tamada, Y., & Ikada, Y. (1993). Cell adhesion to plasma-treated polymer surfaces. *Polymer*, 34(10), 2208-2212.

Tang J, Peng R, Ding J. The regulation of stem cell differentiation by cell–cell contact on micropatterned material surfaces. *Biomaterials* 2010;31(9):2470–6

Thapa, A., Webster, T. J., & Haberstroh, K. M. (2003). Polymers with nano-dimensional surface features enhance bladder smooth muscle cell adhesion. *Journal of Biomedical Materials Research Part A*, 67(4), 1374-1383.

Thevenot, P., Hu, W., & Tang, L. (2008). Surface chemistry influence implant biocompatibility. *Current topics in medicinal chemistry*, 8(4), 270.

Thompson, L. F., Willson, C. G., & Bowden, M. J. (1994). Introduction to Microlithography, 1994. Washington, DC: ACS.

Triffitt, J. T. (1996). The stem cell of the osteoblast. *Principles of bone biology*, 39-50.

Tuan, R. S., Boland, G., & Tuli, R. (2003). Adult mesenchymal stem cells and cell-based tissue engineering. *Arthritis Research and Therapy*, 5(1), 32-45.

Uccelli, A., Moretta, L., & Pistoia, V. (2008). Mesenchymal stem cells in health and disease. *Nature Reviews Immunology*, 8(9), 726-736.

Valamehr B et al. Hydrophobic surfaces for enhanced differentiation of embryonic stem cell-derived embryoid bodies. *Proc Natl Acad Sci USA* 2008;105(38):14459–64.

Vater, C., Kasten, P., & Stiehler, M. (2011). Culture media for the differentiation of mesenchymal stromal cells. *Acta Biomaterialia*, 7(2), 463-477.

Vert, M. (2007). Polymeric biomaterials: strategies of the past vs. strategies of the future. *Progress in Polymer Science*, 32(8), 755-761.

Vesel, A., & Mozetic, M. (2012). Surface modification and ageing of PMMA polymer by oxygen plasma treatment. *Vacuum*, 86(6), 634-637.

Vogel, V., & Sheetz, M. (2006). Local force and geometry sensing regulate cell functions. *Nature reviews molecular cell biology*, 7(4), 265-275.

Voldman, J., Gray, M. L., & Schmidt, M. A. (1999). Microfabrication in biology and medicine. *Annual review of biomedical engineering*, 1(1), 401-425.

Wan, Y., Qu, X., Lu, J., Zhu, C., Wan, L., Yang, J., & Wang, S. (2004). Characterization of surface property of poly (lactide-co-glycolide) after oxygen plasma treatment. *Biomaterials*, 25(19), 4777-4783.

Wan, Y., Wang, Y., Liu, Z., Qu, X., Han, B., Bei, J., & Wang, S. (2005). Adhesion and proliferation of OCT-1 osteoblast-like cells on micro-and nano-scale topography structured poly (L-lactide). *Biomaterials*, 26(21), 4453-4459.

Wang, P. Y., Clements, L. R., Thissen, H., Tsai, W. B., & Voelcker, N. H. (2015). Screening rat mesenchymal stem cell attachment and differentiation on surface chemistries using plasma polymer gradients. *Acta biomaterialia*, 11, 58-67.

Wang, Y. X., Robertson, J. L., Spillman Jr, W. B., & Claus, R. O. (2004). Effects of the chemical structure and the surface properties of polymeric biomaterials on their biocompatibility. *Pharmaceutical research*, 21(8), 1362-1373.

Wang, Y., Kim, H. J., Vunjak-Novakovic, G., & Kaplan, D. L. (2006). Stem cell-based tissue engineering with silk biomaterials. *Biomaterials*, 27(36), 6064-6082.

Watari, S., Hayashi, K., Wood, J. A., Russell, P., Nealey, P. F., Murphy, C. J., & Genetos, D. C. (2012). Modulation of osteogenic differentiation in hMSCs cells by submicron topographically-patterned ridges and grooves. *Biomaterials*, 33(1), 128-136.

Wei, J., Igarashi, T., Okumori, N., Igarashi, T., Maetani, T., Liu, B., & Yoshinari, M. (2009). Influence of surface wettability on competitive protein adsorption and initial attachment of osteoblasts. *Biomedical Materials*, 4(4), 045002.

Weiner, S., & Wagner, H. D. (1998). The material bone: structure-mechanical function relations. *Annual Review of Materials Science*, 28(1), 271-298.

Weiss, P. (1934). In vitro experiments on the factors determining the course of the outgrowing nerve fiber. *Journal of Experimental Zoology*, 68(3), 393-448.

Wennerberg, A. (1998). The importance of surface roughness for implant incorporation. *International Journal of Machine Tools and Manufacture*, 38(5), 657-662.

Wenzel, R. N. (1936). Resistance of solid surfaces to wetting by water. *Industrial & Engineering Chemistry*, 28(8), 988-994.

Wilson, C. J., Clegg, R. E., Leavesley, D. I., & Pearcy, M. J. (2005). Mediation of biomaterial-cell interactions by adsorbed proteins: a review. *Tissue engineering*, 11(1-2), 1-18.

Wong, J. Y., Leach, J. B., & Brown, X. Q. (2004). Balance of chemistry, topography, and mechanics at the cell–biomaterial interface: Issues and challenges for assessing the role of substrate mechanics on cell response. *Surface Science*, 570(1), 119-133.

Wong, J. Y., Velasco, A., Rajagopalan, P., & Pham, Q. (2003). Directed movement of vascular smooth muscle cells on gradient-compliant hydrogels. *Langmuir*, 19(5), 1908-1913.

Yamamoto, K., Sokabe, T., Watabe, T., Miyazono, K., Yamashita, J. K., Obi, S., & Ando, J. (2005). Fluid shear stress induces differentiation of Flk-1-positive embryonic stem cells into vascular endothelial cells in vitro. *American Journal of Physiology-Heart and Circulatory Physiology*, 288(4), H1915-H1924.

Yang, M. T., Fu, J., Wang, Y. K., Desai, R. A., & Chen, C. S. (2011). Assaying stem cell mechanobiology on microfabricated elastomeric substrates with geometrically modulated rigidity. *Nature protocols*, 6(2), 187-213.

Yang, Y., Kulangara, K., Lam, R. T., Dharmawan, R., & Leong, K. W. (2012). Effects of topographical and mechanical property alterations induced by oxygen plasma modification on stem cell behavior. *ACS nano*, 6(10), 8591-8598.

Yao, X., Peng, R., & Ding, J. (2013). Effects of aspect ratios of stem cells on lineage commitments with and without induction media. *Biomaterials*, 34(4), 930-939.

Yeong, W. Y., Chua, C. K., Leong, K. F., & Chandrasekaran, M. (2004). Rapid prototyping in tissue engineering: challenges and potential. *Trends in biotechnology*, 22(12), 643-652

Yildirim, S. (2013). Isolation Methods of Dental Pulp Stem Cells. *In Dental Pulp Stem Cells* (pp. 41-51). Springer New York.

Yim, E. K., Pang, S. W., & Leong, K. W. (2007). Synthetic nanostructures inducing differentiation of human mesenchymal stem cells into neuronal lineage. *Experimental cell research*, 313(9), 1820-1829.

Zhao, L., Liu, L., Wu, Z., Zhang, Y., & Chu, P. K. (2012). Effects of micropitted/nanotubular titania topographies on bone mesenchymal stem cell osteogenic differentiation. *Biomaterials*, 33(9), 2629-2641.

Zhao, Y., Tan, K., Zhou, Y., Ye, Z., & Tan, W. S. (2016). A combinatorial variation in surface chemistry and pore size of three-dimensional porous poly (ε-caprolactone) scaffolds modulates the behaviors of mesenchymal stem cells. *Materials Science and Engineering: C*, 59, 193-202.

Zheng, Q., Lv, C., Hao, P., & Sheridan, J. (2010). Small is beautiful, and dry. *Science China Physics, Mechanics and Astronomy*, 53(12), 2245-2259.

Zhou, X., Novotny, J. E., & Wang, L. (2009). Anatomic variations of the lacunar–canalicular system influence solute transport in bone. *Bone*, 45(4), 704-710.

APPENDICES

APPENDIX A

ALAMAR BLUE CALIBRATION CURVE

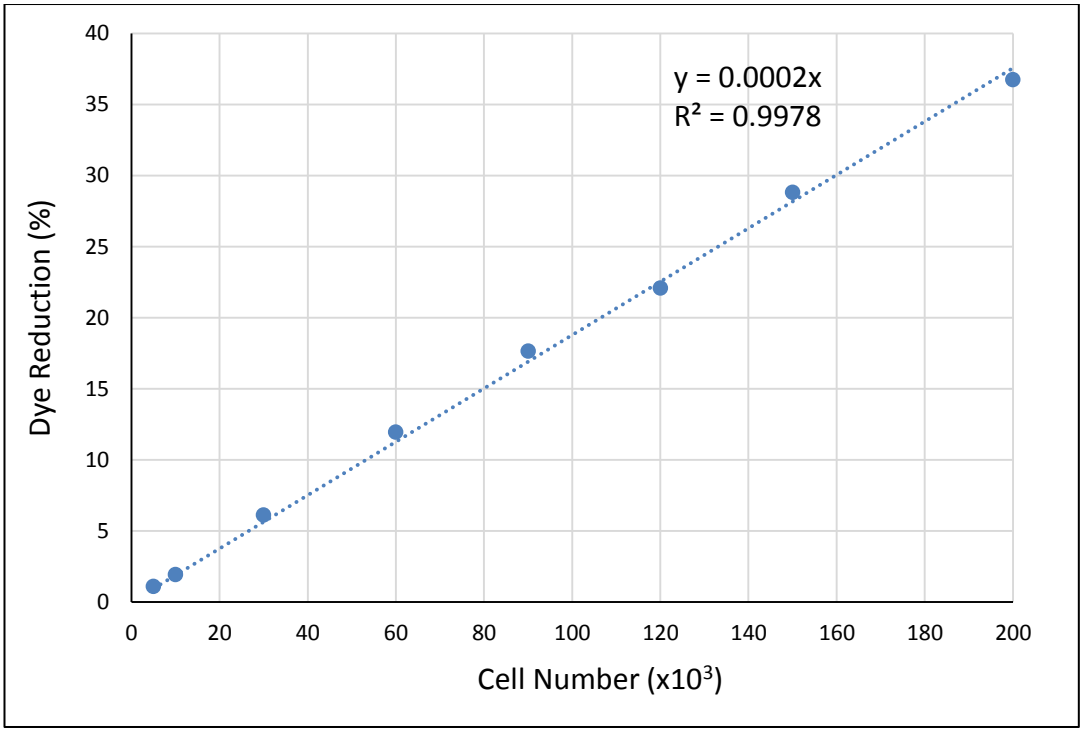

Figure A.1. Calibration curve of the Alamar Blue cell viability assay for DPSCs.

APPENDIX B

NUMERICAL RESULTS OF THE ANALYSES

Table B.1. Young's moduli and ultimate tensile strength values of the PMMA films produced by using three different molecular weights.

Molecular Weight (kDa)	Young's Modulus (E) (MPa)	Ultimate Tensile Strength (UTS) (MPa)
120	870.3 ± 6.2	25.2 ± 0.5
350	1285.4 ± 28.7	41.6 ± 2.1
996	1255 ± 14.7	41.5 ± 0.3

Table B.2. Water contact angle values of the unpatterned PMMA films upon oxygen plasma modification with different plasma power and durations.

Plasma Parameters		Water Contact Angle (Degrees)
Power (W)	**Duration (min)**	
0	0	87.3 ± 3.8
20	2.5	67
30	2.5	55
50	2.5	42
75	2.5	35
100	2.5	32
100	10	12.5 ± 0.3

Table B.3. Water contact angle values of all PMMA substrates before and after oxygen plasma modification (100W 10 min).

Sample	Water Contact Angle (Degrees)	
	Untreated	**Plasma Treated**
Unpatterned Control	87.4 ± 3.8	14.5 ± 0.3
P4G4	131.6 ± 1.3	14.6 ± 0.6
P8G8	119.8 ± 2.4	17.9 ± 1.0
P16G16	113. 3 ± 1.2	18.7 ± 0.2

Table B.4. Numbers of DPSCs on TCPs and PMMA substrates 16 h after cell seeding. Seeding density was $2x10^4$.

Sample	Cell Number ($x10^3$)	
TCPs	21.8 ± 3.1	
	Untreated	**Plasma Treated**
Unpatterned Control	2.1 ± 0.7	10.9 ± 0.4
P4G4	8.2 ± 0.6	9.6 ± 1.7
P8G8	5.7 ± 0.3	11.2 ± 1.6
P16G16	4.9 ± 0.8	14. 8 ± 1.5

Table B.5. Number of DPSCs on TCPs and PMMA substrates determined by Alamar Blue cell viability assay on Days 3, 7, 14 and 21.

	Cell Number (x10^4)							
Time	**Day 3**		**Day 7**		**Day 14**		**Day 21**	
Plasma Modification / **Samples**	-	+	-	+	-	+	-	+
Unpatterned Control	0.31 ± 0.04	2.18 ± 0.23	1.58 ± 0.08	13.48 ± 0.30	15.04 ± 0.62	25.65 ± 0.54	28.00 ± 1.22	34.60 ± 1.28
P4G4	0.37 ± 0.03	0.88 ± 0.08	0.81 ± 0.08	5.01 ± 0.25	8.34 ± 0.23	20.61 ± 0.65	24.13 ± 1.09	33.18 ± 0.95
P8G8	0.4 ± 0.03	1.45 ± 0.09	1.06 ± 0.06	12.10 ± 0.47	14.98 ± 0.18	25.03 ± 0.34	27.83 ± 1.21	33.64 ± 1.47
P16G16	0.47 ± 0.07	1.69 ± 0.09	1.84 ± 0.03	15.53 ± 0.30	18.55 ± 0.23	23.23 ± 0.25	29.00 ± 1.22	32.60 ± 0.82
TCPs	3.10 ± 1.27		15.69 ± 0.21		36.58 ± 0.99		41.73 ± 1.19	

Table B.6. Proliferation rate on TCPs and PMMA substrates between days 3-7, 7-14 and 14-21.

	Proliferation Rate (Cells/Day, x 10^4)					
Tine Interval	**Days 3-7**		**Days 7-14**		**Days 14-21**	
Plasma Modification / **Sample**	-	+	-	+	-	+
Unpatterned Control	0.32 ± 0.02	2.82 ± 0.1	1.92 ± 0.09	1.74 ± 0.09	1.85 ± 0.2	1.28 ± 0.2
P4G4	0.11 ± 0.02	1.03 ± 0.06	1.07 ± 0.04	2.23 ± 0.1	2.26 ± 0.16	1.79 ± 0.16
P8G8	0.16 ± 0.02	2.66 ± 0.12	1.99 ± 0.03	1.85 ± 0.08	1.84 ± 0.17	1.23 ± 0.22
P16G16	0.34 ± 0.02	3.46 ± 0.08	2.39 ± 0.03	1.10 ± 0.05	1.35 ± 0.18	1.34 ± 0.12
TCPs	3.15 ± 0.06		2.98 ± 0.14		0.74 ± 0.22	

Table B.7. Fold changes in the expressions of stemness and osteogenic markers by DPSCs cultured on TCPs in osteogenic differentiation media for 14 and 28 days.

	Fold Change (OM(+)/OM(-))	
Time (Days) / **Marker**	**14**	**28**
Oct3/4	1.49 ± 0.58	1.65 ± 0.49
Nanog	0.49 ± 0.10	052 ± 0.22
Osx	10.47 ± 0.31	0.93 ± 0.38
ALP	2.49 ± 0.42	10.13 ± 1.07
OC	3.13 ± 1.03	11.20 ± 3.42

Table B.8. Fold changes in the expressions of stemness and osteogenic markers by DPSCs cultured on untreated and plasma treated micropillar decorated PMMA films for 14 and 28 days.

	Fold Change (Sample/Unpatterned Control)											
Time	**Day 14**						**Day 28**					
Sample	**P4G4**		**P8G8**		**P16G16**		**P4G4**		**P8G8**		**P16G16**	
Plasma Modification	-	+	-	+	-	+	-	+	-	+	-	+
Marker												
Oct3/4	0.72 ± 0.01	0.56 ± 0.00	0.56 ± 0.13	1.29 ± 0.21	0.63 ± 0.10	0.98 ± 0.16	1.49 ± 0.27	0.47 ± 0.05	2.90 ± 1.06	0.81 ± 0.15	1.30 ± 0.31	1.09 ± 0.02
Nanog	0.69 ± 0.15	0.45 ± 0.09	1.40 ± 0.28	0.58 ± 0.15	1.12 ± 0.28	0.70 ± 0.13	0.60 ± 0.11	0.44 ± 0.03	1.77 ± 0.05	0.48 ± 0.01	1.13 ± 0.03	1.04 ± 0.31
Osx	0.48 ± 0.01	1.03 ± 0.07	0.36 ± 0.01	0.79 ± 0.12	0.52 ± 0.01	0.77 ± 0.14	0.71 ± 0.08	1.87 ± 0.04	0.76 ± 0.02	1.56 ± 0.37	0.60 ± 0.05	0.94 ± 0.07
ALP	3.61 ± 0.18	1.00 ± 0.16	4.01 ± 0.21	1.25 ± 0.28	1.37 ± 0.51	1.04 ± 0.06	5.21 ± 0.35	0.48 ± 0.03	5.73 ± 0.47	0.87 ± 0.13	1.25 ± 0.55	0.88 ± 0.12
OC	0.39 ± 0.03	0.95 ± 0.14	0.48 ± 0.05	0.83 ± 0.06	0.75 ± 0.13	0.88 ± 0.01	0.40 ± 0.05	0.70 ± 0.16	0.34 ± 0.01	0.82 ± 0.20	0.54 ± 0.01	0.65 ± 0.07

APPENDIX C

STANDARD AND MELT CURVES OF GENE SPECIFIC PRIMERS

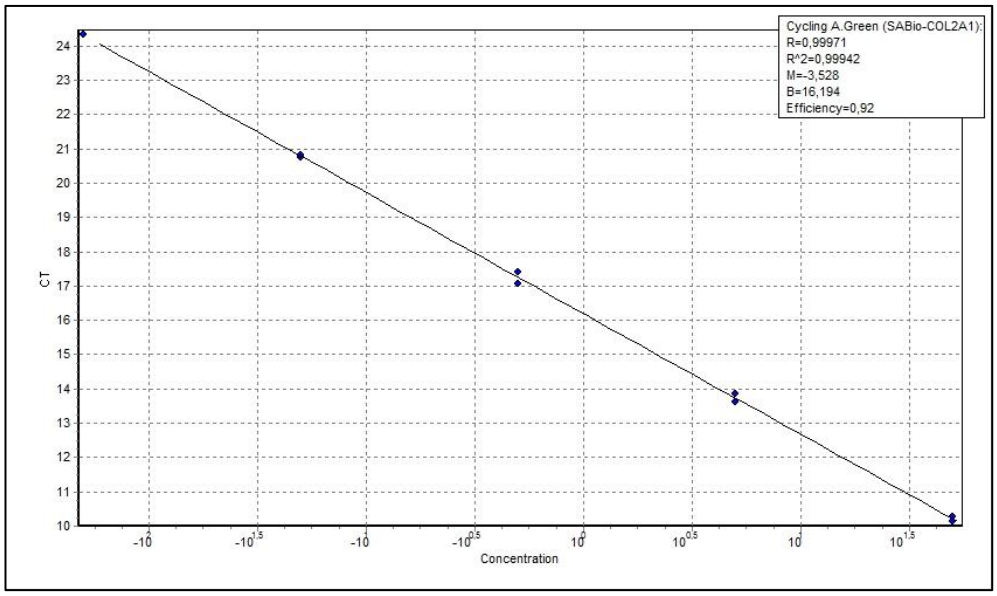

Figure C.1. Standard curve of GAPDH specific primer pair.

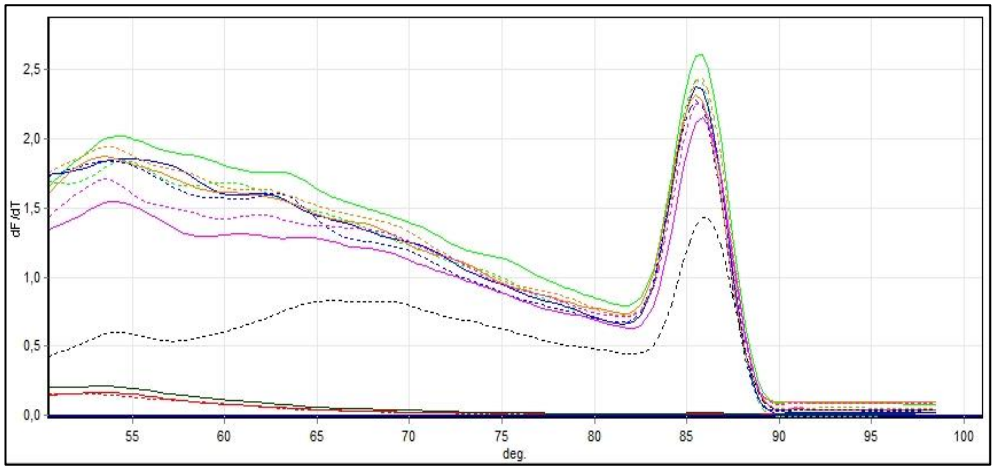

Figure C.2. Melt curve of the products of GAPDH specific primer pair.

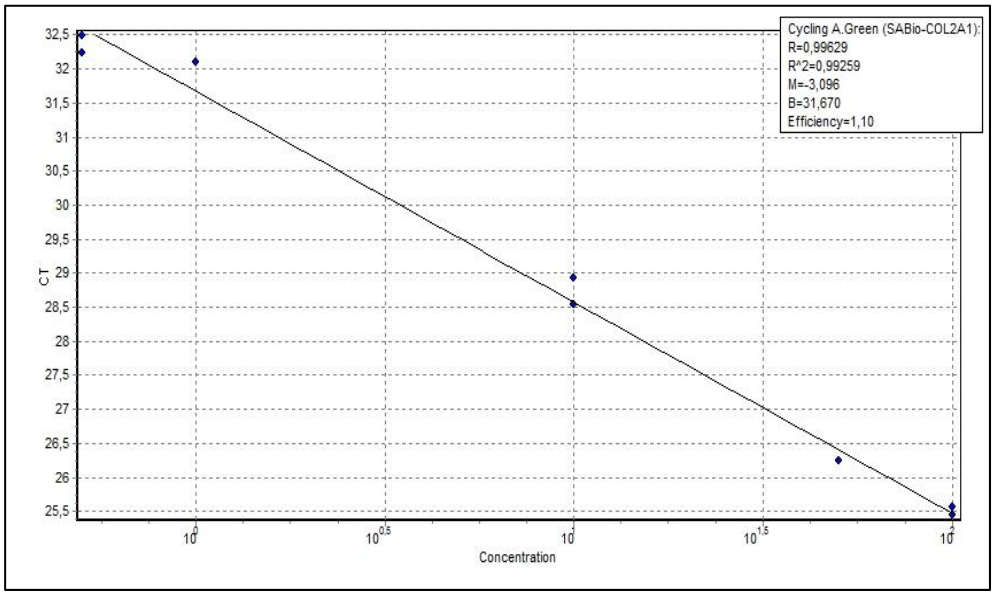

Figure C.3. Standard curve of Oct3/4 specific primer pair.

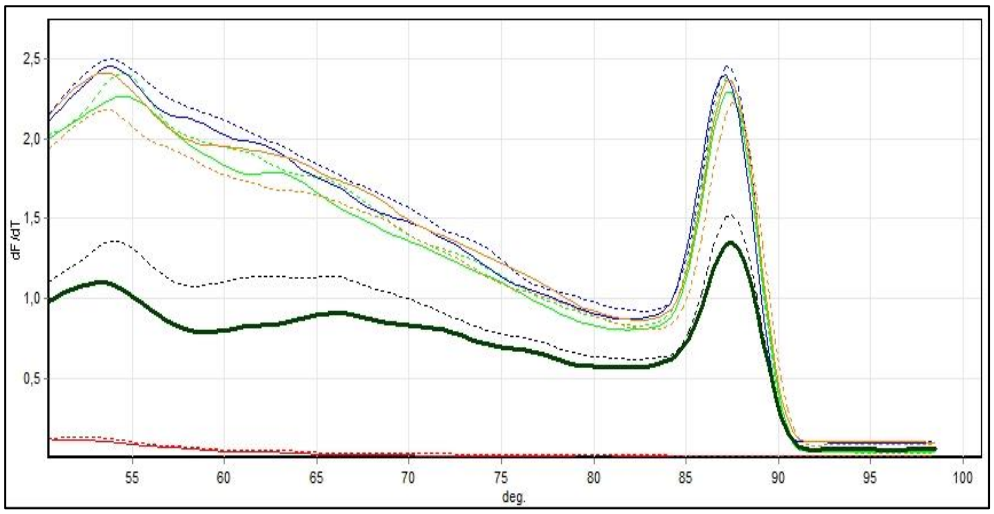

Figure C.4. Melt curve of the products of Oct3/4 specific primer pair.

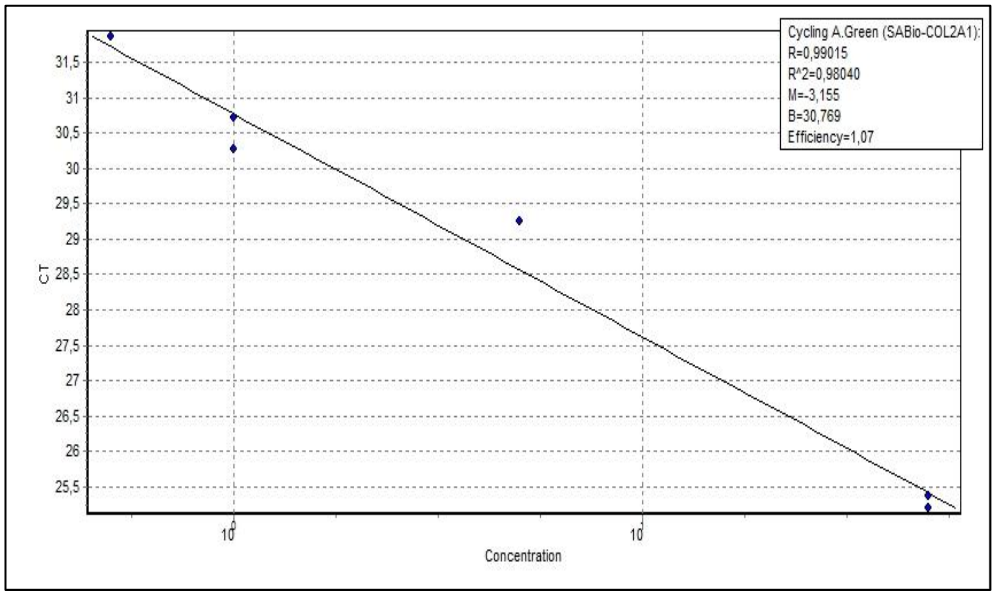

Figure C.5. Standard curve of Nanog specific primer pair.

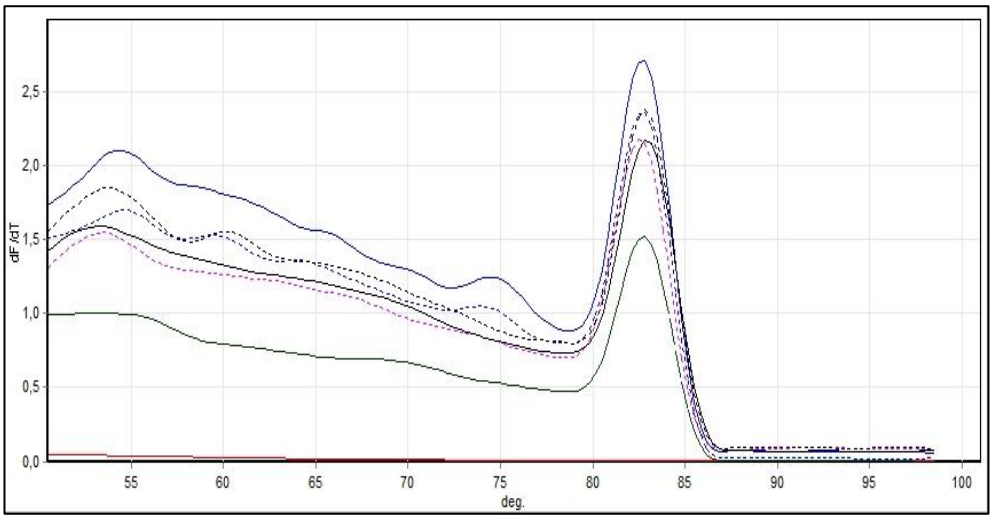

Figure C.6. Melt curve of the products of Nanog specific primer pair.

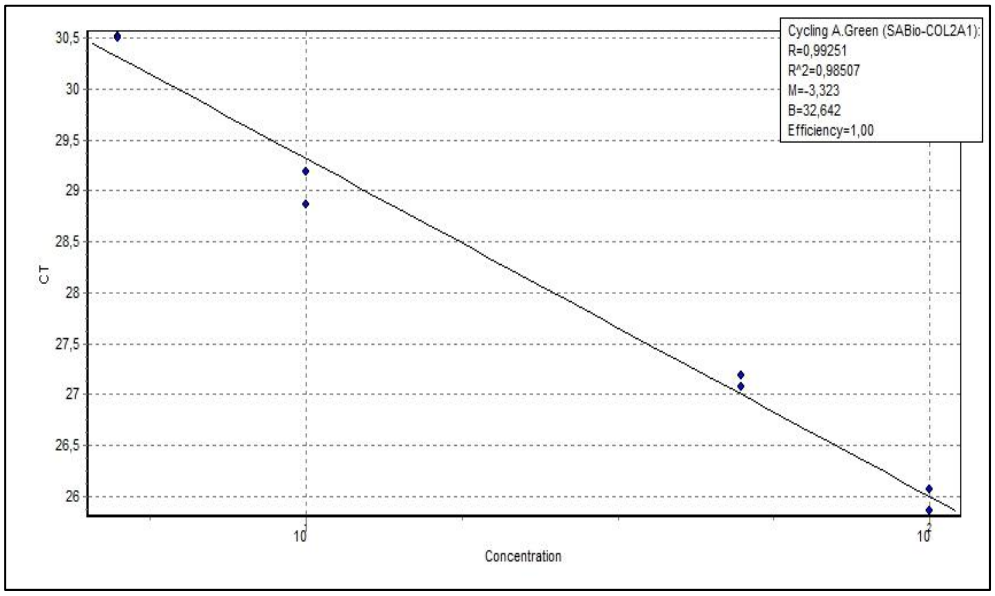

Figure C.7. Standard curve of Osx specific primer pair.

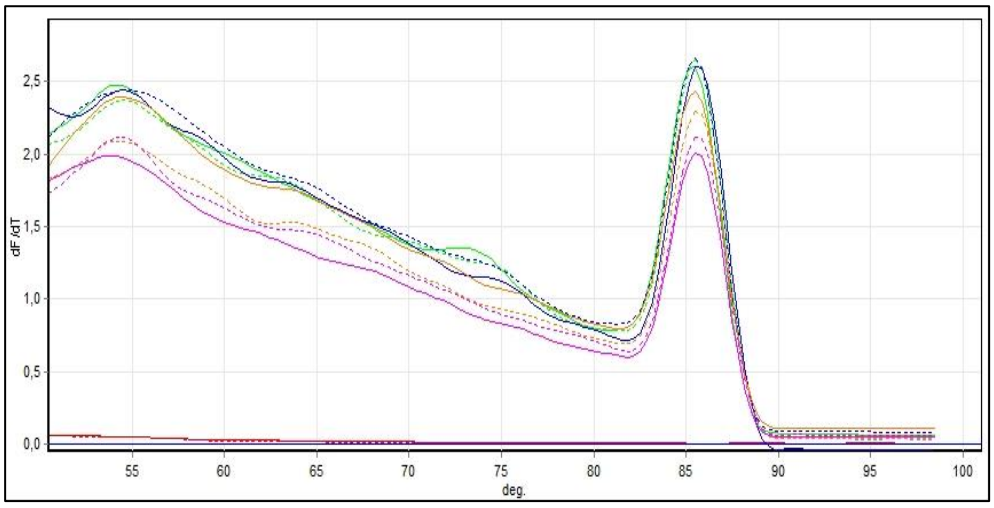

Figure C.8. Melt curve of the products of Osx specific primer pair.

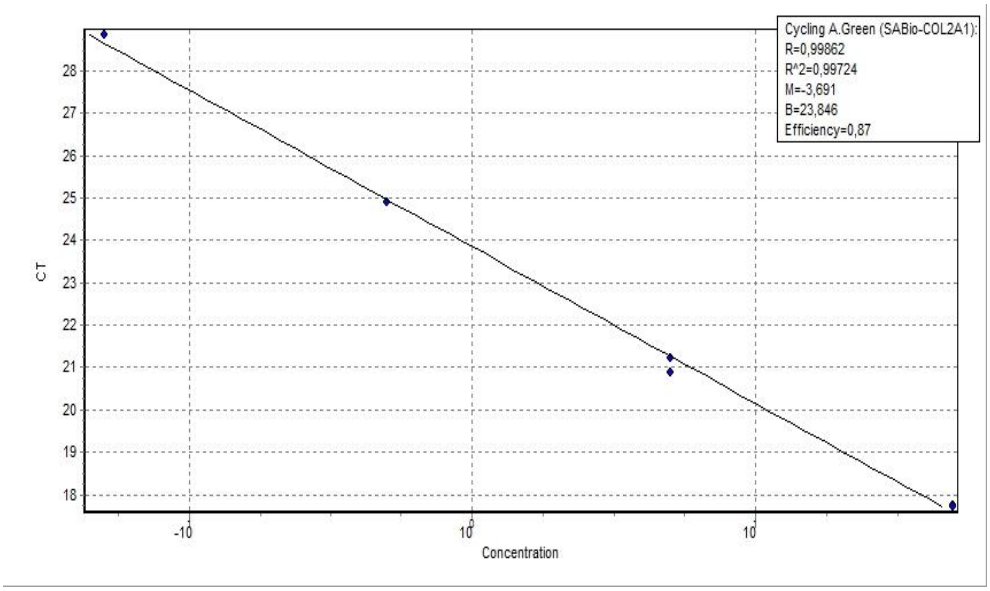

Figure C.9. Standard curve of ALP specific primer pair.

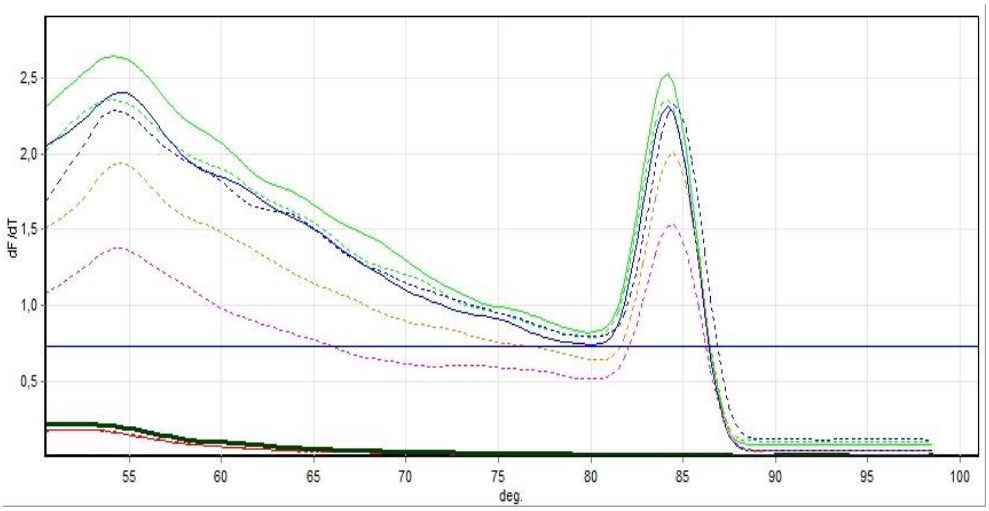

Figure C.10. Melt curve of the products of ALP specific primer pair.

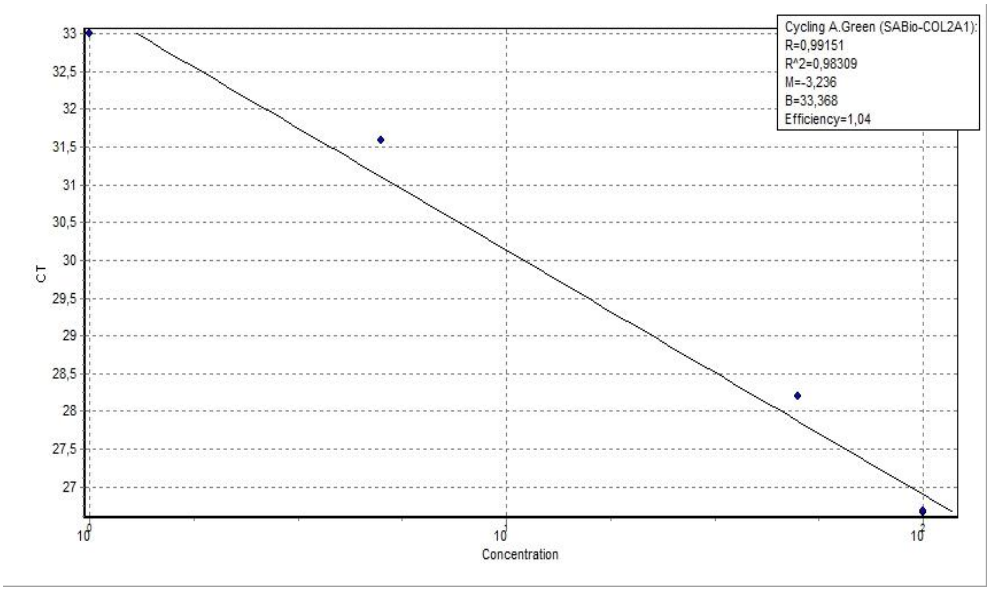

Figure C.11. Standard curve of OC specific primer pair.

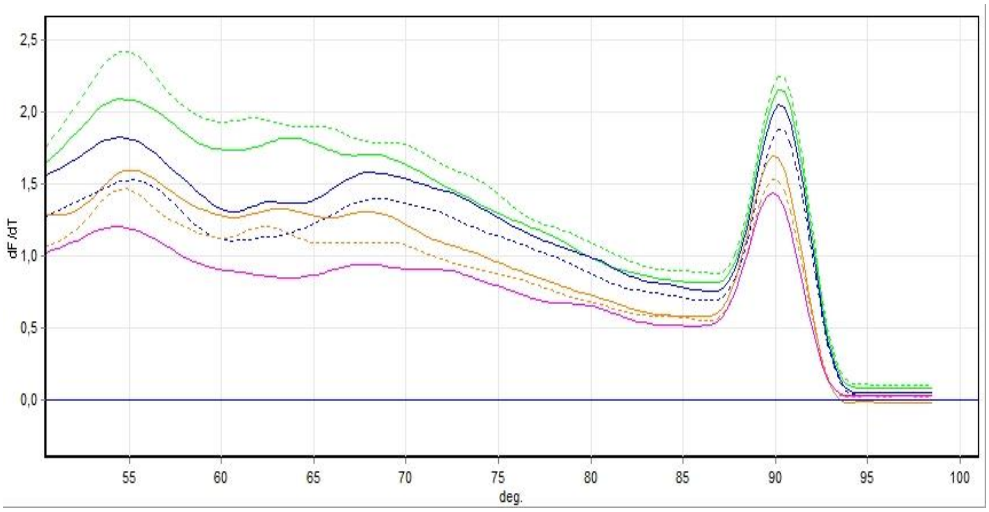

Figure C.12. Melt curve of the products of OC specific primer pair.

APPENDIX D

ETHICS COMMITTEE REPORT

FEN BİLİMLERİ ENSTİTÜSÜ
GRADUATE SCHOOL OF NATURAL AND APPLIED SCIENCES

ORTA DOĞU TEKNİK ÜNİVERSİTESİ
MIDDLE EAST TECHNICAL UNIVERSITY

DUMLUPINAR BULVARI 06800
ÇANKAYA ANKARA/TURKEY
T: +90 312 210 22 92
F: +90 312 210 79 59
www.fbe@metu.edu.tr
www.fbe.metu.edu.tr

Sayı: 28620816/ 505-69

17.11.2014

Gönderilen : Prof. Dr. Vasıf Hasırcı
BIOMATEN

Gönderen : Prof. Dr. Canan Sümer
IAK Başkanı Vekili

İlgi : Etik Onayı

Danışmanlığını yapmış olduğunuz Biyoteknoloji Bölümü öğrencisi Onur Hastürk'ün "İmplant Yüzeylerindeki Mikrodesenlerin İnsan Mezenkimal Kök Hücre Farklılaşma Yönü Üzerine Etkileri" isimli araştırması "İnsan Araştırmaları Komitesi" tarafından uygun görülerek gerekli onay verilmiştir.

Bilgilerinize saygılarımla sunarım.

Etik Komite Onayı

Uygundur

17/11/2014

Prof.Dr. Canan Sümer
Uygulamalı Etik Araştırma Merkezi
(UEAM) Başkanı Vekili
ODTÜ 06531 ANKARA